Characterizing Cerebral Degeneration in Amyotrophic Lateral Sclerosis with Texture Analysis

by

Abdullah Ishaque

A thesis submitted in partial fulfillment of the requirements for the degree of

Doctor of Philosophy

in Neuroscience

Neuroscience and Mental Health Institute
University of Alberta

Abstract

Amyotrophic lateral sclerosis (ALS) is a neurodegenerative disease that is hallmarked by unrelenting and progressive wasting and paralysis of voluntary muscles. The classic pathology in ALS features neuronal loss, gliosis, and abnormal protein deposition in the upper and lower motor neurons (UMN and LMN). Most patients diagnosed with ALS die within five years of symptom onset due to respiratory failure. Studies have used magnetic resonance imaging (MRI) techniques to capture the neurodegenerative processes in the brain *in vivo* and have consistently shown abnormalities in the motor cortices, corticospinal tract, and frontotemporal regions. However, the longitudinal course of cerebral degeneration remains poorly understood. Additionally, clinical trials are hampered by a lack of feasible objective biomarkers that can monitor the disease and provide a means to mitigate the detrimental effects of the heterogeneity of disease in ALS.

In this dissertation, the overall objectives were to study cerebral degeneration in ALS using routinely acquired MR images and texture analysis. Texture analysis is an image processing technique that quantifies variations and relationships between voxel intensities in an image. Secondly, the longitudinal changes in gray and white matter structures in ALS were investigated to study the progressive course of cerebral degeneration in the disease.

To accomplish these objectives, the dissertation was divided into three experiments. First, 3-dimensional (3D) texture analysis was applied to T1-weighted MR images of ALS patients and controls. Baseline group comparisons identified abnormalities in texture of T1-weighted images in the motor cortex, insula, frontal lobe, basal ganglia, parahippocampal regions, and corticospinal tract in ALS patients. Furthermore, patients with survival of less than 20 months

had greater involvement of frontotemporal regions than patients with longer lengths of survival. In the second experiment, the discriminatory accuracy of these texture features from the corticospinal tract was evaluated in two independent cohorts. Additionally, the association between texture of the corticospinal tract from T1-weighted images and its diffusion metrics from diffusion tensor imaging were investigated. Binary logistic regression models using texture features of the corticospinal tract were able to discriminate ALS patients from controls. Several texture features correlated with diffusion metrics and these features were also significantly different along the length of the corticospinal tract, particularly in the regions of the corona radiata and internal capsule, between ALS patients and controls. These experiments highlight the ability of texture analysis to quantify gray and white matter degeneration using a single T1-weighted image sequence. In the last experiment, the longitudinal progression of cerebral degeneration was investigated. Here, progressive texture abnormalities in the internal capsule in ALS patients over four- and eight-month intervals in the absence of clinical UMN decline were found. Clinical UMN dysfunction also correlated specifically with texture of the corticospinal tract. Longitudinal gray matter progressive changes were characterized by a frontotemporal spatial spread, instead of worsening degeneration within the motor structures. Longitudinal findings differed between fast and slow progressing ALS subgroups; the slow progressing ALS subgroup had greater progressive texture change in the internal capsule than the fast progressing ALS subgroup. On the other hand, the fast progressing ALS subgroup had greater progressive texture changes in the precentral gyrus.

In summary, this dissertation has revealed important insights into the longitudinal gray and white matter degeneration in the brain in ALS and their relationship to their clinical phenotype. Particularly, progressive degeneration along the corticospinal tract occurs over a

short period of time in the absence of clinical UMN decline. Over the same period, the longitudinal course of gray matter pathology is characterized by a frontotemporal spatial spread instead of progressive degeneration within the motor structures. Texture analysis of T1-weighted images successfully recapitulated the known *in vivo* spatial pathological cerebral characteristics of ALS with abnormalities in the motor cortex, frontotemporal regions, and the corticospinal tract. Texture-based abnormalities of the corticospinal tract correlated with clinical UMN dysfunction, highlighting the importance of this structure as a suitable marker for UMN disease. Therefore, texture analysis of T1-weighted images has emerged as a potential objective biomarker due to its feasibility in clinical application. Based on the results, it can serve and fulfil the roles of multiple types of biomarkers including diagnostic and prognostic markers.

Preface

The dissertation is an original work of Abdullah Ishaque. Chapter 3 of this dissertation has been published as:

- Ishaque, A., Mah, D., Seres, P., Luk, C., Eurich, D., Johnston, W., Yang, Y.H. and Kalra, S., 2018. Evaluating the cerebral correlates of survival in amyotrophic lateral sclerosis. *Annals of clinical and translational neurology*, 5(11), pp.1350-1361.

The study was designed by me, with assistance from Kalra, who also served as the senior author along with Yang, Y.H. I was responsible for data analysis and manuscript writing and editing. Mah and Seres were involved with recruitment of participants and data acquisition. Luk, Johnston, and Kalra were responsible for clinical examination of patients ALS. Eurich provided guidance for statistical analysis. The final manuscript was approved by all authors.

Chapter 4 of this dissertation has been published as:

- Ishaque, A., Mah, D., Seres, P., Luk, C., Johnston, W., Chenji, S., Beaulieu, C., Yang, Y.H. and Kalra, S., 2019. Corticospinal tract degeneration in ALS unmasked in T1-weighted images using texture analysis. *Human brain mapping*, 40(4), pp.1174-1183.

The study was designed by me, with assistance from Beaulieu, Yang, and Kalra. Mah and Seres were responsible for recruitment of participants and data acquisition. Luk, Johnston, and Kalra. were responsible for clinical examination of ALS patients. Chenji provided guidance for statistical analysis. The final manuscript was approved by all authors.

Chapter 5 of this dissertation has been submitted for publication as:

- Ishaque, A., Ta, D., Khan, M., Zinman, L., Korngut, L., Genge, A., Dionne, A., Briemberg, H., Yang, Y.H., Emery, D., Eurich, D., Frayne, R., Graham, S., Wilman, A., Kalra, S., and Dupré, N. Progressive Cerebral Degeneration in Amyotrophic Lateral Sclerosis: A T1-weighted Texture Study.

I was responsible for the design of the study, data analysis, and manuscript writing and editing with assistance from Kalra. Ta and Khan assisted with data collation and parts of processing. Zinman, Korngut, Genge, Dionne, Briemberg, and Kalra were responsible for recruitment and clinical assessments of participants from multiple centres across Canada. Emery and Kalra were involved with the clinical review of magnetic resonance imaging (MRI) scans of participants included in the study. Frayne, Graham, and Wilman were responsible for the creation and implementation of a harmonized MRI acquisition protocol across multiple sites.

Due to the paper-based nature of this dissertation, each experimental chapter is followed by a reference list formatted in accordance with the accepting/submitting journal's formatting style. The final References chapter at the end of the dissertation lists all references in the order they appear in the introductory and discussion chapters.

Several ethics applications (approved) were put in place at the University of Alberta for the research projects I was involved in during the time of the PhD program:

1) MRI Biomarkers in ALS (Pro00036028)
2) Hudson Imaging Study (Pro00061945)
3) Multimodal Imaging of MND (Pro00011079)
4) Phase 4 – MRI Biomarkers in ALS (Pro00042912)
5) Post-mortem Evaluation of ALS and MND (Pro00090736)

Acknowledgements

To Dr. Sanjay Kalra, I owe my sincerest and deepest gratitude for the supervision and mentorship during my time in your research laboratory. You provided me with the best training environment a student can ask for. I have learned so much from you that will have a lasting impact in my future career as a neuroscientist, and I am eager to start on that journey. Your passion for caring for patients with ALS is unrelenting and I hope to one day serve my patients the same way.

To my supervisory committee members, Dr. Herb Yang, Dr. Christian Beaulieu, and Dr. Sumit Das, I thank you for your guidance and support. Your questions and our discussions have taught me to thinking critically, to always present data and results in the most accurate and transparent manner, and have inspired me to work outside my comfort zone. Never did I think that I would one day use computing science techniques, learn about ways to study the inner-wirings of the brain, or that I would be learning neuroanatomy in a neuropathology laboratory. I am grateful for the opportunities you have afforded me.

To the members of Dr. Kalra's laboratory, my experience of working with you, learning from you, and teaching some of you has been a highlight of my research training. From research coordinators to graduate students to volunteers – to attempt to name all would be futile – I appreciate you all greatly. I am thankful for the long-lasting friendships we created, and I look forward to working with you again in the future.

To the unsung heroes of this dissertation, the research participants and their families. This work, and work from Dr. Kalra's laboratory, would simply not be possible without your support and investment of your time. Words cannot describe how thankful I am that because of people

like you, I was able to do research at a high-level. I only hope that my work offers some justification for your time and energy. Thank you for believing in our research.

I would like to offer a special thanks and recognition to ALS Canada. Their support for my research has propelled me to places I never thought I could achieve. Dr. David Taylor, the passion with which you tirelessly work towards finding a cure for ALS has been inspiring. The Annual ALS Canada Forum was an exciting venue for me to network and place my research in the bigger picture. I would also like to thank my table tennis partner and co-champion, Kristiana Salmon. We had a fun run!

This work was made possible thanks to operating grants from the Canadian Institutes of Health Research, ALS Association, ALS Society of Canada, Brain Canada, Shelly Mrkonjic Research Fund, Queen Elizabeth II Graduate Scholarship (Master's), Alberta Graduate Student Scholarship, H Jean McDiarmaid Scholarship, Dr. Eli and Charlotte Wershof Scholarship, Queen Elizabeth II Graduate Scholarship (Doctoral), ALS Canada-Brain Canada Doctoral Trainee Award, Alberta Innovates MD-PhD Studentship, and Faculty of Medicine and Dentistry Dean's Doctoral Award.

And lastly, to my family and friends, I would not have been able to get through the rigours of my training without your support. To Raheel Syed, thank you for always encouraging and believing in me at times when others and even myself could not. The friendship we have built over my time in Edmonton is one for the books. Your support has not gone unacknowledged.

Table of Contents

List of Tables

List of Figures

Chapter 1

Chapter 2

images were acquired at 1 x 1.5 x 1 mm3. Study 3 and 4 were pooled together because their images were acquired at 1 x 1 x 1 mm3. The graph on the top shows autocorrelation values from regions where it was significantly decreased in patients on whole-brain analysis. The regions included the motor cortex, insula, hippocampus, and subcortical frontal white matter. The graph below shows autocorrelation values from regions where it was significantly increased in patients on whole-brain analysis. The regions included only the corticospinal tract. The raw data presented here is not corrected for age and gender and is segregated by the study.

Supplementary Figure 2 Significant differences in autocorrelation between patients and controls ($p < 0.001$, cluster size > 10) in separate studies at different resolutions. Study 1 images were acquired at 1 x 1 x 1.5 mm3 and Study 2 images were acquired at 1 x 1.5 x 1 mm3. Study 3 and 4 were pooled together because their images were acquired at 1 x 1 x 1 mm3. Areas in red are regions where autocorrelation was significantly decreased in patients and areas in blue are regions where autocorrelation was significantly increased in patients.

Chapter 4

Figure 1 Correlations were observed between DTI metrics of the CST and the texture features autocorrelation, energy, and inverse difference normalized in the primary cohort. AD = axial diffusivity, RD = radial diffusivity, FA = fractional anisotropy, FDR = false discovery rate correction

Figure 6 Differences in textures from T1W images within the CST between patients and controls in the independent cohort overlaid on a sample T1W image. FDR = false discovery rate correction, L = left, R = right

Figure 7 Representative 3D texture map for *autocorrelation* (top row) and the corresponding T1W image (bottom row) from a control (left) and a patient (right) in the independent cohort. In the control participant, the CST is homogenously hypointense on an *autocorrelation* map. In a patient, however, the CST appears to be more heterogenous with hyperintense areas in the centrum semiovale and in posterior limb of the internal capsule. The T1W image, in comparison to the texture map, shows no overt differences between the control and patient.

Figure E1 Flow chart depicting a summary of the analytical steps involved in texture analysis. Steps: 1) 22 textures were calculated, 2) redundant textures were removed, 3) white matter-sensitive textures were identified by correlating the unique textures to DTI metrics, 4) white matter-sensitive textures were used for voxel-wise analysis in both the primary and the independent cohorts, 5) texture values from the primary cohort were used to generate a binary regression model, and 6) used to evaluate the diagnostic performance of the white matter-sensitive textures in both cohorts.

Figure E2 Gray (top) and white (bottom) matter VBM analyses for participants in the primary cohort. Significant differences at $p < 0.001$ with a cluster size threshold of 20 or more voxels were found. The results did not survive multiple comparison correction with FDR. VBM results are overlaid on a

autocorrelation decreased in the posterior corpus callosum and increased in the left internal capsule. (C) In fast progressing ALS, autocorrelation decreased in the posterior corpus callosum and left insular cortex. Autocorrelation was not increased in this subgroup. The color bars show the range of T-values.

Figure 4 Texture differences between ALS compared to controls at T_0 (A) and T_{max} (B). In panels (A) and (B), regions in red indicate areas of significantly ($P < 0.0005$, cluster size > 50) altered autocorrelation in ALS patients compared to controls. The color bars show the range of F-values. Images on the right show a merged glass-brain representation of the differences in ALS patients at T_0 and T_{max}. Regions in blue indicate significant clusters present only at T_0, regions in purple indicate significant overlapping clusters present at T_0 and T_{max}, and regions in red indicate significant clusters present only at T_{max}.

Figure 5 Texture differences in controls, ALS, and ALS subgroups between various timepoints in (A) the posterior limb of the internal capsule (PLIC) and (B) the precentral gyrus regions of interests. Data is represented as the mean ± 95% confidence interval at each point. The numbers inside in the bars in (A) represent the sample sizes of each group in the respective analyses.

Figure 6 Cerebral associations between texture and clinical measures in ALS patients. Regions in yellow indicate areas of significant ($P < 0.0005$, cluster size > 50) positive correlations between autocorrelation and (A) ALSFRS-

Abbreviations

ALS	amyotrophic lateral sclerosis
FTD	frontotemporal dementia
MRI	magnetic resonance imaging
UMN	upper motor neuron
LMN	lower motor neuron
MND	motor neuron disease
TDP-43	transactive response DNA-binding protein 43
SOD1	amyotrophic lateral sclerosis functional rating scale-revised
TARDBP	transactive response DNA-binding protein
FUS	fused in sarcoma
C9ORF72	chromosome 9 open reading frame 72
BMAA	β-*N*-methylamino-L-alanine
CSF	cerebrospinal fluid
EAAT2	excitatory amino acid transporter-2
MRS	magnetic resonance spectroscopy
PET	positron emission tomography
hnRNP	heterogenous ribonucleoprotein

NFL	low molecular weight neurofilament
DPR	dipeptide-repeat
p-UMN	predominant UMN
EMG	electromyography
fMRI	functional MRI
PLS	primary lateral sclerosis
PMA	progressive muscular atrophy
ECAS	Edinburg cognitive and behavioural screen
ALSFRS-R	ALS functional rating scale-revised
FVC	forced vital capacity
NAA	*N*-acetylaspartate
PEG	percutaneous endoscopic gastronomy
NIV	non-invasive ventilation
CPAP	continuous positive airway pressure
BiPAP	bilevel positive airway pressure
H&E	hematoxylin and eosin
LFB	Luxol fast blue
GFAP	glial fibrillary acidic protein
DTI	diffusion tensor imaging

3D	three-dimensional
ROI	region of interest
VBM	voxel-based morphometry
FA	fractional anisotropy
MD	mean diffusivity
NAA	*N*-acetylaspartate
Cr	creatinine
Cho	choline
mI	myo-inositol
Glu	glutamate
GABA	gamma aminobutyric acid
BOLD	blood oxygenation level-dependent
DMN	default mode network
GLCM	gray-level co-occurrence matrix
MCI	mild cognitive impairment
CALSNIC	Canadian ALS Neuroimaging Consortium

Chapter 1 Amyotrophic Lateral Sclerosis

French neurologist Jean-Martin Charcot coined the term *"sclérose latérale amyotrophique"* (amyotrophic lateral sclerosis) in the 1860s and 1870s in a series of clinical-pathological correlation studies.[1] Charcot noted that some of his patients exhibited signs of muscle atrophy and spasticity. At autopsy, he observed atrophy of the cranial and spinal nerve roots and degeneration of the lateral spinal cord columns in these patients. By viewing the patients' clinical presentation in light of their post-mortem findings, he associated muscular atrophy (amyotrophy) to pathology in the cranial and spinal nerves and spasticity to sclerosis in the lateral columns of the spinal cord (lateral sclerosis). Although the division of the motor system into upper and lower motor neurons (UMN and LMN) had not yet been made in the literature, Charcot effectively recognized ALS as a disease of UMN (spasticity) and concomitant LMN (muscle atrophy) dysfunction.[1]

The contemporary understanding of ALS has greatly evolved since its initial characterization as a motor neuron disease (MND). Approximately 15% of ALS patients present with clinical FTD and upwards of 40% of patients have signs of cognitive impairment on detailed examination.[2] The disease is thought to be stochastic and focal at onset and its clinical progression is underscored by progressive involvement of contiguous body regions.[3] Pathologically, ALS is defined as a transactive response DNA-binding protein 43 (TDP-43) proteinopathy in an overwhelming majority of its cases.[4, 5] Several genetic causes have now been identified including mutations in superoxide dismutase 1 (*SOD1*), transactive response DNA-binding protein (*TARDBP*), fused in sarcoma (*FUS*), and chromosome 9 open reading frame 72

(*C9ORF72*) genes.[6] In this introductory chapter, an overview of ALS pertaining to its epidemiology, pathophysiology, and clinical presentation and management will be provided.

Epidemiology

The annual incidence rates of ALS in adults from high-quality, prospective European population-based registries are established between 2 – 3/100,000 person years.[7, 8] Canadian population-based studies have reported rates between 1.6 – 2.4/100,000 person years.[9] Substantially higher rates are reported from certain parts of the world, such as the Faroe Islands, which may represent a genetic founder effect and homogenous populations.[10, 11] The incidence of ALS is higher in males than in females by a factor of 1.1 – 1.5, and it is primarily driven by a higher incidence of spinal onset ALS in males.[7, 8] Across the globe, the mean age of onset for ALS is around 62 years, however, disparities exist between studies due to true variations or differences in study design.[10] For example, in a clinic-based prospective cohort study from China, the mean age of symptom onset was 50 years.[12] Incident rates increase with age irrespective of gender and reach their peak between the sixth and seventh decade of life.[8, 10] To put this in perspective, the incidence rates of Parkinson's disease, which is the second most common neurodegenerative disorder, are between 8 – 18/100,000 person years.[13] The prevalence rates of ALS range between 4 – 8/100,000 person years depending on the study.[10]

Recent studies suggest that ancestral origin may play a role in the non-uniform world-wide distribution of ALS. Genetic factors, such as the founder effect, may influence disease phenotype at the population-level and increase incidence rates in genetically isolated or homogenous populations. This is evident in the Sardinian and Finnish populations where founder mutations in the *TARDBP* and the *C9ORF72* genes, respectively, are responsible for one-third of all ALS cases and increased rates of comorbid clinical FTD.[14-16] In Cuba, persons with equal

parts European and African ancestral backgrounds had lower rates of mortality from ALS than did persons of primarily either European or African ancestries.[17] In the United States, self-reported ethnic minorities had lower risks of ALS and ALS-linked mortality than white participants, even after adjusting for socioeconomic status and type of health insurance, suggesting a true race-based difference in the risk of ALS.[18] These studies point towards underlying genetic or environmental risk factors for ALS that may be prevalent in certain populations.

Etiology and pathophysiology

Genetic causes

The first causative factor for ALS was identified with the discovery of mutations in *SOD1* in individuals with a family history of ALS (familial ALS).[19] It has since become evident that even in sporadic cases, genetic variations are present in the established genes known to cause familial ALS.[20] Studies have proposed an oligogenic etiology of ALS with mutations in two or more established genes in certain cases.[21] Furthermore, ALS is increasingly recognized as a disease with complex underlying genetics associated with a polygenic rare variant architecture that governs its onset and phenotypic variability.[22] Notwithstanding, there are several key genes implicated in the genetic etiology of ALS that account for half of all familial cases and 5% of sporadic cases.[20] These include mutations in *SOD1*,[19] *TARDBP*,[23] *FUS*,[24, 25] and *C9ORF72*[14, 26] genes.

SOD1. Most mutations in *SOD1* in ALS follow an autosomal dominant pattern of inheritance;[19] however, a recessive form also exists in Scandinavian populations.[27] Mutant *SOD1* is found in almost 20% of familial and 1% of sporadic ALS cases.[20] Higher rates of *SOD1*

mutations are observed in Asian countries compared to European countries. Considerable phenotypic variability exists between different types of *SOD1* mutations. The A4V mutation, which is a missense mutation on codon 4, causes an aggressive form of the disease with limited UMN involvement and leads to death typically within a year of symptom onset.[28] In contrast, the D90A mutation is associated with particularly prominent UMN involvement and survival close to 10 years.[27] *SOD1* mutations are not known to cause cognitive or behavioural impairments in ALS.

TARDBP. Pathological TDP-43 was discovered to be a major component of the hallmark ubiquitin-positive neuronal inclusions in a majority of ALS and FTD cases.[4, 5] These findings led to the discovery of mutations in the *TARDBP* gene, which encodes for TDP-43, that follow an autosomal dominant inheritance pattern in familial ALS.[23] Despite the high prevalence of TDP-43-positive inclusions in ALS, mutations in the *TARDBP* gene account for less than 5% of familial and 1% of sporadic cases.[20] Phenotypically, mutations in *TARDBP* are associated with increased rates of bulbar and cognitive involvement compared to *SOD1* mutations.[29]

FUS. *FUS* mutations, similar to *TARDBP* mutations, occur in less than 5% of familial and 1% of sporadic cases of ALS.[20] FUS is also functionally similar to TDP-43 in that it regulates RNA metabolism.[24, 25] The discovery of mutations in *FUS* further highlighted the role of altered RNA metabolism and processing in the pathogenesis of ALS.[30] Neuropathological findings of ALS with *FUS* mutations are positive for FUS cytoplasmic inclusions, but they lack the hallmark TDP-43-positive inclusions.[31] *FUS* mutations typically cause an aggressive form of ALS with a younger age of onset and shorter survival.[29]

C9ORF72. Genetic linkage studies[32, 33] and subsequent large-scale genome-wide association studies[15, 34] identified a gene on chromosome 9p21 that was mutated in sporadic and

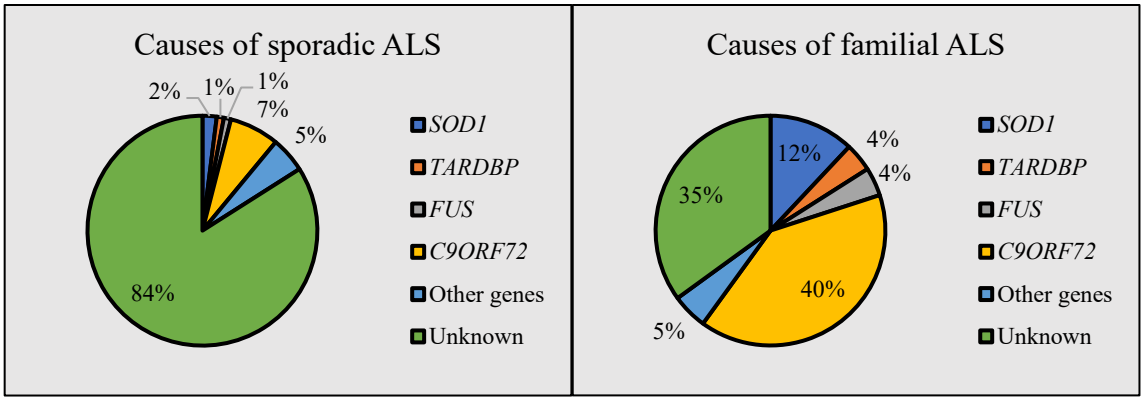

Figure 1: Genes known to carry causative ALS mutations. Values represent percentages of ALS explain by each gene in European populations. Taken from Renton AE, Chiò A, Traynor BJ. State of play in amyotrophic lateral sclerosis genetics. Nature neuroscience. 2014 Jan;17(1):17.

familial cases of ALS and FTD. This mutation was later identified as a pathogenic repeat expansion of the hexanucleotide GGGGCC in the non-coding region of *C9ORF72*.[26] This gene defect accounts for upwards of 40% of familial and almost 10% of sporadic ALS cases in certain European populations.[35] Additionally, the mutant *C9ORF72* repeat expansion also genetically links ALS and FTD with more than 50% of familial and almost 20% of sporadic ALS-FTD cases carrying the pathogenic mutation.[36] The pathogenic hexanucleotide expansion in *C9ORF72* follows an autosomal dominant inheritance pattern and is thought to drive neurodegeneration through toxic gain of function mechanisms.[37] Population-based studies suggest that ALS with the *C9ORF72* mutation exhibits a phenotype characterized by younger age of onset, presence of cognitive and behavioural impairment, and reduced survival.[38]

Despite these advances in our understanding of the genetic causes of ALS, the etiology of more than 80% of sporadic cases, which constitute 95% of all ALS cases,[39] is not known (Figure 1). There is, however, a likely misclassification of some true familial ALS cases as sporadic due to factors such as low disease penetrance, small family sizes, and misdiagnosis.[40] Furthermore, as ALS continues to be regarded as a member of a disease spectrum rather than a singular entity,

the definition of familial ALS must also evolve to include related disorders such as FTD and other MNDs.

Environmental risk factors

External exposures have been studied as potential risk factors for ALS based on clinical observations and anecdotal lines of evidence. It has been reported that individuals who develop ALS have a lower body mass index and a greater proclivity to have participated in varsity-level sports prior to disease onset.[41, 42] This feature is not observed in individuals who develop other neurological disorders. Further support is provided by studies that demonstrate a negative association between pre-diagnostic body fat and ALS mortality.[43] Studies have not, however, found a dose-response relationship between levels of physical activity and risk of ALS.[44] Instead, ALS patients had increased levels of leisure time physical activity than controls. These findings point to an increased risk of ALS associated with genetic predispositions or lifestyles that promote physical activity rather than with levels of physical activity. However, this has not yet been replicated in other studies.[45]

Evidence-based analysis suggests that smoking can be considered an establish risk factor for sporadic ALS.[46] Prospective population-based studies also provide evidence for a dose-response relationship between the number of years spent smoking with the risk of ALS.[47] Interestingly, the association between smoking and increased risk of ALS is largely found in females.[48] This suggests that lifestyle risk factors may interact with biological factors to establish the final risk of ALS.

Exposure to chemicals and heavy metals have also been investigated as risk factors for ALS. Studies have suggested exposure to lead and pesticides leads to increased risk of ALS.[49, 50]

Environmental exposure to a neurotoxin called β-*N*-methylamino-L-alanine (BMAA) has also been studied as a potential risk factor for ALS.[51] Studies have linked dietary exposure to BMAA in certain clusters of ALS patients in Europe.[52] Initial evidence for the risk of ALS from BMAA exposure was based on the high incidence rates of a rare ALS variant in Guam where there were high levels of dietary BMAA.[53] However, definitive epidemiological evidence to establish a risk of ALS due to BMAA consumption is currently lacking.

A gene-time-environment model of neurodegeneration has been proposed for ALS.[54] The model speculates that the genetic burden for the risk of ALS is established at birth and its onset is mitigated by interactions between time (age) and lifetime exposure to environmental factors. Within the model, it is possible that certain genetic profiles are sensitive to particular environmental exposures.[54] However, more studies are needed to further elucidate these relationships.

Pathophysiology

The pathophysiology of ALS is complex and closely linked to causative and risk-conferring genetic variations.[55] With the discovery of mutations in *TARDBP*, *FUS*, and *C9ORF72* genes, however, it is clear that certain mechanisms, such as aberrant RNA biology, transect multiple pathogenic pathways and play a central role in the overall disease. Regardless of the underlying mechanisms, the end result in the pathogenesis of ALS is the degeneration of motor neurons and disruption of extra-motor neural networks.[56] The mechanisms that confer a selective vulnerability to pyramidal motor neurons and disease-resistance to ocular motor neurons are the subject of investigation.[57] One hypothesis explaining this phenomenon is that ALS is a disease of the neocortex with subsequent susceptibility to descending corticofugal pathways.[58, 59] Nevertheless, findings from basic studies have contributed to the understanding of

the cellular biology of ALS. Several major themes in the pathophysiology of ALS have emerged that will be reviewed here.

Glutamate excitotoxicity. A well-established and one of the earliest proposed mechanisms underlying ALS is glutamate excitotoxicity. Glutamate is the primary excitatory neurotransmitter in the central nervous system, and its altered metabolism has widespread implications in neurodegeneration.[60] Glutamate-mediated excitotoxicity in ALS occurs when abnormally high levels of glutamate in the synapse induce repetitive neuronal firing causing an excessive influx of calcium leading to neuronal death.[61] Initial *in vivo* evidence for this mechanism in ALS came from a study measuring excitatory neurotransmitter levels from the cerebrospinal fluid (CSF) in patients.[62] Patients were found to have an almost threefold increase in the CSF concentration of glutamate compared to controls. This finding was replicated in a larger study of almost 400 ALS patients that also showed higher CSF glutamate concentrations compared to controls and patients with other neurological disorders.[63] *In vivo* measurements of glutamate and glutamine (an important precursor for glutamate) with magnetic resonance spectroscopy (MRS) also show elevated levels in motor regions in the brain.[64, 65] These measures correlate with decreased motor function and clinical UMN dysfunction.

Astrocytes, which are a type of glial cells, play an important regulatory role by their uptake of excess glutamate from the synaptic cleft via the excitatory amino acid transporter-2 (EAAT2) to prevent repetitive firing of the postsynaptic neuron.[61] EAAT2 protein levels are markedly reduced in post-mortem motor cortex and spinal cord tissue from ALS patients.[66] Decreased levels of EAAT2 in mice causes elevated extracellular glutamate levels and neuron death.[67] Furthermore, in the *SOD1*^{G93A} transgenic mouse model, reduction of EAAT2 expression occurs pre-symptomatically[68] and its overexpression can delay the onset of motor symptoms.[69]

These studies suggest that glutamate excitotoxicity in ALS is mediated by dysfunctional or loss of EAAT2 from astrocytes.

Non-cell autonomous mechanisms. The important role of glial cells is highlighted in the pathogenesis of ALS by studies of microglia, which mediate neuroinflammatory responses, and oligodendrocytes, which are responsible for myelinating axons in the central nervous system. In an ALS mouse model, it was demonstrated that by selectively silencing a mutant *SOD1* gene in microglia, survival is increased.[70] This was further corroborated by another study that showed prolonged disease duration and survival in *SOD1* mutant mice that received microglia from wild-type mice.[71] In humans, post-mortem evidence of activated microglia is associated with clinical symptoms of UMN dysfunction[72] and executive function impairments.[73] Furthermore, a study using positron emission tomography (PET) imaging showed first *in vivo* evidence of widespread cerebral microglial activation in patients with ALS.[74] Increased microglia activation in the motor cortex was also linked to increased clinical UMN burden. These studies suggest that microglia are a major contributor to disease progression and are potential targets for future therapies.[75]

Oligodendrocytes are vital glial cells that provide structural and functional support to neurons. Oligodendrocytes metabolically support axons by supplying them with lactate, which is an essential metabolic substrate for axons, through monocarboxylate transporter 1 (MCT1).[76] In patients with ALS, MCT1 expression in the motor cortex is reduced by more than 50%.[76] Furthermore, patches of demyelination are observed in the motor cortex and in the anterior horn gray matter in the spinal cord of ALS patients that is further suggestive of oligodendrocyte dysfunction.[77] Oligodendrocyte dysfunction is considered an early event in the pathogenesis of ALS as morphological changes occur prior to disease onset in mouse models.[77, 78] Furthermore, selectively removing mutant SOD1 from oligodendrocytes delays disease onset and prolongs

survival.[77] Knocking down SOD1 from oligodendrocytes in sporadic and familial cases of ALS also greatly improves survival of motor neurons. This finding is not observed in cases of *C9ORF72* mutations, which highlights the importance of patient subgroups in trials involving targeted oligodendrocyte therapies.[79]

Dysfunctional protein homeostasis. Several lines of evidence suggest that ALS is a disease involving aberrant protein homeostasis. From a neuropathological view, the disease is hallmarked by abnormal cytoplasmic protein aggregates in neuronal and glial cells in the central nervous system.[80] These aggregates are immunoreactive for ubiquitin[81] and ubiquitin-binding protein p62.[82] Ubiquitin and p62 are key players in the cellular ubiquitin-proteasome system that is responsible for the selective degradation of misfolded, damaged, or otherwise abnormal proteins in all eukaryotic cells.[83] Their presence in proteinaceous aggregates signals a failure of cellular protein turnover that can be a cause or a result in neurodegenerative diseases.[84] TDP-43, which is localized primarily in the nucleus under normal conditions, is the main component of ubiquitinated cytoplasmic inclusions in ALS.[4, 5] The ubiquitination of mislocalized TDP-43 is thought to be a late event that overburdens the ubiquitin-proteasome system leading to a dysfunction of protein degradation pathways.[85] Several mutations in sequestosome 1[86] and ubiquilin 2[87] genes have also been identified in cases of sporadic and familial ALS that further suggest the involvement of aberrant protein degradation pathways in the pathogenesis of ALS. Additionally, though the function of the C9ORF72 protein in humans is still poorly understood, it has recently been shown to be involved in the regulation of autophagy pathways as an effector protein in experimental systems.[88, 89]

Altered RNA biology. The role of RNA biology in the pathogenesis of ALS was highlighted with the discovery of ubiquitinated TDP-43 in cytoplasmic aggregates in neurons

and glial cells in a vast majority of ALS cases.[4, 5] Soon after, mutations in the genes encoding for TDP-43 and FUS were identified as causal factors of ALS, which suggested that abnormalities in these proteins can cause neurodegeneration.[23-25] TDP-43 is a DNA/RNA binding protein that is structurally and functionally analogous to the heterogenous ribonucleoprotein (hnRNP) family of proteins.[90] It plays a role in stabilizing the mRNA of low molecular weight neurofilament (NFL) protein,[91] which also forms aggregates in ALS and is a neuropathological feature.[92] Reductions in NFL mRNA levels are observed in patients that are thought to be related to alterations in TDP-43.[91, 93, 94] Similar to TDP-43, FUS has an N-terminal RNA-recognition motif and a C-terminal region where ALS-linked mutations localize almost exclusively.[30] TDP-43 and FUS bind to thousands of RNA targets in neurons[95-97] and dysfunction in these proteins could have wide-ranging deleterious effects in normal neuronal function. Indeed, depletion of TDP-43 and FUS results in altered splicing of hundreds of pre-mRNAs, some of which are implicated in ALS and FTD. Mutations in these RNA-binding proteins can cause motor neuron death due to aberrant RNA splicing in the absence of protein aggregation[98] and malfunctioning glial cells.[99] Conversely, toxic gain-of-function mechanisms have also been proposed as a cause for neuronal degeneration. In mice, overexpression of exogenous FUS with impaired nuclear import resulted in an ALS-like phenotype.[100] This occurred in the absence of dysfunction of endogenous nuclear FUS and indicates that mislocalization and aggregation of the protein can result in the disease phenotype. Furthermore, reduced levels of ataxin-2, which is also an RNA-binding protein associated with an increased risk of ALS,[101] in *TARDBP* transgenic mice decreases aggregation of TDP-43, increases survival, and improves motor function.[102] As such, mitigating gain-of-function mechanisms of TDP-43 in ALS might provide an effective therapeutic strategy.

Pathogenic mechanisms of the *C9ORF72* mutation. Mutations in the *C9ORF72* gene account for a majority of the known genetic causes of ALS and ALS-FTD.[6] The mutation is a repeat expansion of the hexanucleotide GGGGCC in a non-coding region of the gene.[14, 26] Healthy individuals carry less than 25 repeats of the hexanucleotide, whereas pathogenic repeats are in the order of 50 or more repeats.[14, 26, 103] Though the normal function of the C9ORF72 protein in humans is not yet fully understood, three main pathological mechanisms of mutant C9ORF72 have been studied in the context of ALS-FTD: loss of function, gain of toxic functions, and faulty nucleocytoplasmic transport. Mice with *C9ORF72* knockdown do not undergo motor neuron degeneration or show evidence of classic ALS pathological features.[104] Additionally, reduced *C9ORF72* RNA levels in mice do not cause motor or behavioural deficits reminiscent of ALS-FTD.[105] These findings raise the possibility that defects in *C9ORF72* mediate pathology through gain of toxic function mechanisms rather than loss of functions. GGGGCC RNA repeats are known to accumulate in the nucleus of cells of the central nervous system in carriers of *C9ORF72* mutations.[26, 105] These RNA foci sequester RNA-binding proteins, such as those from the hnRNP family, in many neurodegenerative disorders and cause alterations RNA splicing.[106] In ALS-FTD, hnRNP A3 binds to the GGGGCC repeats and is thought to disrupt *C9ORF72* pre-mRNA transport between the nucleus and cytoplasm.[107] This implies a toxic gain of function mechanism whereby expanded repeats reduce levels of proteins vital to RNA metabolism in neuronal cells. Recent lines of converging evidence also suggest that aberrant nucleocytoplasmic trafficking is the final pathway in *C9ORF72* mutations. Evidence from flies,[108, 109] mice,[110] yeast,[111] and human induced pluripotent stem cells[108, 109] models demonstrate that GGGGCC repeats interact and sequester proteins directly involved

nucleocytoplasmic transport. Moreover, rescuing levels of the affected proteins ameliorates neuronal toxicity, therefore, providing a possible therapeutic approach.

It is clear that the pathogenesis of ALS is multifaceted involving various genetic influences, cellular pathways, and environmental variables. The culmination of the pathogenic mechanisms is the degeneration of UMNs, primarily the corticospinal and corticobulbar tracts, and LMNs in disease-specific cranial nerve nuclei and in the anterior horn of the spinal cord. The disease is believed to propagate in the brain through axonal pathways via "prion-like" mechanisms, a feature common to several neurodegenerative diseases.[112] These biological complexities result in vast clinical phenotypic heterogeneity with respect to the degree of UMN versus LMN involvement, cognitive and behavioural dysfunction, and neuropathological findings.

Clinical presentation and management

Motor symptoms at presentation

Onset based on body region. Approximately two-thirds of all patients present with limb onset ALS. The most common presenting symptom is progressive muscle weakness in an arm or leg.[113] This can be associated with fasciculations and muscle cramps in the affected limb at onset.[113] There is a relative concordance between handedness and the laterality of the site of onset in the arms.[114] In ALS with onset in the upper limbs, 64% patients report first symptoms in their dominant limb. Bulbar onset ALS is evident in about 30% of all patients where weakness or dysfunction begins in the muscles required for speech articulation, mastication, or swallowing.[7] These patients present with symptoms of dysarthria (for example, slurred speech and hoarse

voice) and dysphagia (for example, difficulties with chewing and swallowing). Less than 5% of incident ALS cases have a respiratory onset that is characterized by shortness of breath.[7]

Site of symptom onset is influenced by genetic factors. Patients with *SOD1* mutations rarely present with bulbar onset ALS,[115, 116] whereas patients with *C9ORF72* mutations have the highest rates of bulbar onset ALS.[117] *TARDBP* and *SOD1* mutations have near identical limb to bulbar onset ALS ratios; however, *TARDBP* mutations are associated with symptom onset in the upper limbs, whereas the SOD1 mutations are associated with symptom onset in the lower limbs.[29, 118] Patients with *FUS* mutations have varied sites of onset consistent with sporadic ALS.[29] These observations are in contrast with the hypothesis that the site of symptom onset is a stochastic process in ALS.[3]

Motor neuron level involvement in ALS. In humans, a majority of the UMNs originate from the primary motor cortex (precentral gyrus) and the premotor areas in the cortex and their projecting axons form the descending corticospinal and corticobulbar tracts (Figure 2). Other fibers originate from the parietal areas including the sensory cortex. Corticospinal tracts decussate in the lower medulla and provide input to alpha motor neurons in the anterior horn of the spinal cord. Corticobulbar tracts project to the cranial nerve motor nuclei in the brainstem. LMNs cell bodies are located in the brainstem and anterior horn of the spinal cord and their axons directly innervate muscle fibers (Figure 2). In the brainstem, LMNs send out their axons via cranial nerves, whereas in the spinal cord, LMNs called alpha motor neurons send out their axons via the spinal nerves. Diagnosis of ALS requires the presence of signs of both UMN and LMN degeneration.[119] UMN signs include hyperreflexia, spasticity, and loss of dexterity and LMN signs include hyporeflexia, muscle hypotonia, muscle atrophy, and fasciculations. Around 20% of ALS patients present with a predominant UMN (p-UMN) phenotype.[120] p-UMN ALS is

clinically characterized by severe UMN signs such as spastic paraparesis, spastic dysarthria, and the presence of pathological reflexes such as the Babinski and Hoffmann signs.[121] Evidence of mild LMN signs typically begins in the distal upper limbs and later progress to involve proximal upper limbs, whereas LMN signs in the lower limbs are evident only in the later stages of the disease.[120] Conversely, a subgroup of less than 20% of ALS patients presents with progressive LMN signs of weakness and muscle atrophy restricted to either upper or lower limbs for at least

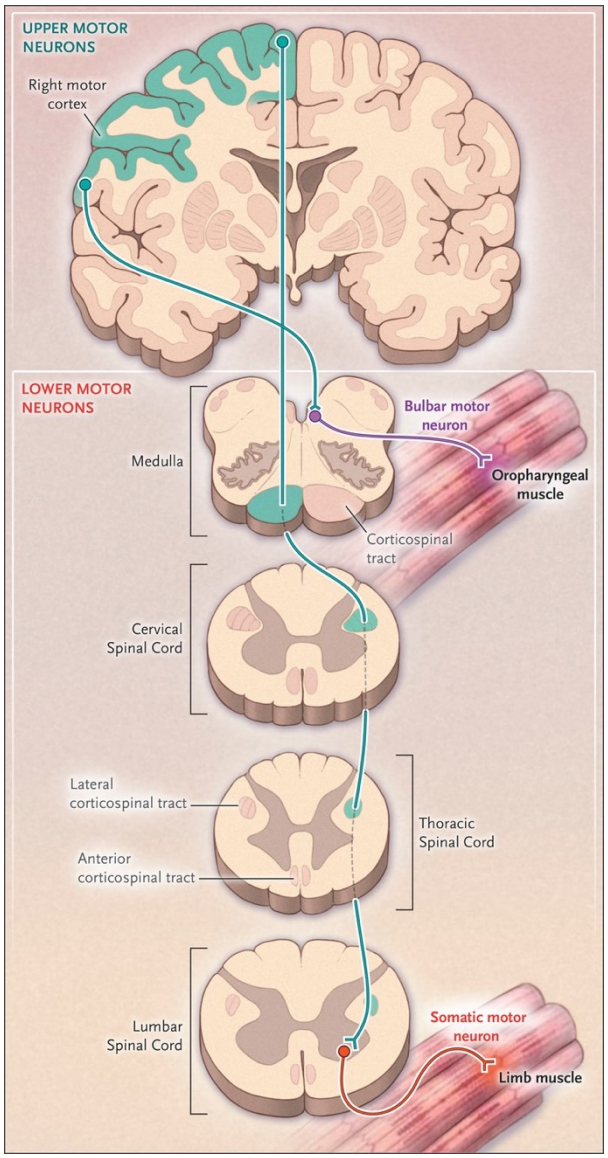

Figure 2: Anatomy of the upper and lower motor neurons in the central nervous system. Taken from Brown RH, Al-Chalabi A. Amyotrophic lateral sclerosis. New England Journal of Medicine. 2017 Jul 13;377(2):162-72.

12 months.[7, 122] These variants are termed flail arm and leg syndromes, respectively, and predominantly involve proximal muscles of the upper limbs and distal muscles of lower limbs. Patients with LMN variants may exhibit hyperreflexia, but do not develop hypertonia in the affected limbs over the course of their disease.[122]

SOD1 mutations generally confer an LMN-dominant disease, whereas *TARDBP* mutations result in equal involvement of UMN and LMN dysfunction.[29] ALS patients who carry

C9ORF72 mutations display UMN and LMN dysfunctions similar to the typical characterization of ALS.[117]

Diagnostic criteria, classification, and staging

The clinical motor presentation of ALS, as briefly outlined above, is widely heterogenic. This variability has implications for research study designs because clinical features of the disease are known to impact patient outcomes. Though the diagnosis of ALS in clinical practice is relatively clear in the presence of progressive signs of UMN and LMN degeneration, efforts are being made to further stratify the disease.[123] The original El Escorial criteria was developed in 1994 to stratify patients by diagnostic certainty to aid enrollment in clinical trials.[124] According to the criteria, diagnostic certainty was defined by the extent of topographical distribution of UMN and LMN signs along four body regions: bulbar, cervical, thoracic, and lumbosacral. Diagnostic certainty was classified as suspected ALS, possible ALS, probable ALS, and definite ALS based on the number of body regions demonstrating motor neuron dysfunction on clinical evaluation.[124] These criteria were revised to improve their diagnostic sensitivity.[119] The revision removed "suspected ALS" and added "laboratory-supported probable ALS" as a category. The latter was assigned to cases of possible ALS with documented LMN dysfunction on electromyography (EMG) studies (Table 1).

The revised El Escorial criteria have remained the mainstay for defining the inclusion criteria for research studies and clinical trials because of their standardized nature.[125, 126] These criteria do, however, have several weaknesses. Firstly, they do not address the heterogeneity in the patient population; for example, there is no distinction between UMN and LMN dominant disease, or between limb and bulbar onset ALS. As such, the levels of diagnostic certainty are poor prognostic indicators, with the exception of cases of definite ALS that demonstrate worse

survival in some studies.[127] Secondly, cognitive dysfunction, which impacts around 50% of ALS patients,[128] is not considered in these criteria. Though the presence or absence of cognitive dysfunction may not alter the formal diagnosis of ALS, it may have implications for patient stratification in clinical trials to optimize efficacy of novel therapeutics. Clinically, there also remains an average delay of one year from the onset of symptoms to diagnosis.[129] The Awaji criteria for the diagnosis of ALS were proposed in 2008 in an attempt to mitigate to the delay in diagnosis and improve diagnostic sensitivity.[130] These criteria advocate for the use of EMG in the diagnostic workup and equate electrophysiological evidence of LMN dysfunction to clinical findings of LMN involvement. Prospective studies have suggested that the Awaji criteria have higher diagnostic sensitivity than the El Escorial criteria and can potentially improve enrollment in clinical trials.[131, 132]

Table 1: Revised El Escorial criteria for ALS.

Possible ALS	Laboratory-supported probable ALS	Probable ALS	Definite ALS
• UMN and LMN signs in only one region, or • UMN signs alone in two or more regions	• UMN and LMN signs in only one region, or • UMN signs alone in one region and • Electrophysiological evidence of LMN signs in at least two regions	• UMN and LMN signs in at least two regions	• UMN and LMN signs in three regions

Staging systems have been proposed to quantify clinical disease progression. The King's Clinical Staging System categorizes clinical milestones in the natural history of the disease into distinct stages (Table 2).[133] The first three stages correspond to the incremental functional involvement of the four regions used in the El Escorial criteria and the last stage characterizes the need for intervention (gastrotomy or non-invasive ventilation). Contrary to the El Escorial criteria, however, involvement of a body region is marked by neurogenic weakness in that region

and not by the presence of signs of both UMN and LMN dysfunction. This staging system has predictable intra- and inter-stage transition times that make it suitable for use in clinical trials as an objective marker for disease progression.[133, 134] Furthermore, recent studies show that cognitive and behavioural deficits increase with later disease stages in ALS.[135] This suggests that cognitive and behavioural impairments should be an integral part of future staging systems.

Table 2: King's staging system for ALS.

Stage 1	Stage 2A	Stage 2B	Stage 3	Stage 4A	Stage 4B
• Symptom onset in one region	• Diagnosis	• Involvement of second region	• Involvement of third region	• Need for gastronomy	• Need for respiratory support

Spectrums of amyotrophic lateral sclerosis

MND spectrum. As previously described, patients with ALS present with variable involvement of UMN and LMN dysfunction. At the extremes of the UMN and LMN continuum are primary lateral sclerosis (PLS) and progressive muscular atrophy (PMA). PLS is an adult-onset MND that is characterized by the presence of only UMN findings on clinical exam; on the other end, PMA is characterized by the presence of only LMN findings (Figure 3).[136] These extreme MND entities are rare and constitute to less than 10% of all cases.[7]

PLS typically presents in the fifth decade of life as slow progressing leg spasticity and weakness and spastic weakness of the bulbar muscles.[137] Patients report stiffness and poor coordination as initial symptoms that is reflective of UMN dysfunction. PLS progresses slowly over time and reports indicate patients' survival can extend beyond 10 years, which is markedly longer than in patients with ALS.[138] A diagnosis of PLS can only be made after four years of restricted clinical UMN involvement as some patients who initially present with UMN dysfunction develop signs of LMN dysfunction between 3 – 4 years after symptom onset;[139]

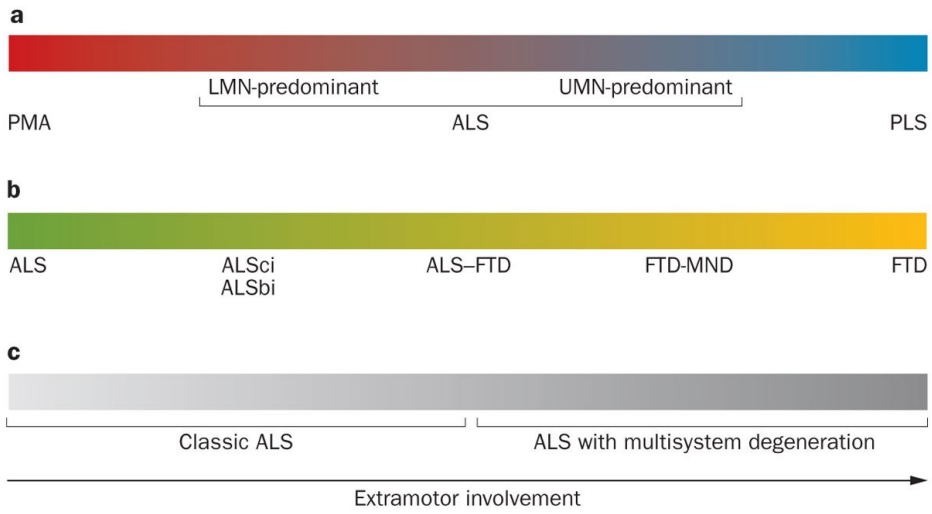

Figure 3: Spectrums of motor and extra-motor features in ALS. ALSbi = ALS with behavioural impairment; ALSci = ALS with cognitive impairment; PMA = primary muscular atrophy; PLS = primary lateral sclerosis; FTD = frontotemporal dementia. Taken from Swinnen B, Robberecht W. The phenotypic variability of amyotrophic lateral sclerosis. Nature Reviews Neurology. 2014 Nov;10(11):661-70.

however, some patients do develop LMN disease after four years.[140] Reports at autopsy, albeit few, also show that a remarkable number of PLS patients have neuropathological evidence of LMN disease.[140] These findings suggest that PLS is on the same disease spectrum as ALS with subclinical or very late LMN involvement.

PMA is clinically diagnosed in the presence of LMN signs and symptoms in the absence of UMN dysfunction. A subset of patients can, however, develop UMN signs within two years of diagnosis.[141] Furthermore, neuroimaging studies have provided evidence of subclinical corticospinal tract and extra-motor involvement in PMA.[142] These observations suggest that PMA is on the same disease spectrum as ALS. This hypothesis is supported by neuropathological studies that demonstrate UMN degeneration in over 50% of PMA cases.[143, 144]

The main motivation to distinguish between these variants is their differences in prognosis. On average, patients with PLS live the longest, followed by patients with PMA and then ALS. This may indicate that biologically, the burden of concomitant UMN and LMN disease leads to the poor survival in ALS and isolated UMN or LMN dysfunctions cause less

severe forms of disease. Additionally, this spectrum raises the importance of identifying homogeneous patient populations for future studies and clinical trials.

ALS-FTD spectrum. Approximately 10-15% of patients with ALS meet clinical criteria for FTD (ALS-FTD) (Figure 3).[2, 128, 145] Mutations in *C9ORF72* genetically reaffirm the ALS-FTD disease spectrum as they account for a remarkable percentage of ALS, FTD, and ALS-FTD cases.[6] A pathological link between ALS and FTD was established with the discovery of TDP-43 as the major component of the characteristic inclusions in both ALS and FTD.[4, 5] Clinically, FTD represents a range of dementias that are characterized by progressive impairments in behaviour, executive function, and language caused by frontotemporal lobar degeneration.[146] Behavioural-variant FTD is typified by behavioural disinhibition, apathy, loss of sympathy, and executive dysfunction[147] and is the most common FTD variant associated with ALS-FTD.[148] In large population-based studies, 50% of patients with ALS without clinical FTD are also found to have some degree of cognitive impairment on formal neuropsychological testing.[2, 145] Behavioral dysfunction is observed in approximately 30% of patients,[149] with apathy being the most common impairment.[150] Comorbid cognitive dysfunctions in ALS, particularly deficits in executive function, are associated with worse motor function decline and survival.[145, 151, 152] Therefore, extra-motor impairments in ALS have significant implications for patient outcomes and play an important role in the pathogenesis of the disease. Owing to the pervasiveness, heterogeneity, and clinical implications of these extra-motor findings, criteria have been developed to characterise mild cognitive and behavioural impairments in ALS without clinical dementia.[153]

Executive dysfunction is the most common cognitive impairment in ALS.[2, 128] Executive functions are responsible for mental processes involving inhibitory control, working memory,

and cognitive flexibility.[154] The most striking and consistent executive deficit in ALS is found in tests of verbal fluency.[155] Verbal fluency tasks, such as asking participants to respond with words that begin with a certain letter in a limited period of time, assess cognitive flexibility associated with frontal regions of the brain.[156] PET studies[157, 158] and functional MRI (fMRI) studies[159] have localized deficits in verbal fluency in ALS to abnormalities in the dorsolateral prefrontal cortex, premotor cortex, and medial prefrontal cortex. There is also increasing evidence of language impairment in ALS.[155] In particular, it may be at least as prevalent as executive dysfunction in non-demented patients with ALS; however, executive dysfunction accounts for almost half of the variation in language composite test scores.[160] This suggests that language impairments in ALS may be a consequence of executive dysfunction. Evidence from neuroimaging studies establishing the anatomical substrates of language impairments is currently lacking.

Social cognition deficits are also being increasingly recognized in patients with ALS. In particular, patients exhibit impairments in facial emotion recognition and Theory of Mind.[161] Theory of Mind reflects an individual's ability to infer the mental states of oneself and others and aids in the understanding of social behaviour. These impairments are associated with alterations in the long association fibers in the white matter, anterior cingulate gyrus, orbitomedial prefrontal cortex, and dorsolateral prefrontal cortex in patients with ALS.[162-165] Similar to language impairments, however, current evidence suggests that deficits in social cognition are a function of executive dysfunction in ALS.[166] Notwithstanding, impaired social cognition is a hallmark feature of behavioural-variant FTD and its prevalence in ALS along with executive dysfunction implicates a cognitive continuum between ALS and behavioural-variant FTD.[155]

The high prevalence of cognitive and behavioural impairments in ALS prompted the development of the Edinburgh Cognitive and Behavioural ALS Screen (ECAS).[167] ECAS is a

clinical screening tool used to identify the cognitive and behavioural impairment profile in patients without dementia. The cognitive screen assesses ALS-specific domains (executive function and fluency, language, and social cognition) and ALS non-specific domains (memory and visuospatial functions) using a series of written and verbal tests. The behavioural screen involves a caregiver interview to assess five behaviour domains: behavioural disinhibition, apathy, loss of sympathy, compulsive behaviours, and altered food preferences. When measured with ECAS, the most prevalent deficits occur in the language and executive functions domains in patients with ALS.[167] Importantly, ECAS has been validated against formal neuropsychological evaluation as a screening tool with high sensitivity and specificity to characteristic impairments in ALS.[168]

Clinical progression and survival

Clinical progression. ALS is described as focal at onset with maximal UMN and LMN signs appearing in the initially involved body region.[3] The symptoms then spread outwardly from the initial region to contiguous neuroanatomic regions. The phenotypic heterogeneity during the disease course is complicated by the differing anatomical features at the UMN and LMN levels: UMNs are organized somatotopically along the primary motor cortex mediolaterally over a small distance; whereas, LMNs are organized somatotopically along the spinal cord rostrocaudally over a larger distance. Furthermore, the spread is considered independent in the two motor neuron systems. At the UMN level, disease spreads to ipsilateral body regions followed by contralateral regions (Figure 3). Conversely, at the LMN level, disease preferentially spreads to the contralateral body region and subsequently to ipsilateral body regions that are further along the spinal cord.[169-173]

The progression and severity of ALS is most commonly quantified by the ALS Functional Rating Scale-Revised (ALSFRS-R).[174] The ALSFRS-R is a series of questions that interrogates a patient's status with respect to four functional domains: bulbar, fine motor, gross motor, and respiratory. It is measured out of a maximum score of 48 (12 questions with 4 points each) and its decline over the disease course follows a curvilinear trajectory.[175] The rate of decline is influenced by genetics,[176] age and site of onset,[175, 177] and motor neuron level involvement.[121] Some MRI studies demonstrate that the ALSFRS-R score correlates with changes in the corticospinal tract,[178] whereas other studies have not found this association.[179] This inconsistency is in part due to the insensitivity of the ALSFRS-R to UMN dysfunction.

Survival and prognostic factors. ALS is largely defined by poor survival rates. The median survival from the time of diagnosis is approximately two years and death typically occurs between 1 – 4 years; survival rates are 76% and 23% one and five years after diagnosis, respectively.[45] Only 12% of patients survive for longer than a decade. The end stage of ALS is punctuated by weakness in respiratory muscles that causes difficulty with breathing,[180] and the most common cause of death is respiratory failure.[180, 181]

Several prognostic factors for decreased survival in ALS have been identified.[127] Older age and bulbar onset are most commonly associated with worse survival in population-based studies. Respiratory function is clinically very relevant for patient care and is also a good prognostic indicator. Forced vital capacity (FVC), a surrogate marker of respiratory status, measured at diagnosis strongly predicts survival even after adjusting for age and site of onset in clinical populations.[182, 183] The rate of disease progression measured at presentation is also significantly associated to patients' prognosis.[184] It is defined as the decline in the ALSFRS-R score at diagnosis since the onset of symptoms [(patient ALSFRS-R score – 48)/symptom

duration]. The rate of disease progression at presentation is typically around 0.6 points per month; at longitudinal follow-up, the ALSFRS-R declines at an average rate of 1 point per month in large clinical trials.[185, 186] The presence of comorbid cognitive and behavioural dysfunction has also been the subject of investigation for its impact on survival in ALS. Interestingly, it has been found that executive dysfunction, in particular, is predictive of poor survival.[152, 187] Behavioral impairments are also found to be associated with poor survival.[187, 188] Not surprisingly, the presence of clinical dementia in the form of FTD also confers a worse survival in ALS. These findings suggest that an overall increased pathological burden in the brain is responsible for the poor outcomes in ALS. Genetic influences also contribute to altered survival in ALS. Patients with mutated *C9ORF72* have shorter survival than patients without the mutated gene.[38] The A4V mutation in the *SOD1* gene confers a particularly aggressive form of the disease that is thought to be because of LMN involvement.[28, 189] In contrast, the D90V mutation in *SOD1* leads to an indolent form of ALS with a protracted survival of longer than 10 years.[27]

Clinical management

Despite the recent advances in the understanding of ALS, there is no cure for the disease. The primary objective of clinical care remains management of symptoms and maintaining quality of life in the face of worsening disability. Currently, only two drugs are approved for treating ALS: riluzole and edaravone. Several supportive interventions and therapies are offered to patients that revolve around nutritional support and preserving respiratory function.[190]

Riluzole. Riluzole was the first drug approved for the treatment of ALS. Randomized clinical trials show that riluzole increases survival by approximately three months.[191] The mechanisms by which riluzole exerts its effects remain an area of study. One potential pathway is by inhibition of presynaptic release of glutamate via a reduction in calcium influx.[192] Others

have proposed that riluzole promotes uptake of glutamate.[193] These lines of evidence suggest that riluzole, at least in part, asserts its neuroprotective functions by reducing glutamate excitotoxicity in the central nervous system. *In vivo* evidence in humans for this hypothesis comes from MRS studies that show recovery in the levels of *N*-acetylespartate (NAA), a metabolic marker for neuronal integrity, three weeks after administration of riluzole in patients with ALS.[194]

Edaravone. Edaravone was approved for treating ALS in 2017 in the United States of America and in the following year in Canada.[195] Initially, this drug was developed as an antioxidant, neuroprotective agent to reduce free radicals in the brain after an ischemic stroke.[196] Oxidative stress is a pathogenic theme in the mechanisms causing ALS and therefore, edaravone is thought to mitigative oxidative injury in vulnerable motor neurons. An early clinical trial has demonstrated a marginal reduction in the rate of decline in the ALSFRS-R score over 24 weeks compared to placebo groups.[126] However, edaravone is not yet widely utilized in clinical practice due to several challenges.[197] Particularly, edaravone is deemed efficacious in only a restricted subset of patients and the treatment regimen is very resource intensive requiring intravenous infusions for up to weeks every month. Furthermore, the impacts of this drug on survival are not yet known.

Multidisciplinary care. Specialized multidisciplinary care is recommended for patients with ALS by clinical practice guidelines.[198, 199] In multidisciplinary clinics, patients receive care from physicians, physical therapists, dietitians, social workers, and nurses. Studies have shown that patients who attend multidisciplinary clinics have longer survival by up to 10 months when compared to patients who attend general neurological clinics.[200, 201] These patients also have a higher proclivity to receive riluzole and other supportive treatments such as nutritional and respiratory support. It is important to note that patients who attend multidisciplinary clinics are

also typically younger than those who do not, potentially reflecting a bias in patient cohorts in survival analysis.[200, 201] In a well-matched study, patients who attended multidisciplinary clinics were found to have better quality of life and mental health.[202]

Nutritional support. Declining body weight at diagnosis and during follow-up is associated with worse survival in ALS.[203] Energy metabolism balance is altered in patients with ALS due to reduced food intake caused by dysphagia and resting hypermetabolism.[204] As such, nutritional support in the form of altered food consistencies and nutritional supplements are strongly recommended to maintain body weight.[198, 205] Eventually, a percutaneous endoscopic gastronomy (PEG) may be needed to provide an alternate access to deliver nutrients in progressively worse swallowing dysfunction. Studies have demonstrated that patients using PEG have improved body weight profiles compared to patients who refuse the intervention.[206] Furthermore, improved survival by four months was also observed in these patients after six months of intervention.

Respiratory function preservation. Maintaining respiratory function is vital as most deaths in ALS occur due to respiratory dysfunction. Non-invasive ventilation (NIV) methods, such as continuous positive airway pressure (CPAP) and bilevel positive airway pressure (BiPAP) machines, are recommended in patients with less than 50% FVC.[205] In a randomised control trial investigating the efficacy of NIV therapies compared to standard of care, NIV improved the survival of patients, particularly in patients with better bulbar function who experienced an extended median survival by 7 months.[207] Additionally, use of NIV methods are recommended to improve the quality of life as patients report better sleep quality, improved energy and vitality, and decreased depression.[205] Invasive methods of ventilation, such as

tracheostomy, are recommended if respiratory function is not maintained with NIV or if NIV is not tolerated.

Histopathology

Macroscopic pathology

Typical cases of ALS do not have overt macroscopic changes in the brain on post-mortem evaluation. In cases of ALS-FTD, mild to moderate cortical atrophy in the frontal and anterior temporal lobes can be appreciated reflecting the FTLD disease process.[208] In cases of PLS, marked atrophy of the precentral gyrus is observed.[209, 210] Differences in atrophy of the precentral gyrus between ALS and PLS are largely reflective of the longer disease duration in PLS. The spinal cord in ALS often displays atrophy, or thinning, of the anterior nerve roots that supply LMNs to skeletal muscles.[80] In clinical practice, the thickness of the anterior nerve root can be assessed by comparing it with the thickness of the posterior nerve root, which is comprised of afferent sensory fibers and remains unaffected in ALS. No macroscopic abnormalities occur in the cerebellum in ALS.

Microscopic pathology

Microscopic pathology of the central nervous system is routinely evaluated by staining tissue sections (several micrometers thick) with chemicals that are sensitive to various cellular structures. Most commonly used chemicals are the hematoxylin and eosin (H&E) stain used to evaluate neurons and glia and the Luxol fast blue (LFB) stain used to evaluate myelinated structures. Immunohistochemistry (IHC) is used to selectively stain and identify proteins via the binding of antibodies to specific antigens. IHC staining can identify cell types and pathological protein inclusions.

Upper motor neuron pathology. The classic UMN pathology in ALS is characterized by loss of layer V pyramidal neurons, particularly Betz cells, in the primary motor cortex.[211-213] Betz cells are large pyramidal UMNs that send their axons down the descending corticospinal and corticobulbar tracts. Other changes in the Betz cells include degeneration of dendrites, accumulation of lipofuscin, and reactive astrocytic gliosis around the cell soma.[214, 215] Betz cells are identified on routine H&E stain and make up less than 10% of the pyramidal tract system.[216] As such, some studies have found no change in the overall number of neurons in the primary motor cortex, even in light of *in vivo* MRS evidence of neuronal loss and metabolic dysfunction.[217]

Initial reports of reactive astrogliosis were associated with degenerating neurons in the primary motor cortex. Astrocytes react to various central nervous system injuries, such as ischemia, trauma, and inflammation, with changes in their morphology and in severe cases, with glial scar formation.[218] In ALS, patchy reactive astrogliosis was first reported in layers II and III and occasionally in layers IV and V of the motor cortex when stained with glial fibrillary acidic protein (GFAP).[219] In this study, neuronal loss was widespread in the motor cortex rather than limited to the scattered regions of astrogliosis. Increased reactivity to GFAP is also observed at the gray-white matter junction and in the subcortical region of the primary motor cortex in ALS.[220, 221]

Pathology of the corticospinal tract in the white matter is marked by degeneration of myelinated axons. Myelin pallor, or decreased levels of myelin staining due to loss of myelinated axons, is observed along the length of the descending UMNs in the centrum semiovale, internal capsule, and spinal cord.[72, 211, 222] Sections of the cervical cord often exhibit remarkable myelin pallor in the lateral descending corticospinal tracts. Activated microglia on CD68 stains are

observed in areas of degenerating corticospinal tracts.[72, 223] Microglia phagocytose myelin debris from degenerating myelinated axons and therefore are expected to be present in areas of degenerating white matter.[224] Microglia involvement is also implicated in the pathogenesis in ALS, and its degree at post-mortem is associated with clinical disease progression and UMN burden.[72]

Lower motor neuron pathology. LMN pathology in ALS is evaluated from sections of the brainstem and the spinal cord. Neuronal cell loss in the hypoglossal nucleus of cranial nerve XII and nucleus ambiguus of cranial nerve X is regarded as a cardinal feature of ALS.[211] These medullary nuclei contain LMNs that serve the motor functions of speech and swallowing. This is consistent with evidence of frequent clinical bulbar dysfunction in ALS on formal testing, even in cases with no bulbar symptoms.[225, 226] Cranial nerves III, IV, and VI, which control muscles of eye movement, are rarely involved pathologically and this corroborates the sparring of eye movement function in ALS. Loss of alpha motor neurons in the anterior horns of the spinal cord is well-documented in ALS.[222, 227, 228] On average, patients experience a loss of 10 – 90% of their LMNs with the greatest loss in the neuraxis level corresponding to the region of the onset.[171] Studies have also shown a strong association between the number of remaining alpha motor neurons and the corresponding body region's remaining muscle fibers.[229] This provides a direct relationship between LMN loss and muscle atrophy. Reactive astrogliosis is also evident in the anterior horns of the spinal cord at multiple levels.[230] Activated microglia are present in the anterior horns and their degree of involvement is related to clinical disease progression.[72, 231, 232]

Bunina bodies are considered a specific hallmark of LMN pathology in ALS.[233] They are visualized on H&E staining as small, round inclusions in the cytoplasm and dendrites of neurons.[234] Bunina bodies are frequently observed in the surviving LMNs in the brainstem and

the spinal cord.[222] These inclusions, at least in part, are responsible for the clinical manifestations of LMN dysfunction since they are not observed in PLS cases.[235] Furthermore, they maintain their specificity to LMN pathology even in long-duration ALS cases.[236] Approximately 60% of PMA cases also show evidence of Bunina bodies in their surviving LMNs, whereas in ALS, greater than 80% of cases exhibit these inclusions.[144, 222]

Proteinaceous inclusions. Ubiquitinated aggregates of aberrant proteins in inclusion bodies are a defining pathological feature of neurodegenerative diseases.[237] Presence of ubiquitinated proteins in pathological inclusion bodies represents a failure of their metabolism and degradation pathways. Specific protein inclusions, along with their unique anatomical distribution in the central nervous system, are synonymous with certain diseases. For example, the presence of pathological alpha-Synuclein in substantia nigra is pathognomonic for Parkinson's disease.

In ALS, ubiquitin-positive inclusions in LMNs of the brainstem and spinal cord are detected with anti-ubiquitin antibodies in IHC analysis.[238] Large autopsy studies have suggested that they are present in surviving LMNs in 100% of ALS cases.[222] Ubiquitin pathology in UMN is less consistent; some studies have shown no ubiquitin-positive inclusions in the motor cortex,[230] whereas others have demonstrated UMN ubiquitin pathology in less than 50% of cases.[239, 240] In a vast majority of ALS cases, the pathological ubiquitinated protein in these cytoplasmic inclusions is TDP-43.[4, 5] There is also a loss of normal nuclear TDP-43 staining and hyperphosphorylation of pathological cytoplasmic TDP-43. TDP-43 mislocalization from the nucleus to the cytoplasm is considered an early event in neurodegeneration.[241] Evidence suggests that retention of nuclear TDP-43 staining in ALS is associated with a slower disease course.[242] In

sporadic ALS, pathological TDP-43 immunoreactivity is observed in neuronal and glial cytoplasmic inclusions in both UMN and LMN systems.[243]

Clinicopathological studies of TDP-43 pathology patterns have provided insight into their specificity to clinical phenotypes across the ALS-FTD spectrum. TDP-43 pathology can be used to differentiate between ALS and other neurodegenerative processes. In a study of behavioural-variant FTD, ALS-FTD, Alzheimer's disease, and neurologic controls, TDP-43 pathology in the hypoglossal nucleus identified ALS with a 98% accuracy.[244] In contrast, the severity of TDP-43 pathology in the anterior cingulate gyrus identified behavioural-variant FTD with a 99% accuracy. Furthermore, cases of behavioural-variant FTD with positive TDP-43 pathology in the hypoglossal nucleus are strongly associated with evidence of possible or probable ALS according to clinical criteria.[245] TDP-43 pathology in the brain and spinal cord correlates with neuronal loss and is presumed to be the antecedent event.[246, 247] Additionally, severity of neuronal involvement along the spinal cord neuraxis is strongly associated with site of clinical onset of disease in spinal ALS.

The genetic profile of patients with ALS substantially impacts their pathological features.[248] In particular, the composition of proteinaceous inclusions in *SOD1*, *FUS,* and *C9ORF72* mutants deviates from the pathology of sporadic ALS as described above. Pathological TDP-43 inclusions are remarkably absent in ALS with *SOD1* mutations.[249, 250] Interestingly, however, hyaline inclusions with ubiquitin immunoreactivity are still present and considered a hallmark for *SOD1* mutation pathology. These inclusions are thought to contain SOD1 and various chaperone proteins[251, 252] and not generally found in sporadic ALS.[253] Furthermore, studies using antibodies that label misfolded SOD1 with specific conformational changes have identified misfolded SOD1 in intraneuronal inclusions in *SOD1*-linked familial

ALS, but not in sporadic ALS.[254, 255] These findings, however, have been challenged by studies demonstrating misfolded SOD1 in sporadic ALS neurons and glia.[256] A recent large-scale study of non-*SOD1* and *SOD1*-linked familial ALS and sporadic ALS autopsy cases refuted these claims by showing evidence of misfolded SOD1 in *SOD1*-linked familial ALS, but not in other cases.[257] This suggests that SOD1 misfolding may not be a critical component of sporadic ALS.

ALS patients with *FUS* mutations also have marked absence of pathological TDP-43 inclusions.[258, 259] Instead, immunostaining for FUS demonstrates FUS-positive cytoplasmic inclusions in UMNs and LMNs.[24, 25, 258, 259] Specific *FUS* mutations have been associated with disease severity and pathological patterns. Patients with P525L *FUS* mutations have an early-onset, rapid disease course with numerous FUS-positive neuronal cytoplasmic inclusions, particularly in the primary motor cortex.[260] In contrast, the R521C mutation has a more typical ALS phenotype, but with less frequent FUS-positive inclusions in the primary motor cortex and a preponderance of involvement basal ganglia structures. Recent studies have also shown that FUS-positive inclusions are present in surviving LMNs in sporadic ALS, non-*SOD1* familial ALS, and ALS-FTD.[261] Furthermore, FUS-positive inclusions co-localize with TDP-43, ubiquitin, and p62 immunoreactivities in sporadic and familial ALS, except for *SOD1*-linked familial ALS, which has a unique signal on IHC analysis including C9ORF72-positive inclusions.[261, 262]

The neuropathology associated with *C9ORF72* mutations is distinctive when compared with all other cases of ALS.[263] With respect to TDP-43 pathology, *C9ORF72* expansion mutation carriers are indistinguishable from sporadic ALS. They harbour ubiquitinated TDP-43 cytoplasmic inclusions in neurons and glia in both UMN and LMN with concurrent neuronal loss in the respective regions.[35, 264] These findings do not differ between *C9ORF72*-linked ALS and

ALS-FTD cases.[265] The defining pathological feature of this genetic mutation are ubiquitinated, p62-positive neuronal inclusions that are remarkably negative for TDP-43.[35, 264, 266] These star-shaped cytoplasmic inclusions are typically found in the pyramidal cells in the CA4 region of hippocampus and in the Purkinje cells of cerebellum. These inclusions contain pathological dipeptide-repeat proteins encoded from the *C9ORF72* expanded genes.[267] The role of these proteins in the pathogenesis and clinical expression of the disease is subject of ongoing investigations.[268]

Extra-motor pathology. Progressive degeneration of both UMN and LMN systems is the primary pathological feature of ALS. However, accumulating evidence supports the view that pathologically, similar to its clinical expression, ALS is a multisystem disease that affects extra-motor regions. Central to neuropathological evaluation in sporadic ALS, ubiquitin IHC analysis reveals cytoplasmic inclusions in the non-motor frontal areas, temporal lobe, and the subcortical gray matter structures of the brain.[222, 269] The severity of the extra-motor ubiquitin pathology is worse in ALS-FTD disease.[269] Systemic studies of TDP-43 pathology in sporadic ALS also reveal a multisystem pattern of involvement.[270] The motor system is most frequently affected, followed by involvement of the basal ganglia, thalamus, cingulate gyrus, frontal lobe, temporal lobe, hippocampus, and amygdala (Figure 4). Clinicopathological investigations suggest that extra-motor cortical and subcortical TDP-43 pathology is more prevalent in ALS-FTD compared to ALS without evidence of clinical dementia.[243, 247, 271] The association of greater TDP-43 extra-motor involvement in ALS-FTD also persists in *C9ORF72*-linked ALS and ALS-FTD cases.[265] Synaptic loss in the prefrontal cortex is associated with TDP-43 pathology and considered a substrate of cognitive decline in ALS.[56] Executive dysfunction, the most common form of cognitive impairment in ALS, is also associated with greater TDP-43 pathology in the middle

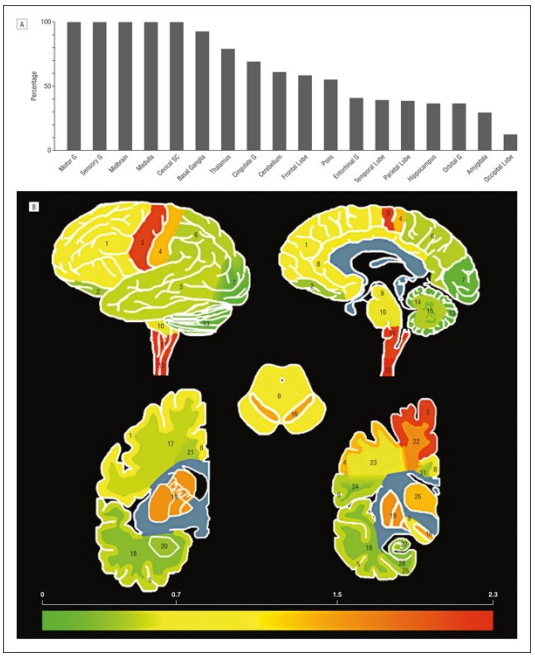

Figure 4: Frequency and heat map of the deposition of abnormal TDP-43 in the brain in ALS. Taken from Geser F, Brandmeir NJ, Kwong LK, Martinez-Lage M, Elman L, McCluskey L, Xie SX, Lee VM, Trojanowski JQ. Evidence of multisystem disorder in whole-brain map of pathological TDP-43 in amyotrophic lateral sclerosis. Archives of neurology. 2008 May 1;65(5):636-41.

frontal gyrus.[73] Interestingly, severe striatal TDP-43 pathology is a consistent feature of *C9ORF72*-linked disease.[264, 272, 273] However, striatal pathology rarely manifests clinically in ALS. Cluster analysis reveals that greater TDP-43 pathology, both in terms of extent and severity, is associated with cognitive impairment.[272]

Pathological staging

Propagation of pathology in characteristic spatial patterns is a hallmark of neurodegenerative diseases.[112] In ALS, a stereotypical spread of pathological TDP-43 across regions of the brain in discrete stages has been proposed to reconcile motor and extra-motor pathology.[274] Each increasing stage is demarcated by the presence of abnormal intraneuronal TDP-43 in unique regions in addition to the pathology in the preceding stages. In the brain, TDP-43 pathology is thought to spread sequentially through four neuropathological stages. Stage 1 is

characterized by the presence of phosphorylated TDP-43 in the cytoplasm of projection neurons in the motor cortex (Betz cells), motor neurons of cranial nerves V, VII, and X – XII, and in alpha motor neurons of the anterior horn of the spinal cord. Stage 2 is primarily characterized by the involvement of precerebellar brainstem nuclei including the inferior olive, medullary reticular formation, and the red nucleus. Clinical motor dysfunction related to cerebellar pathology, however, is not observed in ALS. In stage 3, TDP-43 pathology extends to prefrontal and temporal neocortical areas. Additional TDP-43 pathology is observed in the caudate, putamen, and ventral striatum at this stage. The final stage of TDP-43 is characterized by involvement of the hippocampal formation and nearby anteromedial temporal structures.

It should be noted that this pathological staging system was derived from an autopsy cohort of ALS patients, which by definition precludes a longitudinal analysis. The extent of the topographical distribution, and not the degree of TDP-43 pathology, was used to assign cases to a given stage. Additionally, increasing stages were not associated with disease duration in this study.[274] Therefore, though this system offers preliminary evidence of a sequential pattern of pathological progression in ALS, it needs to be replicated and validated in future studies. Longitudinal data is further required to provide evidence for the *in vivo* propagation of the TDP-43 pathology in ALS.

Spreading of TDP-43 pathology through these neuropathological stages is believed to occur via axonal pathways. Structures involved in stages 1 and 2 are connected by major descending tracts from the motor cortex including corticospinal, corticobulbar, and corticopontine tracts. Propagation to stage 3 can occur via association tracts connecting the precentral gyrus with prefrontal areas[275] and the cortico-basal ganglia loop.[276] Direct evidence for the dissemination of TDP-43 pathology from the motor to the frontal and temporal regions,

however, is currently lacking. Studies have aimed to recapitulate the neuropathological stages of TDP-43 spread *in vivo* by evaluating the white matter integrity of tracts that are hypothesized to be susceptible at the different stages: corticospinal tract (stage 1), corticorubral and corticopontine tracts (stage 2), corticostriatal tracts (stage 3), and perforant tract (stage 4).[277, 278] In cross-sectional analysis, progressively more significant differences between ALS patients and controls were found in the diffusion profiles of tracts corresponding to higher disease stages.[277] Additionally, longer disease duration correlated with the higher disease stages according to this *in vivo* imaging-based staging scheme. In a follow-up longitudinal study, 27% of ALS patients were observed to increase in their ALS stage as defined by this *in vivo* scheme; that is, diffusion abnormalities were sequentially observed in tracts associated with high disease stages over time.[278] These studies suggest that patient-level TDP-43 pathology staging is feasible and sensitive to longitudinal progression; however, further work is required to validate their clinical significance.

Chapter 2 Magnetic Resonance Imaging in Amyotrophic Lateral Sclerosis

As discussed previously, ALS is a complex disease with no objective tests or measures to detect and monitor disease progression. There is an urgent need for markers that can be used in the clinical management of patients and also aid clinical trials to evaluate novel therapeutics. Various markers for ALS have been proposed, including "wet" biomarkers from blood and CSF of patients.[279] MRI and its various modalities have emerged as leading candidates in providing markers for ALS because of their superior neuroanatomical specificity and sensitivity to unique disease processes. In particular, T1-weighted imaging and diffusion tensor imaging (DTI) are structural MRI techniques that have been widely applied in ALS in efforts to understand the pathogenesis of the disease and discover the much-needed markers. MRS and fMRI are other MRI modalities that have also made significant contributions. MRS studies have highlighted alterations in the metabolic profile of neurons and glia in ALS.[280] fMRI studies have been particularly useful in providing the neuroanatomical basis of functional impairments in the motor and extra-motor domains in ALS.[281]

The focus of the work here is on structural MRI and its application in ALS. Markers of structural damage can serve as objective measures of disease and its evolution over time, and they are ideal candidates for use in clinical trials. MRI-based measures have already proven to be

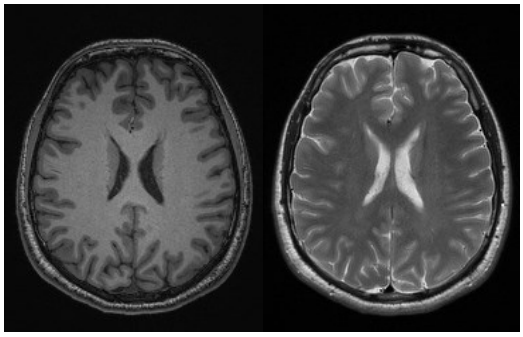

Figure 1: T1-weighted (left) and T2-weighted (right) magnetic resonance imagines in a healthy person.

vital markers of pathology in Alzheimer's disease[282] and progress has been made towards markers for ALS.[283] As such, this chapter will provide an overview of the findings on advanced MRI modalities in ALS, their phenotypic manifestations, and their longitudinal evolution. The basic principles of structural MRI and its analytical methods will be also presented to prime the reader for the forthcoming sections. Later, texture analysis as an MRI-based marker will be formally introduced alongside its current neurological applications in the literature.

Basics of structural magnetic resonance imaging

T1-weighted MRI

T1-weighted MRI is most commonly used to study gray matter structures in the brain. This imaging technique provides a three-dimensional (3D) image reconstruction of the brain where various tissue classes (gray matter, white matter, and CSF) are identifiable based on their "contrast", or voxel intensity. In T1-weighted images, the image contrast is such that CSF appears black, gray matter structures appears gray, and white matter appears lighter than gray matter (Figure 5). The contrast between tissue classes is a result of the biophysical properties of tissues (namely, their spin-lattice and spin-spin relaxation times) and the sensitization of acquisition protocols towards those properties.[284] Consequently, in the presence of pathological processes in disease states, tissue properties vary that lead to alterations in their image intensities.

For example, tumours typically occur as darker regions in the brain on T1-weighted images; however, in T2-weighted images that are sensitized to fluid content, a tumour may appear bright due to edema in the surrounding tissue.

In clinical practice, T1-weighted images are used to detect macroscopic structural abnormalities that are detectable to the human eye, such as tumours or severe atrophy. In research, due to the excellent contrast, T1-weighted images can be segmented into the various tissue classes and be used to assess gray matter structures by measuring cortical thickness, volume, and density. These measurements can be obtained manually by outlining a region of interest (ROI) that is in question for a study. There are a number of freely available software packages that can automatically segment structures of the brain from a T1-weighted image with sufficiently high resolution. The structures can then be quantified with measurements of surface area, shape, volume, or cortical thickness.[285-287] This data is used to assess group-level differences and correlations with clinical tests and measures. In addition, automated pipelines exist that are capable of evaluating gray matter density differences between groups across the whole brain in a voxel-by-voxel manner. The most commonly used approach is called voxel-based morphometry (VBM) that enables an unbiased, whole-brain evaluation of gray matter densities and regional atrophy from T1-weighted images.[287] For example, a VBM study may find reduced gray matter density in the hippocampal region in patients with Alzheimer's disease when compared to controls. Similarly, regional differences in cortical thickness can be evaluated at the group-level in whole-brain analysis.[285] These methods are advantageous because they enable analysis of the whole brain without *a priori* hypotheses and can investigate the neuroanatomical correlates of clinical data obtained from the study participants.

Diffusion tensor imaging

Even though T1-weighted images provide a contrast between gray and white matter structures, they are not suitable to analyze white matter structures using the aforementioned techniques. In normal anatomy, regions of white matter are composed of nerve fibers that form a complex network of pathways connecting different parts of the brain and the spinal cord. On T1-weighted images, however, this detailed anatomy is not captured as white matter appears as homogenous tissue without anatomical variations. To enable analysis of white matter structures, neuroimaging studies most commonly use diffusion tensor imaging (DTI). DTI is an MRI technique that relies on the Brownian motion of water.[288] In an unrestricted environment, water molecules can freely diffuse in any direction. In white matter, however, diffusion of water is restricted by the presence of fiber bundles and their microstructures.[289] Thus, the displacement of water molecules in white matter is approximately elliptical in shape, with the greatest diffusion occurring along the direction of axons and restricted diffusion in the perpendicular direction due to barriers such as axonal membranes, myelin, and other microstructures. Alterations in the diffusion profile of water, for example, increased diffusion in the perpendicular direction, can therefore mirror pathogenic states, such as the breakdown of axonal membranes. A diffusion tensor model is then used to describe these diffusion properties of water within the tissue. This model is typically quantified into two summary measures in most neuroimaging studies: fractional anisotropy (FA) and mean diffusivity (MD). FA measures the strength of directionality in the diffusion of water, whereas MD measures the overall displacement of water due to diffusion. In white matter regions, FA is generally high due to preferential diffusion along the nerve fibers; in gray matter regions, FA is lower due to absence of organized structures restricting the diffusion of water. MD, however, is similar in both gray and white matter regions in the adult human brain. Damage to white matter regions typically results in a reduction in FA

and an increase in MD. The pattern of alterations in the DTI metrics can sometimes reveal additional information regarding the characteristics of degenerative processes;[290] however, caution must be undertaken in interpreting results as these measures are non-specific .[291, 292]

Similar to analyzing gray matter from T1-weighted images, DTI permits ROI and whole-brain analysis. DTI data can be used to virtually "dissect" specific white matter pathways, or tracts, to create 3D ROIs via a method called tractography. The diffusion profile of these tracts can then be analyzed between groups in ROI-based analyses. Earlier DTI studies utilized simple 2D ROIs to study diffusion in disease-relevant regions, such as the internal capsule in ALS.[293] Experimental DTI pipelines also permit whole-brain evaluation via VBM and tract-based spatial statistics of FA and MD images. In the later method, voxel-by-voxel analysis of DTI metrics is conducted along the major white matter pathways in the brain.[294] Irrespective of the analytic technique, between-group comparisons of diffusion profiles and correlations between clinical variables and DTI metrics are feasible.

Structural abnormalities in amyotrophic lateral sclerosis

Primary motor cortex

Reduced gray matter density in the precentral gyrus is a common finding in whole-brain VBM studies comparing ALS patients with controls.[295] There are some instances of divergent results with studies showing no change in VBM analysis.[296, 297] However, variations in VBM findings in ALS studies are known to be affected by the choice of image processing pipeline and statistical models.[298] Disease heterogeneity paired with small study sample sizes is also a contributing factor for the varying results. Studies analyzing cortical thickness have

demonstrated thinning of the primary motor cortex and largely mirror VBM findings of reduced gray matter density in ALS.[299-302]

Involvement of the primary motor cortex has been shown to relate to the functional motor involvement in ALS. In particular, in subgroup analyses comparing limb- and bulbar-onset ALS, patterns of focal cortical atrophy along the motor homunculus are associated with site of symptom onset and severity of motor impairment measured with the ALSFRS-R in corresponding body regions[301, 303, 304] This is in line with the hypothesis that ALS has a focal onset of disease and is mediated, at least in part, by cortical degenerative processes. Few studies have assessed the involvement of the primary motor cortex in relation to the degree of clinical UMN involvement. Patients with p-UMN phenotypes, including patients with PLS, consistently show worse atrophy in the motor cortex compared to patients presenting with classic ALS symptoms.[301, 304, 305] Therefore, cortical thinning in the motor regions of the brain, potentially due to the loss of UMNs, is reflective of clinical UMN dysfunction in ALS and related disorders. Degeneration of the primary motor cortex and its role in survival in ALS, however, is not fully understood. No direct association between survival and cortical thickness of the precentral gyrus was found in one study.[301] In another study, the cortical thickness of the right precentral gyrus was found to significantly correlate with survival only in univariate analysis and not in multivariate analysis.[306]

The diagnostic utility of using cortical thickness of the primary motor cortex as a measure to detect ALS has been evaluated in a few studies. Initial reports suggest that a cortical thickness of less than 2.42 mm in the precentral gyrus can different patients with ALS from controls with 82% specificity and 84% sensitivity.[300] A follow-up study that included ALS-mimicking disorders, such as multifocal motor neuropathy and spinobulbar muscular atrophy, found that

cortical thickness had a 76% specificity and 72% sensitivity in differentiating ALS from ALS mimics and controls.[301] Though promising, these studies need to be replicated in different datasets with patients that are earlier in their disease stage for further validation.

Corticospinal tract and corpus callosum

DTI studies have consistently reported a pathological change in DTI metrics, particularly with reduced FA, of the corticospinal tract in ALS in comparison to controls.[293, 307-309] This observation is thought to reflect degerenation and overall loss of descending white matter fibers in ALS.[310] Furthermore, abnormal DTI findings in the corticospinal tract are evident in ROI,[293, 308] tractography,[142, 309] and TBSS studies,[311-313] suggesting the robustness of this finding. A study recently proposed evaluating the pathological TDP-43 stages *in vivo* in ALS using DTI.[277] In the proposed scheme, presence of DTI abnormalities in the corticospinal tract, corticorubral and corticopontine tracts, corticostriatal tract, and the perforant tract corresponds to stages 1 – 4 of TDP-43 pathology, respectively. The study also found that later stages were associated with lower ALSFRS-R scores.

Clinically, abnormal diffusion profile of the corticospinal tract is most often found to associate with disease progression rate in ALS.[307, 312, 314] This correlation is most prominent in the internal capsule where decreasing FA values correlate with faster disease progression rates.[314] Clinical UMN dysfunction has also shown to associate with the diffusion profile of the corticospinal tract; two studies demonstrated that worsening of DTI metrics correlate with increased UMN burden on clinical exam.[315, 316] Decreasing ALSFRS-R scores have positively correlated with FA of the corticospinal tract in some studies,[313] whereas in other studies, no correlation is observed.[307, 317] This possibly reflects the lack of specificity of the ALSFRS-R

score as a measure of UMN dysfunction in ALS. Interestingly, FA of the corticospinal tract demonstrates a weaker association to survival compared to ALSFRS-R score in univariate and multivariate analyses.[318] It could be hypothesized that UMN dysfunction, when measured with DTI, does not substantially contribute to overall survival. On the other hand, overall disability measured by the ALSFRS-R score, which is predominantly affected by LMN disease, plays a more important role in predicting survival. Several studies have investigated the involvement of the corticospinal tract with DTI in patients with PMA and LMN phenotypes. Subclinical reductions in FA of the corticospinal tract are evident patients with PMA in unbiased, whole-brain analysis when compared to controls.[319-321] These findings are congruent with pathological findings of UMN degeneration in PMA patients with no history of clinical UMN dysfunction.[143, 144] Compared with ALS patients, patients with PLS have lower FA along the entire corticospinal tract, suggestive of a more severe form of UMN disease.[312, 322] These findings, however, are not consistent as studies have shown PLS patients have disease restricted to the rostral parts of the corticospinal tract.[323]

The diagnostic accuracy of DTI in ALS was evaluated in two meta-analysis studies. Based on group-level statistics, the pooled sensitivity and specificity of using FA to distinguish between ALS and controls was 65% and 67%, respectively, using data from 30 published studies.[324] This is corroborated by an individual patient data meta-analysis that demonstrated 68% sensitivity and 73% specificity.[325] Therefore, further work is needed to improve the utility of DTI in the diagnostic workup of ALS.

Decreased FA in the corpus callosum is also reported as a consistent DTI feature in patients with ALS.[326, 327] Specifically, the greatest severity of damage occurs in the region of the corpus callosum where interhemispheric fibers connecting the motor regions of the brain pass

through. The significance of degenerating callosal fibers is not yet established; however, some studies suggest that it is related to the failure of inhibitory circuitry in the brain in ALS.[328, 329] It has also been suggested that the topography corpus callosum damage mirrors the cortical degeneration patterns in ALS and other MNDs.[330] Neuropathological studies have demonstrated degenerative changes in corpus callosum with increased gliosis.[331, 332] However, more studies are needed to clearly elucidate the role of the corpus callosum in the pathogenesis of ALS.

Frontal and temporal lobe involvement

Extra-motor features in ALS are well-recognized in clinical and post-mortem investigations. Likewise, extra-motor structural abnormalities in the form of decreased gray matter density and cortical thinning of the frontal and temporal lobes is evident in classical ALS without clinical dementia.[301, 303, 333-336] The frontotemporal pattern of cortical atrophy is worse in clinically defined ALS-FTD compared to controls and ALS.[337-339] Similarly, DTI studies have provided convincing evidence of widespread degeneration of frontal and temporal pathways across the ALS spectrum.[179, 307, 333, 334, 340, 341] These results are in line with the concept that ALS is a multisystem disorder.

Studies over the last five years have increasingly sought to delineate the cognitive and behavioural manifestations of frontotemporal degeneration in ALS. Studies assessing language deficits in ALS using syntactic comprehension and semantic knowledge tasks have found their performance to correlate with atrophy in the anterior temporal regions and insula[342-344] and associated degeneration of the white matter tracts.[345] Patients with semantic-variant primary progressive aphasia, a subtype of FTD with severe language impairments,[346] also exhibit the same pattern of temporal lobe degeneration.[347] Indeed, language functions in humans,

particularly syntactic comprehension, are performed by complex circuitry involving the temporal lobes and Broca's area.[348]

Executive dysfunctions in ALS, on the other hand, are primarily associated with degenerative processes in the frontal regions of the brain. Impaired verbal fluency has been shown to correlate with decreased gray matter density in the dorsolateral prefrontal region.[316] Scores from the frontal assessment battery, a set of tests to executive functioning, correlate with atrophy in the orbitofrontal gyrus.[349] A multimodal study evaluating structural correlates of cognitive and behavioural impairment found that white matter integrity measured with DTI metrics is the major contributing factor towards extra-motor dysfunction in ALS.[350] In particular, altered DTI metrics of the major association fibers such as the cingulum and superior longitudinal fasciculus were found to be associated with executive dysfunction. Fluency deficits have also demonstrated strong correlations with inferior longitudinal fasciculus, inferior fronto-occipital fasciculus, and superior longitudinal fasciculus in ALS.[351, 352]

Apathy, which is a hallmark behavioural dysfunction in ALS, is consistently associated with degeneration of the cingulate in ALS. Studies have shown that increased apathy is associated with decreased FA of the anterior cingulum bundle.[353] In another study, various behavioural dysfunction phenotypes including apathy and disinhibition in ALS were associated with thinning of the orbitofrontal and cingulate cortex.[354] Lack of emotional empathy, a substrate of impaired social cognition, is also associated with worse gray matter density in the anterior cingulate cortex.[163] Cingulate gyrus and its white matter fibers are limbic structures in the human brain. Limbic structures are important modulators of emotions and memory.[355] Hippocampus, which is another limbic structure, also exhibits atrophy in formal volumetric analyses in ALS.[356,

[357] Although memory loss is not a hallmark feature, approximately 25% of ALS patients exhibit impaired immediate and delayed recall that is associated with hippocampal volume loss.[297]

Progressive structural changes in amyotrophic lateral sclerosis

Literature considerations

The progressive structural changes in the brain in ALS are poorly understood. This is partly due to scarcity of longitudinal studies and small study sample sizes. To date, there have been 33 published reports that have aimed at evaluating longitudinal structural changes in ALS (Table 3). More than half of these studies had less than 20 patients that were followed longitudinally and only seven studies reported results with 30 or more patients. This is problematic because given the complexity and heterogeneity of ALS, it is difficult to interpret results and draw meaningful conclusions from studies with small sample sizes. Furthermore, cerebral structural changes are well-documented in healthy aging over the adult lifespan.[358] The majority of longitudinal studies in ALS do not include control participants and therefore fail to account for changes that occur as part of the normal ageing processes.

It is important to investigate both gray and white matter structures to fully understand the scope of longitudinal change in ALS. Currently, only eight published reports have studied both gray and white matter structures simultaneously using a multimodal MRI approach.[305, 316, 359-364] A majority of the longitudinal studies have focused on alterations in DTI metrics, with some limited to the corticospinal tract. Studies with lengthy multimodal MRI protocols and clinical evaluations are difficult for patients because of fatigue and functional motor impairments,

Table 1: Longitudinal DTI and T1-weighted imaging studies in ALS.

Authors	Year of publication	MRI modality	Patients with follow-up, *n*	Length of follow-up	Main longitudinal findings
Jacob et al.[365]	2003	DTI	3	9 months	14% reduced anisotropic diffusion in the internal capsule
Sage et al.[366]	2007	DTI	7	5 – 11 months	No significant reductions in the FA of the corticospinal tract
Blain et al.[315]	2007	DTI	11	6 – 12 months	No significant reductions in the FA of ROIs along the corticospinal tract
Mitsumoto et al.[367]	2007	DTI	30	6 – 15 months	No significant reductions in the FA of the internal capsule
Nickerson et al.[368]	2009	DTI	2	3 – 12 months	Qualitative decline in the FA of the internal capsule
Avants et al.[369]	2009	T1	4	5.3 months	Atrophy in the premotor cortex, motor cortex, and parietal lobes in ALS-FTD
Agosta et al.[370]	2009	DTI	17	6 – 12 months	No significant reductions in the FA of the corticospinal tract
Agosta et al.[371]	2009	T1	16	6 – 12 months	Atrophy in the premotor cortex and basal ganglia. Fast progressing ALS showed greater atrophy in the motor and extra-motor regions
van der Graaf et al.[142]	2011	DTI	16	6 months	Reduced FA along the corticospinal tract, corpus callosum. Extra-motor reductions in FA more prominent in bulbar-ALS
Zhang et al.[372]	2011	DTI	17	8.1 months	Reduced FA in the corticospinal tract and the corpus callosum
Senda et al.[363]	2011	DTI, T1	17	6 months	Reduced gray matter density in frontal and temporal regions. Reduced FA in the corticospinal tract and frontal lobe regions
Keil et al.[373]	2012	DTI	15	6 months	Reduced FA in the cerebral peduncles and the temporoparietal region
Menke et al.[314]	2012	DTI	19	5 – 7 months	Increased axial diffusivity in the internal capsule
Verstrate et al.[300]	2012	T1	20	3 – 10 months	No significant cortical thinning observed in whole-brain analysis
Kwan et al.[305]	2013	DTI, T1	9	1.3 years	Reduced cortical thickness of the precentral gyrus on ROI-based analysis. No significant reduction in the FA of the corticospinal tract
Schuster et al.[374]	2014	T1	51	3 – 15 months	Reduced cortical thickness in the frontal and temporal lobes in classic ALS. Cortical thinning of the precentral gyrus observed in LMN variants
Menke et al.[316]	2014	DTI, T1	27	16 months	Reduced gray matter density in the motor regions, frontotemporal regions, and deep gray nuclei. Increased MD in the corpus callosum and increased axial diffusivity in the corticospinal tract ROI
Verstraete et al.[375]	2014	DTI	24	3 – 12 months	Expanding network of reduced FA in white matter tracts
Westeneng et al.[376]	2015	T1	39	5.5 months	Decreased volume of the hippocampus and increased ventricular volume
Steinbach et al.[377]	2015	DTI	16	3 months	Increased connectivity between the hippocampus and the visual cortex
Walhout et al.[301]	2015	T1	39	3 – 12 months	Reduced cortical thickness in the temporal lobe
Cardenas-Blanco et al.[360]	2016	DTI, T1	34	6 months	No significant reduction in the cortical thickness or gray matter density. Reduced FA of the corticospinal tract in ROI-based analysis
Floeter et al.[378]	2016	T1	11	5.7 months	No significant reduction in the cortical thickness of C9+ patients
Baldaranov et al.	2017	DTI	6	26 months	0.2 – 5.6% annual reduction in FA of the corticospinal tract

de Albuquerque et al.[361]	2017	DTI, T1	27	8 months	No significant reduction in the cortical thickness or gray matter density. Increased MD in the corpus callosum
Wirth et al.[379]	2018	T1	4	3 – 39 months	Variability in the longitudinal course of the cortical thickness of the precentral gyrus at the individual level
Bede et al.[359]	2018	DTI, T1	32	4, 8 months	Reduced gray matter density in the insula, hippocampus, precentral gyrus, and the cerebellum after four months. Progressive reductions in the frontotemporal regions after eight months. Reduced FA in the corticospinal tract and the corpus callosum after eight months.
Stampfli et al.[380]	2018	DTI	17	5.6 months	Reduced fiber density in the corticospinal tract, corpus callosum, and extra-motor region
Kassubek et al.[278]	2018	DTI	67	9 months	Decline in the FA of the corticospinal tract and frontal white matter pathways
Floeter et al.[381]	2018	DTI	11	6.4 months	Spreading of reduced FA in the frontoparietal regions; greater reductions in FA observed in C9+ ALS-FTD
Menke et al.[362]	2018	DTI, T1	13	24 months	Reduced gray matter density in frontotemporal regions, deep gray nuclei, and the precentral gyrus. Reduced FA in the corticospinal tract, corpus callosum, and frontal fibers
Shen et al.[364]	2018	DTI, T1	10	6 months	Reduced gray matter density of the precentral gyrus and thalamus. No significant change in DTI metrics
Alruwaili et al.[382]	2019	DTI	23	6 months	No significant change in DTI metrics

MRI = magnetic resonance imaging; DTI = diffusion tensor imaging; FA = fractional anisotropy; MD = mean diffusivity; ROI = region of interest; ALS-FTD = amyotrophic lateral sclerosis-frontotemporal dementia; LMN = lower motor neuron; C9+ = *C9ORF72* mutation

particularly in the later stages of their disease. This is a potential source of selection bias as only the phenotypes with less severe disability may be included in such studies.

Changes in gray matter

Progressive gray matter density reductions in the primary motor cortex have been observed in ALS in VBM studies.[316, 359, 362-364] These changes are typically observed between 6 – 12 months after the initial assessment. A study of 32 patients demonstrated that reductions are detectable even after four months and continue to progress at the eight-month mark.[359] The decline in ALSFRS-R over time in these studies does not correlate with gray matter density reductions. Interestingly, only two of the eight studies that evaluated cortical thickness of the primary motor cortex in ALS demonstrated statistically significant declines over time.[305, 359] In the first study, the mean follow-up time was greater than 12 months for nine patients, and in the second study, cortical thinning was only observed at the eight-month follow-up and not at the four-month follow-up. It is therefore conceivable that degenerative processes in ALS do not result in rapid cortical atrophy of the primary motor cortex, but rather lead to subtle alterations in the gray matter density that progress to overt atrophy. Indeed, time to the follow-up scan has been shown to correlate with the degree of cortical thinning in the percental gyrus.[305]

Progressive extra-motor gray matter damage in ALS has shown variable results. Some studies have demonstrated widespread gray matter changes encompassing the frontal, temporal, and parietal lobes, deep gray nuclei, and the cerebellum.[316, 359, 363] On the other hand, studies have also demonstrated a lack of progressive change in the extra-motor gray matter regions.[360, 361] In one study, patients were stratified based on their longitudinal motor functional decline measured by the ALSFRS-R score.[371] Patients that progressed rapidly exhibited more prominent

extra-motor change in the frontotemporal cortical regions over time after an average of nine months. This dichotomy in the extra-motor degeneration pattern is also evident in cross-sectional studies.[341] This suggests that the motor and frontotemporal cerebral degeneration is linked via network pathways and as such, increased motor impairment is accompanied by progressive frontotemporal atrophy. Furthermore, this points to the need for patient stratification to better understand the nature of progressive degenerative changes. There is some evidence that suggests that deep gray nuclei and cerebellum are also involved in progressive changes in ALS.[316, 362-364, 371] A study found progressive reduction in the volume of the thalamus over six months in participants with a *C9ORF72* gene mutation.[378] Another study found declining, but not statistically significant, volumes of deep gray structures including the caudate and putamen after a mean follow-up of 5.5 months.[376] Decreased gray matter density was observed in the caudate and thalamus after at least six months of follow-up in 27 patients with ALS.[316] Decreased volumes of deep gray structures, including structures of the limbic system, have been found to associate with poor survival and cognitive dysfunction.[357, 376]

Changes in white matter

Initial longitudinal DTI studies demonstrated no significant progressive changes in the cerebral white matter in ALS.[315, 366, 367, 370] These early studies were limited by sample sizes as some of them followed less than 10 patients over time.[365, 366, 368] Furthermore, longitudinal DTI assessments were limited to ROI-based approaches, primarily in the internal capsule.[315, 367, 368] This method precludes assessment along the length of the corticospinal tract and other white matter pathways that are affected in ALS.

Since the early studies, many reports have demonstrated longitudinal changes in the white matter in ALS. A study detected progressive decreases in FA along the corticospinal tract 6 months after the initial scan.[142] In particular, subcortical white matter and regions of the cerebral peduncles and internal capsule were affected in limb- (n = 7) and bulbar-onset ALS (n = 9). Similarly, a three time-point study identified decreased FA in the corticospinal tract after eight months and failed to do so after four months.[359] This suggests that progressive damage to the core white matter pathology is slow in ALS and perhaps well-established by the time of symptomatic disease. Clinical burden of UMN dysfunction also shows limited variability with progression of the disease, which correlates with corticospinal tract involvement.[316] The rate of decline in the FA of the corticospinal tract correlated with the rate of decline in the ALSFRS-R score;[278] however, this is not a consistent finding between studies.[361] Progressive damage to the corticospinal tract after 6 – 8 months, albeit relatively small in magnitude, has since been shown in many longitudinal DTI studies.[278, 314, 316, 359, 360, 362, 363, 372, 373] Similar progressive damage to the body and the genu regions of corpus callosum has also been reported in some studies.[142, 316, 359, 361, 362, 372, 380]

Relatively limited extra-motor white matter changes have been noted in longitudinal DTI studies. A study where 27 ALS patients were examined at least six months apart found progressive alterations in DTI metrics only in the regions of the corticospinal tract and the corpus callosum on whole-brain analysis.[316] Similar findings were found in another study that follow 32 patients with ALS over three time-points, four months apart.[359] In this study, no changes in white matter were observed at the second time-point; however, at the third time point at eight months, progressive decreases were observed in the central white matter regions pathways. Some studies have observed changes in the frontal and temporal lobes and a progressive failure of expanding

extra-motor white matter networks in ALS over time.[363, 373, 375] Recently, a longitudinal analysis in 67 patients with ALS demonstrated that 30% of the patients show an increase in the disease stage after six months according to the *in vivo* DTI staging scheme described earlier[278]. Rate of decline of the ALSFRS-R scores was also shown to correlate with rate of decreased in FA in stage-related white matter tracts. This suggests that white matter pathology slowly spreads to involve extra-motor regions. Alterations in white matter pathways in the dorsolateral prefrontal cortex and the inferior frontal gyrus have been noted in bulbar- and not in limb-onset ALS.[142] Furthermore, a study found that the expansive white matter pathology is related to patients that are positive for *C9ORF72* mutations and patients with ALS-FTD.[381]

Thus far, only six studies have investigated gray and white matter changes together in whole-brain analysis.[316, 359, 361-364] Based on these studies, it is believed that progressive structural damage to gray matter structures is prevalent even in symptomatic patients diagnosed with ALS. On the other hand, the core white matter pathology may already be established by the time patients are examined and exhibit very slow progression over time. This is corroborated by evidence of limited or no decline in the DTI measurements of the corticospinal tract even when there is a rapid deterioration in the functional status of patients.[305, 360] Two studies completed for sample size calculations for future longitudinal experiments. In one study, the number of patients with ALS needed to detect a treatment effect of 25% change in the rate of ALSFRS-R decline at 80% power and an alpha level of 0.05 was 94; in comparison, to detect the same effect in the FA of the corticospinal tract, 567 patients would have been needed.[360] In another study with 11 follow-up ALS patients, power calculations demonstrated that 46 patients would be needed to detect a longitudinal effect with 80% power at 95% alpha level.[315]

Alterations in cerebral metabolism and activity in amyotrophic lateral sclerosis

Abnormalities in cerebral metabolites

MRS is the preferred modality for probing the complex neurochemical milieu of the central nervous system. MRS techniques can quantify the concentration of various metabolites that are relevant to, or are involved in, the neuronal and gliotic structure and function. In contrast to structural MRI where protons of water molecules are of interest, MRS targets protons in other molecules, or metabolites. The most commonly studied metabolite in ALS is *N*-acetylaspartate (NAA).[280] NAA is highly specific to neurons with complex and wide-ranging roles in the nervous system, some of which include neuronal transport, neuronal peptide synthesis, and energy metabolism in the mitochondria.[383] Due to its widespread implications, levels of NAA are frequently regarded as markers for general "neuronal health". The absolute concentration of NAA in a particular region is dependent on both biological (cell type, compartments) and technical aspects such as acquisition parameters and post-processing techniques. As such, it is common practice to report NAA as a fraction of reference metabolites unaffected by disease states, such as creatine (Cr) or choline (Cho).

Within the motor cortex, levels of NAA are consistently found to be decreased in ALS.[384-386] Decreasing levels of NAA have also shown to associate with greater clinical UMN dysfunction on neurological exam[387-389] and slowed finger tapping speed.[367, 386] Importantly, decreased in NAA/Cho ratio in the motor cortex in ALS patients was associated with shorter survival in the first study that investigated neurochemical correlates of survival in this disease.[390] These findings directly implicate degeneration of the cortical UMN system to the clinical

phenotype of the disease. Similarly, NAA ratios from the corticospinal tract are known to decline in ALS when compared to controls in the centrum semiovale and the internal capsule.[391, 392] Longitudinal MRS studies in ALS remain scarce, though some reports have demonstrated progressive decline in NAA in the motor cortex.[384, 385, 393]. These studies suffer from small sample sizes for longitudinal analyses. In one study with 30 ALS patients with a follow-up assessment at 3 months, there was a non-statistically significant decline in NAA/Cr.[367] One study, however, found a subclinical increase in NAA/Cr in the motor cortex of ALS patient one day after administration of Riluzole, an anti-glutamatergic drug.[394] This finding is thought to further provide evidence for the glutamate excitotoxicity hypothesis and also suggests that subclinical cerebral changes are detectable in short time intervals. This was corroborated by a follow-up study that demonstrated sustained increases in NAA/Cr after 3 weeks in ALS patients receiving Riluzole treatment.[194] Given the modest survival benefit from Riluzole, the relevance of glutamate excitotoxicity to the overall survival in patients is questionable. However, it is clear that NAA is a dynamic marker that is sensitive to progressive cerebral changes.

Reduced NAA levels are also evident in extra-motor regions in ALS. Reports have shown declining NAA in the dorsolateral and medial prefrontal cortices, cingulate gyrus, and basal ganglia structures.[395-398] One study found abnormal NAA levels in the prefrontal cortex in ALS patients without clinical evidence of cognitive decline, providing further supporting the ALS-FTD spectrum.[398] In addition, lower NAA/Cr from the dorsolateral prefrontal cortex correlates with poorer performance in executive function tasks in ALS patients.[395, 396] Regions of the brain that are not affected in ALS, such as the parietal and occipital lobes, are spared from abnormalities in metabolite levels on MRS.[395, 396, 399] Taken together, these studies provide convincing evidence of neurochemical imbalances in the frontotemporal and deep brain

structures in ALS. Whether or not these are primary or secondary insults, however, is not yet understood.

Other metabolites including myo-inositol (mI), glutamate (Glu), and more recently gamma aminobutyric acid (GABA) have also been the subject of investigations in ALS. mI is believed to be sensitive to astrocytic proliferation, or astrocytosis, as evidenced by studies in multiple sclerosis,[400] schizophrenia,[401] and brain tumours.[402] In ALS, mI levels correlate positively with glial activation on PET imaging when measured by a radiotracer for a glial protein.[403] Although mI has not been as extensively studied as NAA in ALS, studies have shown an increase in its levels in the motor cortex.[64, 399, 404] These findings are in line with evidence of gliosis on PET imaging[74] and histology.[232] MRS studies of glutamate and GABA have reported conflicting results thus far. It should be noted that measuring these metabolites requires specialized acquisition sequences at high (3) or ultra-high field (7 tesla) magnetic field strength scanners. The paucity of this technology further renders studies to selection bias and small sample sizes. There are reports of decreased,[399] normal,[386] and increased[405] levels of glutamate in the motor cortex in ALS. Abnormalities in GABA, the primary inhibitory neurotransmitter in the brain, are of interest because there is evidence to suggest impaired inhibitory function in the motor cortex in ALS.[406] MRS studies, however, have not yet convincingly demonstrated alterations in GABA as some report reduced,[407] while others report normal[408] levels. Interestingly, however, a study using a ligand for GABA receptors in PET imaging found decreased uptake in regions of motor and prefrontal cortices.[409] It is likely that the discrepancies are contributed in large part by the diversity in acquisition and processing methodology of MRS data. More studies are needed to further the understanding of these important neurotransmitters in ALS.

A number of studies have also sought to combine MRS with other modalities to improve diagnostic ability of neuroimaging techniques to discriminate ALS patients from controls. Studies suggest that the combination of MRS and structural MRI techniques increase the diagnostic accuracy when compared to using either of the techniques in isolation. A study measuring FA of the corticospinal tract and NAA, mI, and GABA from the motor cortex found that a model combining all measures had a 93% sensitivity and 85% specificity in discriminating ALS patients from controls.[410] In comparison, using FA alone had 86% sensitivity and 70% specificity. Similarly, other studies have demonstrated a 14 – 33% improvement in diagnostic accuracy when NAA levels from the motor cortex are combined with signal intensity changes on structural images.[411, 412] Despite the early success in experimental studies, the feasibility of multimodal techniques in a clinical setting still remains poor and hinders their widespread application.

Insights from functional magnetic resonance imaging

fMRI studies have provided a unique perspective into the abnormalities in cerebral activity in ALS. fMRI relies on the blood oxygenation level-dependent (BOLD) signal in the brain. The BOLD signal is nested in the assumption that local neuronal firing, or activity, increases metabolic demands that causes a parallel increase in local blood flow. This shift in local cerebral hemodynamics increases the concentration of oxygenated hemoglobin to supply increased oxygen demands relative to deoxygenated hemoglobin, two molecules with different magnetic susceptibilities. This relative shift in the local abundance of oxygenated and deoxygenated hemoglobin species leads to a "BOLD response" that is detected by fMRI.[413] One of the earliest studies that demonstrated changes in cerebral blood flow in ALS, however, utilized PET imaging.[414] This study made two critical observations in ALS patients: (1) reduced

blood flow at rest in cortical regions associated with motor function is suggestive of absolute neuronal loss and (2) widened area of increased cortical blood flow in response to a simple motor task compared to controls is representative of cortical reorganization or compensation for the loss of motor neurons. These findings were further substantiated by evidence from fMRI studies.

Two broad categories of fMRI studies exist: task-based and resting-state. Task-based fMRI paradigms measure BOLD signal changes in response to a motor or cognitive task. Simple motor tasks, such as finger flexion and extension and button pressing, demonstrate cerebral activation in contralateral motor cortices in both ALS patients and controls.[415, 416] This represents the normal function of the human motor system; the left side of the motor homunculus (precentral gyrus) controls movements on the right side of the body and vice versa. In ALS patients, however, the recruitment of a greater cerebral cortex area, particularly of the premotor area, in response to the motor task is noted to be a consistent finding similar to the earlier PET studies.[415-418] Studies have also attempted to replicate these findings while controlling for limb weakness by designing movement imagination and action observation tasks. Similar to motor execution tasks, these studies demonstrate wider area of cortical recruitment in ALS patients compared to controls in response to movement imagination and action observation.[418-420] These findings are considered to reflect the failing inhibitory cortical drive in ALS as the neuronal activity spreads unchecked to neighbouring cortical regions. Another leading hypothesis is that the greater recruitment of cortical regions represents a compensatory mechanism secondary to motor neuron loss.[421] Further evidence supporting these hypotheses comes from studies utilizing DTI and fMRI techniques in unison. Within regions of decreased structural integrity, increased functional connectivity was noted in ALS patients compared to controls.[422] Importantly, this finding correlated positively with disease progression rate, which suggests that altered cerebral

activity may not represent a mere secondary phenomenon, but rather an active disease process related to the loss of inhibitory function.

Beside motor tasks, alterations in cerebral activity in response to cognitive tasks have also been studied in ALS. In one study, ALS patients demonstrated increased cerebral activation compared to controls in response to a Stroop effect, a measure of executive function, in the regions of the left middle and superior temporal gyri and the left anterior cingulate gyrus.[423] Similarly, another study reported increased cerebral activation in ALS patients compared to controls during social cognition and executive function tasks.[424] Increased activity in the prefrontal cortex has also been observed in ALS patients in response to an emotional regulation task, a component of social cognition.[425] In this study, the authors observed increased activation of the dorsal lateral prefrontal cortex and the anterior cingulate cortex in ALS patients in response to an emotional stimulus. It should be noted that there are studies that have also observed decreased activation during executive function[159] and social cognition tasks.[426] It is possible that these studies are capturing various timepoints in the disease pathophysiology where there are both successful and failed compensatory processes taking place over time. Longitudinal studies with sufficiently large sample sizes are therefore warranted to untangle the progression of cerebral activity in ALS with respect to specific cognitive domains.

More recently, resting-state fMRI study designs have become increasingly prevalent in ALS and other neurodegenerative disease. These studies investigate the spontaneous BOLD signal alterations in the absence of external stimuli, or during a “resting state”. Pioneering fMRI studies identified neural networks in which spatially distinct cerebral regions demonstrated consistent correlations of spontaneous and intrinsic activity at rest.[427] The most well-studied network is the default mode network (DMN).[428] The DMN is a set of brain regions that are more

active at rest than during attention-demanding tasks. This network includes the ventral medial prefrontal, dorsal medial prefrontal cortex, posterior cingulate gyrus including the precuneus, and lateral parietal cortex.[428] Another commonly studied network in ALS is the sensorimotor network. It should be noted that resting-state fMRI studies are often difficult to compare to one another because of their methodological differences. These methodical approaches can be characterized into two broad categories: data-driven and hypothesis-driven. Data-driven approaches rely on complex algorithms to parse out nonoverlapping brain networks automatically. Hypothesis-driven approaches, on the other hand, rely on *a priori* hypotheses and anatomical knowledge to define ROIs for signal analyses.

Early studies with resting-state fMRI demonstrated reduced activity in the DMN and the sensorimotor networks in ALS patients compared to controls.[429, 430] These findings are substantiated by studies that demonstrate an interhemispheric disconnect and overall decreased motor cortex activity in ALS at rest.[431] Importantly, this decline in cerebral activity was found to correlate with a decline in the limb function measured by the ALSFRS-R. On the contrary, other studies have also demonstrated increased functional activity in the motor cortex[422, 432] and in temporal and parietal regions.[433] Associations between increasing white matter damage and increased functional activity have also been observed.[422, 433] These studies proport that with progressive structural damage in the brain in ALS, more regions of the brain are recruited as a compensatory mechanism to maintain function. This also lends indirect support to the hypothesis of loss of inhibitory neurons in the disease. A recent study attempted to reconcile these differences and found no differences in the DMN between ALS patients and controls, but it showed a positive correlation between DMN connectivity and disease progression rate.[434]

Longitudinal resting-state fMRI studies are therefore needed to further explore the alterations in cerebral activity in ALS.

Texture analysis

Introduction to image texture

Texture analysis is an umbrella term that describes a range of techniques that can quantify intensity patterns and relationships between pixels in an image. It was first conceived as a method to perform pattern recognition in photographs taken from high-altitudes.[435] Over the last two decades, an increasing number of medical imaging studies have implemented texture analysis techniques for the classification and characterization of pathology. A cursory search in PubMed of terms "texture analysis" and "MRI" and "CT" (computed tomography) yields more than 1000 results from the last five years. In the following paragraphs, the discussion will focus on the application of texture analysis to structural MRI studies of the brain; however, it should be noted that texture analysis is utilized across the spectrum of medical imaging modalities including ultrasound imaging.[436] The aim of using texture analysis is usually to explore subtle changes in intensity and patterns in an image to enable the characterization of pathology with greater detail, or in some cases, to allow the detection of disease processes from seemingly normal images. To accomplish this, the following general steps are needed in a study: pre-processing, texture feature extraction, and texture feature selection.

Pre-processing. This step includes the standard procedures of quality assurance, image intensity bias correction, and image processing that are common to most structural MRI studies. For texture analysis, a further step of quantization of gray-levels is implemented. This scales images from their full dynamic range of thousands of gray-levels to between 8 – 64 gray-levels.

The purpose of quantization is to reduce redundancies in the image and computing time for later steps. It has been shown that larger dynamic ranges are not required for optimal sensitivity and specificity in the performance of texture analysis.[437] These findings are also supported by results from unpublished experiments performed locally.

Texture feature extraction. Texture analysis characterizes an image by calculating, or extracting, "texture features". The term "texture" in everyday language refers to tactile features. For example, a surface can be "rough" or "smooth" depending on its topographical profile. In MRI, "texture" refers to the variations in the distribution and relationships of gray-levels in an image. Texture of an image can similarly be regarded as "homogeneous", "heterogenous", "bright", or "dark" in lay terms depending on the degree of variation in the pixel intensities in local regions. Similar to estimating FA and MD from DTI to characterize the diffusion of water in regions of the brain, texture features provide an objective means of characterizing regions based on their intensity patterns and variations.

There are numerous approaches to extracting texture features including run-length matrix and wavelet transform.[438] A common method used in medical imaging, and one that is implemented in this dissertation, is to extract texture features from a gray-level co-occurrence matrix (GLCM).[435] This is a second-order statistical technique of quantifying texture. A GLCM is constructed by tabulating the frequency of co-occurring pixel intensity combinations in an image. It is defined as an $N \times N$ matrix where N is the total number of gray levels in the image. Each cell in the GLCM (i, j) contains the number of times the gray level i co-occurs with the gray level j in a particular direction over a specific distance. Values in each cell are then normalized by dividing them by the sum of all co-occurrences in the matrix. Figure 6 provides a schematic guide to the construction of a single GLCM from a hypothetical ROI in a T1-weighted

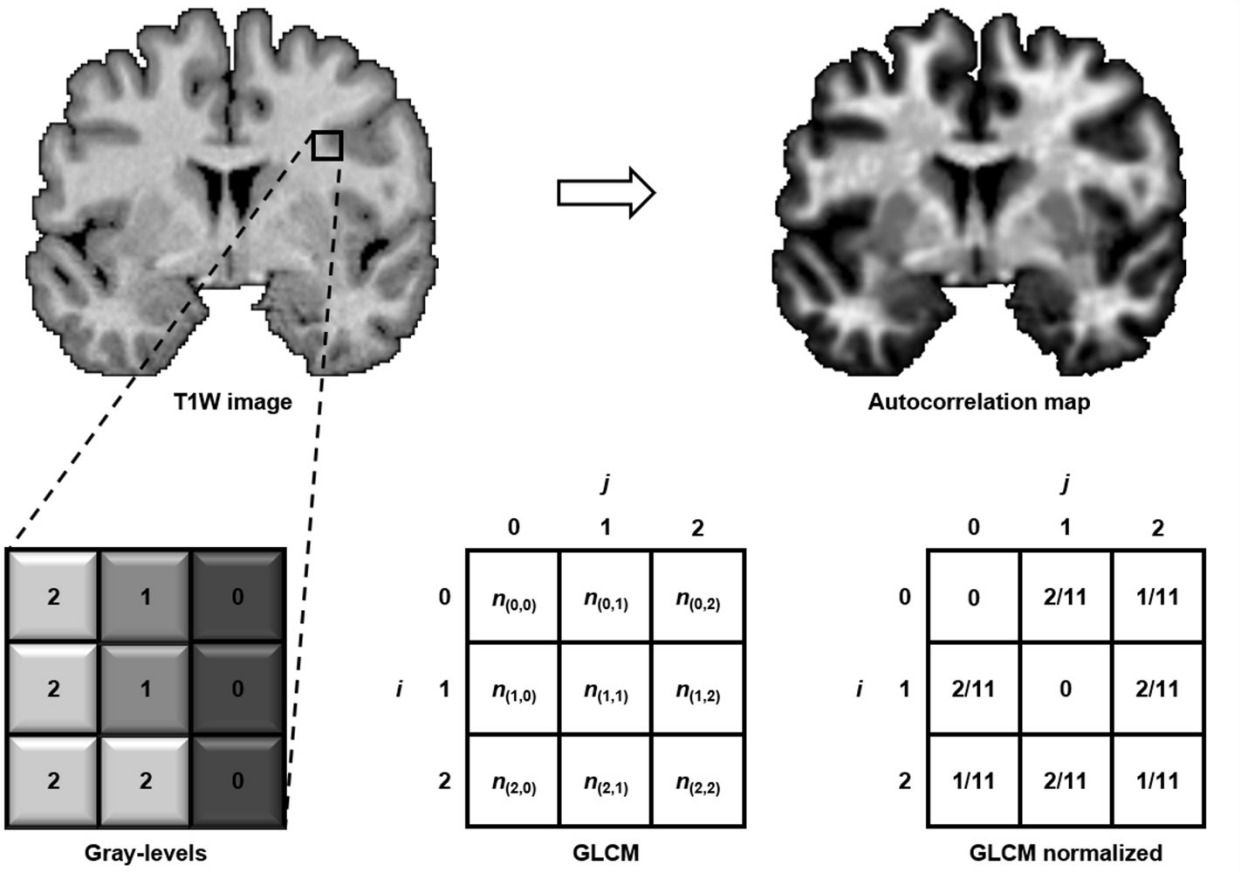

Figure 2: Schematic representation of the creation of a gray level co-occurrence matrix (GLCM) in a neighborhood of pixels in an image. Each cell in the GLCM matrix represents the number of times a certain pixel combination (i,j) co-occurs in a particular direction. In this example, the GLCM is evaluated for θ = 0° (left-right direction). Values are then normalized in the GLCM by dividing them by the sum of all co-occurrences in the GLCM. Texture feature autocorrelation is then calculated from the normalized GLCM in every direction in each orthogonal plane (i.e. in three dimensions) to produce an autocorrelation map for each T1W image. Autocorrelation is a texture feature calculated from GLCM. Areas of increased autocorrelation (hyperintensity on the maps) represent regions where there is an increased probability of co-occurrence of gray levels. Taken from Ishaque A, Mah D, Seres P, Luk C, Eurich D, Johnston W, Yang YH, Kalra S. Evaluating the cerebral correlates of survival in amyotrophic lateral sclerosis. Annals of clinical and translational neurology. 2018 Nov;5(11):1350-61.

image. GLCMs can be computed for pixel distance, $d = 1, \ldots, n$ and direction, $\theta = 0°, \pm 45°, \pm 90°, \pm 135°$, and $\pm 180°$. Several texture features can then be calculated from each combination of d and θ. Table 4 provides the derivation of commonly utilized texture features in neuroimaging literature from the GLCM method. Detailed mathematical steps are beyond the scope of this dissertation as the focus here is on the application of this texture analysis approach in ALS. For more technical details, the reader is referred to previously published literature.[435, 439, 440]

Texture feature selection. The next step is to select a texture feature, or a subset of texture features, to characterize an image or an ROI. This is undertaken to avoid overfitting and limiting high rates of false-positives in subsequent classification or discriminatory analyses. This can be accomplished with either an *a priori*, or data-driven approach. Data-driven approaches include principal component analysis[441] and Fisher coefficients;[442] these are automatic methods that require large sample sizes that outnumber the number of texture features being investigated. *A priori* methods include removing redundant texture features based on their degree of intercorrelation or selecting texture features based on prior results. *A priori* approaches consequently are at an increased risk of bias. There is currently no consensus on the optimal method of texture feature selection, and it is largely study-specific.

Table 2: Formula for commonly used GLCM-based texture features. p(i,j) in these equations is the (i,j)-th entry in the normalized GLCM

Texture feature	Formula	Description
Autocorrelation	$\sum_{i=1}^{N}\sum_{j=1}^{N}(ij)p(i,j)$	Measurement of fineness and coarseness of texture, related to the linear dependency of gray levels in a neighbourhood
Contrast	$\sum_{i=1}^{N}\sum_{j=1}^{N}(i-j)^2p(i,j)$	Measurement of the amount of gray level variation in a neighbourhood
Energy	$\sum_{i=1}^{N}\sum_{j=1}^{N}p(i,j)^2$	Measurement of the uniformity in the gray level distribution of a neighbourhood
Entropy	$-\sum_{i=1}^{N}\sum_{j=1}^{N}p(i,j)\log\left[p(i,j)\right]$	Measurement of the degree of disorder in the gray level distribution of a neighbourhood

Texture analysis in neuroimaging

The application of GLCM and other approaches of texture analysis to structural imaging techniques is predicated on the assumption that pathological processes in the brain cause subtle stereotypic alterations in pixel/voxel intensities and their relationships. When a patient suspected of suffering from a neurological condition undergoes an MRI evaluation, structural images (T1-,

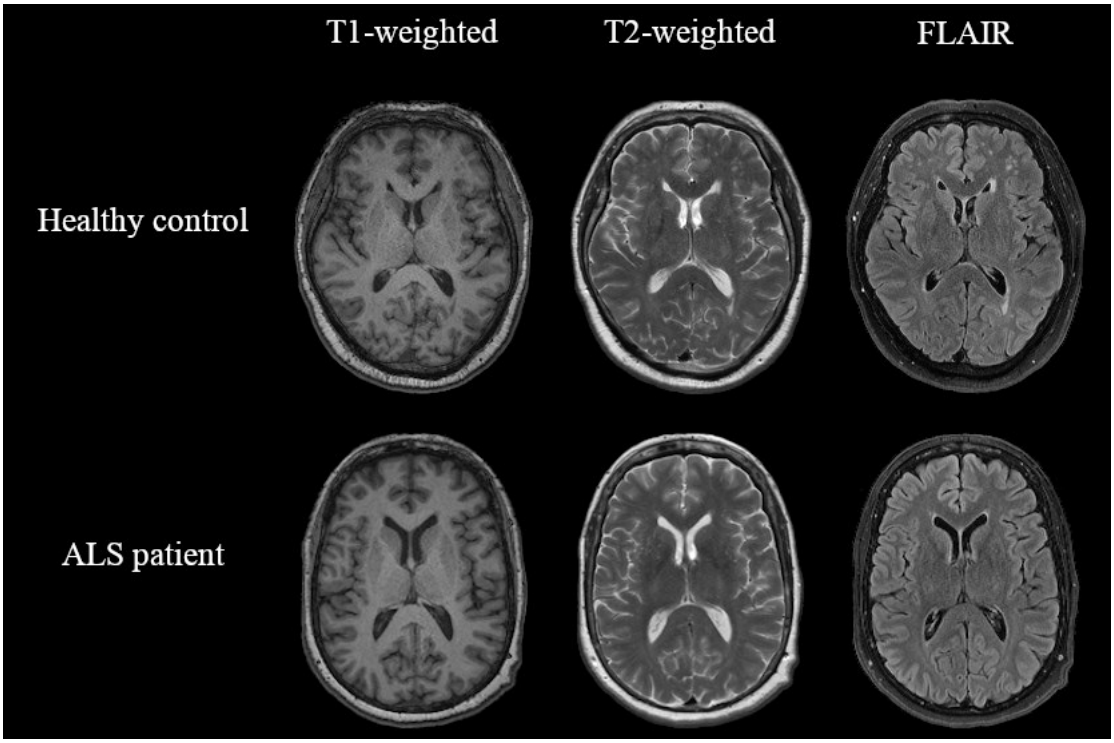

Figure 3: MRI scans of a healthy control and an ALS patient. No obvious structural differences are present between the images of these two subjects, making diagnosing ALS with clinical MRI assessment impossible. FLAIR = fluid-attenuated inversion recovery

T2-, and fluid-attenuated inversion recovery weighted) are generally acquired to rule out gross anatomical abnormalities that can explain the patient's symptomatology. Barring detecting congenital deformations, lesions, and marked global atrophy, clinical MRI sequences do not serve diagnostic or prognostic purposes for neurodegenerative disorders (Figure 7). A large body of research, however, now suggests that texture features can detect subtle signal changes in the brain in routine structural images that can be used for classification and prognostication purposes.

One of the pioneering studies of texture analysis in neuroimaging sought to evaluate the value of MRI texture features as a diagnostic marker for Alzheimer's disease.[443] The authors used GLCM texture features extracted from T1-weighted images of the brain to classify patients with Alzheimer's disease from a group of normal subjects using linear discriminant analysis. The results demonstrated that texture features correctly classified 91% of the subjects.[443] Recent ROI-

based studies have demonstrated altered texture signature in the medial temporal lobe in Alzheimer's disease.[444] Furthermore, altered GLCM-based textures from the ROIs containing the hippocampus and entorhinal cortex, regions known to be affected in the early stages of the disease,[445] correlated with worsening cognition in these patients.[444, 446] Other studies have also demonstrated similar texture abnormalities on T1-weighted images in the corpus callosum and thalamus in this disease.[446, 447] These studies point to the presence of altered texture-based signals on structural images of patients with Alzheimer's disease. A major question in the Alzheimer's disease literature revolves around the accurate prediction of patients developing the disease from mild cognitive impairment (MCI). To address this, studies have simultaneously investigated volumetric and texture measures of hippocampus to predict which patients with MCI progress to develop Alzheimer's disease.[448, 449] These studies successfully detected early texture changes in patients with MCI that who eventually progressed to having Alzheimer's disease. Importantly, these studies found that texture of the hippocampus outperformed its volume measurements at baseline in predicting the future progression.[448, 449] It was postulated that texture features are sensitive to intensity variations caused by early pathological processes, such as protein accumulation, preceding overt atrophy that is detected by volume changes.

Similarly, texture analysis using the GLCM method has been applied to multiple sclerosis in ROI-based studies.[450] Initial work focusing on *in vivo* texture alterations in the spinal cord of multiple sclerosis patients revealed significant differences when compared to normal controls.[451] Importantly, texture differences were detected between controls and relapsing-remitting multiple sclerosis patients prior to detectable atrophic changes in the spinal cord. In a longitudinal study of relapsing-remitting multiple sclerosis, texture abnormalities, particularly increased heterogeneity, were increased in new lesions, which then recovered over a course of eight

months.[452] On the other hand, texture was noted to be stable in normal appearing white matter and gradually worsening in chronic lesions. These findings suggest that texture features not only can capture static differences, but are also capable of monitoring changes over time. Due to the mathematical and often abstract nature of texture features, it is difficult to rationalize the underlying pathological forces that manifest as abnormalities in texture. Animal models of multiple sclerosis have suggested that increases in texture heterogeneity and coarse texture in structural images correspond to inflammatory and demyelinating pathology.[453, 454] This is supported by an *ex vivo* study of human post-mortem brain tissue that showed that MRI texture heterogeneity is closely associated with myelin density, followed by the degree of inflammation on histological analysis.[455] These studies provide early support of specific MRI texture-neuropathological correlations that can inform future studies.

Prior to the work presented in this dissertation, there had been two studies that investigated texture abnormalities in ALS on structure MRI using 2D manually drawn ROI.[456, 457] In the first study, the authors used texture analysis to study changes in deep structures of the brain (caudate nucleus, putamen, thalamus, and cerebral peduncles) on T1-weighted images in ALS patients. Texture was significantly altered in bilateral thalami and right caudate nucleus in ALS patients compared to controls.[456] The second study was conducted by the author of this dissertation to investigate the texture changes in ALS from T2-weighted images. Texture features were quantified from a coronal slice encompassing the motor structures (motor cortex, corticospinal tract).[457] Texture features were different between ALS patients and healthy controls and correlated with measures of clinical upper motor neuron dysfunction and functional disability. Additionally, the classification accuracy of texture features and visual assessment of

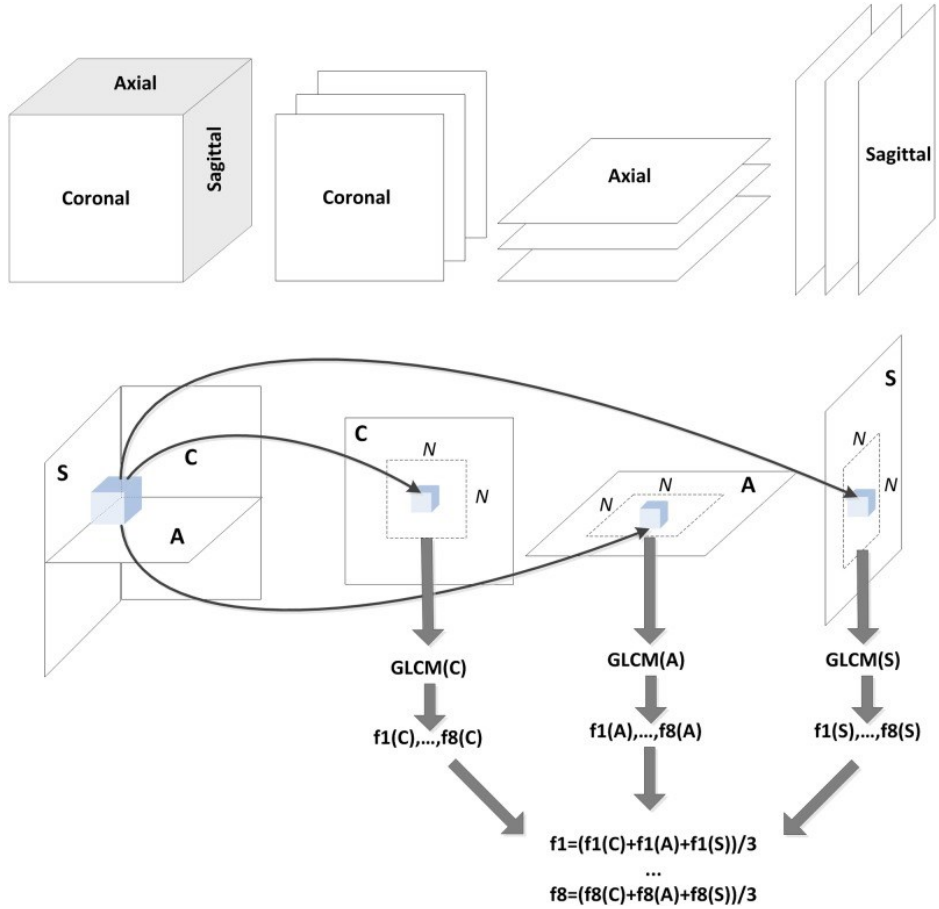

Figure 4: Schematic diagram demonstrating the three-dimensional adaptation of the GLCM technique. At each voxel, texture features are calculated in each of the three orthogonal planes and subsequently averaged to produce a texture value at the voxel. Taken from Maani R, Yang YH, Kalra S. Voxel-based texture analysis of the brain. PloS one. 2015;10(3).

the T2-weighted images by expert reviewers was tested. A model combining texture features with visual assessment showed the best performance in discriminating ALS patients from controls. This study thus provided initial support for the use of texture analysis in a clinical setting. However, due to the 2D quantification of texture features from a large section of the images, the study lacked spatial sensitivity.

Studies using GLCM-based texture analysis to analyze structure MRI thus far have been restricted to ROI-based approaches. Using this approach, texture features are quantified into numerical values from discrete regions of the brain for statistical analyses. This has several limitations: (1) inability to perform unbiased whole-brain analyses, (2) requirement of an *a priori*

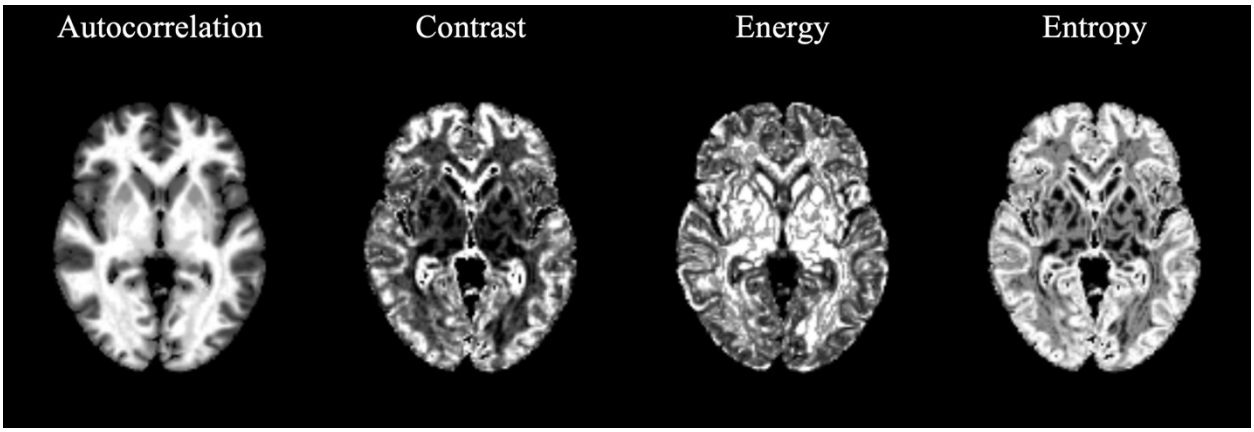

Figure 5: Three-dimensional maps of commonly used GLCM-based texture features extracted from a T1-weighted image of a healthy control.

hypothesis regarding the anatomical region to be investigated, and (3) inability to visualize texture features. To mitigate these issues, Maani et al.[440] developed a tool to generate 3D "texture maps" of GLCM texture features. These maps are created in the three orthogonal planes and allow for novel visualization and statistical analysis of texture features in a voxel-by-voxel manner, similar to VBM. In brief, this method generates a GLCM for each voxel in each of the three planes (axial, coronal, and sagittal). The texture value in each plane is averaged from all eight directions over a particular voxel distance. The final texture feature value at the particular voxel is the average of texture in the three planes. This is illustrated in Figure 8. Figure 9 provides an example of texture maps generated from a T1-weighted image. The original study validated this approach to texture analysis on T1-weighted images with artificially-created lesions and from patients with Alzheimer's disease.[440] This technique of 3D texture analysis has since been further used in the study of Alzheimer's disease where it has successfully recapitulated its classic pathological findings.[440, 448] These studies showed texture abnormalities in the regions of bilateral hippocampus, amygdala, and inferior parietal lobe in patients with Alzheimer's disease compared to healthy controls on T1-weighted images.

This novel technique was applied to ALS in a pilot study of 19 patients with ALS and 20 healthy controls.[439] T1-weighted images were acquired from all participants and subsequent whole-brain voxel-wise texture analysis was performed to assess group differences. The results revealed texture changes in the regions of the internal capsule and precentral gyrus.[439] These regions demonstrated upwards of 90% sensitivity and specificity in distinguishing participants with ALS from controls. Importantly, correlations with symptom duration and UMN dysfunction were also seen with texture of the internal capsule.[439] Thus, this proof-of-concept study uncovered the hallmark pathological gray and white matter features of ALS using an unbiased, whole-brain approach of texture analysis of T1-weighted images.

Rationale, Aims, and Hypotheses of the Dissertation

ALS is a neurodegenerative disease with a very poor prognosis. As detailed in the previous sections, the disease is complicated by its vast heterogeneity in etiology, pathogenic mechanisms, and clinical presentation. Most patients die from the illness within five years of symptom onset due to respiratory failure. There currently is no cure for the disease and clinical management is aimed at supportive therapies to improve quality of life. The only two medications currently available – Riluzole and Edaravone – provide only modest improvements to survival rates, which are in the order of two to three months.

The present lack of treatment options is not for a lack of testing new therapeutics in clinical trials. At the time of writing, there were 68 clinical trials actively recruiting for ALS around the globe according to the clinicaltrials.gov registry. Despite these efforts, however, patients continue to succumb to the relentless course of the disease. The biggest challenge facing clinical trials is the lack of objective measures that can be used as primary endpoints or to stratify patients into homogenous subgroups. The most commonly used primary endpoint is the ALSFRS-R score that subjectively assesses a patient's functional status.[125, 395, 458] Importantly, this measure is not specific to either UMN or LMN pathology. The ALSFRS-R also does not evaluate cognitive processes, which are affected to varying degrees in almost half of all patients with ALS. This tool also does not capture the complexity in the 3D progression of the disease throughout the central nervous system. Due to these reasons, it is possible that some medications fail clinical trials due to the nonspecific nature of the endpoints being used. Another challenge is that clinical trials adhere to the El Escorial criteria for inclusion of patients into their studies. As detailed above, UMN signs and symptoms are often masked by severe LMN dysfunction and some patients do not meet the criteria until they have reached advanced stages of the disease. As

such, these patients may miss their window of therapeutic opportunity and not respond to potential treatments.

An objective biomarker is therefore needed to mitigate these issues and pave the way towards better treatment and a cure for ALS. This potential biomarker can improve diagnostics in cases of unclear UMN dysfunction, potentially ameliorating the diagnostic delay. Furthermore, such a tool should also be sensitive to the longitudinal progression of the disease, both in its severity and spatial distribution. To this end, neuroimaging techniques are considered strong candidates to provide the much-needed biomarker.[283, 459] Neuroimaging allows in-depth investigations of the structure, function, and neurochemistry of the central nervous system. As detailed previously, several neuroimaging techniques including T1- and T2-weigted images, DTI, fMRI, and MRS have been extensively studied in ALS as potential biomarkers. However, no single MRI modality has so far emerged as being able provide a comprehensive measure and assessment of the *in vivo* cerebral pathology in ALS. T1- and T2-weighted images are limited by their inability to evaluate white matter changes with current analytical methods. FA of the corticospinal tracts shows only modest diagnostic capabilities. MRS studies are technically challenging to perform and are not yet widely accessible. Furthermore, sufficient longitudinal neuroimaging studies with large enough sample sizes to account for the heterogeneity in ALS have not been conducted to answer the questions regarding the progressive pathology of the disease.

3D texture analysis is a possible source of biomarkers that are sensitive to the pathology in ALS. It has so far been applied to a small dataset of T1-weight images where it detected both gray and white matter alterations in ALS with a high classification accuracy in characterizing patients with ALS and healthy controls. This 3D application was significant because it revealed

in an unbiased manner the core pathological characteristics of the disease from routine T1-weighted images. A foreseeable advantage to this technique is its ability to detect the disease process in the brain in a comprehensive manner from a single MRI modality. This has implications for clinical applications as it may enable objective diagnostic and monitoring capabilities for ALS through routine MRI assessments instead of requiring advanced or multimodal techniques. More work is needed to replicate these initial findings, delineate the biological underpinnings, and assess texture features' ability to monitor disease progression.

The rationale for this dissertation is thus born out of (1) the urgent need for an objective biomarker for ALS and (2) the limited understanding in the longitudinal progression of the disease. Texture analysis may be able to provide answers to these pressing questions. Therefore, this dissertation will seek to study ALS through texture analysis of T1-weighted images. To this end, the dissertation was designed with several overarching aims:

Aim 1: to apply 3D texture analysis in a large sample of patients with ALS. This aim will serve to confirm the findings of the pioneering study in independent, larger T1-weighted image datasets and rule out the possibility of false positive and spurious results. Furthermore, accomplishing this aim will provide evidence either for or against the sensitivity of 3D texture analysis towards the widespread cerebral degeneration seen in ALS. It is evident that ALS harbours pathology in the frontotemporal areas of the brain, and it will be investigated whether texture features are able to detect these changes in addition to the degenerative processes of the motor system.

Aim 2: to examine the clinical validity of texture features in the context of ALS. It is important to examine whether abnormalities in a biomarker are associated with clinically meaningful outcomes. It is imperative for a diagnostic biomarker for ALS to be sensitive to

subclinical pathology to enable earlier diagnosis of the disease and stratify patients in clinical trials appropriately. Additionally, the neuroanatomical correlates of survival of ALS are poorly understood. Population-based and clinical-cohort studies have provided initial insight into the possible risk factors of poor prognosis; however, direct associations between prognosis and brain structure remain yet to be elucidated. Thus, this aim will seek to evaluate whether abnormalities in MRI-based texture in patients with ALS are associated with diagnostic accuracy, clinical UMN dysfunction, and survival.

Aim 3: to examine the longitudinal progression of disease in ALS. The longitudinal pattern of the disease course in ALS is controversial. As stated above, there is no consensus regarding the disease progression in gray or white matter. The dissertation will seek to monitor patients with ALS over time with texture analysis of their T1-weighted images. This will allow the study of whole-brain pathology in an unbiased manner. Furthermore, the utility of texture features in monitoring longitudinal disease progression will be assessed and compared with clinical measures.

To accomplish these aims, a series of experiments will be performed using local datasets and data from the Canadian ALS Neuroimaging Consortium (CALNSIC). CALSNIC is a national initiative aimed at increasing the research capacity for ALS studies. It operates at research centres in Canada and the United States of America and enrolls patients with ALS and related disorders. In addition to MRI assessments, participants undergo clinical phenotyping with neurological exams and cognitive evaluations. These data were made available for the experiments in this dissertation.

It is hypothesized that (1) abnormalities in texture of T1-weighted images will be detected in the motor and the frontotemporal regions in ALS; (2) texture of the motor regions of

the brain, including the precentral gyrus and the corticospinal tract, will be associated with clinical UMN dysfunction; (3) texture abnormalities of the corticospinal tract are associated with changes in its diffusion measures (4) the presence of pathology in frontotemporal regions will be associated with worse survival in ALS; and (5) longitudinal progression in ALS will be marked by worsening of the spatial burden in gray matter and progressive degeneration of the corticospinal tract.

Chapter 3 Evaluating the Cerebral Correlates of Survival in Amyotrophic Lateral Sclerosis

* As published in *Ishaque A, Mah D, Seres P, Luk C, Eurich D, Johnston W, Yang YH, Kalra S. Evaluating the cerebral correlates of survival in amyotrophic lateral sclerosis. Annals of clinical and translational neurology. 2018 Nov;5(11):1350-61.*

Abstract

Objective: To evaluate cerebral degenerative changes in ALS and their correlates with survival using 3D texture analysis.

Methods: A total of 157 participants were included in this analysis from four neuroimaging studies. Voxel-wise texture analysis on T1-weighted brain magnetic resonance images (MRIs) was conducted between patients and controls. Patients were divided into long- and short-survivors using the median survival of the cohort. Neuroanatomical differences between the two survival groups were also investigated.

Results: Whole-brain analysis revealed significant changes in image texture (FDR $p < 0.05$) bilaterally in the motor cortex, corticospinal tract (CST), insula, basal ganglia, hippocampus, and frontal regions including subcortical white matter. The texture of the CST correlated ($p < 0.05$) with finger- and foot-tapping rate, measures of upper motor neuron function. Patients with a survival below the media of 19.5 months demonstrated texture change (FDR $p < 0.05$) in the motor cortex, CST, basal ganglia, and the hippocampus, a distribution which corresponds to stage 4 of the distribution TDP-43 pathology in ALS. Patients with longer survival exhibited texture changes restricted to motor regions, including the motor cortex and the CST.

Interpretation: Widespread gray and white matter pathology is evident in ALS, as revealed by texture analysis of conventional T1-weighted MRI. Length of survival in patients with ALS is associated with the spatial extent of cerebral degeneration.

Introduction

Amyotrophic lateral sclerosis (ALS) is a neurodegenerative disease that is characterized by progressive motor decline. It is accompanied by cognitive impairment in up to 50% of patients[1]. Clinical diagnosis requires concurrent evidence of upper and lower motor neuron (UMN and LMN) signs on physical examination. Patients have a median survival of 26 months from diagnosis, with considerable variability in longevity amongst individuals[2]. Marked clinical heterogeneity poses significant challenges to development of therapies in this disease with no curative treatment.

The identification of prognostic factors is vital for the evaluation of novel therapeutics, as they could assist in the selection of more homogeneous patient sub-types for clinical trials[3]. Older age, shorter time to diagnosis, bulbar onset, as well as the presence of comorbid cognitive deficits, particularly executive dysfunction, are regarded as negative prognostic factors in ALS[3-5].

Magnetic resonance imaging (MRI) is considered the leading tool for biomarker discovery in ALS[6]. Imaging studies have corroborated the pathological elements of neurodegeneration in ALS *in vivo*. Namely, degeneration of the motor (motor cortex and corticospinal tract (CST))[7-9] and extra-motor (frontotemporal)[7, 10] regions. Few studies have emerged that examine the role of neuroimaging in the prognostication of ALS[11-13]. These studies have associated degeneration of motor regions as predictive of survival; however, the implications of extra-motor degeneration have not yet been explored.

Despite the contributions of neuroimaging studies towards the understanding of ALS, the clinical purpose of MRI is limited to ruling out ALS-mimics. The pathological processes in the

gray and white matter—neuronal loss[14, 15], protein inclusions[16], gliosis[14, 17], and demyelination[17, 18]—cause unique alterations in the MRI signal intensity; however, these changes are inaccurately measured by current analytical methods[19, 20].

Texture analysis of MR images has been utilized to detect and characterize cerebral changes on routine MRI scans[21]. It is a quantitative approach that can detect subtle local signal intensity and pattern variations in an image. In focal cortical dysplasia, texture analysis techniques have demonstrated superior classification accuracy when compared to visual inspection[22]. Studies in multiple sclerosis have identified the pathological correlates of altered texture on T2-weighted (T2W) MRI[23]. In an initial study of 19 patients, a 3-dimensional (3D) texture analysis approach localized changes in the CST and the motor cortex from T1W images in ALS[24].

The objectives of this work are two-fold: (1) to evaluate the spatial distribution of cerebral degeneration in a large cohort of patients with ALS as reflected by changes in texture of T1W images, and (2) to investigate the neuroanatomical correlates of survival with texture. Based on the previous literature, it was hypothesized that (1) texture analysis will detect motor and extra-motor pathology, and (2) it will demonstrate differences in the spatial distribution of cerebral degeneration between long- and short-surviving patients. The successful application of texture analysis in ALS could aid in detecting pathological changes on conventional MRI and provide prognostic indicators with clinical relevance.

Methods

Participants

Participants were recruited from the University of Alberta between 2003 and 2018 as part of four different prospective MRI studies (herein referred to as Study 1, 2, 3, and 4). Patients with ALS were recruited for these studies from a multidisciplinary ALS clinic if they had no history of other neurological or psychiatric disorders. Healthy controls with no neurological or psychiatric disorders were also recruited in each of the four studies. All participants provided informed written consent prior to their involvement in their respective studies, which were approved by the local research ethics review board.

Patients had UMN and LMN signs on clinical examination and met criteria for possible, probable lab-supported, probable, or definite ALS according to the El Escorial criteria[25]. Patients with frontotemporal dementia (FTD), or those with a family history of ALS were also included. All patients underwent neurological assessments according to their specific study protocol. For the present work, UMN examination data was included for analysis. Patients from Study 2, 3, and 4 had performed finger- and foot-tapping tests as a measure of their UMN function. Finger- and foot-tapping rates were calculated by averaging the total number of taps in 10 seconds over two trials. Scores from the left and right side were averaged to give a single score for each patient's finger- and foot-tapping rate. Patient's functional disability was measured using the ALS functional rating scale-revised (ALSFRS-R). The scale ranges from 0 to 48, with lower scores reflecting greater disability. Two patients were assessed using the ALSFRS (range 0 – 40), an older version that does not assess respiratory symptoms. Symptom duration was recorded as the date from their reported onset of symptoms to the date of their MRI scan. Disease progression rate was calculated by (48 – patient ALSFRS-R score)/symptom duration for every

patient. For the two patients with ALSFRS scores, disease progression rate was calculated as (40 – patient ALSFRS score)/symptom duration.

MRI protocols

Participants in Study 1 and 2 were scanned in a Siemens 1.5 T scanner, and participants in Study 3 and 4 were scanned on a Siemens 3 T and a Varian 4.7 T scanner, respectively. T1W images for all participants were acquired with a 3D magnetization-prepared rapid gradient-echo sequence. The images in Study 1, 3, and 4 were acquired axially and images for Study 2 were acquired coronally (Table 1).

Image processing and texture analysis

Image processing and subsequent voxel-wise analyses were conducted in Statistical Parametric Mapping 12 version 6685 (SPM12; http://www.fil.ion.ucl.ac.uk/spm/software/spm12/) and Computational Anatomy Toolbox 12.1 (CAT12; http://dbm.neuro.uni-jena.de/cat12/). T1W images were first assessed for quality assurance, which included a visual check for subject motion and scanner artifacts. They were then aligned along the anterior and posterior commissures to ensure anatomical alignment across participants for 3D texture analysis and image registration procedures. Images were corrected for non-uniformity intensity bias and segmented into gray and white matter in their native space. The gray and white matter segments were combined to create a custom whole-brain mask for each participant. T1W images were normalized using a high-dimensional approach[26] to the Montreal Neurological Institute (MNI) template provided by CAT12—the forward deformation fields were saved for later transformations into the standard space. Normalized gray matter

segments were smoothed with a 6 *mm* full-width at half maximum (FWHM) Gaussian kernel for statistical analyses.

Texture analysis was performed using the gray level co-occurrence matrix (GLCM) method, a second-order statistical approach for extracting texture features[21, 27]. Methodological details regarding the 3D adaptation of GLCM to generate 3D texture maps from T1W images are provided elsewhere[28]. Briefly, the GLCM was defined for each voxel and its adjacent voxels (referred to as the reference voxel and its neighbourhood) in all three orthogonal planes for a T1W image. A GLCM is an $N \times N$ matrix, where N is the total number of gray levels in an image. To reduce computation time, T1W images were scaled down to 8 gray levels. Each cell in the GLCM (i,j) specifies the number of times gray level i co-occurs with gray level j over a distance d and in a particular direction θ within the neighbourhood. In this study, a distance of one and four directions—0°, 45°, 90°, and 135°—were considered for the construction of the GLCMs. The GLCMs for all four directions were summed and normalized to represent the probability of co-occurrence between gray levels in the neighbourhood. This was carried out in the axial, coronal, and sagittal planes to generate three GLCMs per voxel. A texture feature could then be calculated from the GLCMs and averaged over the three planes to compute a single 3D texture value for each voxel. Figure 1 illustrates a schematic representation of the creation of the GLCM.

In this work, whole-brain autocorrelation maps were computed from the GLCMs of T1W images. The texture feature autocorrelation has been shown to be sensitive to cerebral degeneration in ALS and in Alzheimer's disease using 3D texture analysis[24, 28]. It can be best understood as a measure of the linear dependency in the gray level, or as being sensitive to repetitive patterns in pairs of gray levels in a local neighbourhood; the higher the autocorrelation

value, the higher the likelihood that a pair of gray levels will co-occur. Autocorrelation is calculated as follows:

$$Autocorrelation = \sum_{i=1}^{N}\sum_{j=1}^{N}(ij)p(i,j)$$

where $p(i,j)$ is the probability of co-occurrence between gray levels i and j in a neighbourhood. The texture maps were normalized to the MNI template by applying the forward deformation fields obtained earlier and smoothed with a 6 *mm* FWHM Gaussian kernel for statistical analyses.

Statistical analysis

All statistical tests were conducted in MedCalc Statistical Software version 18.2.1 (MedCalc Software bvba, Ostend, Belgium; http://www.medcalc.org). One-way analysis of variance (ANOVA) was used to ensure participant demographic characteristics did not differ between the MRI studies. Demographic differences between patients and controls were assessed with independent samples *t*-tests and χ^2 tests. Statistical significance was defined at $p < 0.05$. Whole-brain voxel-wise analyses were performed in SPM12 for the normalized and smoothed texture maps. Statistical significance was defined as $p < 0.05$ after correcting for multiple comparisons with the false discovery rate (FDR) method with a cluster size of 10 voxels. A second-level full factorial model was designed to examine whole-brain voxel-wise differences in autocorrelation between patients and controls while controlling for age, sex, and MRI protocol. Autocorrelation values from significant clusters in the motor regions were extracted and correlated with finger- and foot-tapping scores. Partial correlations were used to control for MRI protocol and statistical significance was defined at $p < 0.05$. Voxel-based morphometric (VBM)

analysis of gray matter density was also conducted for comparison with texture analysis. A threshold mask of 0.2 was applied to the gray matter segments to exclude noise and other tissue classes from the analysis. The full factorial model additionally controlled for total intracranial volume to control for differences in head sizes[29].

Patients were dichotomized at their median survival into long- and short-surviving patients. The two groups' texture maps were directly compared using a second-level full factorial model while controlling for age and MRI protocol. Additional models compared autocorrelation in long-surviving patients with controls and short-surviving patients with controls. Patients' five-year survival analysis using Cox proportional-hazards regression models was conducted in MedCalc. Univariate and stepwise multivariate models were carried out with age, sex, site of onset, ALSFRS-R score, symptom duration, and disease progression rate as covariates. Survival was defined as the time from the T1W scan to death. Patients were censored if they were alive at the time of the analysis or lost to follow-up.

Results

Demographics

A total of 157 participants (patients = 83, controls = 74) with T1W images were included in this study. Patients' mean age, symptom duration, ALSFRS-R score, and progression rate did not differ between the 4 MRI studies. Patients' mean age (58.7 ± 10.8 years) did not differ significantly from controls' mean age (55.8 ± 11.3 years). There were 50 male and 33 female patients, and 31 male and 43 controls (χ^2 $p < 0.05$). 76.8% of the patients had limb onset and 23.2% of the patients had bulbar onset. One patient did not have information regarding their site of onset. Three patients had concomitant FTD on clinical examination. The mean ALSFRS-R

score was 38.7 ± 5.6. Two patients completed the ALSFRS and had scores of 29 and 25. The mean and median symptom duration were 22.9 ± 15.4 months and 17.3 months (range 2 – 86 months), respectively. The mean and median disease progression rates were 0.67 ± 1.08 and 0.41 (range 0.07 – 9.09), respectively.

Texture differences between patients and controls

Significant regional differences in autocorrelation were observed in the whole-brain voxel-wise analysis (FDR $p < 0.05$). Autocorrelation was decreased in patients in bilateral motor cortex, insula, prefrontal cortex, bilateral hippocampus, thalamus, caudate, cingulate gyrus, and subcortical frontal regions (Figure 2A, Supplementary Figure 1). Autocorrelation was increased in the CST in patients bilaterally (Figure 2B, Supplementary Figure 1). No other regions of increased autocorrelation were observed. An *F*-test was conducted to ensure that these voxel-wise group differences were not biased by an interaction effect caused by the different MRI studies. No interaction effect was found between the main effect of group and the main effect of studies on autocorrelation (FDR $p < 0.05$). Additionally, supplementary whole-brain voxel-wise analyses were repeated separately for studies that acquired images at different resolutions to ensure the heterogeneity in voxel sizes did not impact the results. Study 1 and 2 were analyzed separately and Study 3 and 4 were pooled together because their images were acquired at 1 x 1 x 1 mm^3 (Table 1). The results are reported in Supplementary Figure 2.

Correlation between UMN function and texture

Autocorrelation values were extracted from patients in Study 2, 3, and 4 from the significant clusters of between-group differences in the motor cortex and the CST region. Finger-tapping scores were available for 55 patients and foot-tapping scores were available for 53

patients. Significant correlations ($p < 0.05$) were found between autocorrelation values from the CST and finger- ($r = -0.28$) and foot-tapping scores ($r = -0.31$) (Figure 3). No significant correlations were found between autocorrelation values from the motor cortex and either tapping scores.

Gray matter density differences between patients and controls

Significant reductions in gray matter density were detected in patients in the whole-brain VBM analysis. Gray matter density was decreased bilaterally in the motor cortex, gyrus rectus, and frontal gyri (Figure 4). The thalamus, cingulate gyrus, and the insula also demonstrated reductions in gray matter density (Figure 4).

Regional gray matter density reductions did not completely overlap changes in autocorrelation. Notably, gray matter density was not reduced in the hippocampi of patients, even at lower statistical thresholds (uncorrected $p < 0.001$). Changes in the lateral motor cortex were evident in gray matter density and autocorrelation values; however, only autocorrelation demonstrated reductions in the medial motor cortex region. Furthermore, gray matter density was reduced largely in the anterior subsection of the insula, whereas autocorrelation was reduced more extensively in its anterior and posterior subsections.

Survival analysis

One patient had missing survival information and was excluded from this analysis ($n = 82$). The mean time from MRI scan to outcome did not differ significantly between MRI studies. At the time this analysis was performed, 64 patients had died, and 18 patients were censored (17 alive and one lost to follow-up). The median survival was 19.5 months, which was used to dichotomize patients into long- and short-survivors (Table 2). Long-survivors had a mean

survival of 40.3 ± 24.6 months, whereas short-survivors had a mean survival of 11.9 ± 5.1 months. Short-survivors were significantly older (62.0 ± 10.3 years) than long-survivors (55.2 ± 10.3 years) at the time of the MRI scan. The two groups did not differ on any other demographic detail.

Relative to controls, the two groups of patients demonstrated significant differences in autocorrelation (FDR $p < 0.05$). Long-survivors displayed bilateral decreases in the motor cortex and increases in the region of the CST in comparison with controls (Figure 5A). Small significant clusters of decreased autocorrelation values were observed in the frontal regions. No differences were noted in the hippocampi, insula, or basal ganglia.

Short-survivors had significantly decreased autocorrelation values in bilateral motor cortex and frontal regions. In contrast to the long-survivor group, reductions were also found in the insula right hippocampus, and thalamus (Figure 5B). Comparable to the long-survivor group, autocorrelation was significantly increased in the CST in short-survivors, although this was reported at a lower statistical threshold (uncorrected $p < 0.001$). A direct comparison between long- and short-survivors did not reveal significant regional differences in autocorrelation.

Patients' age, sex, site of onset, ALSFRS-R score, symptom duration, and progression rate were evaluated as predictors of five-year survival in univariate and multivariate models. Univariate analysis revealed age (HR = 1.04, 95% confidence interval (CI) = 1.01 – 1.06, $p = 0.01$) and symptom duration (HR = 0.98, 95% CI = 0.97 – 1.00, $p = 0.03$) as significant predictors of survival. The multivariate model also selected older age (HR = 1.05, 95% CI = 1.02 – 1.08, $p < 0.01$) and shorter symptom duration (HR = 0.98, 95% CI = 0.96 – 0.99, $p < 0.01$) as significant predictors when all the variables were entered in the model and selected with the stepwise method.

Discussion

In this work, an unbiased whole-brain texture analysis approach was used to study cerebral degeneration in ALS and its impact on survival. Confirming the first hypothesis, both gray and white matter structures of motor and extra-motor regions demonstrated texture differences between patients and controls. Affected gray matter regions closely mirrored the neuroanatomical pattern of pathological TDP-43 inclusions in ALS[16] and the involvement of the CST resembled the hallmark pathology of the disease[17]. Secondly, shorter survival was associated with changes in the extra-motor regions, particularly the basal ganglia and hippocampus. This suggests that survival is potentially mediated by the spatial burden of pathology in ALS. These findings are further discussed below.

Texture analysis and pathology of ALS

Autocorrelation was found to be altered in patients in the motor (motor cortex and CST) and extra-motor regions (frontal, temporal, and subcortical structures). This is in accordance with the view that ALS is a multisystem neurodegenerative disease. Loss of pyramidal neurons in layer V of the motor cortex[14, 15] and ubiquitin-reactive cytoplasmic inclusions in the frontal and temporal regions are consistent pathological features of the disease[16, 18]. In addition, ALS is regarded as a disorder on the larger ALS-FTD spectrum with the identification of the pathological TDP-43 inclusions as the unifying disease protein[30]. Subsequent *in vivo* MRI studies have found similar pathological involvement of gray and white matter structures in the frontal and temporal regions[7, 9].

Autocorrelation was decreased in the motor cortex, frontal regions, basal ganglia structures, and the hippocampus. This spatial pattern is in alignment with the progressive TDP-

43 pathology in ALS[16]. Interestingly, VBM analysis did not detect change in the hippocampus at an identical statistical threshold, consistent with previous VBM studies [7, 10]. Ubiquitin-positive inclusions have been documented on histology in the granular cell layer of the hippocampus in ALS[31]. This feature is not only seen in cases of ALS with clinical dementia, but also in patients without clinical evidence of dementia[32, 33]. Furthermore, TDP-43 inclusions in the hippocampus are characterized as the final pathological stage of the disease[16]. It could be hypothesized that texture analysis is detecting imaging correlates of TDP-43 inclusions in the gray matter that precede atrophic changes that are eventually detectable by VBM analysis. Indeed, in a recent longitudinal study, patients had demonstrable hippocampal atrophy at two-year follow-up[34]. This view is further supported from studies in Alzheimer's disease that suggest that texture analysis is a marker for pre-atrophy amyloid beta plaque accumulation in the hippocampus because of its sensitivity to the subtle pathological variation in the MRI signal caused by the inclusions[35].

The CST demonstrated pronounced increases in autocorrelation in patients along with correlations with UMN function. Pathological demyelination and gliosis of the CST in ALS have been well documented in autopsy[14, 17, 18] and in *in vivo* MRI studies[8]. It is postulated that T1W hyperintensity, otherwise known as T1-shortening, along the CST may be due to the pathological changes including the presence of lipid-laden macrophages and accumulation of intra-axonal neurofilaments[36]. The involvement of the corpus callosum is also a frequent finding in diffusion tensor imaging (DTI) studies and is proposed to be characteristic of Wallerian-type degeneration[37]; however, systematic neuropathological evaluations of the corpus callosum are lacking to support that view. Few autopsy reports have provided initial support for gliosis, but not a demyelinating pathology in the corpus callosum[38, 39]. Phosphorylated TDP-43 inclusions, which are considered a hallmark pathological feature of ALS[16], are also reportedly absent in the

corpus callosum[40]. The corpus callosum did not exhibit any degenerative changes with texture analysis in this study. The contributions of the pathological mechanisms towards the increase in autocorrelation in the CST, but not in the corpus callosum cannot be concluded from this work. It can be speculated that autocorrelation is detecting a specific pathology of the CST, which is not present extensively in the corpus callosum; however, MRI-histological studies are needed to investigate the relationship between textures and the underlying pathological processes. One such study in multiple sclerosis demonstrated that heterogeneity in MRI texture was predictive predominantly of demyelinating pathology, followed by axonal injury, and inflammation[41].

Neuroanatomical correlates of survival in ALS

Survival analysis showed that shorter survival is associated with greater gray matter degeneration. Compared to patients with longer survival, those with shorter survival additionally had degenerative changes in the insula, subcortical frontal white matter, thalamus, and hippocampus. Dysfunction of the insula has been implicated as a contributing factor to verbal-fluency deficits[42], which typify the overall executive dysfunction in ALS[43]. Systematic investigations of the sub-cortical structures have also revealed the involvement of the thalamus and the hippocampus, including its relation to memory-deficits, in ALS[44-46]. Thus, the extra-motor changes in short-survivors potentially reflect the extra-motor phenotype of the disease. Indeed, there is a growing body of evidence that suggests that the presence of comorbid FTD, or executive dysfunction in the absence of other cognitive deficits, are predictors of poor survival in ALS[4, 5].

Recently, Brettschneider et al. proposed a neuropathological staging system in ALS based on the sequential spatial burden of intraneuronal phosphorylated TDP-43 inclusions[16]. Lowest burden of TDP-43 pathology was characterized by inclusions in the motor cortex (stage

1), followed by inclusions in the prefrontal neocortex, precerebellar nuclei, and red nuclei (stage 2)[16]. Later stages included TDP-43 inclusions in the striatum (stage 3) and the hippocampi (stage 4)[16]. It is noteworthy that based on this staging scheme, short-survivors demonstrated regions from all four stages of the disease, including the hippocampus, whereas long-survivors did not demonstrate late-stage structures. Patients in stage 4 also have been shown to have memory deficits associated with hippocampus and perforant pathway degeneration[47, 48]. These results strongly suggest that survival is associated with the spatial burden of the cerebral degeneration in ALS. Initial support for this comes from a large autopsy study that demonstrated that ALS cases with temporal lobe involvement, specifically in the hippocampus, had significantly reduced survival and invariant UMN involvement compared to cases with only UMN involvement[18]. Pending replication and further validation of these findings, future clinical trials evaluating novel therapeutics in ALS should consider prospectively subgrouping patients into short and long disease course patients based on the involvement of extra-motor structures using texture analysis.

Age and symptom duration were associated with shorter survival in this study, which is in accordance with the current literature[3]. There are only three studies in the literature that have investigated *in vivo* cerebral degeneration as a predictor of survival in ALS[11-13]. The first study testing this utilized magnetic resonance spectroscopy of the motor cortex and found N-acetylaspartate/choline ratio, a marker for neuronal loss, to be a significant predictor of survival (HR = 0.24, 95% CI = 0.08 – 0.72, $p = 0.01$)[11]. The second investigated white matter involvement with DTI and identified fractional anisotropy of the CST as a significant predictor of survival (HR = 0.94, 95% CI = 0.89 – 1.00, $p = 0.06$)[12]; however, this study had a small number of patients ($n = 24$) and more than 50% of them were censored at the time of analysis[12]. Finally, the third study evaluated MRI measures of cortical and white matter motor structures

along with clinical indices including age and ALSFRS-R to predict 18-month survival[13]. The study demonstrated that the combination of MRI measures and clinical indices had better predictive accuracy (79.15%) than using clinical indices alone (66.67%); however, the results were not replicated in an independent, albeit small, validation sample[13]. In this work, no overt differences in the degree of motor region involvement between the two survival groups were found and short-survivors displayed more widespread degeneration when compared to controls. Previous studies have not evaluated the influence of extra-motor degeneration on survival in ALS. Incorporating extra-motor regions and multimodal data likely would improve the accuracy of survival models.

Summary and study limitations

Results here suggest that the spatial extent of cerebral involvement is an important prognostic factor, with involvement of extra-motor regions leading to a worse outcome. This conclusion was achieved with the largest study to date in ALS that investigated *in vivo* neuroanatomical correlates of survival. The findings reported in this work indicate that 3D texture analysis of T1W images is efficacious in detecting pathological cerebral changes in ALS. This is an important step towards the development of cerebral markers of the disease. Texture features could play a role in detecting varying neurobiological processes that can lead to the identification of patient subtypes *in vivo*; a biomarker with this property could play a critical role in patient selection in clinical trials.

There are limitations to this study. First, this was an analysis utilizing a large heterogenous dataset. Although the potential effect of MRI protocols on autocorrelation was statistically controlled for and no demographic differences in the patient and control populations from the different studies were found, future studies should be performed on homogenously

acquired data. Conversely, however, the heterogeneity of the data in light of the results also supports the clinical relevance and the robustness of texture analysis. Second, as the clinical datasets were not uniform between studies, correlations with clinical measures including cognitive assessments could not be performed. Lastly, though the regional group differences in autocorrelation between patients and controls and patients of long and short survivorship are in accordance with the current understanding of the pathology in ALS, little is understood about the histopathological basis of these findings. Future studies should further validate texture analysis in ALS with clinical and cognitive assessments and histological studies.

Acknowledgements

The authors would like to thank the participants and their families. This study was supported by funding from ALS Society of Canada, the ALS Association of America, the Canadian Institutes of Health Research, Brain Canada, the MSI Foundation, and the Shelly Mrkonjic ALS Research Fund. Data was made available in part from the Canadian ALS Neuroimaging Consortium (CALSNIC), for which data management and quality control was facilitated by the Canadian Neuromuscular Disease Registry (CNDR).

Author contributions

A. I. contributed to the conception and design of the study, analysis of data, and drafting of the manuscript and figures; S.K., D.M., P.S., C.L., and W.J. contributed to the acquisition of data; D.E., contributed to analysis of data; and Y.Y. and S.K. contributed to the conception and design of the study.

Conflicts of interest

Nothing to report.

References

1. Ringholz G, Appel S, Bradshaw M et al. Prevalence and patterns of cognitive impairment in sporadic ALS. Neurology 2005;65(4):586-590.

2. Pupillo E, Messina P, Logroscino G, Beghi E. Long-term survival in amyotrophic lateral sclerosis: A population-based study. Ann Neurol 2014;75(2):287-297.

3. Chiò A, Logroscino G, Hardiman O et al. Prognostic factors in ALS: A critical review. Amyotrophic Lat Scler 2009;10(5-6):310-323.

4. Olney R, Murphy J, Forshew D et al. The effects of executive and behavioral dysfunction on the course of ALS. Neurology 2005;65(11):1774-1777.

5. Elamin M, Phukan J, Bede P et al. Executive dysfunction is a negative prognostic indicator in patients with ALS without dementia. Neurology 2011;76(14):1263-1269.

6. Turner MR, Grosskreutz J, Kassubek J et al. Towards a neuroimaging biomarker for amyotrophic lateral sclerosis. Lancet Neurol 2011;10(5):400-403.

7. Chang JL, Lomen-Hoerth C, Murphy J et al. A voxel-based morphometry study of patterns of brain atrophy in ALS and ALS/FTLD. Neurology 2005;65(1):75-80.

8. Pyra T, Hui B, Hanstock C et al. Combined structural and neurochemical evaluation of the corticospinal tract in amyotrophic lateral sclerosis. Amyotrophic Lat Scler 2010;11(1-2):157-165.

9. van der Graaff, Maaike M, Sage CA, Caan MW et al. Upper and extra-motoneuron involvement in early motoneuron disease: A diffusion tensor imaging study. Brain 2011;134(4):1211-1228.

10. Agosta F, Pagani E, Rocca M et al. Voxel-based morphometry study of brain volumetry and diffusivity in amyotrophic lateral sclerosis patients with mild disability. Hum Brain Mapp 2007;28(12):1430-1438.

11. Kalra S, Vitale A, Cashman NR et al. Cerebral degeneration predicts survival in amyotrophic lateral sclerosis. Journal of Neurology, Neurosurgery and Psychiatry 2006;77(11):1253-1255.

12. Agosta F, Pagani E, Petrolini M et al. MRI predictors of long-term evolution in amyotrophic lateral sclerosis. Eur J Neurosci 2010;32(9):1490-1496.

13. Schuster C, Hardiman O, Bede P. Survival prediction in amyotrophic lateral sclerosis based on MRI measures and clinical characteristics. BMC neurology 2017;17(1):73.

14. Kawamata T, Akiyama H, Yamada T, McGeer PL. Immunologic reactions in amyotrophic lateral sclerosis brain and spinal cord tissue. Am J Pathol 1992;140(3):691-707.

15. Nihei K, McKee AC, Kowall NW. Patterns of neuronal degeneration in the motor cortex of amyotrophic lateral sclerosis patients. Acta Neuropathol 1993;86(1):55-64.

16. Brettschneider J, Del Tredici K, Toledo JB et al. Stages of pTDP-43 pathology in amyotrophic lateral sclerosis. Ann Neurol 2013;74(1):20-38.

17. Lawyer T, Netsky MG. Amyotrophic lateral sclerosis: A clinicoanatomic study of fifty-three cases. AMA Archives of Neurology & Psychiatry 1953;69(2):171-192.

18. Piao Y, Wakabayashi K, Kakita A et al. Neuropathology with clinical correlations of sporadic amyotrophic lateral sclerosis: 102 autopsy cases examined between 1962 and 2000. Brain pathology 2003;13(1):10-22.

19. Hecht M, Fellner F, Fellner C et al. MRI-FLAIR images of the head show corticospinal tract alterations in ALS patients more frequently than T2-, T1-and proton-density-weighted images. J Neurol Sci 2001;186(1):37-44.

20. Hecht M, Fellner F, Fellner C et al. Hyperintense and hypointense MRI signals of the precentral gyrus and corticospinal tract in ALS: A follow-up examination including FLAIR images. J Neurol Sci 2002;199(1):59-65.

21. Kassner A, Thornhill RE. Texture analysis: A review of neurologic MR imaging applications. AJNR Am J Neuroradiol 2010;31(5):809-816.

22. Bernasconi A, Antel SB, Collins DL et al. Texture analysis and morphological processing of magnetic resonance imaging assist detection of focal cortical dysplasia in extra-temporal partial epilepsy. Ann Neurol 2001;49(6):770-775.

23. Zhang Y, Moore G, Laule C et al. Pathological correlates of magnetic resonance imaging texture heterogeneity in multiple sclerosis. Ann Neurol 2013;74(1):91-99.

24. Maani R, Yang Y, Emery D, Kalra S. Cerebral degeneration in amyotrophic lateral sclerosis revealed by 3-dimensional texture analysis. Frontiers in neuroscience 2016;10:120.

25. Brooks BR, Miller RG, Swash M, Munsat TL. El escorial revisited: Revised criteria for the diagnosis of amyotrophic lateral sclerosis. Amyotrophic Lat Scler 2000;1(5):293-299.

26. Ashburner J. A fast diffeomorphic image registration algorithm. Neuroimage 2007;38(1):95-113.

27. Haralick RM, Shanmugam K. Textural features for image classification. IEEE Trans Syst Man Cybern 1973(6):610-621.

28. Maani R, Yang YH, Kalra S. Voxel-based texture analysis of the brain. PLoS One 2015;10(3).

29. Malone IB, Leung KK, Clegg S et al. Accurate automatic estimation of total intracranial volume: A nuisance variable with less nuisance. Neuroimage 2015;104:366-372.

30. Neumann M, Sampathu DM, Kwong LK et al. Ubiquitinated TDP-43 in frontotemporal lobar degeneration and amyotrophic lateral sclerosis. Science 2006;314(5796):130-133.

31. Okamoto K, Hirai S, Yamazaki T et al. New ubiquitin-positive intraneuronal inclusions in the extra-motor cortices in patients with amyotrophic lateral sclerosis. Neurosci Lett 1991;129(2):233-236.

32. Mackenzie IR, Feldman H. The relationship between extramotor ubiquitin-immunoreactive neuronal inclusions and dementia in motor neuron disease. Acta Neuropathol 2003;105(2):98-102.

33. Stewart H, Rutherford NJ, Briemberg H et al. Clinical and pathological features of amyotrophic lateral sclerosis caused by mutation in the C9ORF72 gene on chromosome 9p. Acta Neuropathol 2012;123(3):409-417.

34. Menke R, Proudfoot M, Talbot K, Turner M. The two-year progression of structural and functional cerebral MRI in amyotrophic lateral sclerosis. NeuroImage: Clinical 2018;17:953-961.

35. Sørensen L, Igel C, Liv Hansen N et al. Early detection of alzheimer's disease using MRI hippocampal texture. Hum Brain Mapp 2016;37(3):1148-1161.

36. Waragai M. MRI and clinical features in amyotrophic lateral sclerosis. Neuroradiology 1997;39(12):847-851.

37. Filippini N, Douaud G, Mackay CE et al. Corpus callosum involvement is a consistent feature of amyotrophic lateral sclerosis. Neurology 2010;75(18):1645-1652.

38. Murray C, Viehman A, Lippa CF. The corpus callosum in pick's disease, alzheimer's disease, and amyotrophic lateral sclerosis: Gliosis implies possible clinical consequence. American Journal of Alzheimer's Disease & Other Dementias® 2006;21(1):37-43.

39. Sugiyama M, Takao M, Hatsuta H et al. Increased number of astrocytes and macrophages/microglial cells in the corpus callosum in amyotrophic lateral sclerosis. Neuropathology 2013;33(6):591-599.

40. Fatima M, Tan R, Halliday GM, Kril JJ. Spread of pathology in amyotrophic lateral sclerosis: Assessment of phosphorylated TDP-43 along axonal pathways. Acta neuropathologica communications 2015;3(1):47.

41. Zhang J, Tong L, Wang L, Li N. Texture analysis of multiple sclerosis: A comparative study. Magn Reson Imaging 2008;26(8):1160-1166.

42. Abrahams S, Goldstein L, Kew J et al. Frontal lobe dysfunction in amyotrophic lateral sclerosis: A PET study. Brain 1996;119(6):2105-2120.

43. Abrahams S, Leigh P, Harvey A et al. Verbal fluency and executive dysfunction in amyotrophic lateral sclerosis (ALS). Neuropsychologia 2000;38(6):734-747.

44. Bede P, Elamin M, Byrne S et al. Basal ganglia involvement in amyotrophic lateral sclerosis. Neurology 2013;81(24):2107-2115.

45. Abdulla S, Machts J, Kaufmann J et al. Hippocampal degeneration in patients with amyotrophic lateral sclerosis. Neurobiol Aging 2014;35(11):2639-2645.

46. Christidi F, Karavasilis E, Zalonis I et al. Memory-related white matter tract integrity in amyotrophic lateral sclerosis: An advanced neuroimaging and neuropsychological study. Neurobiol Aging 2017;49:69-78.

47. Kassubek J, Müller H, Del Tredici K et al. Diffusion tensor imaging analysis of sequential spreading of disease in amyotrophic lateral sclerosis confirms patterns of TDP-43 pathology. Brain 2014;137(6):1733-1740.

48. Lulé D, Böhm S, Müller H et al. Cognitive phenotypes of sequential staging in amyotrophic lateral sclerosis. Cortex 2018.

Table 3: Participants' characteristics and T1W scan protocols.

Study	Patients (M/F)	Mean age (years)	Controls (M/F)	Mean age (years)	TR (*ms*)	TE (*ms*)	Voxel size (mm^3)	B0 (*T*)
1	27 (19/8)	61.2	13 (5/8)	53.6	1600	3.8	1 x 1 x 1.5	1.5
2	19 (10/9)	57.7	23 (11/12)	55.6	1600	3.8	1 x 1.5 x 1	1.5
3	20 (11/9)	57.6	16 (7/9)	57.0	2300	3.4	1 x 1 x 1	3.0
4	17 (10/7)	57.1	22 (8/14)	56.6	508	4.5	1 x 1 x 1	4.7

MRI = magnetic resonance imaging, M = male, F = female, TR = repetition time, TE = echo time, *ms* = milliseconds, *mm* = millimeters, B0 = magnetic field strength

Table 4: Patients' survival and clinical characteristics. Patients were dichotomized at the median survival of 19.5 months. Survival data was not available for one patient and was therefore excluded from the analysis. Where applicable, data is presented as mean ± standard deviation. The p value is presented for group tests between long- and short-survivors.

	All patients	Long-survivors	Short-survivors	*p* value
Outcome				
Deceased	78.0% (64)	70.7% (29)	85.4% (35)	
Censored	22.0% (18)	29.3% (12)	14.6% (6)	
Survival (months)	26.1 ± 22.5	40.3 ± 24.6	11.9 ± 5.1	**< 0.01**[a]
Age (years)	58.6 ± 10.8	55.2 ± 10.3	62.0 ± 10.3	**< 0.01**[a]
Sex (M/F)	50/32	27/14	23/18	0.37[b]
Site of onset (limb/bulbar)	62/19	32/9	30/10	0.75[b]
ALSFRS-R	38.7 ± 5.6	39.6 ± 6.2	37.8 ± 4.9	0.17[a]
Symptom duration (months)	23.1 ± 15.4	25.1 ± 18.8	21.0 ± 10.9	0.24[a]
Disease progression rate	0.67 ± 1.1	0.55 ± 0.68	0.78 ± 1.39	0.34[a]

M = male, F = female, ALSFRS-R = ALS functional rate scale-revised, a = independent samples *t*-test, b = Chi-squared test

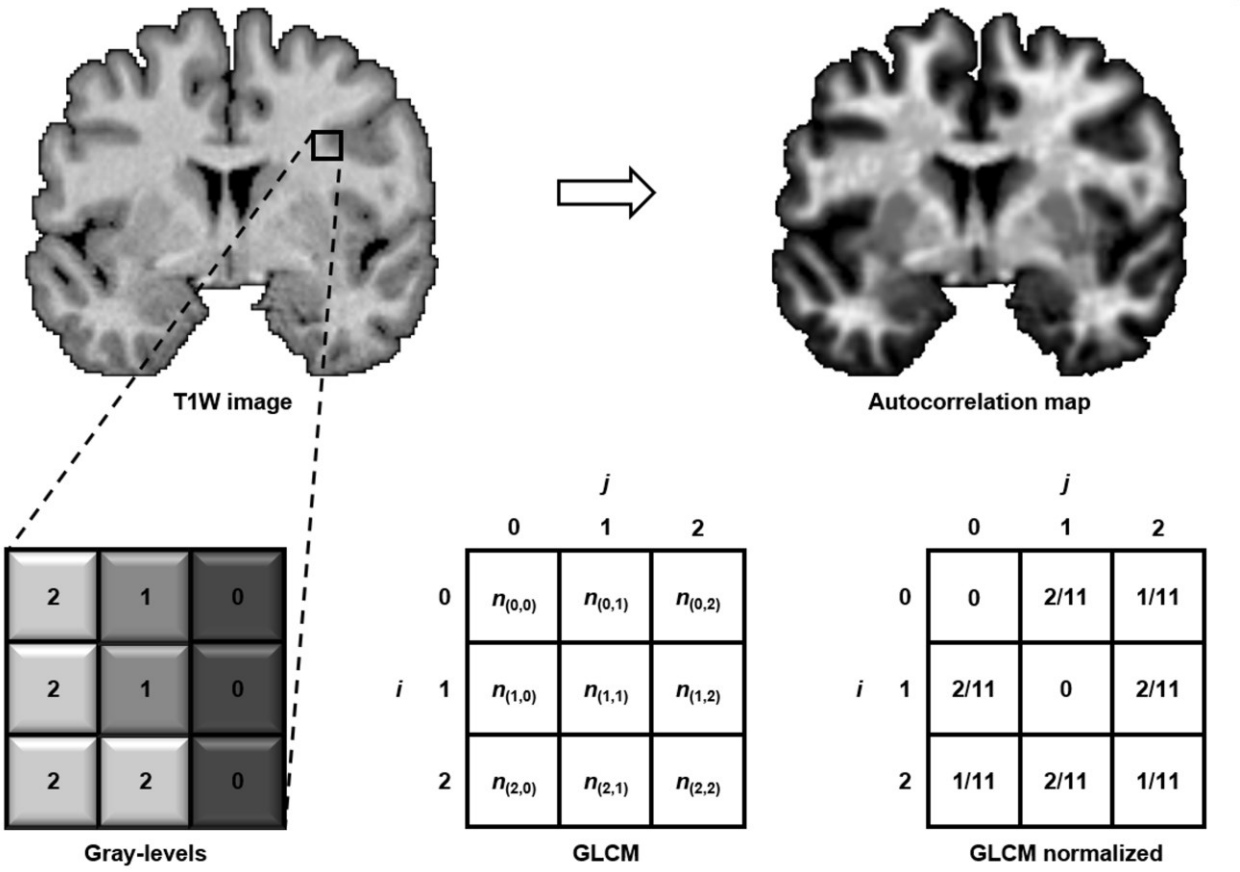

Figure 1: Schematic representation of the creation of a gray level co-occurrence matrix (GLCM) in a neighbourhood of pixels in an image. Each cell in the GLCM matrix represents the number of times a certain pixel combination (i,j) co-occurs in a particular direction. In this example, the GLCM is evaluated for $\theta = 0°$ (left-right direction). Values are then normalized in the GLCM by dividing them by the sum of all co-occurrences in the GLCM. Texture autocorrelation is then calculated from the normalized GLCM in every direction in each orthogonal plane (i.e. in 3 dimensions) to produce an autocorrelation map for each T1W image. Areas of increased autocorrelation (hyperintensity on the maps) represent regions where there is an increased probability of co-occurrence of gray levels.

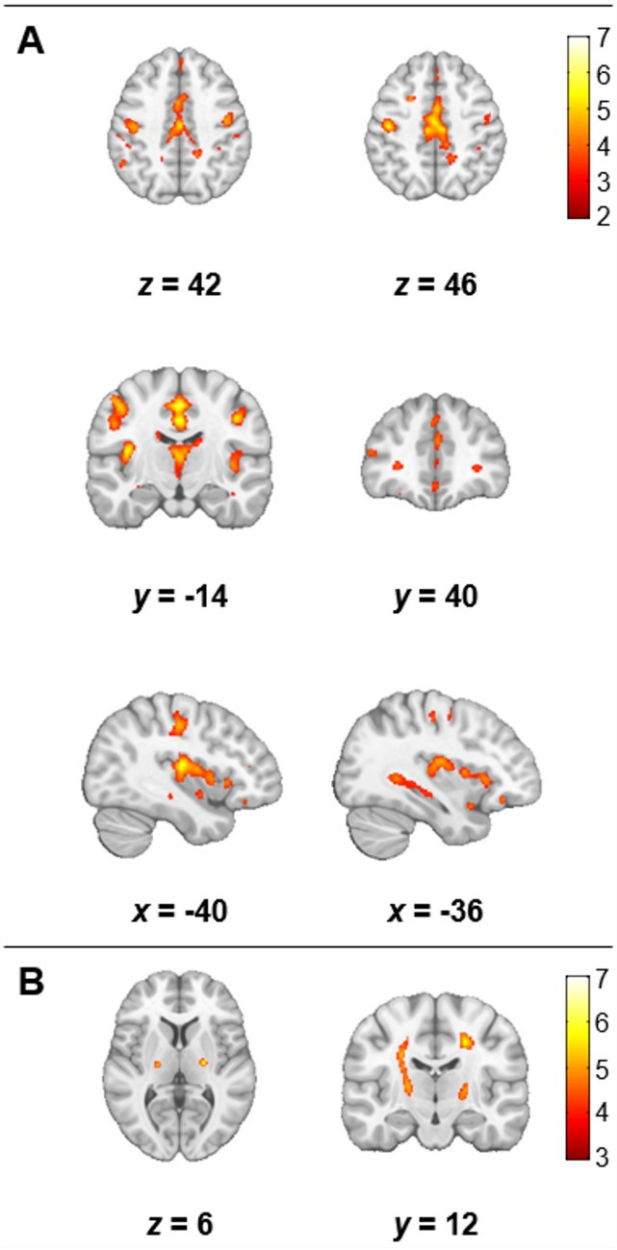

Figure 2: Significant differences in autocorrelation between patients and controls (FDR $p < 0.05$, cluster size > 10). Results are overlaid on the MNI template in neurological convention. Areas of the motor cortex, insula, thalamus, caudate, subcortical white matter, and hippocampus bilaterally had decreased autocorrelation in patients (A). However, autocorrelation was increased along the CST in patients (B). The color bars show the range of *T* values.

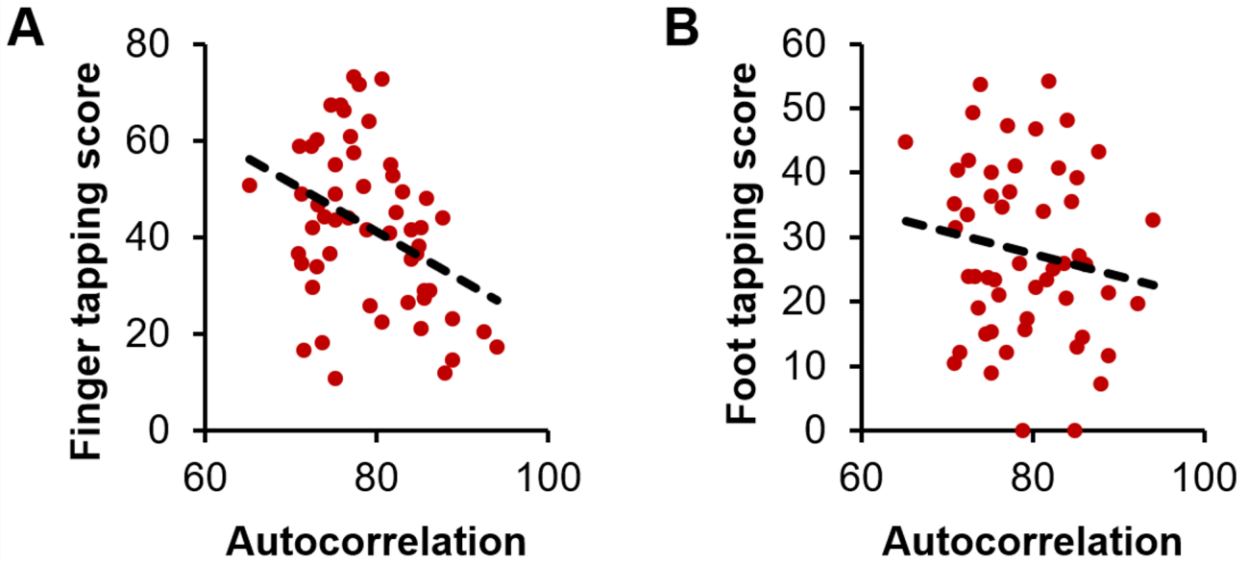

Figure 3: Clinical correlations in patients: autocorrelation in the CST varied with and finger- (A) and foot-tapping rates (B).

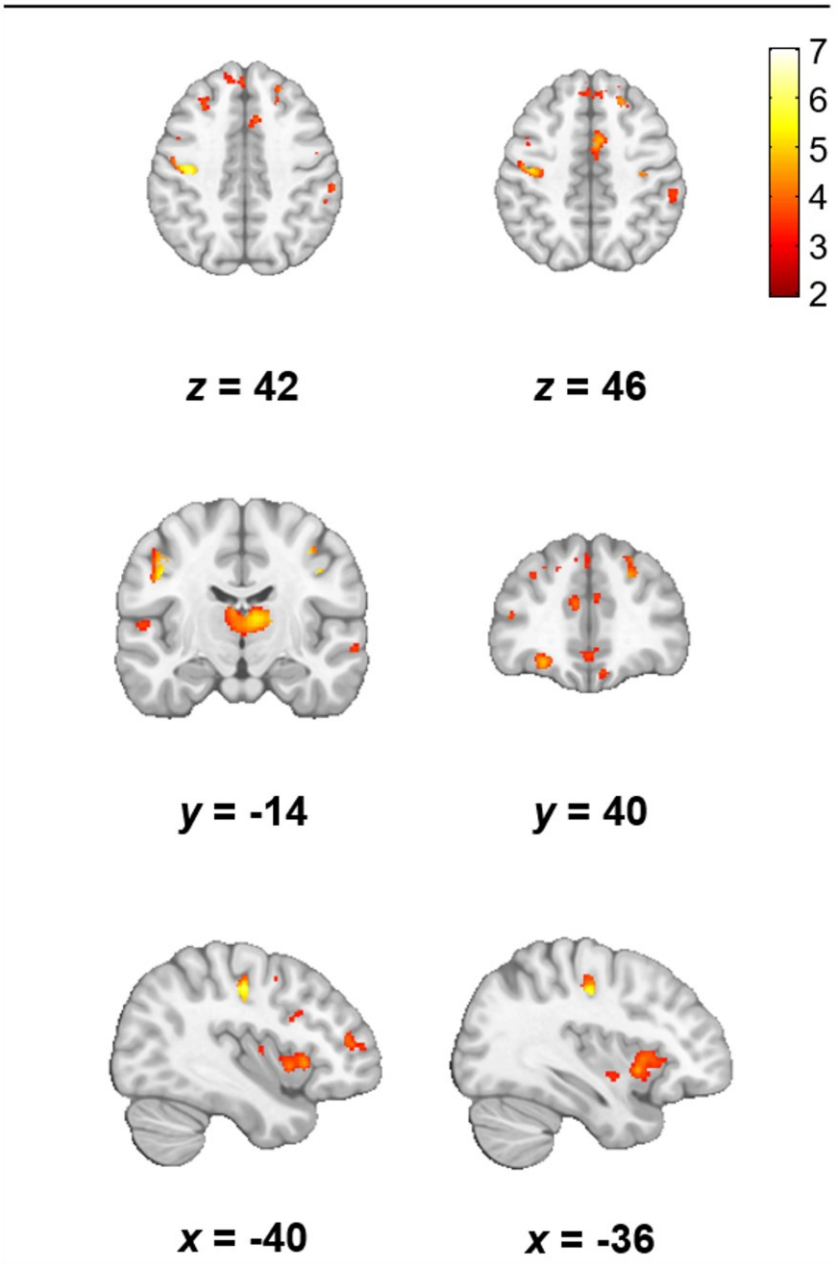

Figure 4: Voxel based morphometry revealed bilaterally decreased gray matter density in the motor cortex, insula, and thalamus in patients (FDR $p < 0.05$, cluster size > 10). Results are overlaid on the MNI template in neurological convention. The color bars show the range of *T* values.

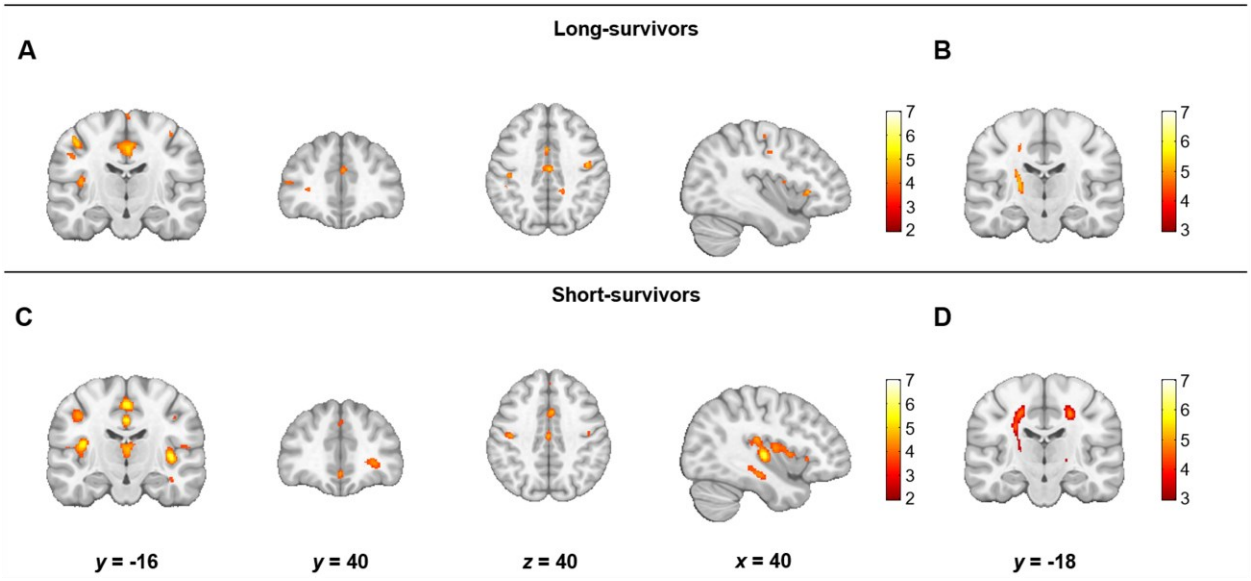

Figure 5: Differences in the texture feature autocorrelation between long-survivors and controls (A, B) and short-survivors and controls (C, D). Panels A and C show the areas of decreased autocorrelation and panels B and D show areas of increased autocorrelation (FDR $p < 0.05$, cluster size > 10). Results are overlaid on the MNI template in neurological convention. The color bars show the range of *T* values. The comparison between short-survivors and controls for significant increases in autocorrelation (D) did not survive FDR correction and is reported at an uncorrected $p < 0.001$ with a cluster threshold of 10 voxels.

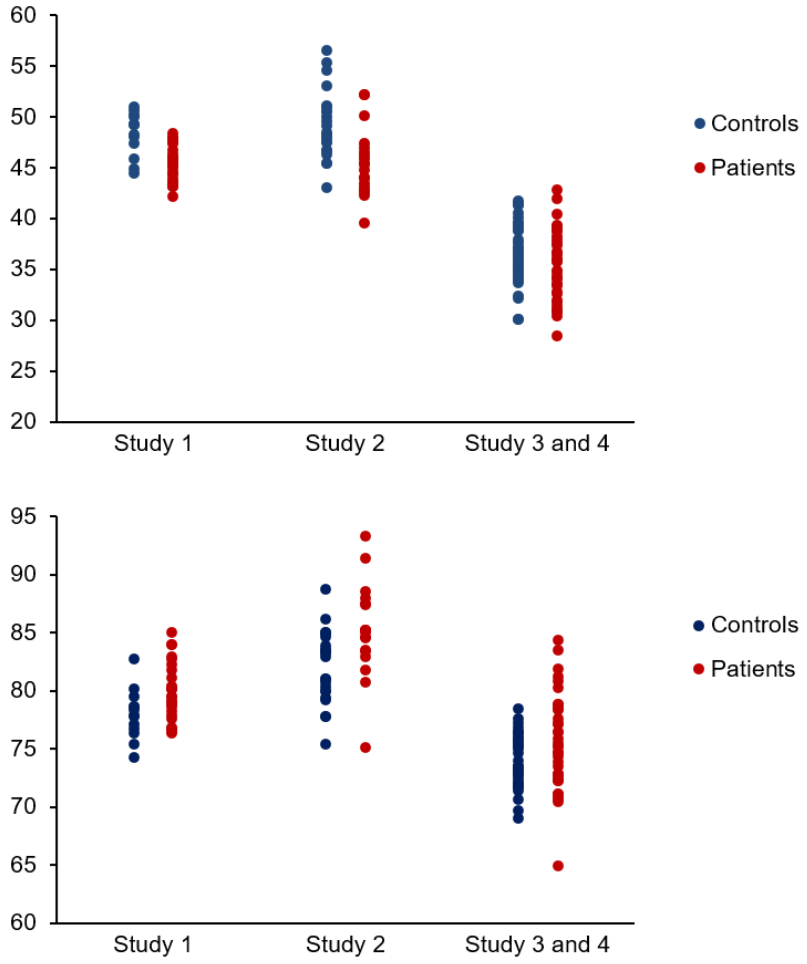

Supplementary Figure 1: Autocorrelation values extracted from the regions of significant differences in the pooled analysis from patients and controls in studies at different resolutions. Study 1 images were acquired at 1 x 1 x 1.5 mm^3 and Study 2 images were acquired at 1 x 1.5 x 1 mm^3. Study 3 and 4 were pooled together because their images were acquired at 1 x 1 x 1 mm^3. The graph on the top shows autocorrelation values from regions where it was significantly decreased in patients on whole-brain analysis. The regions included the motor cortex, insula, hippocampus, and subcortical frontal white matter. The graph below shows autocorrelation values from regions where it was significantly increased in patients on whole-brain analysis. The regions included only the corticospinal tract. The raw data presented here is not corrected for age and gender and is segregated by the study.

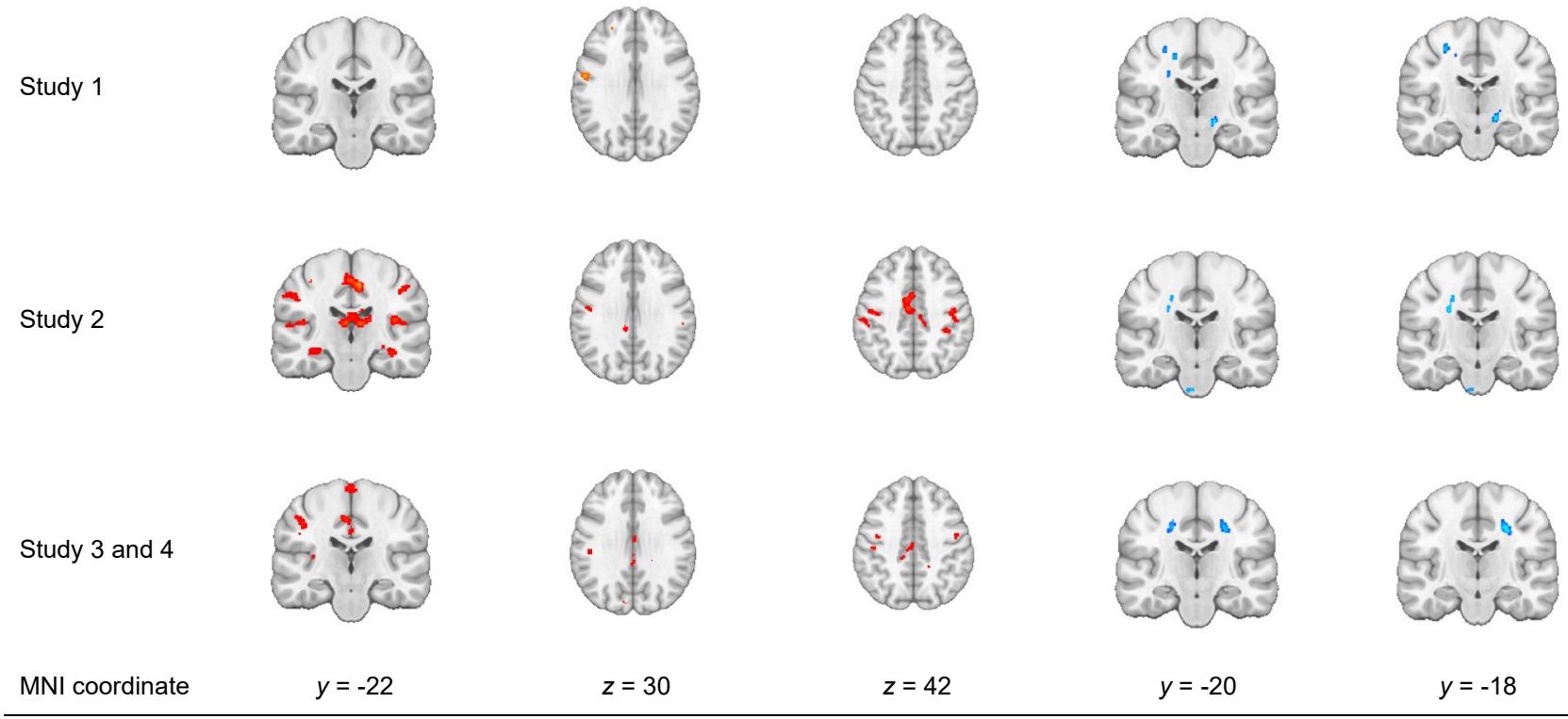

Supplementary Figure 2: Significant differences in autocorrelation between patients and controls ($p < 0.001$, cluster size > 10) in separate studies at different resolutions. Study 1 images were acquired at 1 x 1 x 1.5 mm^3 and Study 2 images were acquired at 1 x 1.5 x 1 mm^3. Study 3 and 4 were pooled together because their images were acquired at 1 x 1 x 1 mm^3. Areas in red are regions where autocorrelation was significantly decreased in patients and areas in blue are regions where autocorrelation was significantly increased in patients.

Chapter 4 Corticospinal Tract Degeneration in ALS Unmasked in T1-weighted Images Using Texture Analysis

* As published in *Ishaque, A., Mah, D., Seres, P., Luk, C., Johnston, W., Chenji, S., Beaulieu, C., Yang, Y.H. and Kalra, S., 2019. Corticospinal tract degeneration in ALS unmasked in T1-weighted images using texture analysis. Human brain mapping, 40(4), pp.1174-1183.*

Abstract

The purpose of this study was to investigate whether textures computed from T1-weighted (T1W) images of the corticospinal tract (CST) in amyotrophic lateral sclerosis (ALS) are associated with degenerative changes evaluated by diffusion tensor imaging (DTI). Nineteen patients with ALS and 14 controls were prospectively recruited and underwent T1W and diffusion-weighted magnetic resonance imaging. 3D texture maps were computed from T1W images and correlated with the DTI metrics within the CST. Significantly correlated textures were selected and compared within the CST for group differences between patients and controls using voxel-wise analysis. Textures were correlated with the patients' clinical upper motor neuron (UMN) signs and their diagnostic accuracy was evaluated. Voxel-wise analysis of textures and their diagnostic performance were then assessed in an independent cohort with 26 patients and 13 controls. Results showed that textures *autocorrelation*, *energy*, and *inverse difference normalized* significantly correlated with DTI metrics ($p < 0.05$) and these textures were selected for further analyses. The textures demonstrated significant voxel-wise differences between patients and controls in the centrum semiovale and the posterior limb of the internal capsule bilaterally ($p < 0.05$). *Autocorrelation* and *energy* significantly correlated with UMN burden in patients ($p < 0.05$) and classified patients and controls with 97% accuracy (100%

sensitivity, 92.9% specificity). In the independent cohort, the selected textures demonstrated similar regional differences between patients and controls and classified participants with 94.9% accuracy. These results provide evidence that T1-based textures are associated with degenerative changes in the CST.

Introduction

Amyotrophic lateral sclerosis (ALS) is a neurodegenerative disorder of the human motor system involving upper and lower motor neurons (UMN and LMN). There are no curative options and patients have a median survival of 26 months from the time of diagnosis (Pupillo, Messina, Logroscino, & Beghi, 2014). Clinical diagnosis of ALS is made in the presence of UMN and LMN physical exam findings and can be supported by electromyographic evaluation of subclinical LMN dysfunction (Brooks, Miller, Swash, & Munsat, 2000). Clinical magnetic resonance imaging (MRI) studies are used to rule out other diagnoses and do not provide an objective assessment of UMN dysfunction. On average, there is a delay of nine to 16 months in reaching the diagnosis due to the inadequate sensitivity of clinical examination (Kraemer, Buerger, & Berlit, 2010).

Classic white matter pathology of ALS is characterized by the degeneration of the corticospinal tract (CST). Intensity variations within the CST have been demonstrated in conventional MRI sequences such as T1-weighted (T1W) and fluid-attenuated inversion recovery (FLAIR), but with subjective visual evaluation and low diagnostic performance (Bowen et al., 2000; Hecht et al., 2001). Recent attempts have also been made to improve the detection of pathological white matter intensity changes in T1W images using voxel-based intensitometry (VBI) (Hartung et al., 2014). Regional cortical thinning on T1W images is a well-characterized feature in ALS. Reductions in cortical thickness are observed in motor (precentral gyrus) and extra-motor (frontotemporal) regions of the brain and are correlated with disease progression and functional disability (Agosta et al., 2012; Bede et al., 2013; Verstraete et al., 2012). The pathological correlates of these *in vivo* MRI findings, however, have not yet been established.

Diffusion tensor imaging (DTI) is an MRI modality that is used to study the microstructural changes in the central nervous system (Beaulieu, 2002). *In vivo* DTI studies have demonstrated altered water diffusion in the CST suggestive of microstructural pathology (Ciccarelli et al., 2006; Ciccarelli et al., 2009; Cosottini et al., 2005; Sarica et al., 2017). Advanced MRI modalities, such DTI, however, are not included routinely in clinical MRI studies and pose feasibility challenges including heterogeneity in sequences, long scan times, and availability on clinical scanners. Therefore, there is a need for an objective marker that is sensitive to the pathological UMN changes in ALS and that can be used clinically to mitigate delays in diagnosis and monitor disease progression.

Texture analysis is a statistical method of quantifying gray-level intensity and patterns in an image that the human eye cannot detect. Studies have applied texture analysis in conventional MR images to characterize and diagnose various neurological diseases including brain tumours and Alzheimer's disease (Kickingereder et al., 2016; Sørensen et al., 2017). A novel 3D voxel-wise texture analysis method also revealed the spatial pattern of pathology involving the medial temporal lobes in Alzheimer's disease in a hypothesis-free study (Maani, Yang, & Kalra, 2015). In ALS, texture changes have been observed in the CST and the deep gray nuclei (Albuquerque et al., 2016; Maani, Yang, Emery, & Kalra, 2016). However, the pathological substrates that underlie texture changes have not yet been investigated.

The purpose of this study was to investigate whether textures of the CST quantified from T1W images are associated with *in vivo* surrogates of white matter degeneration in ALS. It was hypothesized that MRI textures of the CST from T1W images will correlate with DTI metrics of CST degeneration and the clinical UMN burden in patients. Furthermore, the diagnostic utility of T1-based textures in ALS in two independent cohorts was also evaluated for replicability.

Materials and methods

Experiments were first conducted in patients with ALS and controls from a primary cohort to establish a set of textures from T1W images that correlate with DTI metrics. These textures were subsequently tested for voxel-wise texture differences in the CST between patients and controls and evaluated for their diagnostic performance in the primary cohort and in an independent cohort for validation. A summary of the analytical steps of texture analysis in this study are presented in supplementary Figure E1.

Study participants

Patients with ALS were prospectively recruited from a multidisciplinary ALS clinic at the University of Alberta. Patients were required to have an El Escorial designation of clinically possible ALS and, as such, had UMN signs in at least one anatomical region (Brooks et al., 2000). Patients with co-morbid frontotemporal dementia (FTD) and familial ALS were also eligible. Patients were excluded if they were older than 80 years of age, or if they had a history of co-morbid neurological conditions including, but not limited to, multiple sclerosis, stroke, and brain trauma. Healthy control participants without neurological, or psychiatric disorders were recruited. Participants were excluded if they could not tolerate the duration of the MRI scan, or if they had contraindications to having an MRI such as a cardiac pacemaker. All participants provided informed written consent prior to participating in the study, which was approved by the local research ethics review board.

Nineteen patients and 14 controls were enrolled through the Canadian ALS Neuroimaging Consortium (CALSNIC) into the primary cohort. One patient presented with co-morbid FTD and there were no cases of familial ALS. Patients underwent a neurological exam to

assess the extent of clinical UMN involvement in the limbs and bulbar region. An UMN burden score with a maximum score of 12 was calculated. The presence of spasticity and hyperreflexia in the upper and lower limbs, including the Babinski sign and clonus in each foot, were assessed for a maximum possible score of 6 from each side of the body. Twenty-six patients and 13 controls were enrolled into the independent cohort. Disability was quantified with the ALS functional rating scale-revised (ALSFRS-R). Neurological exam data and the ALSFRS-R scores were collected on the same day as the MRI, or from the last clinical visit if it was within four weeks of the MRI scan. A summary of the participants' characteristics is provided in Table 1.

MRI parameters

Participants in the primary cohort were scanned on a Siemens Prisma 3 T scanner. T1W images were acquired axially with a 3D magnetization-prepared rapid gradient-echo (MPRAGE) sequence (slice thickness = 1 mm, voxel size = 1 x 1 x 1 mm^3, TR = 2300 ms, TE = 3.4 s, flip angle = 9°, number of slices = 176). Diffusion-weighted (DW) images were acquired axially using a 2D spin-echo, single-shot echo planar imaging (EPI) pulse sequence (slice thickness = 2 mm, voxel size = 2 x 2 x 2 mm^3, TR = 10000 ms, TE = 90 ms, flip angle 90°, number of slices = 70, b0 images = 5, diffusion gradient directions = 30, b-value = 1000 s/mm^2).

Participants in the independent cohort were scanned on a Siemens Sonata 1.5 T scanner. T1W images were acquired axially with a 3D MPRAGE sequence (slice thickness = 1.5 mm, voxel size = 1 x 1 x 1.5 mm^3, TR = 1600 ms, TE = 3.8 s. flip angle = 15°, number of slices = 128).

T1W image analysis

T1W images were processed in Statistical Parametric Mapping 8 (SPM8 revision 5236) (www.fil.ion.ucl.ac.uk/spm/software/spm8/) running on MATLAB 2014b and were corrected for non-uniformity intensity bias. Gray and white matter were segmented and saved as a unified brain mask for each participant. T1W images were normalized to the Montreal Neurological Institute 152 (MNI152) template using Diffeomorphic Anatomical Registration using Exponentiated Lie algebra (DARTEL) (Ashburner, 2007) and the forward and inverse deformation fields were saved for later transformations of texture maps into MNI space for voxel-wise analysis. Gray and white matter images were smoothed with a 6 mm Gaussian kernel for voxel-wise analysis.

Texture analysis was performed on the bias-corrected T1W images in each participants' native space. 3D orthogonal texture maps were computed for each participant from their respective brain mask in SPM8 using a recently described method (Maani et al., 2015). The texture maps were computed using gray-level co-occurrence matrix (GLCM), a second-order statistical method of examining textures (Haralick & Shanmugam, 1973). A GLCM was defined for each voxel and its adjacent voxels (referred to as the reference voxel and its neighbourhood) in all three orthogonal planes for a T1W image. A GLCM is an $N \times N$ matrix, where N is the total number of gray levels in an image. To reduce computation time, T1W images were scaled down to 16 gray levels. Each cell in the GLCM (i,j) specifies the number of times gray level i co-occurs with gray level j over a distance d and in a particular direction θ within the neighbourhood. In this study, a distance of one pixel and four directions (0°, 45°, 90°, and 135°) adjacent to the central pixel were considered for the construction of the GLCMs. Eight directions (0°, ±45°, ±90°, ±135°and 180°) can be considered in a GLCM; however, because of the

symmetry found in the matrix across the diagonal, opposite directions (for example 0° and 180°) are redundant and were combined. The GLCMs for all four directions were summed and normalized to represent the probability of co-occurrence between gray levels in the neighbourhood. This was carried out in the axial, coronal, and sagittal planes to generate three GLCMs per voxel. A texture feature could then be calculated from the GLCMs and averaged over the three planes to compute a single 3D texture value for each voxel. The following 18 texture feature maps were then computed from the GLCM: *autocorrelation*, *contrast*, *correlation*, *cluster prominence*, *cluster shade*, *dissimilarity*, *energy*, *entropy*, *homogeneity*, *maximum probability*, *sum of squares*, *sum average*, *sum variance*, *sum entropy*, *difference variance*, *difference entropy*, *information measure of correlation*, and *inverse difference normalized*. See (Maani et al., 2015) for a full technical description and details regarding this method. Subsequent analyses of the CST were carried out within an atlas-based CST mask as described in the later sections.

DTI analysis

DW images were processed in ExploreDTI version 4.8.6 and were corrected for temporal signal drift, Gibbs ringing artifacts, motion, eddy current-induced geometric distortions, and EPI distortions (Leemans, Jeurissen, Sijbers, & Jones, 2009; Perrone et al., 2015; Vos et al., 2017). EPI distortions were corrected through non-rigid registration of each participant's DWI data to their respective T1W image. Fractional anisotropy (FA), axial diffusivity (AD), and radial diffusivity (RD) maps were computed from the preprocessed DWI data.

Streamline tractography was performed with the following parameters: FA threshold = 0.2, fiber length range = 50 mm – 500 mm, and angle threshold = 30° using a deterministic approach (Basser, Pajevic, Pierpaoli, Duda, & Aldroubi, 2000). Regions of interests (ROIs) for

the CST were developed on the MNI152 template. Bilateral "AND" operators in the cerebral peduncles and the precentral gyri were used to extract the CST. Contaminating corticopontine tracts and commissural tracts were excluded by placing "NOT" operators in the cerebellum, medial lemniscus, and corpus callosum that were obtained from the MNI structural atlas (Collins, Holmes, Peters, & Evans, 1995; Mazziotta et al., 2001) and the International Consortium of Brain Mapping DTI-81 atlas (Hua et al., 2008). The ROIs were reversed transformed to each participant's native space using their respective inverse deformation fields. The resultant CSTs were segmented between the "AND" ROIs in each participant for anatomical consistency.

Segmented CSTs were resampled to 45 equidistant points for along-tract analysis (Colby et al., 2012). Each unilateral CST bundle was averaged in cross-section along its trajectory at each point. FA, AD, and RD values were computed from the 45 points along the single tract trajectories.

Statistical analysis

Statistical analyses were performed using IBM SPSS for Windows, Version 24.0. Highly correlated textures within the CST were removed to reduce computational load and redundancy. Specifically, a bilateral 3D CST mask was created for each participant by reverse transforming the CST mask from the Jülich histological atlas (Eickhoff et al., 2005) at 25% threshold. Texture values were averaged from the mask and Pearson's r was calculated between every pair of textures. One texture was removed from each pair if Pearson's $r \geq 0.90$.

Textures were validated for sensitivity to white matter properties of the CST by correlating them with DTI metrics of the CST. Each participant's CST mask from the atlas was

overlaid on their FA, AD, and RD maps to obtain averaged DTI metrics. Pearson's *r* was calculated between each texture and DTI metric pair and textures were selected for further analysis if a significant correlation was observed. Statistical significance was accepted at $p < 0.05$ corrected for multiple comparisons using the false discovery rate method (FDR), or at uncorrected $p < 0.05$ if the results did not reach significance after multiple comparison correction. The selected texture feature maps were transformed to the MNI space by applying the participants' respective forward deformation field and smoothed with a 6 mm Gaussian kernel for voxel-wise analyses. Texture maps are inherently slightly blurry when calculated. Therefore, to avoid washing out texture details, a Gaussian kernel less than 8 mm, which is typically used in voxel-wise studies, was used here.

Voxel-wise two-sample *t*-tests were conducted for the microstructural-sensitive textures between the two groups. Age was included as a covariate in all analyses. CST ROI from the atlas was used to create an explicit *a priori* mask in the MNI space. Significance was set at FDR $p < 0.05$, or uncorrected $p < 0.01$. A cluster size threshold of five or more voxels was set to report significant regions. Texture values from the significant clusters in each hemisphere were averaged for all patients and correlated with their contralateral UMN score using Spearman's rank correlation with a statistical significance of FDR $p < 0.05$. The reported textures from the CST were entered in a binary logistic regression model. The model was evaluated for diagnostic performance using receiver operating characteristic (ROC) curve analysis. Whole-brain voxel-based morphometry (VBM) analyses with two-sample *t*-tests to evaluate morphologic changes in gray and white matter were also conducted. Age was included as a covariate in both analyses. Statistical significance was accepted at FDR $p < 0.05$, or uncorrected $p < 0.001$ with a cluster size threshold of 20 or more.

Along-tract analysis of DTI metrics was performed on unilateral CSTs. Between-group differences in FA, AD, and RD were investigated individually by performing multivariate analyses of covariance with the DTI metric value at each location (45 values along the tract) as a dependent variable, group assignment (patients versus controls) as an independent variable, and age as a covariate. To identify the location along the CST responsible for significant between-group differences, comparisons were conducted using two-tailed Student's *t*-tests at each location adjusted for age with a statistical significance of FDR $p < 0.05$. Voxel-wise analysis and the predictive model from the primary cohort were applied to the independent cohort to assess for reproducibility of results.

Results

Correlation of DTI metrics with MRI textures

Ten textures remained after removing redundancies. Of the 10 textures, three demonstrated significant correlations with DTI metrics in the CST (Figure 1): *autocorrelation* correlated with AD ($r = -0.613$) (FDR $p < 0.05$) and RD ($r = -0.556$) (FDR $p < 0.05$); *energy* correlated with FA ($r = 0.416$) (uncorrected $p < 0.05$); and *inverse difference normalized* correlated with FA ($r = 0.510$) (FDR $p < 0.05$), AD ($r = -0.492$) (FDR $p < 0.05$), and RD ($r = -0.675$) (FDR $p < 0.05$).

Between-group texture differences in CST

Voxel-wise analysis revealed significant between-group texture changes in the CST. Specifically, *autocorrelation* was increased in patients (uncorrected $p < 0.01$), whereas *energy* and *inverse difference normalized* were decreased in patients (FDR $p < 0.05$) (Figure 2). Left posterior limb of the internal capsule and bilateral centrum semiovale demonstrated differences

in all three textures. *Energy* and *inverse difference normalized* demonstrated greater involvement of the left CST and bilateral posterior limbs of the internal capsule. Detailed regional analysis is reported in Table E1.

Association of textures in CST with clinical UMN burden

Significant correlations were found between textures in the CST from each hemisphere and the contralateral UMN burden score. *Autocorrelation* ($r = 0.407$) (FDR $p < 0.05$) and *energy* ($r = -0.382$) (FDR $p < 0.05$) correlated with the contralateral UMN burden score, whereas *inverse difference normalized* did not demonstrate a significant correlation (Figure 3).

Diagnostic performance of texture analysis

Textures *autocorrelation*, *energy*, and *inverse difference normalized* were entered in a regression model (predicted value = *autocorrelation**0.81 + *energy**(-0.22) + *inverse difference normalized**(-3.36) + 599.47) and demonstrated 100% sensitivity, 92.9% specificity, and an overall classification accuracy of 97.0%. ROC curve analysis revealed an area under the ROC curve (AUC) of 0.985 (Figure 4).

Between-group VBM analyses

Gray matter VBM analysis revealed significant changes in the motor cortex bilaterally (uncorrected $p < 0.001$). Additional regional differences were observed in the temporal regions bilaterally and the left insula (Figure E2). White matter VBM analysis revealed significant subcortical changes in the right postcentral and precentral region, left parietal regions (uncorrected $p < 0.001$) (Figure E1). No significant differences were observed along the CST. Detailed regional analysis is reported in Table E2.

Along-tract diffusion analysis

One patient's left CST was excluded from along-tract analysis because tractography did not yield any tracts. Significant between-group differences were demonstrated in bilateral CST FA (left: $F = 14.0$, $df = 1$, $p < 0.05$; right: $F = 12.6$, $df = 1$, $p < 0.05$) and RD (left: $F = 17.8$, $df = 1$, $p < 0.05$; right: $F = 14.4$, $df = 1$, $p < 0.05$). No significant between-group difference was detected in AD. Along-tract analysis revealed FA was significantly decreased in patients in the CST bilaterally in the posterior limb of the internal capsule and the centrum semiovale. RD was significantly increased in patients along most of the length of the left CST, and in the posterior limb of the internal capsule and centrum semiovale regions of the right CST (Figure 5).

Independent cohort

Voxel-wise analyses in the independent cohort revealed significant between-group differences of the T1-based textures similar to the primary cohort: *autocorrelation* was increased in patients (FDR $p < 0.05$) and *energy* and *inverse difference normalized* were decreased in patients (FDR $p < 0.05$) (Figure 6). Common areas of change in all three textures were the bilateral posterior limbs of the internal capsule and bilateral centrum semiovale. *Energy* and *inverse difference normalized* were also different in the cerebral peduncles bilaterally. Detailed regional analysis is reported in Table E3. Figure 7 shows a representative *autocorrelation* map and the corresponding T1-weighted image from a control and a patient from this cohort. Application of the regression model derived from the primary cohort with the same weights achieved an overall classification accuracy of 94.9% with 92.3% sensitivity, 100% specificity, and an AUC of 0.991 (Figure 4).

Discussion

In this study, it was shown that texture features of the CST in T1W-images correlate with DTI indices, have discriminatory power in identifying ALS patients from controls, and correlate with clinical measures of UMN dysfunction. This suggests that degeneration of the CST in ALS can be evaluated using texture analysis of T1W-images.

Textures from T1W-images correctly classified patients and controls with 97.0% (100% sensitivity, 92.9% specificity) and 94.9% (92.3% sensitivity, 100% specificity) accuracy in two independent cohorts. This strong discriminatory ability of texture analysis in ALS was observed in a previous study that obtained 95% sensitivity and 90% specificity using textures from the CST in T1W images (Maani et al., 2016). Significant correlations were found between the textures and the UMN burden score indicating that changes detected *in vivo* by texture analysis of T1W images are associated with the underlying pathology of ALS.

T1-based textures of the CST significantly correlated with DTI metrics. Animal models show that FA, AD, and RD are mediated by microstructural factors and processes such as axonal membranes, axonal damage, and myelin damage, respectively (Beaulieu, 2002; Song et al., 2005). This suggests that texture changes from T1W images are sensitive to the characteristic white matter damage of the CST in ALS. The correlation between T1-based textures and DTI metrics has been previously reported, although its biological implications have not been explored (Holli et al., 2010). Current analytical methods for T1W images, including VBM, are not sensitive to subtle intensity changes in white matter that may be mediated by altered microstructural properties. This was corroborated by our results (Figure E2). VBI is a contrast-enhancement technique designed to overcome the current limitations of T1W VBM in evaluating white matter changes. A recent study using VBI in ALS demonstrated widespread white matter

changes on T1W images, including along the CST (Hartung et al., 2014). This shows that pathological variations do exist on T1W images that are not detected with current VBM methods. Therefore, texture analysis can potentially enable white matter analysis from T1W images that reflect pathological alterations.

Textures also demonstrated differences between patients and controls in the centrum semiovale and the posterior limb of the internal capsule. Along-tract analysis of DTI metrics also showed similar regions that were affected in patients compared to controls. Furthermore, FA and RD were altered in patients, whereas AD showed no change. This pattern of change in DTI metrics of the CST has been previously reported in ALS (Blain et al., 2011; Cosottini et al., 2005). Evidence suggests that it is characteristic of Wallerian axonal degeneration involving gliosis and increases in extracellular matrix (Beaulieu, 2002; Pierpaoli et al., 2001). Further evidence from combined MRI-histopathology experiments suggests that T1 signal alterations in ALS are contributed, at least in part, by neuronal loss, myelin dysfunction, and astrocytosis (Meadowcroft et al., 2015). Studies in multiple sclerosis have demonstrated that texture analysis of T2W images is sensitive to the *in vivo* pathological acute inflammatory processes that occur in white matter lesions (Zhang, Zhu, Mitchell, Costello, & Metz, 2009). Zhang et al. (2009) reported that local coarse texture measured using the polar Stockwell transform technique from T2W images increases in acute inflammatory lesions during gadolinium enhancement. They also showed that pre-lesion normal appearing white matter (NAWM) had similar texture to NAWM (Zhang et al., 2009). *Ex-vivo* MRI-pathology studies have further demonstrated that textures from MRI are directly related to tissue pathology. Higher texture heterogeneity was noted in T2W *ex-vivo* MRI in regions of increasing burden of pathology in multiple sclerosis characterized by NAWM, diffusively abnormal white matter, and lesion (Zhang et al., 2013).

Furthermore, Zhang et al. (2013) showed that the degree of texture heterogeneity in T2W images predicted the extent of pathological demyelination in histological analysis. Taken together, the findings of this study and the literature indicate that texture analysis in T1W images is likely detecting a substrate of pathological changes of the CST in ALS; however, MRI-histopathology validation studies are needed in to verify this claim. This is important because T1W images are routinely acquired in the diagnostic workup of suspected patients to rule out gross structural abnormalities without any role in detecting disease pathology. With texture analysis, clinically acquired T1W images may be able to provide objective evidence of UMN involvement during the diagnostic workup.

Recent studies have proposed multimodal MRI as a means of increasing diagnostic yield over the use of a single imaging modality. A study combining DTI and MR spectroscopy reported 93% sensitivity and 85% specificity in discriminating patients from controls (Foerster et al., 2014). In another multimodal study, an 86% sensitivity and 78% accuracy was achieved in discriminating patients and controls using DTI metrics and gray matter densities from T1W images (Schuster, Hardiman, & Bede, 2016). Therefore, although studies support the diagnostic utility of multimodal MRI in ALS, texture analysis on T1W images alone has high diagnostic performance and with greater clinical feasibility since it does not require advanced MRI sequences with long acquisition times that may not be available on all scanners.

T1W images from the primary cohort were acquired from a 3 T scanner, whereas the independent cohort was scanned in a 1.5 T scanner. This has two important implications. First, texture analysis can be applied clinically without requiring high-field MRI scanners. Second, the use of a common predictive model between the two cohorts highlights the robustness of texture analysis considering different MRI scanner vendors and acquisition parameters were used, an

issue commonly present in multicentre studies and clinical trials. Additionally, although ALS is pathologically characterized by UMN and LMN degeneration, it has substantial phenotypic heterogeneity and potential biomarkers must demonstrate diagnostic value across disease phenotypes. In this study, texture analysis demonstrated high diagnostic performance in distinguishing groups of heterogeneous patients from controls in two independent cohorts. Altogether, these results signify the clinical applicability and the utility of the use of textures analysis in ALS.

The study has several limitations. First, it consisted of two relatively small cohorts. Although the diagnostic performance of textures was replicated in an independent cohort, the observations made in this study need to be replicated in studies with larger sample sizes including age- and gender-matched controls. Second, patients in this study comprised of only those with an established diagnosis of ALS. Further studies should investigate the performance of texture analysis in discriminating ALS-mimics and in identifying early-onset patients in whom a diagnosis is uncertain.

In conclusion, this study demonstrates the utility of texture analysis in T1W images in detecting degeneration of the CST in ALS. It also provides clinical validity of texture-based assessment of the CST in ALS given the clinical correlations and high discriminatory performance in independent cohorts. This study supports further analysis of textures from T1W images as MRI-based biomarkers for UMN involvement in ALS.

Acknowledgements

This study was supported by funding from ALS Association, ALS Society of Canada, and Canadian Institutes of Health Research, and Brain Canada. The authors declare no conflict of interests.

References

Agosta, F., Valsasina, P., Riva, N., Copetti, M., Messina, M. J., Prelle, A., . . . Filippi, M. (2012). The cortical signature of amyotrophic lateral sclerosis. *PLoS One, 7*(8), e42816.

Albuquerque, M., Anjos, L. G., Maia Tavares de Andrade, Helen, Oliveira, M. S., Castellano, G., Junqueira Ribeiro de Rezende, Thiago, . . . Cavalcante França Junior, M. (2016). MRI texture analysis reveals deep gray nuclei damage in amyotrophic lateral sclerosis. *Journal of Neuroimaging, 26*(2), 201-206.

Ashburner, J. (2007). A fast diffeomorphic image registration algorithm. *NeuroImage, 38*(1), 95-113.

Basser, P. J., Pajevic, S., Pierpaoli, C., Duda, J., & Aldroubi, A. (2000). In vivo fiber tractography using DT-MRI data. *Magnetic Resonance in Medicine, 44*(4), 625-632.

Beaulieu, C. (2002). The basis of anisotropic water diffusion in the nervous system–a technical review. *NMR in Biomedicine, 15*(7-8), 435-455.

Bede, P., Bokde, A., Elamin, M., Byrne, S., McLaughlin, R. L., Jordan, N., . . . Hardiman, O. (2013). Grey matter correlates of clinical variables in amyotrophic lateral sclerosis (ALS): A neuroimaging study of ALS motor phenotype heterogeneity and cortical focality. *Journal of Neurology, Neurosurgery, and Psychiatry, 84*(7), 766-773. doi:10.1136/jnnp-2012-302674 [doi]

Blain, C. R., Brunton, S., Williams, V. C., Leemans, A., Turner, M. R., Andersen, P. M., . . . Simmons, A. (2011). Differential corticospinal tract degeneration in homozygous 'D90A' SOD-1 ALS and sporadic ALS. *Journal of Neurology, Neurosurgery, and Psychiatry, 82*(8), 843-849. doi:10.1136/jnnp.2010.236018 [doi]

Bowen, B. C., Pattany, P. M., Bradley, W. G., Murdoch, J. B., Rotta, F., Younis, A. A., . . . Quencer, R. M. (2000). MR imaging and localized proton spectroscopy of the precentral gyrus in amyotrophic lateral sclerosis. *AJNR.American Journal of Neuroradiology, 21*(4), 647-658.

Brooks, B. R., Miller, R. G., Swash, M., & Munsat, T. L. (2000). El escorial revisited: Revised criteria for the diagnosis of amyotrophic lateral sclerosis. *Amyotrophic Lateral Sclerosis and Other Motor Neuron Disorders, 1*(5), 293-299.

Ciccarelli, O., Behrens, T., Altmann, D., Orrell, R., Howard, R., Johansen-Berg, H., . . . Thompson, A. (2006). Probabilistic diffusion tractography: A potential tool to assess the rate of disease progression in amyotrophic lateral sclerosis. *Brain, 129*(7), 1859-1871.

Ciccarelli, O., Behrens, T. E., Johansen-Berg, H., Talbot, K., Orrell, R. W., Howard, R. S., . . . Thompson, A. J. (2009). Investigation of white matter pathology in ALS and PLS using tract-based spatial statistics. *Human Brain Mapping, 30*(2), 615-624.

Colby, J. B., Soderberg, L., Lebel, C., Dinov, I. D., Thompson, P. M., & Sowell, E. R. (2012). Along-tract statistics allow for enhanced tractography analysis. *NeuroImage, 59*(4), 3227-3242.

Collins, D. L., Holmes, C. J., Peters, T. M., & Evans, A. C. (1995). Automatic 3-D model-based neuroanatomical segmentation. *Human Brain Mapping, 3*(3), 190-208.

Cosottini, M., Giannelli, M., Siciliano, G., Lazzarotti, G., Michelassi, M. C., Del Corona, A., . . . Murri, L. (2005). Diffusion-tensor MR imaging of corticospinal tract in amyotrophic lateral sclerosis and progressive muscular atrophy. *Radiology, 237*(1), 258-264.

Eickhoff, S. B., Stephan, K. E., Mohlberg, H., Grefkes, C., Fink, G. R., Amunts, K., & Zilles, K. (2005). A new SPM toolbox for combining probabilistic cytoarchitectonic maps and functional imaging data. *NeuroImage, 25*(4), 1325-1335.

Foerster, B. R., Carlos, R. C., Dwamena, B. A., Callaghan, B. C., Petrou, M., Edden, R. A., . . . Feldman, E. L. (2014). Multimodal MRI as a diagnostic biomarker for amyotrophic lateral sclerosis. *Annals of Clinical and Translational Neurology, 1*(2), 107-114.

Haralick, R. M., & Shanmugam, K. (1973). Textural features for image classification. *IEEE Transactions on Systems, Man, and Cybernetics,* (6), 610-621.

Hartung, V., Prell, T., Gaser, C., Turner, M. R., Tietz, F., Ilse, B., . . . Grosskreutz, J. (2014). Voxel-based MRI intensitometry reveals extent of cerebral white matter pathology in amyotrophic lateral sclerosis. *PloS One, 9*(8), e104894.

Hecht, M., Fellner, F., Fellner, C., Hilz, M., Heuss, D., & Neundörfer, B. (2001). MRI-FLAIR images of the head show corticospinal tract alterations in ALS patients more frequently than T2-, T1-and proton-density-weighted images. *Journal of the Neurological Sciences, 186*(1), 37-44.

Holli, K. K., Wäljas, M., Harrison, L., Liimatainen, S., Luukkaala, T., Ryymin, P., . . . Dastidar, P. (2010). Mild traumatic brain injury: Tissue texture analysis correlated to neuropsychological and DTI findings. *Academic Radiology, 17*(9), 1096-1102.

Hua, K., Zhang, J., Wakana, S., Jiang, H., Li, X., Reich, D. S., . . . Mori, S. (2008). Tract probability maps in stereotaxic spaces: Analyses of white matter anatomy and tract-specific quantification. *NeuroImage, 39*(1), 336-347.

Kickingereder, P., Burth, S., Wick, A., Götz, M., Eidel, O., Schlemmer, H., . . . Radbruch, A. (2016). Radiomic profiling of glioblastoma: Identifying an imaging predictor of patient survival with improved performance over established clinical and radiologic risk models. *Radiology, 280*(3), 880-889.

Kraemer, M., Buerger, M., & Berlit, P. (2010). Diagnostic problems and delay of diagnosis in amyotrophic lateral sclerosis. *Clinical Neurology and Neurosurgery, 112*(2), 103-105.

Leemans, A., Jeurissen, B., Sijbers, J., & Jones, D. (2009). ExploreDTI: A graphical toolbox for processing, analyzing, and visualizing diffusion MR data. Paper presented at the *17th Annual Meeting of Intl Soc Mag Reson Med, , 209* 3537.

Maani, R., Yang, Y. H., & Kalra, S. (2015). Voxel-based texture analysis of the brain. *PloS One, 10*(3), e0117759.

Maani, R., Yang, Y. H., Emery, D., & Kalra, S. (2016). Cerebral degeneration in amyotrophic lateral sclerosis revealed by 3-dimensional texture analysis. *Frontiers in Neuroscience, 10*, 120. doi:10.3389/fnins.2016.00120 [doi]

Mazziotta, J., Toga, A., Evans, A., Fox, P., Lancaster, J., Zilles, K., . . . Mazoyer, B. (2001). A probabilistic atlas and reference system for the human brain: International consortium for brain mapping (ICBM). *Philosophical Transactions of the Royal Society of London.Series B, Biological Sciences, 356*(1412), 1293-1322. doi:10.1098/rstb.2001.0915 [doi]

Meadowcroft, M. D., Mutic, N. J., Bigler, D. C., Wang, J., Simmons, Z., Connor, J. R., & Yang, Q. X. (2015). Histological–MRI correlation in the primary motor cortex of patients with amyotrophic lateral sclerosis. *Journal of Magnetic Resonance Imaging, 41*(3), 665-675.

Perrone, D., Aelterman, J., Pižurica, A., Jeurissen, B., Philips, W., & Leemans, A. (2015). The effect of gibbs ringing artifacts on measures derived from diffusion MRI. *NeuroImage, 120*, 441-455.

Pierpaoli, C., Barnett, A., Pajevic, S., Chen, R., Penix, L., Virta, A., & Basser, P. (2001). Water diffusion changes in wallerian degeneration and their dependence on white matter architecture. *NeuroImage, 13*(6), 1174-1185.

Pupillo, E., Messina, P., Logroscino, G., & Beghi, E. (2014). Long-term survival in amyotrophic lateral sclerosis: A population-based study. *Annals of Neurology, 75*(2), 287-297.

Sarica, A., Cerasa, A., Valentino, P., Yeatman, J., Trotta, M., Barone, S., . . . Pucci, F. (2017). The corticospinal tract profile in amyotrophic lateral sclerosis. *Human Brain Mapping, 38*(2), 727-739.

Schuster, C., Hardiman, O., & Bede, P. (2016). Development of an automated MRI-based diagnostic protocol for amyotrophic lateral sclerosis using disease-specific pathognomonic features: A quantitative disease-state classification study. *PloS One, 11*(12), e0167331.

Song, S., Yoshino, J., Le, T. Q., Lin, S., Sun, S., Cross, A. H., & Armstrong, R. C. (2005). Demyelination increases radial diffusivity in corpus callosum of mouse brain. *NeuroImage, 26*(1), 132-140.

Sørensen, L., Igel, C., Pai, A., Balas, I., Anker, C., Lillholm, M., . . . Alzheimer's Disease Neuroimaging Initiative. (2017). Differential diagnosis of mild cognitive impairment and alzheimer's disease using structural MRI cortical thickness, hippocampal shape, hippocampal texture, and volumetry. *NeuroImage: Clinical, 13*, 470-482.

Verstraete, E., Veldink, J. H., Hendrikse, J., Schelhaas, H. J., van den Heuvel, M. P., & van den Berg, L. H. (2012). Structural MRI reveals cortical thinning in amyotrophic lateral sclerosis. *Journal of Neurology, Neurosurgery, and Psychiatry, 83*(4), 383-388. doi:10.1136/jnnp-2011-300909 [doi]

Vos, S. B., Tax, C. M., Luijten, P. R., Ourselin, S., Leemans, A., & Froeling, M. (2017). The importance of correcting for signal drift in diffusion MRI. *Magnetic Resonance in Medicine, 77*(1), 285-299.

Zhang, Y., Moore, G., Laule, C., Bjarnason, T. A., Kozlowski, P., Traboulsee, A., & Li, D. K. (2013). Pathological correlates of magnetic resonance imaging texture heterogeneity in multiple sclerosis. *Annals of Neurology, 74*(1), 91-99.

Zhang, Y., Zhu, H., Mitchell, J. R., Costello, F., & Metz, L. M. (2009). T2 MRI texture analysis is a sensitive measure of tissue injury and recovery resulting from acute inflammatory lesions in multiple sclerosis. *NeuroImage, 47*(1), 107-111.

Table 5: Participant characteristics of ALS patients and healthy controls.

Characteristic	Primary cohort		Replication cohort	
	ALS patients	Healthy controls	ALS patients	Healthy controls
Number of participants	19	14	26	13
Gender (*n*)				
Male	11	6	18	5
Female	8	8	8	8
Age (years)				
Mean ± SD	57.26 ± 10.11	56.93 ± 8.75	61.47 ± 9.22	53.62 ± 10.71
Range	37—74	37—67	42—77	28—65
Onset (*n*)				
Bulbar	4	-	9	-
Limb	15	-	17	-
El Escorial clinical diagnosis category (*n*)				
Definite ALS	3	-	9	-
Probable ALS	10	-	13	-
Probable ALS – Laboratory-supported	0	-	4	-
Possible ALS	6	-	0	-
ALSFRS-R (score)				
Mean ± SD	41.00 ± 4.28	-	36.54 ± 4.93	-
Range	32—47	-	27—45	-
Symptom duration (months)				
Mean ± SD	21.68 ± 14.26	-	19.58 ± 9.02	-

Range	9—60	-	2—38	-

SD = standard deviation; *n* = sample size

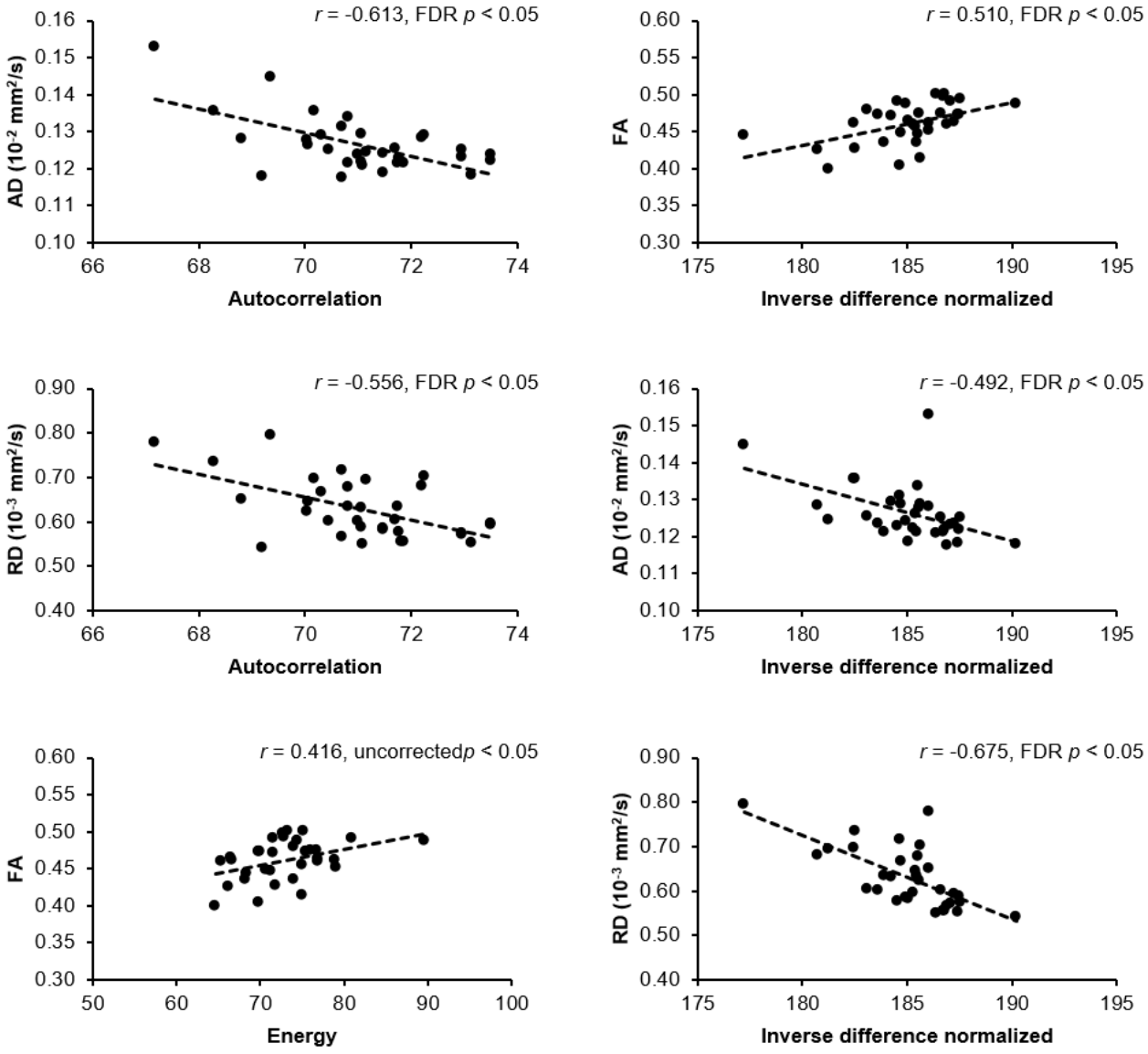

Figure 1: Correlations were observed between DTI metrics of the CST and the texture features autocorrelation, energy, and inverse difference normalized in the primary cohort. AD = axial diffusivity, RD = radial diffusivity, FA = fractional anisotropy, FDR = false discovery rate correction

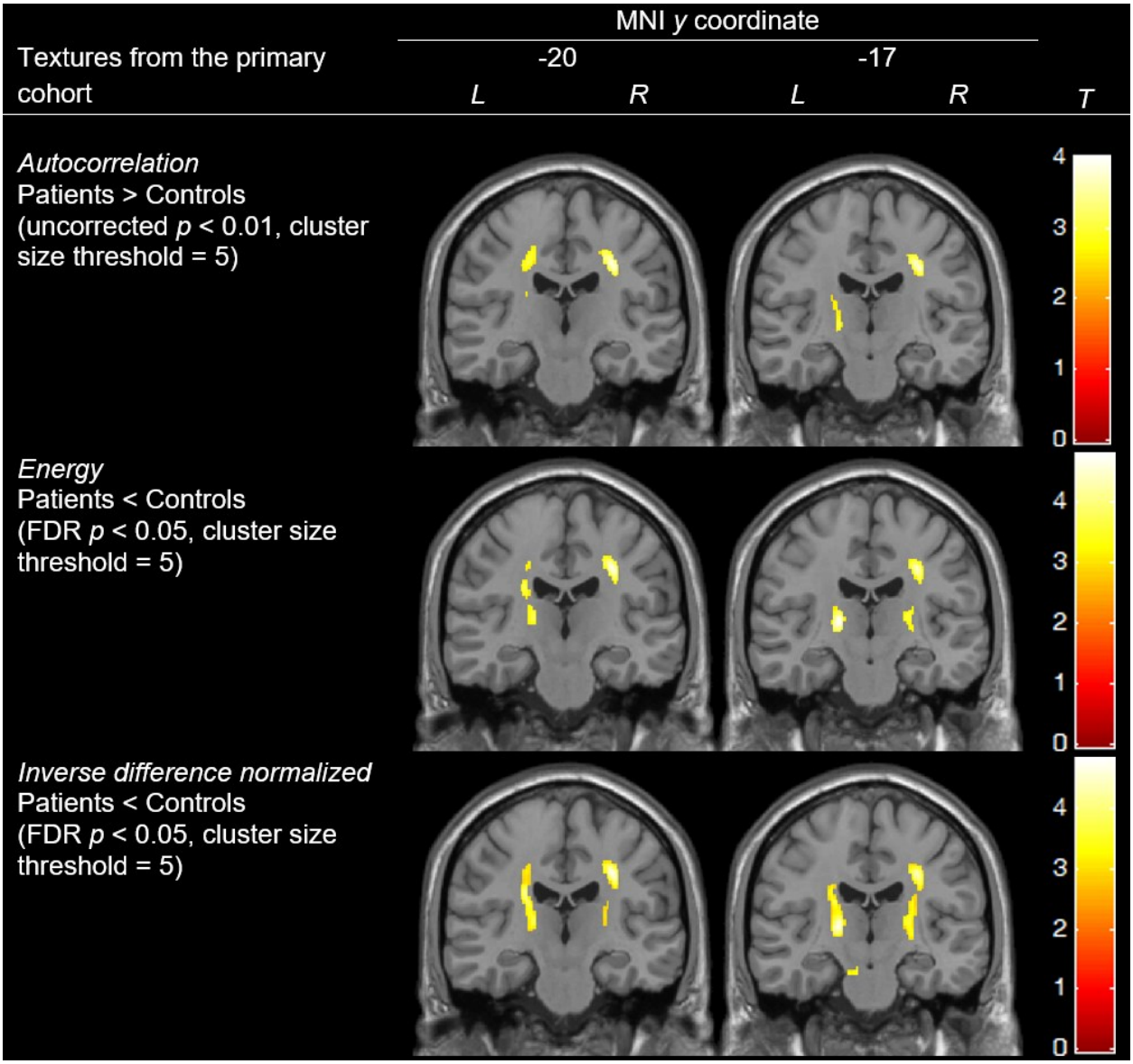

Figure 2: Differences were present in textures in T1W images within the CST between patients and controls in the primary cohort overlaid on a sample T1W image. FDR = false discovery rate correction, L = left, R = right

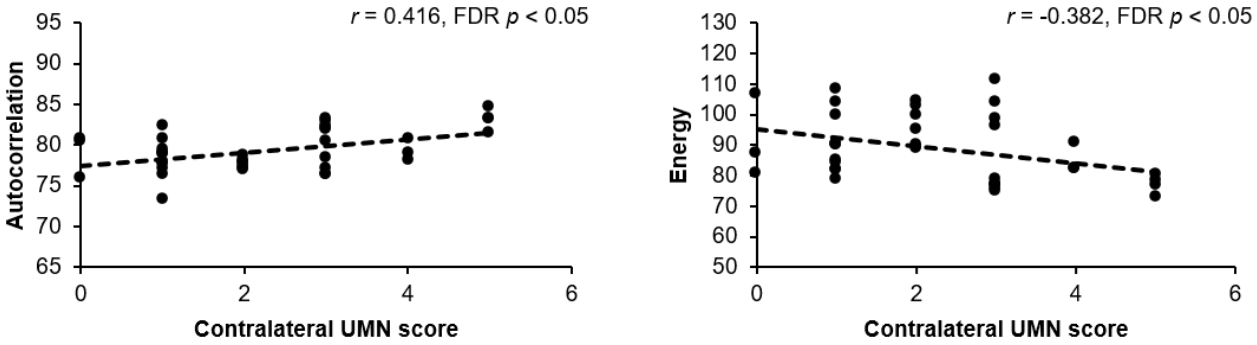

Figure 3: Correlations were observed between textures autocorrelation and energy and the contralateral UMN score among patients in the primary cohort. UMN = upper motor neuron, FDR = false discovery rate correction

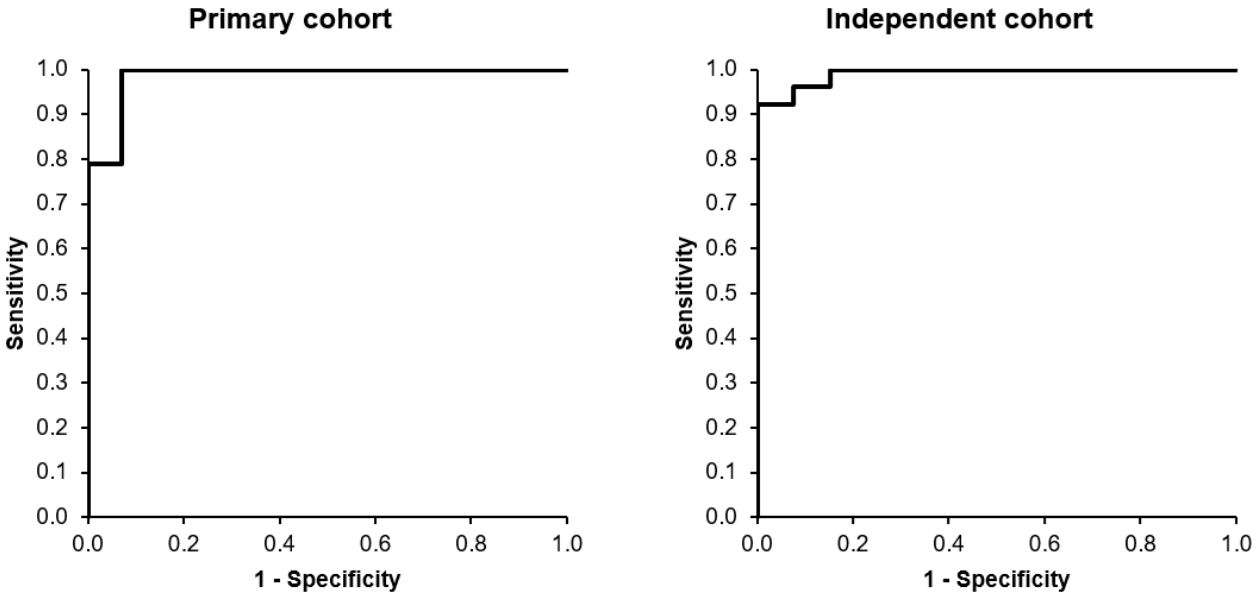

Figure 4: ROC curves for the regression models incorporating autocorrelation, energy, and inverse difference normalized in the primary cohort (left) and the independent cohort (right). The area under the curve (AUC) was 0.985 in the primary cohort (100% sensitivity and 92.9% specificity) and 0.991 in the independent cohort (92.3% sensitivity and 100% specificity) using the predictive model generated from the primary cohort.

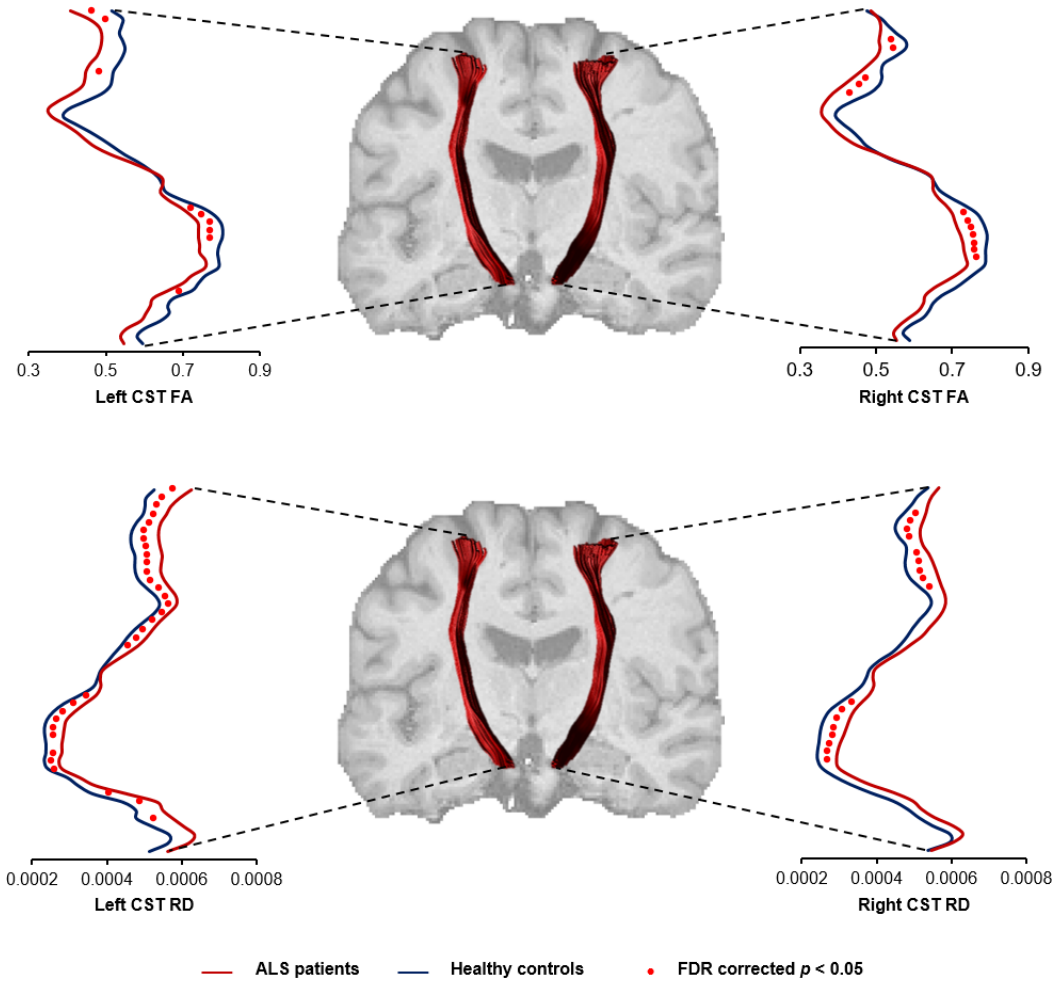

Figure 5: Along-tract analysis of FA (top) and RD (bottom) in the left and the right CST for participants in the primary cohort. A sample corticospinal tract constructed from tractography is superimposed on a sample T1W image to provide anatomical reference to the CST profiles. The x-axes represent the diffusion metric and the y-axes represent the position along the tract. Filled circles indicate points along the tract where the diffusion metric is significantly different in patients compared to controls. Reductions in FA in patients are localized mostly to the internal capsule, whereas RD is increased along most of the left CST and internal capsule and centrum semiovale of the right CST. CST = corticospinal tract, FA = fractional anisotropy, RD = radial diffusivity, FDR = false discover rate correction

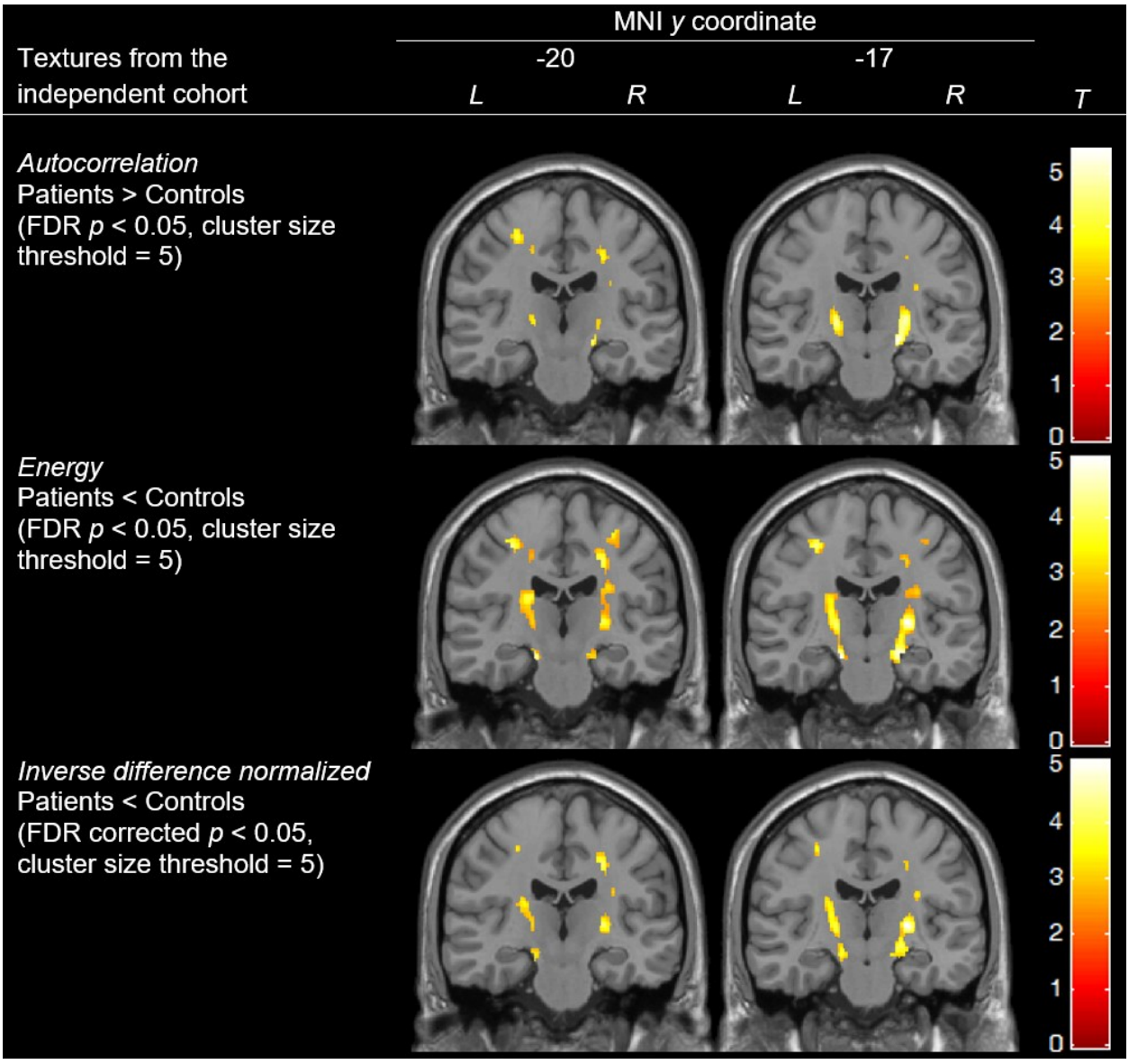

Figure 6: Differences in textures from T1W images within the CST between patients and controls in the independent cohort overlaid on a sample T1W image. FDR = false discovery rate correction, L = left, R = right

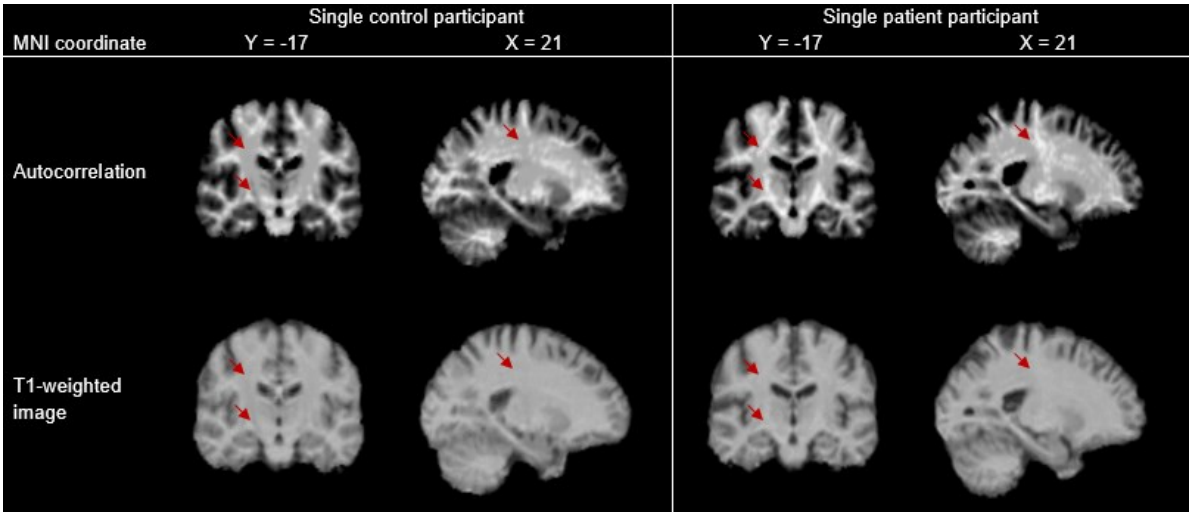

Figure 7: Representative 3D texture map for *autocorrelation* (top row) and the corresponding T1W image (bottom row) from a control (left) and a patient (right) in the independent cohort. In the control participant, the CST is homogenously hypointense on an *autocorrelation* map. In a patient, however, the CST appears to be more heterogenous with hyperintense areas in the centrum semiovale and in posterior limb of the internal capsule. The T1W image, in comparison to the texture map, shows no overt differences between the control and patient.

Table E1: Table shows the cluster size, *T* values, and the MNI coordinates of the all significant regions reported in Figure 2.

Textures from the primary cohort	Cluster size (voxels)	White matter structure	*T*	Peak MNI coordinate		
				x	*y*	*z*
Autocorrelation	218	Left centrum semiovale	-4.00	-19.5	-24	42
	242	Right centrum semiovale	-3.95	27	-18	36
	63	Left posterior limb of the internal capsule	-2.97	-19.5	-16.5	0
		Left posterior limb of the internal capsule	-2.78	-21	-16.5	-10.5
		Left corona radiata	-2.66	-24	-18	18
Energy	193	Right centrum semiovale	4.78	27	-18	37.5
	148	Left posterior limb of the internal capsule	4.73	-19.5	-16.5	6
	16	Left centrum semiovale	3.79	-7.5	-25.5	64.5
	56	Left corona radiata	3.69	-25.5	-19.5	25.5
	54	Right posterior limb of the internal capsule	3.60	21	-16.5	9
		Right posterior limb of the internal capsule	3.23	24	-16.5	1.5
	50	Left centrum semiovale	3.55	-22.5	-21	40.5
Inverse difference normalized	241	Right centrum semiovale	4.81	27	-18	37.5
	473	Left posterior limb of the internal capsule	4.65	-19.5	-16.5	6
		Left corona radiata	4.06	-24	-21	21
		Left centrum semiovale	3.43	-22.5	-21	40.5

63	Right centrum semiovale	3.90	49.5	-4.5	36
23	Left cerebral peduncle	3.83	-9	-13.5	-19.5
165	Right posterior limb of the internal capsule	3.61	21	-16.5	9
	Right posterior limb of the internal capsule	3.42	24	-16.5	1.5
	Right posterior limb of the internal capsule	3.41	24	-16.5	19.5
8	Left centrum semiovale	3.33	-9	-27	63

Table E2: Table shows the cluster size, T values, and the MNI coordinates of the all significant regions reported in Figure E1.

Tissue class	Cluster size (voxels)	Structure	*T*	Peak MNI coordinate		
				x	*y*	*z*
Gray matter	119	Right postcentral gyrus	5.64	60	-31	34
	632	Left occipital lobe	4.84	-45	-67	0
		Left occipital lobe	4.39	-36	-70	4
		Left occipital lobe	4.31	-51	-69	6
	211	Paracentral lobule	4.82	3	-15	49
		Right medial frontal gyrus	4.65	6	-7	60
	213	Left precentral gyrus	4.52	-53	-13	28
	59	Left middle temporal gyrus	4.45	-41	0	-39
	22	Left postcentral gyrus	4.40	-59	-40	45
	31	Right middle temporal gyrus	4.12	56	-49	-14
	135	Left thalamus	4.11	-18	-24	9
	92	Right superior temporal gyrus	4.00	62	-42	6
		Right superior temporal gyrus	3.96	69	-42	1
	59	Left precentral gyrus	3.97	-62	-3	19
	109	Left insula	3.91	-30	20	-5
		Left insula	3.86	-38	15	-3
	31	Paracentral lobule	3.86	-2	-16	64
	26	Right thalamus	3.62	12	-16	13
	24	Right precentral gyrus	3.61	63	-25	46
White matter	197	Right subcortical precentral gyrus	4.64	12	-13	49
	157	Left subcortical parietal lobe	4.31	-47	-51	36

149	Right subcortical postcentral gyrus	4.03	47	-33	40
	Right subcortical postcentral gyrus	3.25	56	-39	48
105	Left subcortical postcentral gyrus	3.74	-47	-39	36
	Left subcortical temporoparietal junction	3.53	-45	-39	22
70	Left subcortical occipital lobe	3.48	-11	-88	9
	Left subcortical occipital lobe	3.41	-3	-85	10
32	Left subcortical temporal gyrus	3.47	-36	-39	13

Table E3: Table shows the cluster size, T values, and the MNI coordinates of the all significant regions reported in Figure 6.

Textures from the independent cohort	Cluster size (voxels)	White matter structure	*T*	Peak MNI coordinate		
				x	*y*	*z*
Autocorrelation	230	Right cerebral peduncle	-5.43	16.5	-18	-9
		Right posterior limb of the internal capsule	-5.00	21	-15	3
	133	Left posterior limb of the internal capsule	-4.76	-19.5	-16.5	1.5
	49	Left centrum semiovale	-3.98	-28.5	-19.5	52.5
	64	Left centrum semiovale	-3.92	-19.5	-22.5	45
	77	Right centrum semiovale	-3.83	22.5	-21	42
	6	Right centrum semiovale	-3.57	13.5	-22.5	60
	26	Right corona radiata	-3.43	28.5	-15	21
Energy	748	Right posterior limb of the internal capsule	5.07	22.5	-15	4.5
		Right cerebral peduncle	5.01	18	-15	-15
		Right corona radiata	3.35	28.5	-12	19.5
	425	Left cerebral peduncle	4.88	-16.5	-16.5	-16.5
		Left posterior limb of the internal capsule	4.18	-19.5	-16.5	3
		Left corona radiata	3.99	-22.5	-18	18
	456	Left centrum semiovale	4.44	-31.5	-18	49.5
		Left centrum semiovale	3.59	-19.5	-22.5	45
		Left centrum semiovale	3.23	-25.5	-22.5	58.5

	488	Right centrum semiovale	4.21	21	-21	42
		Right centrum semiovale	3.90	34.5	-10.5	46.5
		Right centrum semiovale	3.57	28.5	-22.5	60
	11	Left centrum semiovale	3.79	-7.5	-24	57
	19	Left centrum semiovale	3.29	-40.5	-10.5	34.5
	6	Right centrum semiovale	2.74	45	-6	31.5
Inverse difference normalized	424	Right posterior limb of the internal capsule	4.39	22.5	-16.5	3
		Right cerebral peduncle	3.62	18	-16.5	-7.5
		Right corona radiata	3.26	28.5	-13.5	21
	185	Left centrum semiovale	3.82	-40.5	-9	34.5
		Left centrum semiovale	3.62	-31.5	-15	48
		Left centrum semiovale	3.31	-19.5	-22.5	45
	127	Right centrum semiovale	3.78	22.5	-21	42
	33	Left centrum semiovale	3.57	-10.5	-31.5	72
	186	Left posterior limb of the internal capsule	3.56	-19.5	-16.5	3
		Left corona radiata	3.52	-24	-18	18
	72	Left cerebral peduncle	3.44	-15	-16.5	-12
	46	Right centrum semiovale	3.15	33	-12	37.5
	12	Right centrum semiovale	2.94	45	-4.5	30

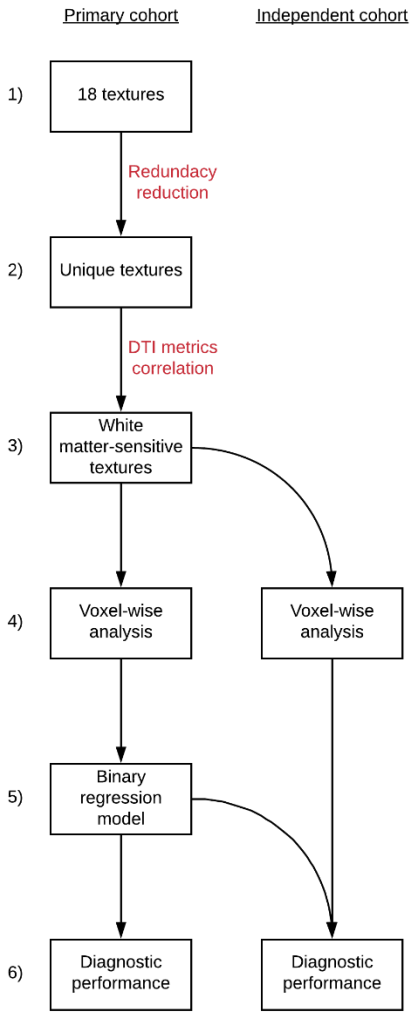

Figure E1: Flow chart depicting a summary of the analytical steps involved in texture analysis. Steps: 1) 22 textures were calculated, 2) redundant textures were removed, 3) white matter-sensitive textures were identified by correlating the unique textures to DTI metrics, 4) white matter-sensitive textures were used for voxel-wise analysis in both the primary and the independent cohorts, 5) texture values from the primary cohort were used to generate a binary regression model, and 6) used to evaluate the diagnostic performance of the white matter-sensitive textures in both cohorts.

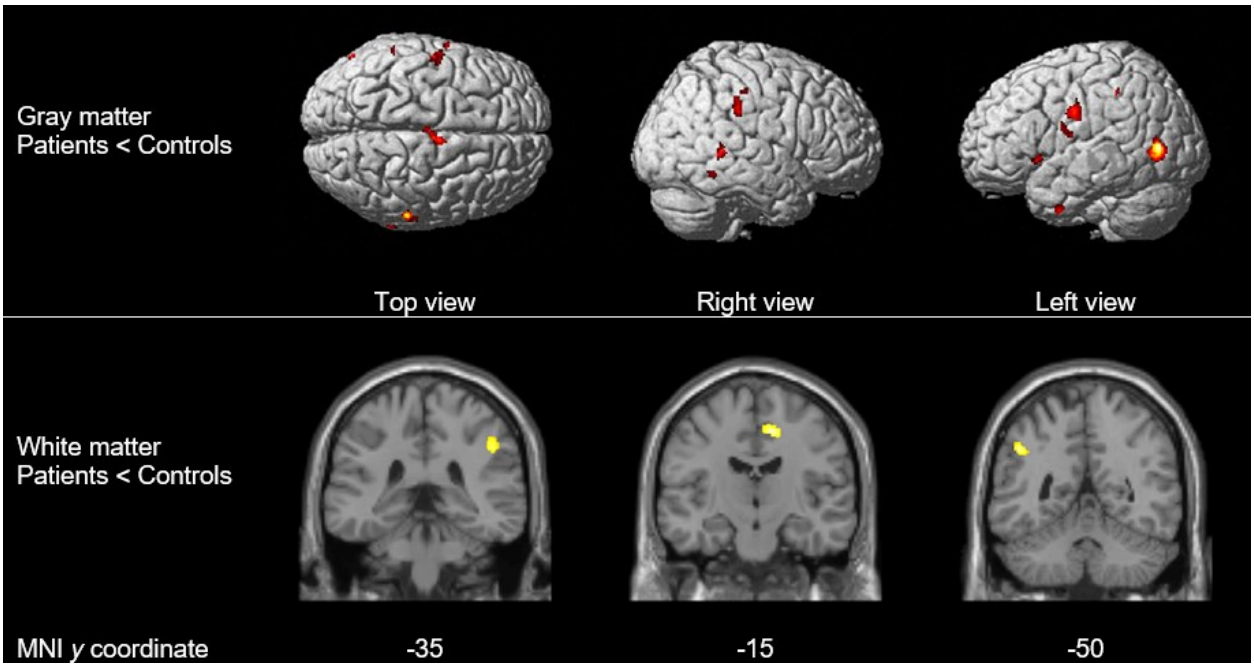

Figure E2: Gray (top) and white (bottom) matter VBM analyses for participants in the primary cohort. Significant differences at $p < 0.001$ with a cluster size threshold of 20 or more voxels were found. The results did not survive multiple comparison correction with FDR. VBM results are overlaid on a sample T1W image in neurological orientation. Detailed results are provided in Table E2. FDR = false discovery rate

Chapter 5 Distinct Patterns of Progressive Gray and White matter Degeneration in Amyotrophic Lateral Sclerosis

Abstract

Progressive cerebral degeneration in amyotrophic lateral sclerosis (ALS) remains poorly understood as most studies are performed in cross-sectional cohorts. Comprehensive investigation of gray and white matter structures requires multimodal image analysis that hampers their feasibility due to their long acquisition and processing times. Here, three-dimensional (3D) texture analysis was used to study the longitudinal gray and white matter degeneration in ALS from routine T1-weighted magnetic resonance imaging (MRI). Furthermore, progressive changes between slow and fast progressing patients were also evaluated. Participants were recruited from six centres as part of the Canadian ALS Neuroimaging Consortium (CALSNIC) and underwent clinical assessments and MRI at baseline (T_0), four (T_4) and eight (T_8) month time intervals. Functional impairment and clinical upper motor neuron (UMN) dysfunction were evaluated for ALS patients. 3D maps of the texture feature autocorrelation, which quantifies the linear dependency and repetitive patterns in pairs of gray levels, were computed from T1-weighted images for voxel-wise and region of interest (ROI) analyses. Two-hundred and fifty-six participants (119 controls and 137 ALS patients) were included in this study and 81 controls and 84 ALS patients returned for at least one follow-up. At baseline, texture changes in ALS patients were detected in the motor cortex, corticospinal tract, insular cortex, and bilateral frontal and temporal white matter. Clinical UMN dysfunction correlated specifically with texture of the corticospinal tract in the voxel-wise analysis, whereas functional impairment was associated with texture in multiple cerebral structures. ALS patients

had greater texture changes in the frontal and temporal structures at T_{max} (last follow-up visit) than at T_0. Direct comparison of texture maps at T_0 and T_{max} in ALS patients showed progressive texture alterations in the temporal white matter, insula, and internal capsule. Within the internal capsule ROI, autocorrelation increased by 0.05 ± 0.02 (mean ± standard error) units/month (P = 0.003) in ALS patients. The slow progressing ALS subgroup had greater progressive texture change in the internal capsule than the fast progressing ALS subgroup. On the other hand, the fast progressing ALS subgroup had greater progressive texture changes in the precentral gyrus. These findings suggest that the characteristic longitudinal gray matter pathology in ALS is the progressive involvement of the frontotemporal regions rather than a worsening pathology within the motor cortex. Furthermore, subclinical degeneration of the pyramidal tracts is detectable at four months with texture analysis.

Introduction

Amyotrophic lateral sclerosis (ALS) is a rapidly progressive neurodegenerative disease with a median survival of 26 months after diagnosis (Pupillo *et al.*, 2014). Its sporadic form typically affects adults between the ages of 60 and 70 years and is characterized by progressive weakness of muscles in the limbs and difficulties with speech and swallowing (Brown and Al-Chalabi, 2017). Frontotemporal dementia (FTD) is present in approximately 10% of patients at the time of diagnosis, with up to 50% of patients demonstrating cognitive and behavioural deficits on detailed neuropsychometric testing (Phukan *et al.*, 2012). Frontotemporal involvement in ALS is further substantiated by studies demonstrating widespread cortical thinning (Agosta *et al.*, 2012; d'Ambrosio *et al.*, 2014), reductions in gray matter density (Menke *et al.*, 2014), and underlying white matter degeneration (Cirillo *et al.*, 2012; Kasper *et al.*, 2014).

Though the cross-sectional cerebral neuroimaging signature of ALS is well-understood as degeneration of the upper motor neuron (UMN) system (including the motor cortex and descending pyramidal tracts) with variable frontotemporal involvement, the progressive degeneration in ALS remains poorly understood. Initial longitudinal studies were limited by small sample sizes ($n < 20$) and a majority of studies have either investigated only gray matter with T1-weighted images (Schuster *et al.*, 2014b; Walhout *et al.*, 2015; Floeter *et al.*, 2016), or white matter with diffusion tensor imaging (DTI) (van der Graaff *et al.*, 2011; Floeter *et al.*, 2018; Kassubek *et al.*, 2018). However, more comprehensive analyses are required in a disease where both gray and white matter structures are affected. Thus far, only four studies have included more than 20 ALS patients with a multimodal MRI protocol to study whole-brain progressive changes (Menke *et al.*, 2014; Cardenas-Blanco *et al.*, 2016; de Albuquerque *et al.*, 2017; Bede and Hardiman, 2018). Two of these studies demonstrated progressive changes in the

corticospinal tract and found no change in gray matter after 6 to 8 months (Cardenas-Blanco *et al.*, 2016; de Albuquerque *et al.*, 2017). In contrast, widespread gray matter degeneration was reported with limited white matter involvement in the other two studies (Menke *et al.*, 2014; Bede and Hardiman, 2018).

Texture analysis is a computational image processing technique that quantifies variations and relationships between voxel intensities in an image, which are difficult to detect by qualitative visual inspection and may not be detectable by common image analysis methods in the field, such as voxel-based morphometry (VBM) and cortical thickness measurements. Autocorrelation is a texture feature that is calculated using the gray-level co-occurrence matrix (GLCM), a second-order texture analysis method (Haralick *et al.*, 1973). It is sensitive to the fineness or coarseness of texture, and it increases with the degree of coarseness. Two-dimensional (2D) texture analysis methods have been utilized extensively in other neurological conditions such as brain tumours, stroke, epilepsy, and multiple sclerosis to detect and classify lesions (Kassner and Thornhill, 2010). Our group developed a 3D extension of GLCM to enable whole-brain voxel-wise analysis of texture features (Maani *et al.*, 2015). With this technique, we showed that autocorrelation calculated from T1-weighted images is decreased in ALS compared to controls in regions of the motor cortex, frontal lobe, and temporal lobe, and increased in the posterior limb of the internal capsule (PLIC) (Maani *et al.*, 2016; Ishaque *et al.*, 2018a). This pattern of cerebral change is in agreement with previously published structural imaging studies in ALS (Li *et al.*, 2012; Shen *et al.*, 2016). Furthermore, alterations in autocorrelation in the corticospinal tract on T1-weighted images in ALS are related to abnormalities observed with DTI metrics (Ishaque *et al.*, 2018b). Texture-based abnormalities in T1-weighted images can therefore successfully recapitulate the known gray and white matter pathology in ALS.

A comprehensive evaluation of progressive cerebral degeneration in ALS is critical to further the understanding of the pathophysiology of the disease. As such, the primary objectives of this study were to (1) examine the cerebral changes in patients with ALS over an eight-month period with texture analysis of T1-weighted images, and (2) to evaluate whether the progressive changes are different between slow and fast progressing patients. Patterns of longitudinal change and the relationships between functional disability, extent of UMN involvement, and texture were also assessed as secondary objectives. The study design included whole-brain and region-of-interest (ROI)-based approaches to investigate the changes in texture. We hypothesized that (1) texture alterations in T1-weighted images are present in gray and white matter and associated with the known pathology and clinical impairment in ALS; (2) progressive cerebral degeneration is evident as texture alterations over time; and (3) progressive cerebral changes in fast progressing patients are greater than the changes in slow progressing patients. To test our hypotheses, we conducted the study in a large, multicentre cohort of ALS patients and controls.

Materials and methods

Participants

Participants for this study were prospectively recruited from six different ALS clinics as part of the Canadian ALS Neuroimaging Consortium (CALSNIC), a multicentre research platform for biomarker studies (Kalra *et al.*, 2019). The CALSNIC research protocol consists of clinical assessments and MRI scans at baseline (T_0), four (T_4) and eight months (T_8); data from all available timepoints were used. T_{max} is the defined as the last follow-up visit attended by the participant. Patients were included in this study if they had signs of UMN and lower motor neuron (LMN) dysfunction in at least one body region on neurological examination. Patients with a family history of ALS and/or FTD, a causative genetic mutation, or comorbid FTD were

not excluded. Control participants with no known neurological or psychiatric disorders were recruited from each site. Institutional ethics approvals were obtained from all recruiting centres and participants provided free and informed written consent prior to their involvement.

Clinical assessment

Patient functional disability was assessed at all timepoints using the ALS Functional Rating Scale-Revised (ALSFRS-R). ALSFRS-R is a 48-point questionnaire that quantifies patient overall disability related to limb, bulbar, and respiratory function with lower scores representing increased disability (Cedarbaum *et al.*, 1999). Symptom duration was calculated as the time in months from symptom onset to the day the ALSFRS-R was administered. Disease progression rate was quantified as (48 – ALSFRS-R score)/symptom duration. Patients underwent a clinical neurological examination of their muscle tone and reflexes at all timepoints by neurologists specializing in ALS. Based on the clinical exam, each patient was assigned a UMN burden score out of 16 where higher scores indicate increased dysfunction; the calculation of the score is provided in Supplementary Table 1. Incomplete neurological exams were excluded from analyses. Bilateral finger and foot tapping scores were measured for each participant at all timepoints. Participants were instructed to tap their finger and foot as fast as possible over a one-minute period for two trials. The final finger and foot tapping scores were calculated as the means of their bilateral scores over the two trials. Tapping scores of 0 were excluded from analyses.

Magnetic resonance imaging

3D T1-weighted images were acquired at 1 *mm* isotropic resolution at all timepoints on 3 T MRI systems as part of the larger CALSNIC MRI protocol (Kalra *et al.*, 2019). Supplementary Table 2 details the MRI acquisition parameters at each of the six recruiting centres.

Image processing

Image processing and analyses were carried out in Statistical Parametric Mapping 12 (SPM12) (https://www.fil.ion.ucl.ac.uk/spm/) and the Computational Anatomy Toolbox 12 (http://www.neuro.uni-jena.de/cat/) software. All T1-weighted images were aligned along the anterior commissure-poster commissure line for optimal image processing and texture analysis. These were then processed using the CAT12 "Segment Data" pipeline where they underwent bias field correction, segmentation into gray and white matter tissue classes, and normalization to the supplied Montreal Neurological Institute (MNI) template using the Diffeomorphic Anatomic Registration Through Exponentiated Lie algebra approach at default settings (Ashburner, 2007). Deformation field maps for the native-to-standard space image transformation were saved for each participant and their individual timepoints.

The 3D GLCM texture analysis was performed using a toolbox developed for SPM (Maani *et al.*, 2015). Whole-brain maps for autocorrelation were calculated from the bias-corrected T1-weighted volume images in their native space. Autocorrelation quantifies the linear dependency and repetitive patterns in pairs of gray levels in a local neighborhood of voxels in an image. Further technical details describing its calculation have been published previously (Maani *et al.*, 2015; Ishaque *et al.*, 2018a). The saved deformation field map for each T1-weighted image was applied to its respective autocorrelation map to transform the map to the MNI space. The

transformed autocorrelation maps were smoothed with a 6 *mm* full-width at half-maximum Gaussian kernel prior to voxel-wise analyses.

The voxel-wise analyses allowed investigations of whole-brain group comparisons and clinical correlations in an unbiased manner. Combined with texture analysis of T1-weighted images, this approach enabled the assessments of both gray and white matter structures without *a priori* hypotheses. In addition, ROI-based analyses of the motor structures were also performed to probe their specific clinical correlations and to quantify their longitudinal progression in ALS. The ROI-based analyses also served a secondary purpose of verifying the results of voxel-wise analyses. Mean autocorrelation values from the precentral gyrus and the PLIC were extracted. The mask for the bilateral precentral gyrus was obtained from the Harvard-Oxford cortical structural atlas at a 25% threshold and the mask for the PLIC was obtained from the John Hopkins University white matter label atlas (Mori *et al.*, 2008). These masks were applied to the unsmoothed autocorrelation maps in the MNI space and their mean autocorrelation value for each region was calculated. This was done for data from all time points.

Statistical analysis

Quantitative demographic, clinical, and ROI data were analyzed in MedCalc Statistical Software version 19.1.3 (MedCalc Software bvba, Ostend, Belgium; https://www.medcalc.org; 2019). Results are presented as mean ± standard deviation unless otherwise stated. Between-group differences were assessed with independent samples *t*-tests, χ^2 tests, and analysis of covariance where appropriate. Pearson correlation coefficient, *r*, was used to test for associations among clinical variables and autocorrelation. Corrections for multiple comparisons were not employed because the testing of individual clinical associations was hypothesis-driven. Patients were classified as “slow progressing” if their disease progression rate was lower than the patient

group's median rate, or as "fast progressing" if it was higher. Statistical significance was defined at $P < 0.05$.

Voxel-wise analyses were conducted in SPM12. Full-factorial models were used to assess between-group, whole-brain differences in autocorrelation. The models included "group" as the variable of interest and age as a covariate. Site was not included as a factor because autocorrelation had previously been shown to have high intra- and inter-site reliability in voxel-wise and ROI-based analyses in an intraclass correlation coefficient study (Ta *et al.*, 2019). As an added measure, the main voxel-wise group analysis was also performed with and without a correctional factor for site (data not shown). The results from both of these models were nearly identical, and thus, site was omitted as a factor for all analyses in favor of simplicity. A *T*-contrast was used to establish the directionality of change in autocorrelation (increased or decreased) in ALS compared to controls. *F*-contrasts were subsequently used to test for the absolute changes in autocorrelation between groups. The following clinical measures were tested as variables of interest at T_0: (1) ALSFRS-R score, (2) UMN burden score, (3) average finger tapping score, and (4) average foot tapping score. Whole-brain voxel-wise paired *t*-tests were conducted in patients to compare their autocorrelation maps at the different timepoints. Regression models were used to assess for whole-brain associations between autocorrelation and clinical variables in ALS patients. Significant clusters were identified at $P < 0.0005$ with a minimum cluster size of at least 50 voxels for all voxel-wise analyses (Sheng *et al.*, 2015; Chen *et al.*, 2018).

Linear mixed-effects models were used to assess the longitudinal progression of clinical measures and autocorrelation in the ROIs in ALS patients. The time interval from T_0 in months was used as the fixed effect. The model intercept and the time interval were used as the random

effects. Longitudinal change in autocorrelation was additionally investigated in the ALS subgroups and controls. The interaction between group assignment and monthly decline in autocorrelation was also tested between ALS and controls, and slow and fast progressing ALS. All linear mixed-effect models were analyzed in SPSS (IBM Corp. Released 2016. IBM SPSS Statistics for Windows, Version 20.0. Armonk, NY: IBM Corp.). Statistical significance was defined at $P < 0.05$.

Results

Study sample characteristics

A total of 256 participants (119 controls and 137 ALS patients) met the inclusion criteria for this study (Table 1). The mean age of ALS patients was higher than controls ($P = 0.02$), and there were proportionally more males than females in the ALS group than in the control group ($P = 0.04$). The mean ALSFRS-R score was 37.8 ± 5.7 ($n = 134$), UMN burden was 5.4 ± 2.9 ($n = 125$), and finger and foot tapping scores were 43.3 ± 13.2 ($n = 94$) and 29.0 ± 12.2 ($n = 80$), respectively. The median disease progression rate for ALS patients was 0.4 (range 0.02 – 2.1) and this was used to divide the patients into slow and fast progressing ALS subgroups. Participants in these two subgroups had no differences in their mean age and gender distribution ($P = 0.4$ and 0.5, respectively; Supplementary Table 3). Participants in the fast progressing ALS subgroup had a higher mean UMN burden score ($P = 0.002$) and a greater proportion of patients with bulbar-onset ALS ($P = 0.004$). Further clinical and demographic details for ALS subgroups are provided in Supplementary Table 3.

Eighty-one controls and 84 ALS patients returned for at least one follow-up MRI scan. Fifty-seven controls had follow-up scans at T_4 and T_8, and 49 ALS patients returned for follow-

up scans at both timepoints. A total of 528 MRI datasets from ALS patients and controls were therefore included in this study (T_0 = 257, T_4 = 159, T_8 = 112). At the time of analysis, not all participants had reached their T_4 and/or T_8 assessments and therefore an attrition rate was not determined. The mean time from T_0 to T_{max} was 243.9 ± 74.6 days and 212.8 ± 68.2 days for controls and ALS patients, respectively. There were no differences in the mean age and gender distribution between ALS patients who returned for a follow-up and those who did not (P = 0.8 and 0.4, respectively). The mean UMN burden score at baseline also did not differ between these two groups (P = 0.7). ALS patients who returned for a follow-up had a higher mean ALSFRS-R score at T_0 (39.0 ± 4.8) compared to those who did not return (35.6 ± 6.5; P < 0.001); however, there was no significant difference between the two groups' disease progression rates (0.4 ± 0.4 versus 0.5 ± 0.4, respectively; P = 0.1). Of the 110 patients with limb-onset ALS at baseline, 74 (67.2%) returned for at least one follow-up MRI scan. In contrast, 10 of the 27 (37.0%) patients with bulbar-onset ALS returned for a follow-up (P = 0.004).

Group differences in texture at baseline

In whole-brain group comparison, ALS patients had decreased autocorrelation compared to controls in bilateral precentral gyri, subcortical white matter, left supplementary motor area, left frontal middle and superior gyri, bilateral frontal white matter, bilateral insular cortex, and bilateral temporal white matter (Fig. 1). Autocorrelation was increased in ALS patients along bilateral pyramidal tracts in regions between the corona radiata and the cerebral peduncles (Fig. 1). Significant clusters in bilateral pyramidal tracts and medial precentral gyrus were present even after the application of progressively restrictive statistical thresholds of P < 0.00005, 0.000005, and 0.0000005 (Supplementary Fig. 1). Clusters in the left insular cortex and thalamic

region appeared at $P < 0.000005$, followed by clusters in the temporal lobe at the lowest statistical threshold of $P < 0.00005$.

Compared to controls, the slow progressing ALS group had alterations in autocorrelation in bilateral precentral gyri, left middle frontal gyrus, bilateral frontal white matter, left insular cortex, and bilateral pyramidal tracts (Fig. 2A). In contrast, the fast progressing ALS group had fewer regions of altered autocorrelation in the frontal cortex, but a greater involvement of bilateral pyramidal tracts, temporal white matter, and parahippocampal regions (Fig. 2B). There were no significant differences between the subgroups when compared directly ($P > 0.001$).

In the ROI-based analysis, autocorrelation was decreased in ALS patients in the bilateral precentral gyrus (estimated marginal mean ± standard error: 42.4 ± 0.2) compared to controls (43.1 ± 0.2) when covaried with age ($P = 0.004$). Similarly, in the PLIC ROI, autocorrelation was significantly ($P < 0.001$) increased in ALS patients (82.9 ± 0.2) compared to controls (81.2 ± 0.2). No significant difference was present in autocorrelation between the subgroups in the precentral gyrus (slow progressing ALS: 42.3 ± 0.3 and fast progressing ALS: 42.6 ± 0.3; $P = 0.3$) or in the PLIC (slow progressing ALS: 82.6 ± 0.3 and fast progressing ALS: 83.2 ± 0.3; $P = 0.1$).

Longitudinal changes in texture

In the whole-brain paired *t*-test comparing ALS patients at T_0 and T_{max} ($n = 84$), autocorrelation was significantly decreased at T_{max} in the posterior corpus callosum, left insular cortex, left temporal white matter, and along the junction of lateral ventricles and bilateral caudate heads compared to T_0 (Fig. 3A). Additionally, autocorrelation was significantly increased in the left internal capsule and right thalamus at T_{max} (Fig. 3A). In the slow progressing

ALS subgroup with at least one follow-up (n = 44), autocorrelation was significantly decreased in the posterior corpus callosum and significantly increased in the left internal capsule at T_{max} compared to T_0. (Fig. 3B). In contrast, autocorrelation was significantly decreased in the posterior corpus callosum, left insular cortex, and at the junction of lateral ventricles and bilateral caudate heads in fast progressing ALS (n = 40) at T_{max} compared to T_0 (Fig. 3C). No areas were significantly increased in this ALS subgroup. No whole-brain differences were found with paired t-test between controls at T_0 and T_{max}.

Progressive changes between all three timepoints were assessed with whole-brain paired t-tests in the subset of ALS patients who returned for all timepoints (n = 49). Between T_0 and T_4, autocorrelation was significantly decreased in the posterior corpus callosum (Supplementary Fig. 2A). Between T_0 and T_8, autocorrelation was significantly decreased in the posterior corpus callosum and along the junction of lateral ventricles and bilateral caudate heads (Supplementary Fig. 2B). Autocorrelation was also significantly increased in the right thalamus in this comparison.

Longitudinal changes in texture in ALS were also assessed with group analyses between ALS patients and controls at T_0 and T_{max}. At T_0, ALS patients had alterations in autocorrelation in the precentral gyrus, bilateral pyramidal tracts, and left insular cortex compared to controls when covaried with age (Fig. 4A). At T_{max}, in addition to the changes observed at T_0, these ALS patients had further alterations in autocorrelation in the frontal lobe white matter, bilateral temporal lobe white matter hippocampus, and thalamus compared to controls (Fig. 4B). Furthermore, there was an increase in the size of the significant clusters at T_{max} compared to T_0.

Linear mixed models were used to investigate the longitudinal evolution of autocorrelation in the precentral gyrus and PLIC ROIs. Controls demonstrated no significant

longitudinal change in autocorrelation in either the precentral gyrus ($P = 0.7$) or the PLIC ($P = 0.5$). In ALS patients, there was no significant decline in autocorrelation within the precentral gyrus ROI over time [0.005 ± 0.009 (standard error) unit/month, $P = 0.4$). Autocorrelation in the PLIC increased significantly at a rate of 0.05 ± 0.02 (standard error) unit/month ($P = 0.003$). When compared directly, the rate of change in autocorrelation over time was significantly different between ALS patients and controls in the PLIC ($P = 0.008$), but not in the precentral gyrus ($P = 0.9$).

In the fast progressing ALS subgroup, there was a trend towards a significant monthly decline in autocorrelation in the precentral gyrus of 0.03 ± 0.01 unit ($P = 0.08$). In the slow progressing ALS subgroup, there was no significant change over time in autocorrelation in the precentral gyrus (0.007 ± 0.01 unit/month, $P = 0.5$). There was a trend towards a significant difference between fast and slow progressing ALS in their rates of change in autocorrelation in the precentral gyrus ($P = 0.09$). In slow progressing ALS, there was a significant increase of 0.06 ± 0.02 unit/month ($P = 0.02$) in the PLIC. The rate of change increase in autocorrelation (0.05 ± 0.03 unit) did not reach significance ($P = 0.08$) in fast progressing ALS. When compared directly, there was no significant difference between the two subgroups in their rates of change in autocorrelation over time in the PLIC ($P = 0.6$). Fig. 5 shows the change in autocorrelation in the precentral gyrus and the PLIC between all timepoints in controls, ALS patients, and ALS subgroups.

Clinical measures: correlations and longitudinal changes

ALSFRS-R scores correlated with UMN burden scores ($r = -0.2$, $P = 0.01$), and finger ($r = 0.5$, $P < 0.001$) and foot tapping scores ($r = 0.4$, $P < 0.001$; Supplementary Fig. 3). UMN

burden scores correlated with finger (r = -0.4, P < 0.001) and foot tapping scores (r = -0.4, P < 0.001; Supplementary Fig. 3). The longitudinal decline in clinical measures was assessed by linear mixed-effect models. An average monthly decline of 0.5 ± 0.06 (standard error) points was observed in the ALSFRS-R score (P < 0.001; Supplementary Fig. 4). UMN burden scores did not demonstrate a significant longitudinal monthly change (0.2 ± 0.03, P = 0.6). Finger (0.6 ± 0.2, P < 0.001) and foot tapping scores (0.5 ± 0.1, P = 0.001) also demonstrated significant monthly declines in ALS patients (Supplementary Fig. 4).

Clinical measures: associations with texture

In whole-brain analysis, the ALSFRS-R displayed widespread positive correlations with autocorrelation in the white matter regions of the frontal lobe, right insula, right precentral gyrus, left postcentral gyrus, bilateral hippocampal and parahippocampal regions, and in the pons of the brainstem (Fig. 6A). Positive correlations between UMN burden score and autocorrelation localized along the bilateral pyramidal tracts in the corona radiata and the internal capsule (Fig. 6B). Additional associations with UMN burden were seen in bilateral caudate head. Finger tapping positively correlated with autocorrelation in ALS patients in the frontal lobe white matter, right middle precentral gyrus, left supplementary motor lobule, and bilateral posterior cingulate gyrus (Fig. 6C). Foot tapping scores demonstrated positive correlations in the frontal lobe white matter and bilateral posterior cingulate gyrus (Fig. 6D).

Autocorrelation from the precentral gyrus ROI significantly correlated with the average finger tapping score (r = 0.3, P = 0.003). Autocorrelation from the PLIC significantly correlated with UMN burden score (r = 0.3, P = 0.002; Supplementary Fig. 5). There were no other significant correlations between autocorrelation and clinical measures.

Discussion

In this study, we set out to investigate progressive cerebral degeneration in ALS with texture analysis of T1-weighted images in a large, multicentre cohort. We first showed that texture-based abnormalities in gray and white matter at baseline were spatially congruent with the cerebral pathology of ALS. Importantly, texture alterations in the pyramidal tract were also found to be highly specific for clinical UMN dysfunction. This was in contrast to ALSFRS-R and finger and foot tapping scores that showed diffuse associations to gray and white matter structures. Furthermore, longitudinal analyses revealed that gray matter progression was characterized by spread of pathology towards the frontotemporal regions. We observed progressive changes in the pyramidal tracts after only four months. This is a novel observation and of importance as clinical UMN dysfunction did not progress over this time. Lastly, we showed that progressive cerebral degeneration in ALS was predicated upon the disease progression rate at baseline. Taken together, these findings also strongly suggest that texture analysis of T1-weighted images is a sensitive marker for longitudinal mapping of disease-related cerebral degeneration in ALS.

Progression of cerebral degeneration in ALS

Though the mechanisms by which progressive cerebral pathology in ALS is disseminated are far from clear, propagation of misfolded proteins via a "prion-like" mechanism is a leading hypothesis (Polymenidou and Cleveland, 2011). Pathological proteins TDP-43 and SOD1 in ALS form seeding aggregates (Watanabe *et al.*, 2001; Johnson *et al.*, 2009) that are believed to propagate via axonal pathways between connected regions leading to a stereotyped spread of disease in the brain (Jucker and Walker, 2013). The four stages of TDP-43 pathology demonstrate a frontotemporal pattern of dissemination with involvement of prefrontal structures

in stage 3 and temporal structures in stage 4 (Brettschneider *et al.*, 2013). Therefore, it is reasonable to hypothesize that longitudinal degeneration in ALS should demonstrate a progressive involvement of frontotemporal structures. In our study, greater texture abnormalities were noted in the frontotemporal and insular regions at follow-up. Atrophic changes in the insula have shown associations with impaired cognitive flexibility in ALS (Evans *et al.*, 2015), and abnormal TDP-43 deposition in the insula is observed in 26 – 49% of patients (Cykowski *et al.*, 2017). Interestingly, we did not find longitudinal change in the precentral gyrus to be different between ALS patients and controls in ROI-based analysis. Indeed, studies investigating longitudinal cortical thickness have demonstrated thinning of the frontal and temporal cortices with sparing of the precentral gyrus (Verstraete *et al.*, 2012; Schuster *et al.*, 2014a; Walhout *et al.*, 2015). This has clinical implications as we previously demonstrated that patients with a shorter survival have greater texture abnormalities in the frontotemporal and insular regions with relatively comparable degeneration of motor cortex compared to patients with a longer survival (Ishaque *et al.*, 2018a). Taken together, these findings suggest that further degeneration within the motor cortex in ALS is limited after a critical level of damage is reached. As such, targeted therapies may play a disease-modifying role if they can halt the disseminative pathology within the gray matter. Future studies should monitor gray matter changes in ALS by assessing the involvement of extra-motor frontal and temporal structures in a staged manner over time, akin to the proposed DTI-based staging system (Kassubek *et al.*, 2014; Kassubek *et al.*, 2018).

Pathology of the pyramidal tracts in ALS is believed to be well-established by the time of diagnosis with limited subsequent longitudinal progression (Menke *et al.*, 2014; Bede and Hardiman, 2018). In particular, a recent study found no change in the pyramidal tracts after four months with DTI analysis (Bede and Hardiman, 2018). In the current study, however,

progressive degeneration of the pyramidal tracts was detected at four months. Strikingly, we did not detect concurrent progressive decline in clinical UMN dysfunction, which is also in agreement with previously published data (Menke *et al.*, 2014). This suggests that texture abnormalities within the pyramidal tracts can monitor subclinical UMN dysfunction and importantly, provide a much-needed marker for ALS. A formal comparison is needed to ascertain whether or not alterations in texture are more sensitive than DTI in detecting longitudinal degenerative changes.

We also noted abnormalities in texture in the corpus callosum in ALS patients over time. Corpus callosum degeneration is a key component of the cross-sectional DTI signature in ALS (Filippini *et al.*, 2010). Longitudinal changes in the corpus callosum have also been noted in other studies (van der Graaff *et al.*, 2011; Zhang *et al.*, 2011; Menke *et al.*, 2014; Bede and Hardiman, 2018). Histologically, inflammatory markers are increased in the corpus callosum with accompanying loss of myelinated axons (Sugiyama *et al.*, 2013; Cardenas *et al.*, 2017), although its role in the pathophysiology of the disease is yet to be elucidated.

In attempting to delineate the relationship between cerebral degeneration and the disease progression rate, patients with fast progressing ALS had greater longitudinal texture alterations in the precentral gyrus compared to patients with slow progressing ALS; however, at baseline, texture abnormalities were similar in both subgroups in this region. Pathology in the motor cortex likely approaches its maximal state, especially in patients with slower disease progression rates, by the time patients are enrolled in clinical studies. In support of this, several studies show correlations between disease progression rate and extra-motor frontotemporal regions in whole-brain cortical thickness analyses (Verstraete *et al.*, 2012; d'Ambrosio *et al.*, 2014; Walhout *et al.*, 2015). It can be postulated from these observations that a faster disease progression rate

implicates a more rapid and greater involvement of the frontotemporal regions. Conversely in the PLIC, patients with slow progressing ALS had greater longitudinal texture change whereas patients with fast progressing ALS had greater abnormalities at baseline. The pyramidal tracts may play a more direct role in regulating disease progression rates with faster rates being associated with greater degeneration at baseline (Menke *et al.*, 2012). This is further substantiated by our observation of greater clinical UMN dysfunction in the fast progressing ALS subgroup at baseline. To the best of our knowledge, no other study has formally investigated the impact of disease progression rate on the progressive degeneration of gray and white matter structures in ALS. It should be noted that even though some of these findings did not satisfy strict statistical significance thresholds, they are of clinical significance and warrant further investigation. If patients with slower disease progression rates do indeed continue to experience progressive pyramidal tract degeneration, this may be an interventional window for future therapies.

Texture of T1-weighted images as a marker for cerebral degeneration in ALS

The most consistent texture abnormalities in ALS are in the motor cortex and in the regions of the pyramidal tracts. Loss of Betz cells (Lawyer and Netsky, 1953; Nihei *et al.*, 1993), astrocytic gliosis (Kamo *et al.*, 1987; Murayama *et al.*, 1991), and aberrant TDP-43 deposition (Brettschneider *et al.*, 2013) are considered the core pathological features in the motor cortex in ALS. Decreased autocorrelation in the motor cortex in patients is likely related to some aggregate of these abnormalities. The derivation of autocorrelation is a function of voxel intensities and the likelihood of co-occurring intensities in an image. Indeed, histological associations, particularly with markers of gliosis, using quantitative *ex vivo* MRI have shown that

these pathological features impact T1 relaxation times in ALS (Meadowcroft *et al.*, 2015). Recent studies have also suggested that T2 shortening in the motor cortex is caused by increased iron accumulation in the microglia (Kwan *et al.*, 2012). Reduced gray matter density (Shen *et al.*, 2016) and cortical thinning (Agosta *et al.*, 2012) are well-known neuroimaging correlates of ALS. It is reasonable to attribute decreased autocorrelation simply to cortical atrophy. However, we showed previously that reduced autocorrelation values in the cortex only partially overlap with reduced gray matter densities and also expand to other disease-related regions (Ishaque *et al.*, 2018a). Texture abnormalities could provide insight into events preceding the later stages of degeneration such as cortical thinning.

Within the pyramidal tracts, loss of myelinated axons and altered myelin sheath morphology are classic pathologic findings in ALS (Lawyer and Netsky, 1953; Smith, 1960). Findings of myelin pallor on Luxol fast blue stains, suggesting myelin loss, are variable and are often present only in cases of marked UMN loss. A study investigating *in vivo* myelin content with myelin water fraction found that there were no abnormalities in ALS patients compared to controls (Kolind *et al.*, 2013). Instead, the authors found increased intra- and extracellular water content that is potentially associated with edema secondary to neuroinflammatory processes. This is in concordance with evidence of widespread cerebral microglial activation in ALS found in neuroimaging (Turner *et al.*, 2004) and histological studies (Kawamata *et al.*, 1992). Additionally, mild qualitative hyperintensities on T1-weighted images (Kato *et al.*, 1997) and increased T2 relaxation times and quantitative proton density in ALS (Ding *et al.*, 2011) are thought to be caused by axonal damage leading to an increase in unbound water. Taken together, we postulate that the increase in autocorrelation observed in the pyramidal tracts in ALS is caused by neuroinflammatory processes involved in the breakdown of myelin content and axonal

loss secondary to cortical neuronal degeneration instead of primary insults to myelin content. Indeed, texture abnormalities in the pyramidal tracts in ALS also correlate with abnormalities in DTI measures that suggest a secondary axonal degeneration process (Ishaque *et al.*, 2018b). This is in contrast with multiple sclerosis where increased texture heterogeneity in lesions and diffusely abnormal white matter was found to be more sensitive to myelin loss compared to axonal injury and inflammation (Zhang *et al.*, 2013). It is therefore imperative that future studies disentangle the multifaceted causes of texture alterations in ALS with direct correlations to histological data to further understand the pathophysiology of the disease.

Clinical-radiological associations have been sought extensively in ALS (Verstraete *et al.*, 2015). The near-exclusive correlation between pyramidal tract changes and UMN burden in this study suggests that the degeneration of this pathway is primarily responsible for the clinical presentation of UMN dysfunction. This was similarly observed in a previous DTI study (Menke *et al.*, 2014). In contrast, the widespread cerebral correlations of ALSFRS-R underscore its poor specificity for UMN function. Studies have shown correlations between ALSFRS-R limb and bulbar sub-scores and the respective gray matter regions in the motor homunculus (Bede *et al.*, 2013; Walhout *et al.*, 2015). Abnormalities in ALSFRS-R sub-scores also correlate with the region of symptom onset (Rooney *et al.*, 2017). The region of symptom onset in ALS is believed to experience the maximal UMN and LMN degeneration (Ravits, 2014). Therefore, ALSFRS-R correlations along the motor homunculus are likely related to an interplay between concurrent UMN and LMN pathology. Finger and foot tapping scores have been used as surrogates for UMN dysfunction in ALS studies (Kent-Braun *et al.*, 1998; Mitsumoto *et al.*, 2007). Here, we found these scores to correlate with clinical UMN dysfunction and as such demonstrate their sensitivity to it; however, they did not show specificity to motor cortex or pyramidal tract

degeneration in whole-brain correlations. Functional MRI studies have demonstrated reduced cortical activity in the prefrontal cortices during voluntary movement tasks in ALS patients (Stanton *et al.*, 2007; Cosottini *et al.*, 2012). This is in line with our finding of frontal lobe associations of finger and foot tapping scores and suggest that motor weakness related to volitional tasks in ALS is associated with failures and compensations in larger networks and not isolated dysfunctions in the UMN system.

Technical considerations and limitations

We have successfully shown here that 3D texture analysis of T1-weighted images enables the assessment of gray and white matter structures for degenerative changes. These changes are associated with clinical dysfunction and can offer insight into the pathophysiology of disease and serve as markers in clinical trials. This technique represents an advancement for neuroimaging studies as it can interrogate both gray and white matter without requiring multimodal MRI protocols that are often challenging for patients with debilitating diseases. Texture features may therefore be considered robust markers for cerebral degeneration that can be rapidly implemented in clinical trials as they only require a T1-weighted image. Future studies must investigate the neuropathological underpinnings for texture features and associations with other relevant MRI modalities (Ishaque *et al.*, 2018b).

We included longitudinal data from controls to ensure the observed findings were not due to healthy ageing, or an artifact of texture analysis. A limitation of this study, however, is that since CALSNIC is actively acquiring data, longer duration and complete follow-up data were not available for all patients and controls. A future study with a larger dataset should aim to replicate the current findings. Furthermore, we did not apply image intensity normalization techniques in this study to account for multicentre data from different MRI systems. It is possible that some of

the observed results were affected by MRI system-specific differences. However, given the relevant clinical correlations, similar results to previous studies, and inclusion of control data from all recruiting sites, that is an unlikely possibility. Additionally, autocorrelation has demonstrated high intra- and inter-site reliability in traveling control datasets (Ta *et al.*, 2019). Nevertheless, it would be worthwhile to optimize texture analysis pipelines to account for possible subtle image intensity variations due to MRI system differences.

In conclusion, we provide evidence for progressive degeneration of white matter in the PLIC in ALS over four- and eight-month intervals in the absence of clinical UMN decline. The longitudinal course of gray matter pathology is characterized by a frontotemporal spatial spread, instead of progressive degeneration within the motor structures. Furthermore, these progressive patterns are influenced by the disease progression rate. This suggests the presence of disease-specific cerebral network vulnerabilities and differential involvement of gray and white matter degeneration in contrast to a simple gradient. Indeed, future studies should look to further parse the factors influencing the longitudinal degeneration in ALS, such as site of symptom onset and cognitive involvement.

Data availability statement

Data can be made available upon submission of a formal request to the corresponding author.

Acknowledgement

We would like to acknowledge and thank the participants and their families for donating their time and energy to this study. We would also like to thank the research support staff at each recruiting centre for their efforts.

Funding

Funding for this study was received from the Canadian Institutes of Health Research, ALS Society of Canada, Alberta Innovates, and Brain Canada.

Competing interests

The authors report no competing financial and non-financial interests in relation to the work described.

References

Agosta F, Valsasina P, Riva N, Copetti M, Messina MJ, Prelle A*, et al.* The cortical signature of amyotrophic lateral sclerosis. PLoS One 2012; 7(8): e42816.

Ashburner J. A fast diffeomorphic image registration algorithm. Neuroimage 2007; 38(1): 95-113.

Bede P, Bokde A, Elamin M, Byrne S, McLaughlin RL, Jordan N*, et al.* Grey matter correlates of clinical variables in amyotrophic lateral sclerosis (ALS): a neuroimaging study of ALS motor phenotype heterogeneity and cortical focality. J Neurol Neurosurg Psychiatry 2013; 84(7): 766-73.

Bede P, Hardiman O. Longitudinal structural changes in ALS: a three time-point imaging study of white and gray matter degeneration. Amyotroph Lateral Scler Frontotemporal Degener 2018; 19(3-4): 232-41.

Brettschneider J, Del Tredici K, Toledo JB, Robinson JL, Irwin DJ, Grossman M*, et al.* Stages of pTDP-43 pathology in amyotrophic lateral sclerosis. Ann Neurol 2013; 74(1): 20-38.

Brown RH, Al-Chalabi A. Amyotrophic Lateral Sclerosis. N Engl J Med 2017; 377(2): 162-72.

Cardenas AM, Sarlls JE, Kwan JY, Bageac D, Gala ZS, Danielian LE*, et al.* Pathology of callosal damage in ALS: An ex-vivo, 7 T diffusion tensor MRI study. Neuroimage Clin 2017; 15: 200-8.

Cardenas-Blanco A, Machts J, Acosta-Cabronero J, Kaufmann J, Abdulla S, Kollewe K*, et al.* Structural and diffusion imaging versus clinical assessment to monitor amyotrophic lateral sclerosis. Neuroimage Clin 2016; 11: 408-14.

Cedarbaum JM, Stambler N, Malta E, Fuller C, Hilt D, Thurmond B*, et al.* The ALSFRS-R: a revised ALS functional rating scale that incorporates assessments of respiratory function. BDNF ALS Study Group (Phase III). J Neurol Sci 1999; 169(1-2): 13-21.

Chen G, Zhou B, Zhu H, Kuang W, Bi F, Ai H*, et al.* White matter volume loss in amyotrophic lateral sclerosis: A meta-analysis of voxel-based morphometry studies. Prog Neuropsychopharmacol Biol Psychiatry 2018; 83: 110-7.

Cirillo M, Esposito F, Tedeschi G, Caiazzo G, Sagnelli A, Piccirillo G*, et al.* Widespread microstructural white matter involvement in amyotrophic lateral sclerosis: a whole-brain DTI study. AJNR Am J Neuroradiol 2012; 33(6): 1102-8.

Cosottini M, Pesaresi I, Piazza S, Diciotti S, Cecchi P, Fabbri S*, et al.* Structural and functional evaluation of cortical motor areas in Amyotrophic Lateral Sclerosis. Exp Neurol 2012; 234(1): 169-80.

Cykowski MD, Powell SZ, Peterson LE, Appel JW, Rivera AL, Takei H*, et al.* Clinical Significance of TDP-43 Neuropathology in Amyotrophic Lateral Sclerosis. J Neuropathol Exp Neurol 2017; 76(5): 402-13.

d'Ambrosio A, Gallo A, Trojsi F, Corbo D, Esposito F, Cirillo M*, et al.* Frontotemporal cortical thinning in amyotrophic lateral sclerosis. AJNR Am J Neuroradiol 2014; 35(2): 304-10.

de Albuquerque M, Branco LM, Rezende TJ, de Andrade HM, Nucci A, Franca MC, Jr. Longitudinal evaluation of cerebral and spinal cord damage in Amyotrophic Lateral Sclerosis. Neuroimage Clin 2017; 14: 269-76.

Ding XQ, Kollewe K, Blum K, Korner S, Kehbel S, Dengler R*, et al.* Value of quantitative analysis of routine clinical MRI sequences in ALS. Amyotroph Lateral Scler 2011; 12(6): 406-13.

Evans J, Olm C, McCluskey L, Elman L, Boller A, Moran E*, et al.* Impaired cognitive flexibility in amyotrophic lateral sclerosis. Cogn Behav Neurol 2015; 28(1): 17-26.

Filippini N, Douaud G, Mackay CE, Knight S, Talbot K, Turner MR. Corpus callosum involvement is a consistent feature of amyotrophic lateral sclerosis. Neurology 2010; 75(18): 1645-52.

Floeter MK, Bageac D, Danielian LE, Braun LE, Traynor BJ, Kwan JY. Longitudinal imaging in C9orf72 mutation carriers: Relationship to phenotype. Neuroimage Clin 2016; 12: 1035-43.

Floeter MK, Danielian LE, Braun LE, Wu T. Longitudinal diffusion imaging across the C9orf72 clinical spectrum. J Neurol Neurosurg Psychiatry 2018; 89(1): 53-60.

Haralick RM, Shanmugam K, Dinstein IH. Textural features for image classification. IEEE Transactions on systems, man, and cybernetics 1973(6): 610-21.

Ishaque A, Mah D, Seres P, Luk C, Eurich D, Johnston W*, et al.* Evaluating the cerebral correlates of survival in amyotrophic lateral sclerosis. Ann Clin Transl Neurol 2018a; 5(11): 1350-61.

Ishaque A, Mah D, Seres P, Luk C, Johnston W, Chenji S*, et al.* Corticospinal tract degeneration in ALS unmasked in T1-weighted images using texture analysis. Hum Brain Mapp 2018b.

Johnson BS, Snead D, Lee JJ, McCaffery JM, Shorter J, Gitler AD. TDP-43 is intrinsically aggregation-prone, and amyotrophic lateral sclerosis-linked mutations accelerate aggregation and increase toxicity. J Biol Chem 2009; 284(30): 20329-39.

Jucker M, Walker LC. Self-propagation of pathogenic protein aggregates in neurodegenerative diseases. Nature 2013; 501(7465): 45-51.

Kalra S, Beaulieu C, Benatar M, Briemberg H, Dionne A, Dupre N*, et al.* The Canadian ALS Neuroimaging Consortium (CALSNIC)(P1. 4-010). AAN Enterprises; 2019.

Kamo H, Haebara H, Akiguchi I, Kameyama M, Kimura H, McGeer PL. A distinctive distribution of reactive astroglia in the precentral cortex in amyotrophic lateral sclerosis. Acta Neuropathol 1987; 74(1): 33-8.

Kasper E, Schuster C, Machts J, Kaufmann J, Bittner D, Vielhaber S*, et al.* Microstructural white matter changes underlying cognitive and behavioural impairment in ALS--an in vivo study using DTI. PLoS One 2014; 9(12): e114543.

Kassner A, Thornhill RE. Texture analysis: a review of neurologic MR imaging applications. AJNR Am J Neuroradiol 2010; 31(5): 809-16.

Kassubek J, Muller HP, Del Tredici K, Brettschneider J, Pinkhardt EH, Lule D*, et al.* Diffusion tensor imaging analysis of sequential spreading of disease in amyotrophic lateral sclerosis confirms patterns of TDP-43 pathology. Brain 2014; 137(Pt 6): 1733-40.

Kassubek J, Muller HP, Del Tredici K, Lule D, Gorges M, Braak H*, et al.* Imaging the pathoanatomy of amyotrophic lateral sclerosis in vivo: targeting a propagation-based biological marker. J Neurol Neurosurg Psychiatry 2018; 89(4): 374-81.

Kato Y, Matsumura K, Kinosada Y, Narita Y, Kuzuhara S, Nakagawa T. Detection of pyramidal tract lesions in amyotrophic lateral sclerosis with magnetization-transfer measurements. AJNR Am J Neuroradiol 1997; 18(8): 1541-7.

Kawamata T, Akiyama H, Yamada T, McGeer PL. Immunologic reactions in amyotrophic lateral sclerosis brain and spinal cord tissue. Am J Pathol 1992; 140(3): 691-707.

Kent-Braun JA, Walker CH, Weiner MW, Miller RG. Functional significance of upper and lower motor neuron impairment in amyotrophic lateral sclerosis. Muscle Nerve 1998; 21(6): 762-8.

Kolind S, Sharma R, Knight S, Johansen-Berg H, Talbot K, Turner MR. Myelin imaging in amyotrophic and primary lateral sclerosis. Amyotroph Lateral Scler Frontotemporal Degener 2013; 14(7-8): 562-73.

Kwan JY, Jeong SY, Van Gelderen P, Deng HX, Quezado MM, Danielian LE*, et al.* Iron accumulation in deep cortical layers accounts for MRI signal abnormalities in ALS: correlating 7 tesla MRI and pathology. PLoS One 2012; 7(4): e35241.

Lawyer T, Jr., Netsky MG. Amyotrophic lateral sclerosis. AMA Arch Neurol Psychiatry 1953; 69(2): 171-92.

Li J, Pan P, Song W, Huang R, Chen K, Shang H. A meta-analysis of diffusion tensor imaging studies in amyotrophic lateral sclerosis. Neurobiol Aging 2012; 33(8): 1833-8.

Maani R, Yang YH, Emery D, Kalra S. Cerebral Degeneration in Amyotrophic Lateral Sclerosis Revealed by 3-Dimensional Texture Analysis. Front Neurosci 2016; 10: 120.

Maani R, Yang YH, Kalra S. Voxel-based texture analysis of the brain. PLoS One 2015; 10(3): e0117759.

Meadowcroft MD, Mutic NJ, Bigler DC, Wang JL, Simmons Z, Connor JR*, et al.* Histological-MRI correlation in the primary motor cortex of patients with amyotrophic lateral sclerosis. J Magn Reson Imaging 2015; 41(3): 665-75.

Menke RA, Abraham I, Thiel CS, Filippini N, Knight S, Talbot K*, et al.* Fractional anisotropy in the posterior limb of the internal capsule and prognosis in amyotrophic lateral sclerosis. Arch Neurol 2012; 69(11): 1493-9.

Menke RA, Korner S, Filippini N, Douaud G, Knight S, Talbot K*, et al.* Widespread grey matter pathology dominates the longitudinal cerebral MRI and clinical landscape of amyotrophic lateral sclerosis. Brain 2014; 137(Pt 9): 2546-55.

Mitsumoto H, Ulug AM, Pullman SL, Gooch CL, Chan S, Tang MX*, et al.* Quantitative objective markers for upper and lower motor neuron dysfunction in ALS. Neurology 2007; 68(17): 1402-10.

Mori S, Oishi K, Jiang H, Jiang L, Li X, Akhter K*, et al.* Stereotaxic white matter atlas based on diffusion tensor imaging in an ICBM template. Neuroimage 2008; 40(2): 570-82.

Murayama S, Inoue K, Kawakami H, Bouldin TW, Suzuki K. A unique pattern of astrocytosis in the primary motor area in amyotrophic lateral sclerosis. Acta Neuropathol 1991; 82(6): 456-61.

Nihei K, McKee AC, Kowall NW. Patterns of neuronal degeneration in the motor cortex of amyotrophic lateral sclerosis patients. Acta Neuropathol 1993; 86(1): 55-64.

Phukan J, Elamin M, Bede P, Jordan N, Gallagher L, Byrne S*, et al.* The syndrome of cognitive impairment in amyotrophic lateral sclerosis: a population-based study. J Neurol Neurosurg Psychiatry 2012; 83(1): 102-8.

Polymenidou M, Cleveland DW. The seeds of neurodegeneration: prion-like spreading in ALS. Cell 2011; 147(3): 498-508.

Pupillo E, Messina P, Logroscino G, Beghi E, Group S. Long-term survival in amyotrophic lateral sclerosis: a population-based study. Ann Neurol 2014; 75(2): 287-97.

Ravits J. Focality, stochasticity and neuroanatomic propagation in ALS pathogenesis. Exp Neurol 2014; 262 Pt B: 121-6.

Rooney J, Burke T, Vajda A, Heverin M, Hardiman O. What does the ALSFRS-R really measure? A longitudinal and survival analysis of functional dimension subscores in amyotrophic lateral sclerosis. J Neurol Neurosurg Psychiatry 2017; 88(5): 381-5.

Schuster C, Kasper E, Dyrba M, Machts J, Bittner D, Kaufmann J*, et al.* Cortical thinning and its relation to cognition in amyotrophic lateral sclerosis. Neurobiol Aging 2014a; 35(1): 240-6.

Schuster C, Kasper E, Machts J, Bittner D, Kaufmann J, Benecke R*, et al.* Longitudinal course of cortical thickness decline in amyotrophic lateral sclerosis. J Neurol 2014b; 261(10): 1871-80.

Shen D, Cui L, Fang J, Cui B, Li D, Tai H. Voxel-Wise Meta-Analysis of Gray Matter Changes in Amyotrophic Lateral Sclerosis. Front Aging Neurosci 2016; 8: 64.

Sheng L, Ma H, Zhong J, Shang H, Shi H, Pan P. Motor and extra-motor gray matter atrophy in amyotrophic lateral sclerosis: quantitative meta-analyses of voxel-based morphometry studies. Neurobiol Aging 2015; 36(12): 3288-99.

Smith MC. Nerve Fibre Degeneration in the Brain in Amyotrophic Lateral Sclerosis. J Neurol Neurosurg Psychiatry 1960; 23(4): 269-82.

Stanton BR, Williams VC, Leigh PN, Williams SC, Blain CR, Jarosz JM*, et al.* Altered cortical activation during a motor task in ALS. Evidence for involvement of central pathways. J Neurol 2007; 254(9): 1260-7.

Sugiyama M, Takao M, Hatsuta H, Funabe S, Ito S, Obi T*, et al.* Increased number of astrocytes and macrophages/microglial cells in the corpus callosum in amyotrophic lateral sclerosis. Neuropathology 2013; 33(6): 591-9.

Ta D, Khan M, Ishaque A, Seres P, Eurich D, Yang YH*, et al.* Reliability of 3D texture analysis: A multicenter MRI study of the brain. J Magn Reson Imaging 2019.

Turner MR, Cagnin A, Turkheimer FE, Miller CC, Shaw CE, Brooks DJ*, et al.* Evidence of widespread cerebral microglial activation in amyotrophic lateral sclerosis: an [11C](R)-PK11195 positron emission tomography study. Neurobiol Dis 2004; 15(3): 601-9.

van der Graaff MM, Sage CA, Caan MW, Akkerman EM, Lavini C, Majoie CB*, et al.* Upper and extra-motoneuron involvement in early motoneuron disease: a diffusion tensor imaging study. Brain 2011; 134(Pt 4): 1211-28.

Verstraete E, Turner MR, Grosskreutz J, Filippi M, Benatar M, attendees of the 4th Ni Sm. Mind the gap: the mismatch between clinical and imaging metrics in ALS. Amyotroph Lateral Scler Frontotemporal Degener 2015; 16(7-8): 524-9.

Verstraete E, Veldink JH, Hendrikse J, Schelhaas HJ, van den Heuvel MP, van den Berg LH. Structural MRI reveals cortical thinning in amyotrophic lateral sclerosis. J Neurol Neurosurg Psychiatry 2012; 83(4): 383-8.

Walhout R, Westeneng HJ, Verstraete E, Hendrikse J, Veldink JH, van den Heuvel MP*, et al.* Cortical thickness in ALS: towards a marker for upper motor neuron involvement. J Neurol Neurosurg Psychiatry 2015; 86(3): 288-94.

Watanabe M, Dykes-Hoberg M, Culotta VC, Price DL, Wong PC, Rothstein JD. Histological evidence of protein aggregation in mutant SOD1 transgenic mice and in amyotrophic lateral sclerosis neural tissues. Neurobiol Dis 2001; 8(6): 933-41.

Zhang Y, Moore GR, Laule C, Bjarnason TA, Kozlowski P, Traboulsee A*, et al.* Pathological correlates of magnetic resonance imaging texture heterogeneity in multiple sclerosis. Ann Neurol 2013; 74(1): 91-9.

Zhang Y, Schuff N, Woolley SC, Chiang GC, Boreta L, Laxamana J*, et al.* Progression of white matter degeneration in amyotrophic lateral sclerosis: A diffusion tensor imaging study. Amyotroph Lateral Scler 2011; 12(6): 421-9.

Table 1: Baseline characteristics of study participants. Data is represented as mean ± standard deviation, or median (range) if data did not follow a normal distribution (Shapiro-Wilk test, $P < 0.05$). Significant between-group differences ($P < 0.05$) are highlighted in bold.

	Controls	ALS	*P* value
n	119	137	
Age (years)	55.8 ± 10.4	59.1 ± 10.5	**0.01**[a]
Gender, male/female	58/61	85/52	**0.03**[b]
Site of symptom onset, limb/bulbar	-	110/27	
ALSFRS-R	-	39 (20 – 47)	
Symptom duration (months)	-	23.4 (5.7 – 151.7)	
Disease progression rate	-	0.4 (0.02 – 2.1)	
UMN burden score	-	5 (1 – 12)	
Average finger tapping score	59.0 ± 12.2	43.3 ± 13.2	**< 0.001**[a]
Average foot tapping score	43.4 ± 8.5	29.0 ± 12.2	**< 0.001**[a]

UMN = upper motor neuron; ALSFRS-R = amyotrophic lateral sclerosis functional rating scale-revised; disease progression rate = (48 – ALSFRS-R)/symptom duration; [a] = independent samples *t*-test; [b] = chi-squared test

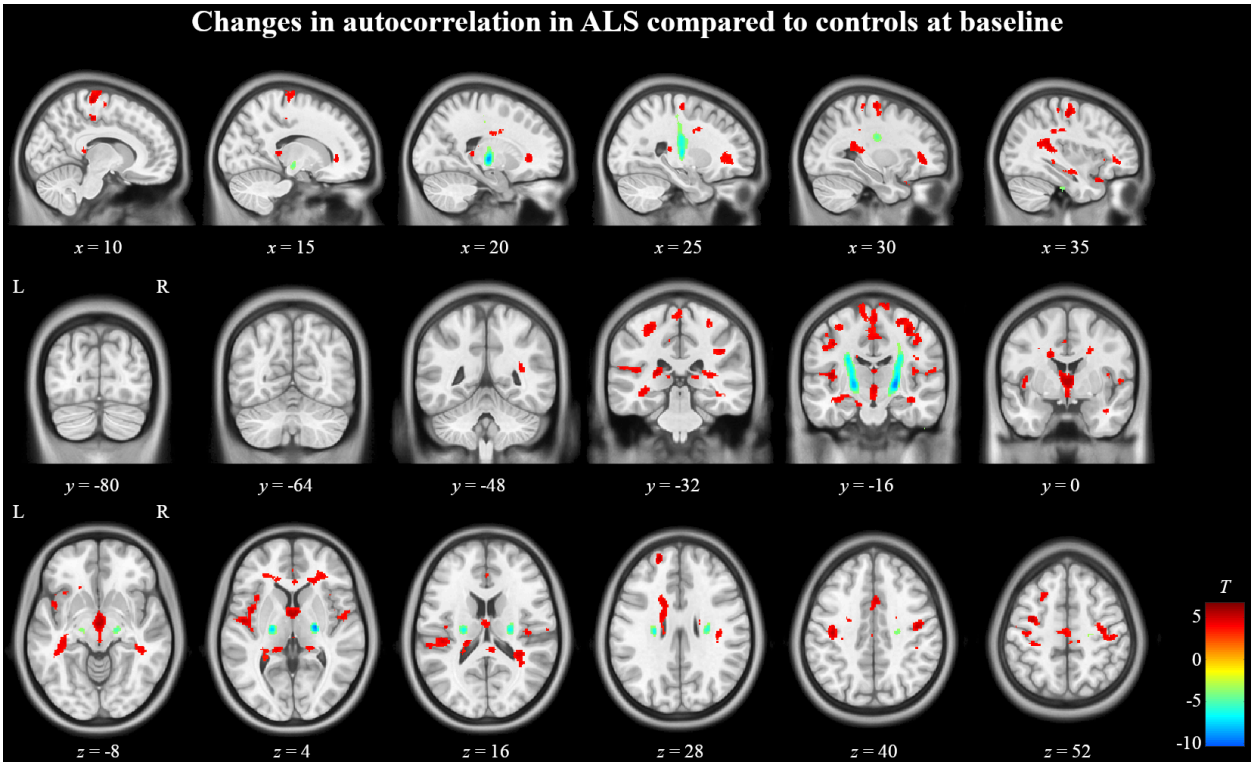

Figure 1: Texture differences between ALS patients and controls at T_0. Regions in red indicate areas of significantly ($P < 0.0005$, cluster size > 50) decreased autocorrelation in ALS patients and regions in blue indicate areas of significantly increased autocorrelation. The color bar on the bottom right shows the range of T-values for the contrast controls > ALS patients.

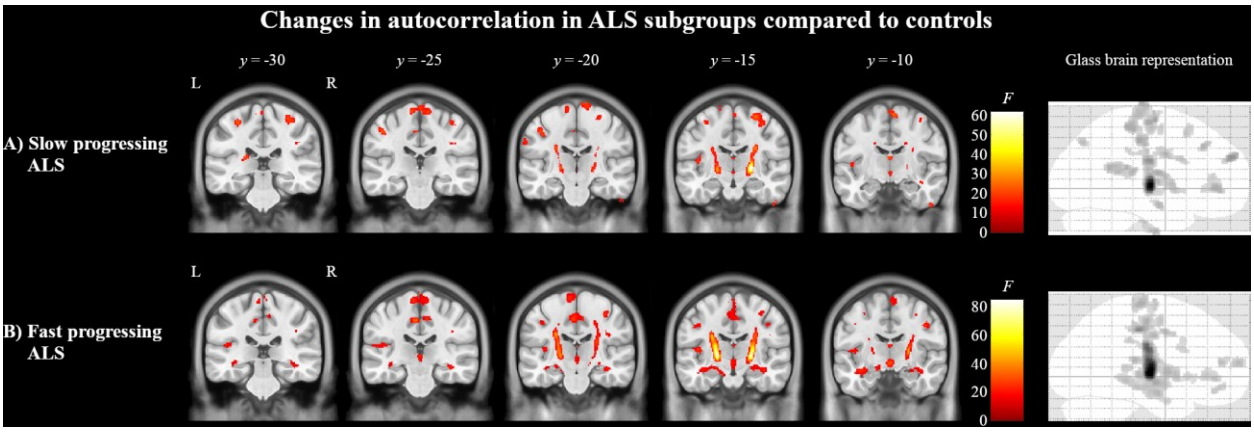

Figure 2: Texture differences between ALS subgroups of slow and fast progressing patients compared to controls at T_0. In panel (A), regions in red indicate areas of significantly ($P < 0.0005$, cluster size > 50) altered autocorrelation in slow progressing ALS patients compared to controls. In panel (B), regions in red indicate areas of significantly altered autocorrelation in fast progressing ALS patients compared to controls. The color bars show the range of F-values.

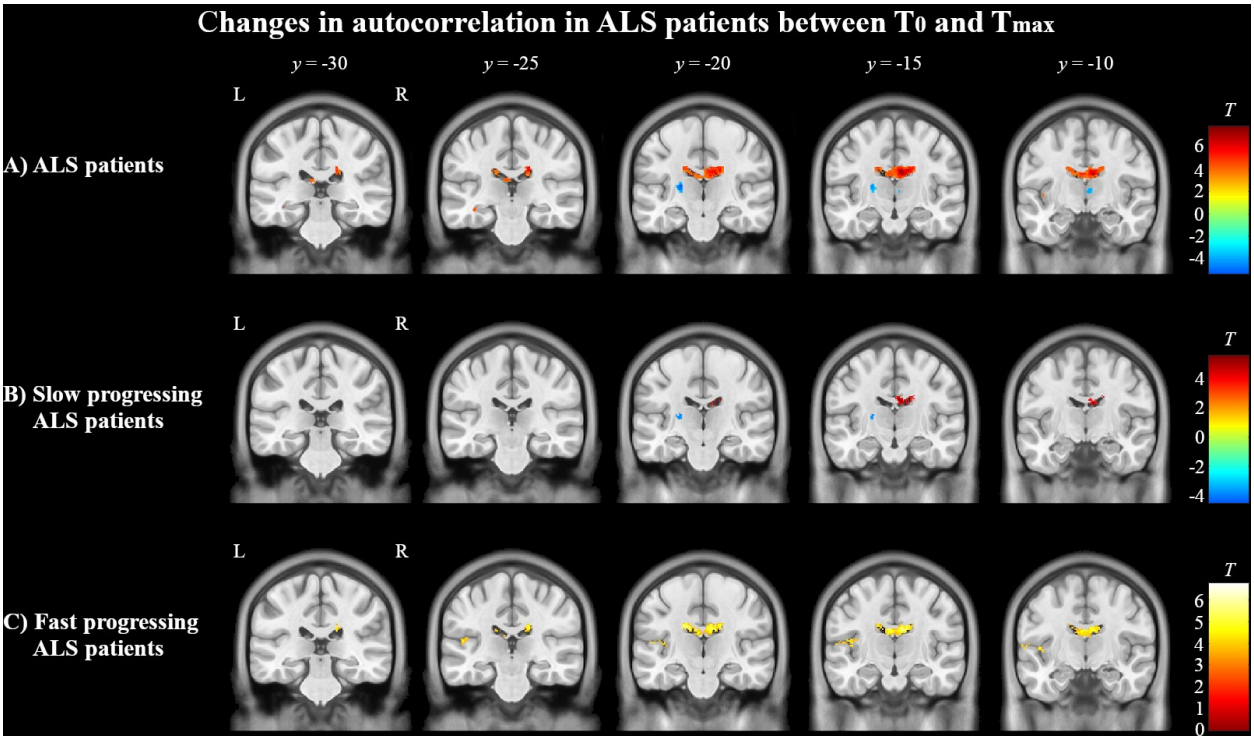

Figure 3: Longitudinal changes in texture in (A) ALS patients and (B) slow and (C) fast progressing subgroups from T_0 to T_{max} evaluated using paired t-tests ($P < 0.0005$, cluster size > 50). (A) In all ALS patients, autocorrelation decreased longitudinally (red) in the posterior corpus callosum, left insular cortex, and at the junction of lateral ventricles and bilateral caudate heads. Autocorrelation increased (blue) in the left internal capsule and right thalamus. ($P < 0.0005$, cluster size > 50). (B) In slow progressing ALS, autocorrelation decreased in the posterior corpus callosum and increased in the left internal capsule. (C) In fast progressing ALS, autocorrelation decreased in the posterior corpus callosum and left insular cortex. Autocorrelation was not increased in this subgroup. The color bars show the range of T-values.

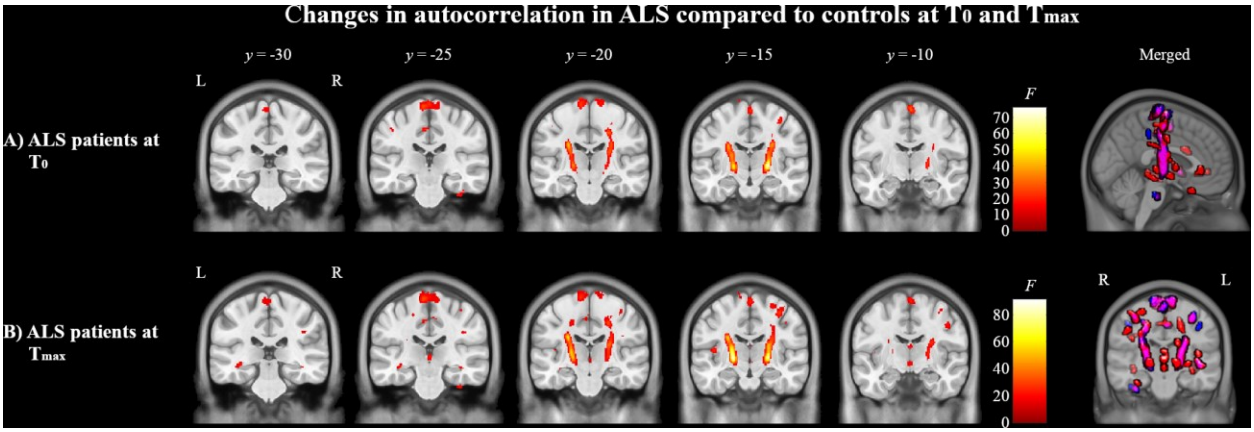

Figure 4: Texture differences between ALS compared to controls at T_0 (A) and T_{max} (B). In panels (A) and (B), regions in red indicate areas of significantly ($P < 0.0005$, cluster size > 50) altered autocorrelation in ALS patients compared to controls. The color bars show the range of F-values. Images on the right show a merged glass-brain representation of the differences in ALS patients at T_0 and T_{max}. Regions in blue indicate significant clusters present only at T_0, regions in purple indicate significant overlapping clusters present at T_0 and T_{max}, and regions in red indicate significant clusters present only at T_{max}.

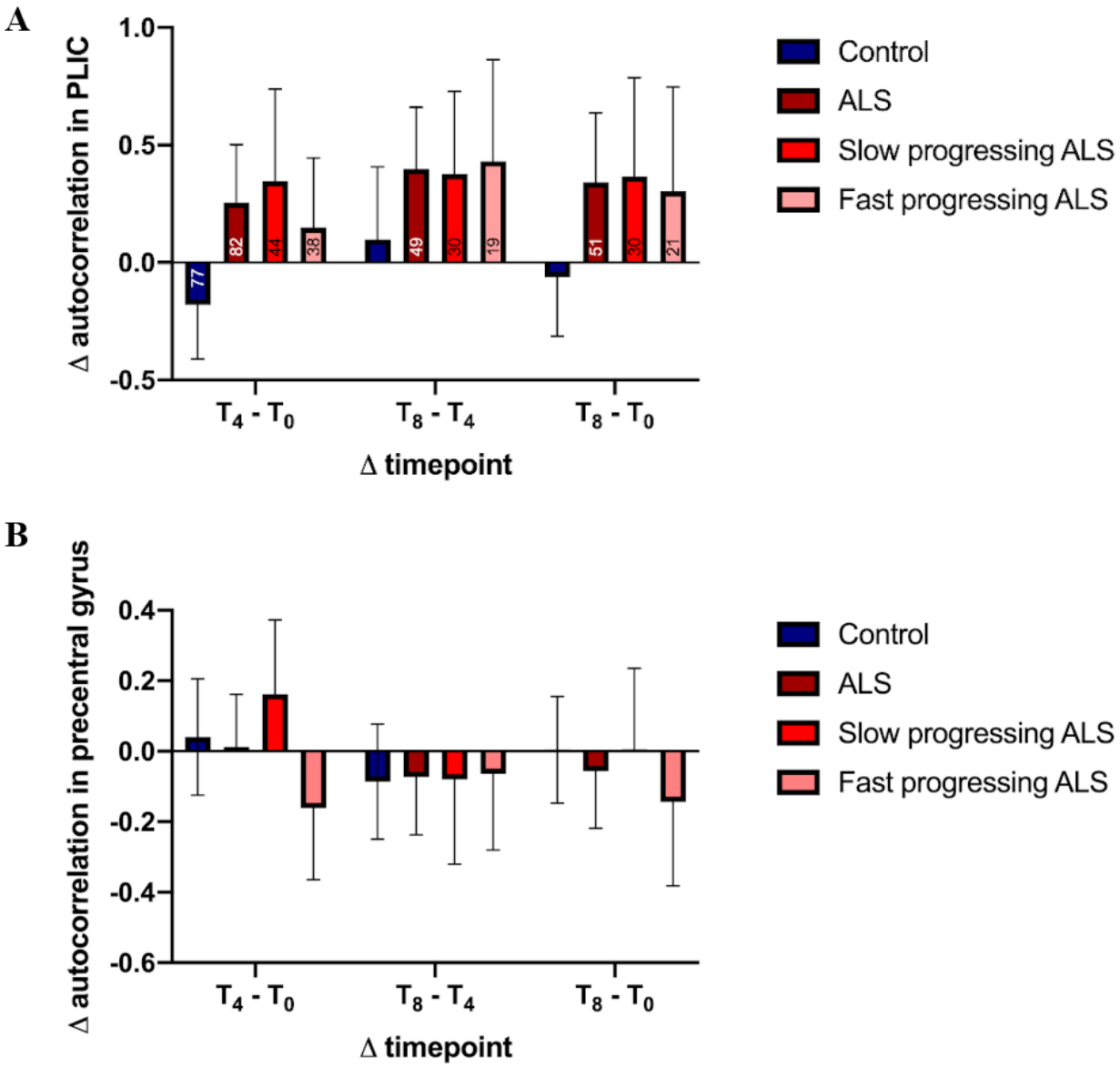

Figure 5: Texture differences in controls, ALS, and ALS subgroups between various timepoints in (A) the posterior limb of the internal capsule (PLIC) and (B) the precentral gyrus regions of interests. Data is represented as the mean ± 95% confidence interval at each point. The numbers inside in the bars in (A) represent the sample sizes of each group in the respective analyses.

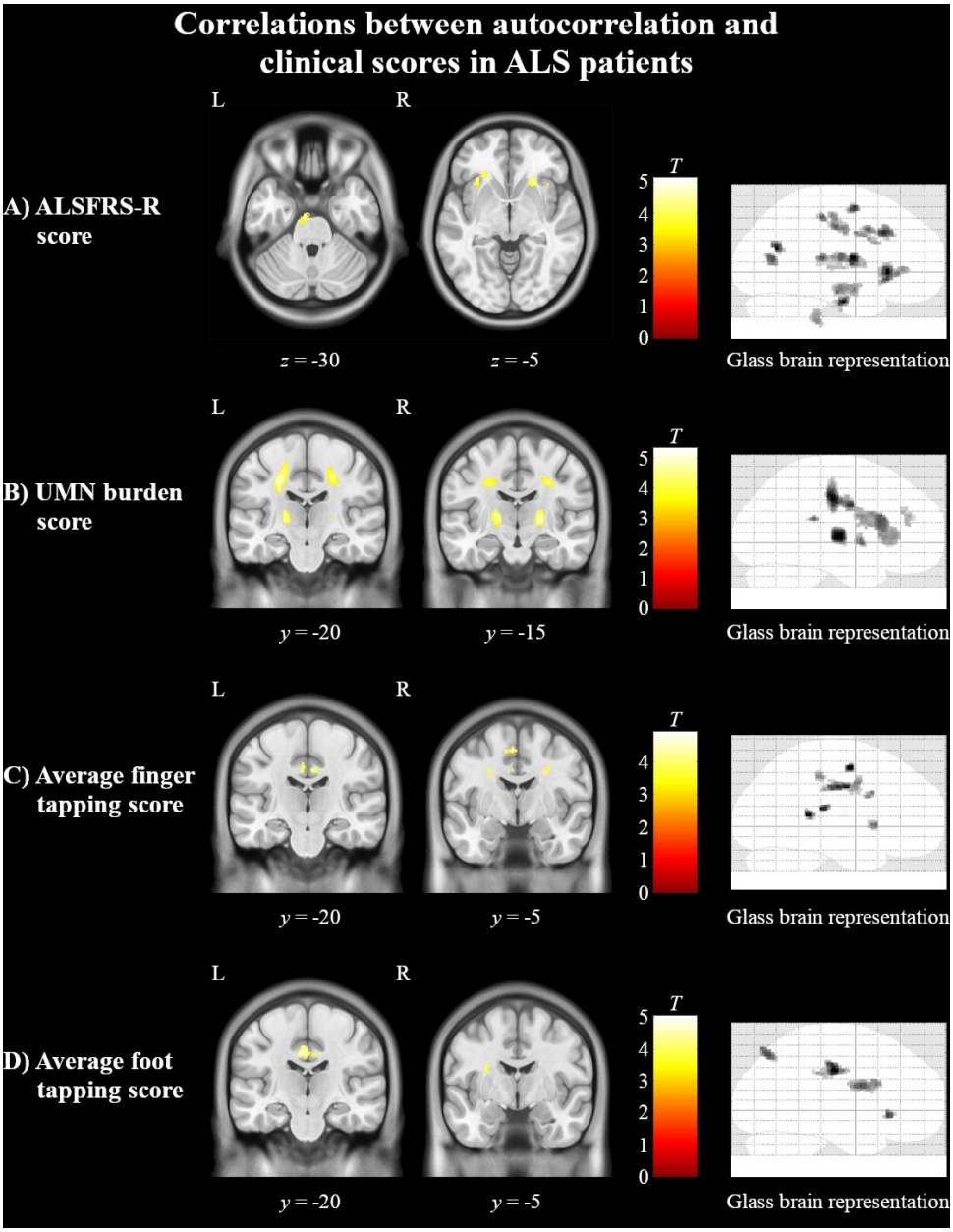

Figure 6: Cerebral associations between texture and clinical measures in ALS patients. Regions in yellow indicate areas of significant ($P < 0.0005$, cluster size > 50) positive correlations between autocorrelation and (A) ALSFRS-R, (B) UMN burden score, (C) average finger tapping score, and (D) average foot tapping score. The color bars show the range of T-values. ALSFRS-R = ALS functional rate scale-revised; UMN = upper motor neuron

Supplementary Table 1: Calculation of the upper motor neuron burden score. Muscle tone and limb reflexes were tested bilaterally in arms and legs. The score associated with the presence of the clinical sign is provided in parentheses.

Clinical exam	Neurological sign and score
Muscle tone (x4)	Hypertonia (1)
Reflexes	
Jaw reflex	Hyperreflexia (1), clonus (2)
Limb reflexes (x4)	Hyperreflexia (1), clonus (2)
Babinski reflex (x2)	Positive (1)
Total UMN burden score	16

UMN = upper motor neuron

Supplementary Table 2: MRI acquisition parameters for 3D T1-weighted scans (all 1 mm isotropic) at the six centres included in this study. Most centres implemented two different protocols as part of the Canadian ALS Neuroimaging Consortium.

Centres	University of British Columbia	University of Calgary		University of Alberta	
	Protocol 1	Protocol 1	Protocol 2	Protocol 1	Protocol 2
n (controls/patients)	10/9	9/9	11/7	19/17	26/21
Scanner vendor	Philips	General Electric	General Electric	Siemens	Siemens
Head coil channels	8	12	32	20	64
Acquisition matrix	240 x 240	256 x 256	224 x 256	256 x 256	232 x 256
Field of view (mm^2)	240 x 240	256 x 256	256 x 256	256 x 256	232 x 256
Slice thickness (*mm*)	1	1	1	1	1
Orientation	Axial	Axial	Sagittal	Axial	Sagittal
Number of slices	150	176	176	176	176
Repetition time (*ms*)	7.9	7.4	8.1	2300	1700
Echo time (*ms*)	3.5	3.1	3.2	3.4	2.2
Inversion time (*ms*)	950	400	400	900	880
Flip angle (°)	8	11	16	9	10

Centres	University of Toronto		McGill University		Laval University
	Protocol 1	Protocol 2	Protocol 1	Protocol 2	Protocol 1
n (controls/patients)	11/23	8/20	6/12	10/8	9/11

Scanner vendor	General Electric	Siemens	Siemens	Siemens	Philips
Head coil channels	8	64	32	64	8
Acquisition matrix	256 x 256	232 x 256	256 x 256	232 x 256	256 x 256
Field of view (mm^2)	256 x 256	232 x 256	256 x 256	232 x 256	256 x 256
Slice thickness (*mm*)	1	1	1	1	1
Orientation	Axial	Sagittal	Axial	Sagittal	Sagittal
Number of slices	176	176	176	176	176
Repetition time (*ms*)	7.7	1700	2300	1700	7.1
Echo time (*ms*)	2.9	2.2	3.4	2.2	3.4
Inversion time (*ms*)	400	880	900	880	950
Flip angle (°)	11	10	9	10	10

Supplementary Table 3: Characteristics of slow and fast progressing ALS patients at baseline. Data is represented as mean ± standard deviation. Significant between-group differences ($P < 0.05$) are highlighted in bold.

	Slow progressing ALS	Fast progressing ALS	*P* value
n	67	67	
Age (years)	59.7 ± 11.1	58.2 ± 9.2	0.4[a]
Gender, male/female	44/23	40/27	0.5[b]
Site of symptom onset, limb/bulbar	61/6	47/19	**0.004[b]**
ALSFRS-R	40.0 ± 4.9	35.5 ± 5.7	**< 0.001[a]**
Symptom duration (months)	45.2 ± 28.8	19.5 ± 11.2	**< 0.001[a]**
Disease progression rate	0.2 ± 0.09	0.7 ± 0.4	**< 0.001[a]**
UMN burden score	4.6 ± 2.5	6.3 ± 3.0	**0.002[a]**
Finger tapping score	46.6 ± 12.2	40.6 ± 13.8	**0.03[a]**
Foot tapping score	31.2 ± 11.7	26.9 ± 12.6	0.1[a]

UMN = upper motor neuron; LMN = lower motor neuron; ALSFRS-R = amyotrophic lateral sclerosis functional rating scale-revised; disease progression rate = (48 – ALSFRS-R)/symptom duration; $\Delta T_{0\text{-}max}$ = time interval between baseline and last follow-up MRI; [a] = independent samples *t*-test; [b] = chi-squared test

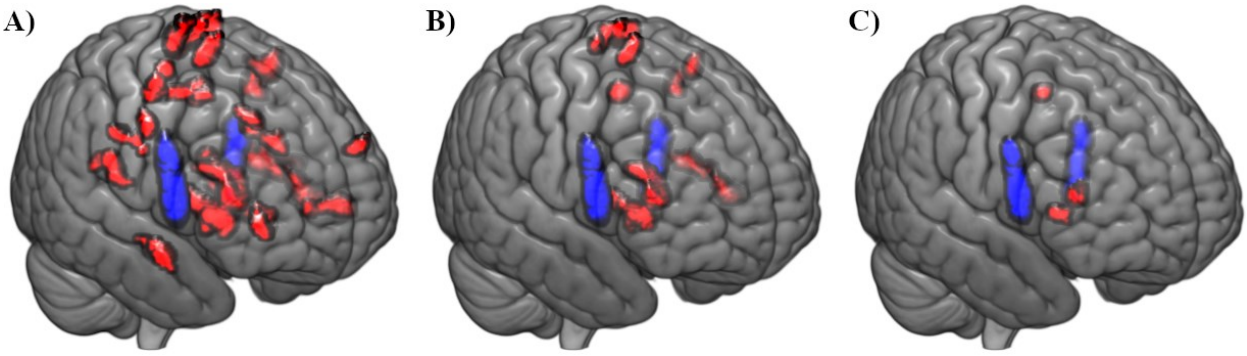

Supplementary Figure 1: Glass brain representations of group differences in texture between controls and ALS patients at different statistical thresholds. Red regions indicate decreased autocorrelation and blue regions indicate increased autocorrelation in ALS patients. At the lowest threshold (A), diffuse gray matter regions showed altered autocorrelation, including left frontal white matter, bilateral temporal white matter, cingulate gyrus, and thalamic region. At the intermediate threshold (B), left lateral precentral gyrus and left insular cortex demonstrated differences in autocorrelation between the two groups. At the highest statistical threshold (C), differences were found in the left medial precentral gyrus. Bilateral pyramidal tracts had increased autocorrelation at all statistical thresholds.

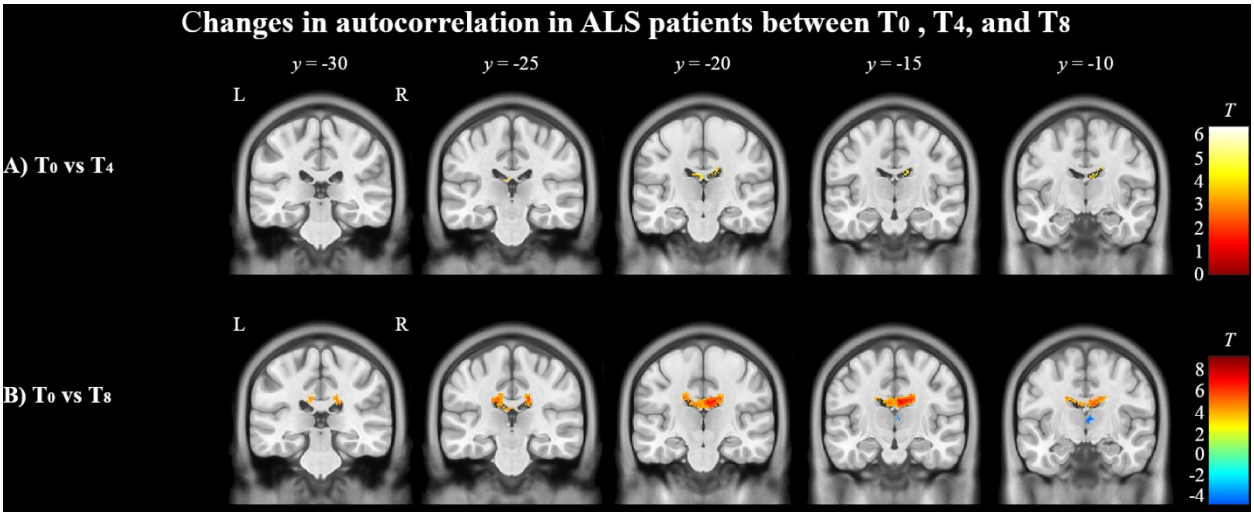

Supplementary Figure 2: Longitudinal changes in texture in ALS between T_0, T_4, and T_8 ($P < 0.0005$, cluster size > 50). (A) Between T_0 and T_4, autocorrelation decreased in the posterior corpus callosum in ALS patients. Autocorrelation did not increase between these timepoints. (B) Between T_0 and T_8, autocorrelation decreased in the posterior corpus callosum and at the junction of the lateral ventricles and bilateral caudate heads. Autocorrelation also increased in the right thalamus. The color bars show the range of T-values.

A **Correlation between ALSFRS-R and UMN burden**

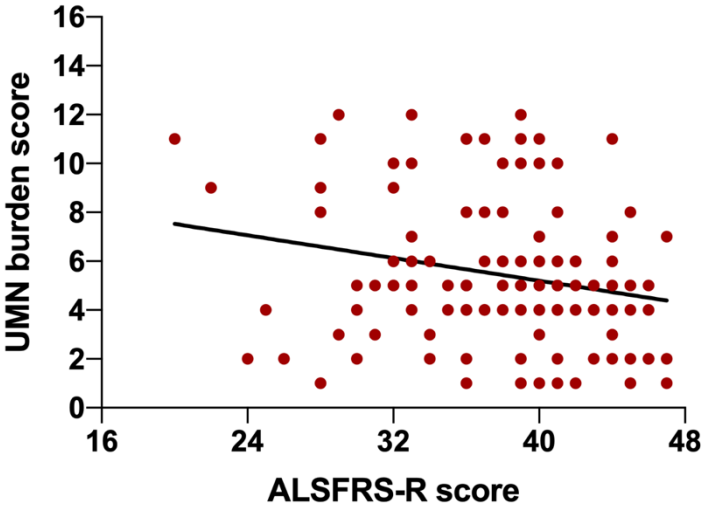

B **Correlation between ALSFRS-R and finger tapping**

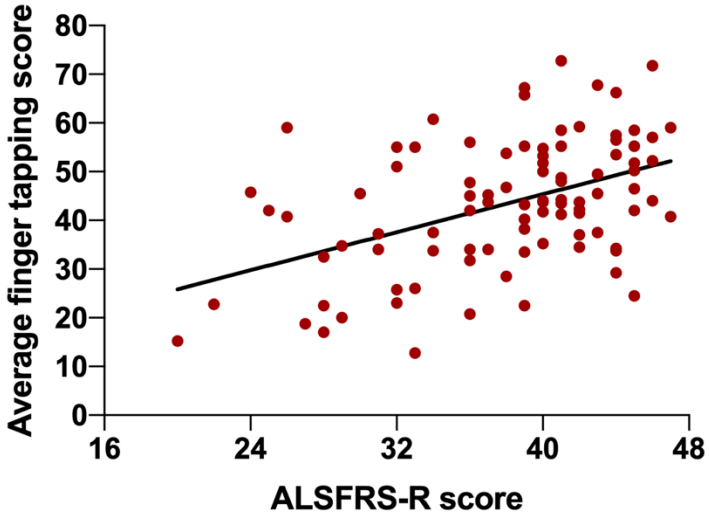

C **Correlation between ALSFRS-R and foot tapping**

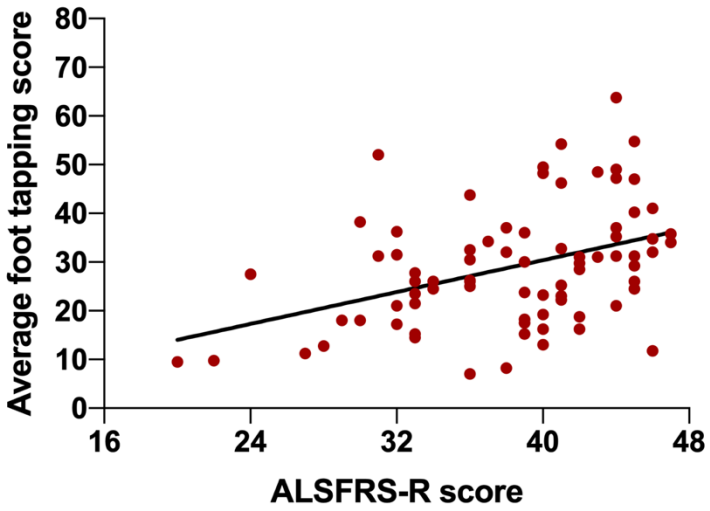

D **Correlation between UMN burden and finger tapping**

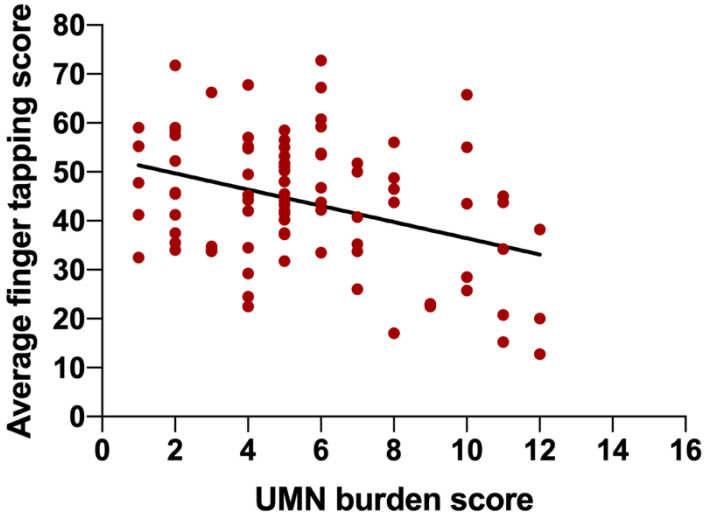

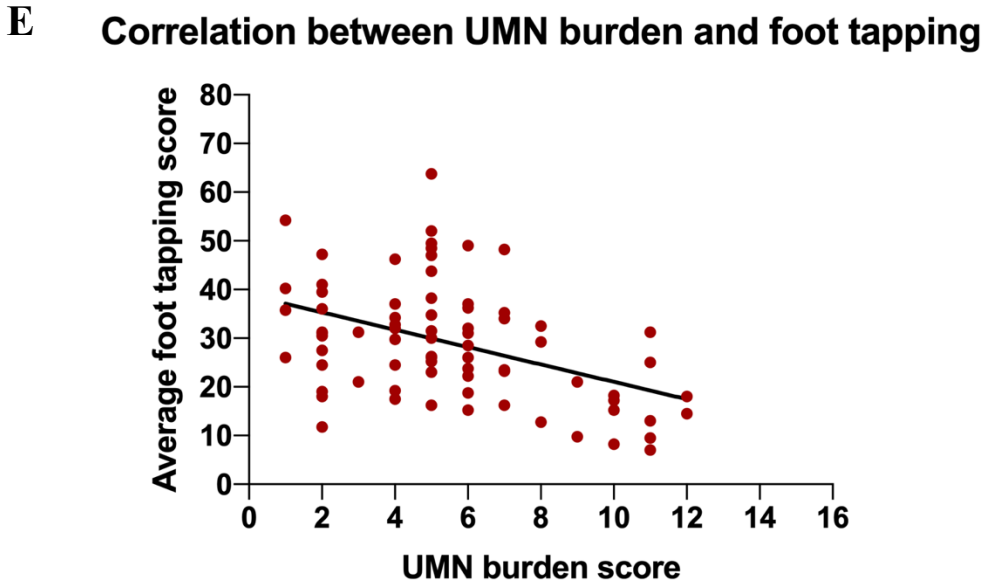

Supplementary Figure 3: Correlations between clinical measures at baseline in ALS patients. ALSFRS-R score significantly correlated with (A) UMN burden score ($r = -0.2$, $P = 0.01$), (B) average finger tapping score ($r = 0.5$, $P < 0.001$), and (C) average foot tapping score ($r = 0.4$, $P < 0.001$). UMN burden score significantly correlated with (D) average finger tapping score ($r = -0.4$, $P < 0.001$) and (E) average foot tapping score ($r = -0.4$, $P < 0.001$).

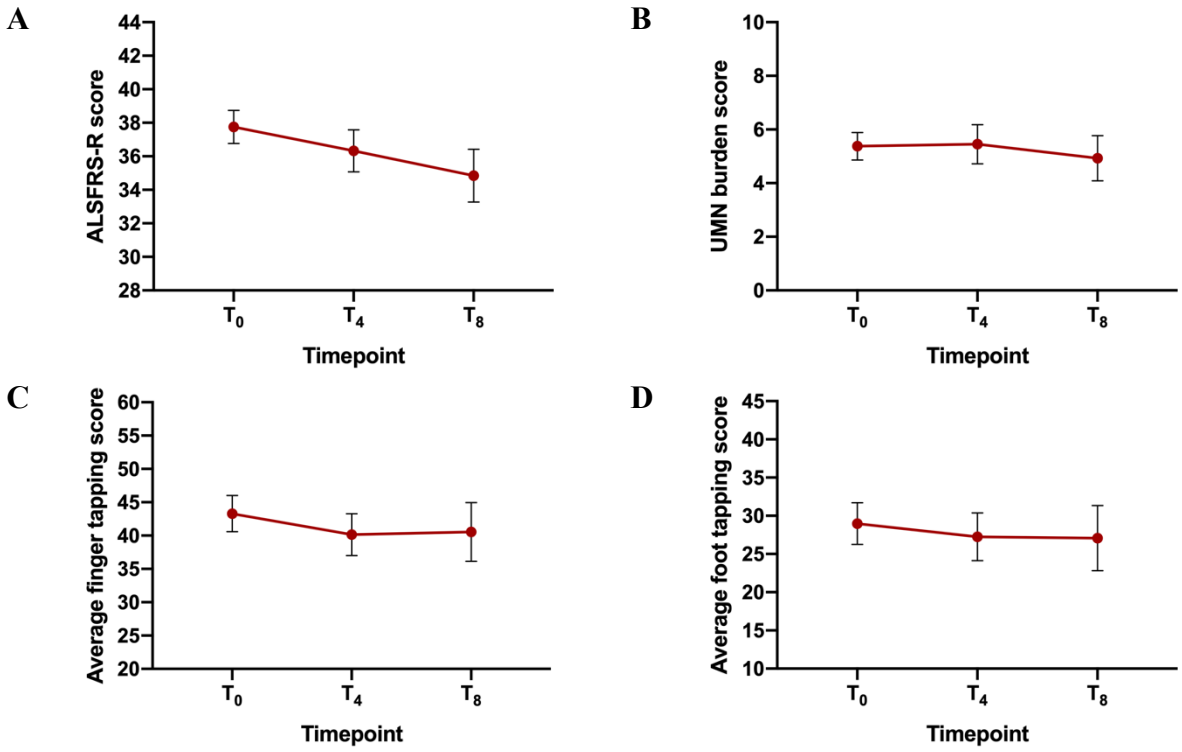

Supplementary Figure 4: Clinical measures of all ALS patients at T_0, T_4, and T_8. Data is represented as the mean ± 95% confidence interval at each timepoint.

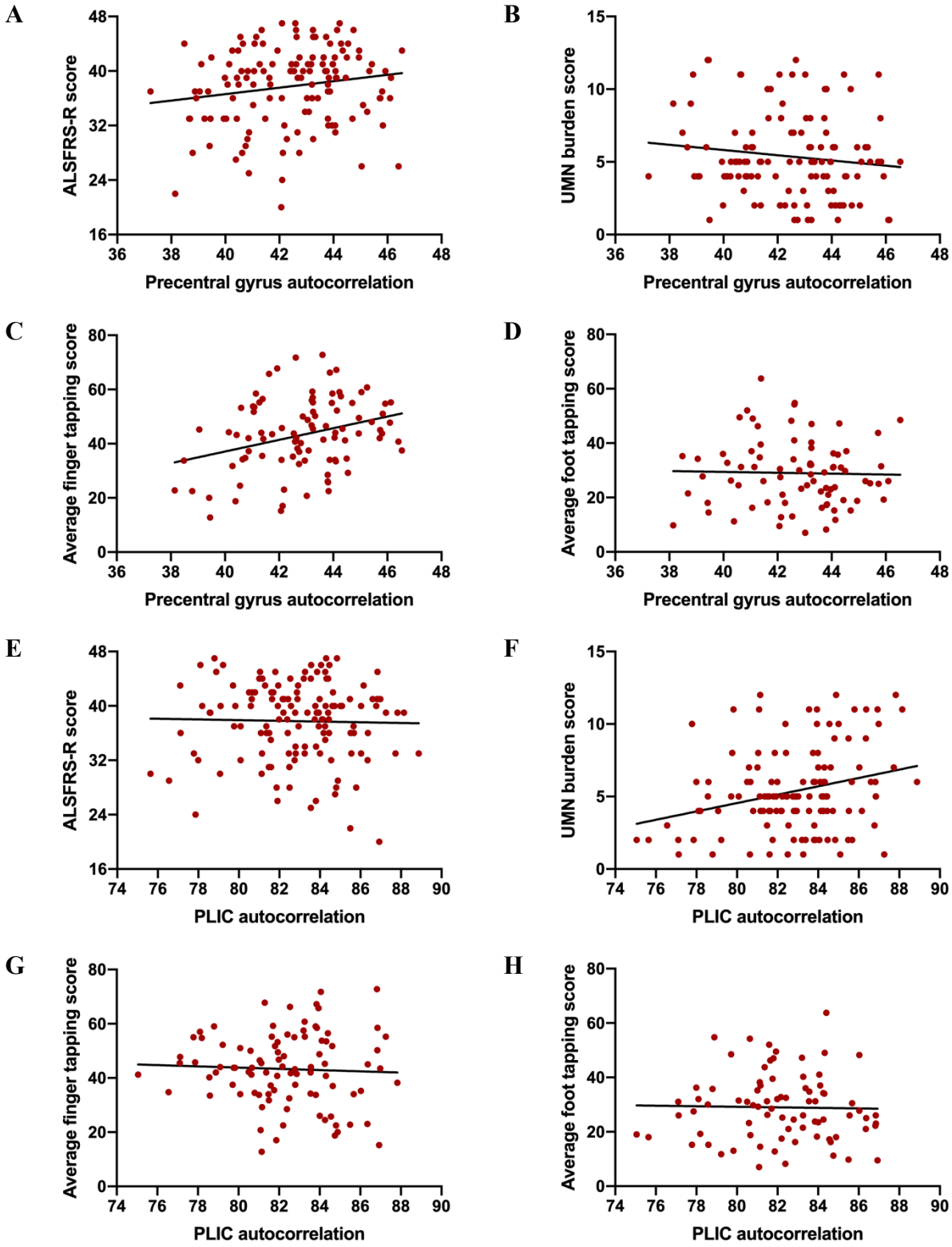

Supplementary Figure 5: Associations between texture of the precentral and the posterior limb of the internal capsule (PLIC) and clinical measures in ALS patients. Significant correlations (P

< 0.05) were found between autocorrelation of the precentral gyrus and average finger tapping score (C, r = 0.3). Autocorrelation of the PLIC correlated significantly with UMN burden score (F, r = 0.2).

Discussion and Conclusion

Each experimental chapter has detailed Discussion and Conclusion sections. Here, the overarching contributions to the understanding of the ALS pathology from a neuroimaging point-of-view will be discussed with respect to the aims and hypotheses initially outlined in this dissertation. The potential of texture analysis as a source of non-invasive biomarkers for ALS will be described and at the end, limitations of this dissertation and future directions will be presented.

Neuroimaging and the pathology of amyotrophic lateral sclerosis

The neuroimaging literature in ALS has provided ample evidence of degenerative changes in the motor cortex, frontotemporal regions, and variably in the deep gray nuclei. These changes range from cortical thinning, volume reductions, and altered metabolism and function. In the white matter, the core signature of disruptions in the corticospinal tract and corpus callosum microarchitecture is also recognised along with disruptions in the frontotemporal networks. These abnormalities in gray and white matter region are confirmed with the study of T1-weighted images using the novel 3D texture analysis technique. Abnormalities in the texture feature autocorrelation were present in the motor cortex and frontotemporal regions in ALS patients. Furthermore, a strong signal of texture alteration in the corticospinal tract was consistently observed. It is worth highlighting that texture abnormalities in the corpus callosum, namely with texture feature autocorrelation, were not detected in the cross-section analyses. This is at odds with DTI studies that suggest that changes in the diffusion profile of this white matter structure are part of its characteristic neuroimaging signature. A possible explanation for this discrepancy is that different texture features are variably sensitive to different microarchitectural

and pathologic features on MRI. The pyramidal tract in humans is comprised of small- (1 – 4 μm) and large-diameter (up to 20 μm) axons of varying axonal densities as they descend through the cerebrum.[460] These tracts have increased extracellular water and thicker myelin sheaths that cause their uniquely hyperintense signal on T2-weighted images compared to adjacent structures.[461] In ALS, large calibre motor neurons, the Betz cells, are preferentially affected and small diameter axons are spared. The corpus callosum, on the other hand, is largely composed of densely packed smaller diameter axons (< 5 μm).[462] The increase in autocorrelation along the descending pyramidal tracts may reflect the increase in extracellular water content secondary to the loss of large-diameter axons. In the corpus callosum, this phenomenon may be diminished due to the higher axonal density. Detailed histological and morphological evaluations of the fibers of the corpus callosum in ALS, however, are currently lacking to further substantiate this claim. The experiments in this work primarily focused on the texture feature autocorrelation and it is entirely possible that other texture features exhibit different behaviours in response to the pathology in ALS. Nevertheless, these findings suggest that subtle variations on routine T1-weighted images are present and can serve as biomarkers for detection of the disease. Furthermore, unique texture alterations on routine MRI modalities such as T1- and T2-weighted and FLAIR images may provide further pathological insights as they are each sensitive to unique microscopic properties of tissue.

Several clinical associations were also established in this work. First, an association between extra-motor involvement and worse survival was demonstrated in ALS patients. These findings are further strengthened by a recent study.[463] This MRS study found that the ratio of NAA/mI from the prefrontal cortex contributed to the prediction of survival after a two-year period. These findings place the ALS-FTD spectrum in spotlight for discussions of disease-

modifying therapies. Consideration should be given to drugs that can limit the spread of pathology within the brain in ALS and not just to protect the motor regions from progressive degeneration. It follows that clinical trials should not only evaluate motor function-related endpoints, but also assess frontotemporal involvement over the course of their experiments. A shift in the approach to designing future clinical trials with respect to primary endpoints is therefore recommended. In addition, patients with an established ALS-FTD syndrome may benefit from a different therapeutic approach and should not be grouped together in clinic trials with patients with only motor findings. Secondly, the ALSFRS-R score was found to associate with widespread cortical regions. This is in accordance with the view that the ALSFRS-R, though sensitive to longitudinal decline in ALS, does not represent specificity to a brain structure or function. The ALSFRS-R may instead represent global cerebral disease burden along with LMN dysfunction, and therefore it should be not used as a surrogate measure for UMN dysfunction in ALS. On the other hand, clinical evaluation of UMN burden was found to closely associate with abnormal texture along the corticospinal tract. This suggests that the clinical UMN dysfunction observed in ALS is largely a function of disruptions in the pyramidal tracts. The location a of insult along the motor cortex is more closely associated with the clinical phenotype as it pertains to limb- versus bulbar-onset phenotypes. This is in accordance with the theory of a focal disease onset in ALS and is supported by neuroimaging findings of focal damage to the motor cortex that mirror the clinical motor phenotype.

The longitudinal experiment results suggest that the pathology in ALS spreads across the gray matter in an anterolateral direction from the motor cortex. Progressive degenerative changes within the motor cortex are limited once the disease is established clinically. Longitudinal cortical degeneration in ALS thus can be characterized as the sequential involvement of cortical

structures that are connected via axonal pathways. Future studies should consider quantifying the rate and pattern of spatial spread of disease across the cortex. For example, the proposed pathological stages of abnormal TDP-43 deposition could represent an *in vivo* stepwise involvement of cortical structures. This, along with the association between survival and frontotemporal involvement, suggests that drugs that can prevent the spread of pathology in the brain may have a neuroprotective role in ALS. In contrast, progressive texture abnormalities within the corticospinal tract suggest that degenerative processes continue to take place over time in the descending pyramidal tracts. The observed dichotomy in the degeneration pattern of gray and white matter structures in ALS is a novel finding that has implications for future studies. These findings lend support to the hypothesis that ALS is a disease mediated by corticofugal axons. In this view, the continued degeneration of the pyramidal tracts could mirror the increasing cortical pathological burden. On the other hand, one can argue that the lack of progressive changes within the motor cortex in light of degenerating pyramidal tracts support the "dying-back" hypothesis where the failure of the UMN system is triggered by LMNs. However, the inevitable cortical spread is not yet accounted for with this point-of-view. Neuroimaging studies have the potential to answer these important questions and further disentangle the pathophysiology of the ALS. Future studies show focus on pre-symptomatic, or early-diagnosis ALS patients to monitor the longitudinal progression of the disease.

Texture analysis and its potential role as a biomarker

This work represents the first comprehensive use of 3D texture analysis to uncover abnormalities in routine MRI scans in a neurodegenerative disorder. In clinical settings, T1-weighted images are acquired to exclude other causes of the signs and symptoms of ALS and serve no diagnostic purpose for patients. Here, it was demonstrated that T1-weighted images

harbour subtle pathological abnormalities that texture features accurately detected, notably in region of the pyramidal tracts. DTI has been the MRI modality of choice to characterize white matter alterations in ALS and other diseases of the central nervous system because of its remarkable sensitivity for microstructural alterations. However, DTI techniques have not yet made inroads towards clinical use for neurodegenerative disease. Texture features as biomarkers have unique advantages because they can be quantified from routine MRI modalities and do not require advanced acquisition and processing techniques to detect pathogenic changes. T1-weighted images are a part of routine neuroimaging work-up for ALS and therefore present an opportunity for earlier diagnoses with texture analysis. This highlights the practicality of texture analysis in providing biomarkers that can clearly improve the diagnostics of ALS, and provide a tool to monitor patients' progression.

A notable characteristic of neurodegenerative disorders is the presence of pathological processes that precede overt atrophy measurable on MRI. These processes include aberrant protein deposition, immune-mediated responses such as gliosis, and metabolic alterations. Volume loss and cortical thinning are frequently used as biomarkers from T1-weighted images in ALS. These features represent the end-stage manifestation of degeneration and cannot be used to detect the earlier stages of the disease where volume loss has not yet taken place. Alterations in texture features, however, are sensitive to signal changes in gray matter independent of volume or thickness measurements. As such, texture features may serve as biomarkers of early-stage ALS. This hypothetical approach of identifying the pathological cascade at various stages of a disease using biomarkers has been utilized in Alzheimer's disease.[282] In light of this approach, abnormalities in texture features can mark the antecedent events in the pathological cascade of

ALS. Thus, texture analysis is not only a source of early biomarkers for ALS, but may also be sensitive to early pathological events that can improve the understanding of its pathophysiology.

Lastly, this work highlights the usefulness of texture analysis in monitoring longitudinal changes in ALS. For a biomarker to be implemented in any clinical trial, it should be sensitive in detecting the natural history of a disease and the response to a therapeutic intervention. The lack of such a biomarker is one of the biggest challenges facing the development of treatment drugs for ALS. Here, texture features detected progressive abnormalities at four- and eight-months follow-up in the absence of measurable clinical decline. This is significant because it underscores the ability of texture features to detect subclinical cerebral changes in a short time interval. Clinical trials can use therefore texture-based biomarkers to study anatomically-specific cerebral responses to various treatments. This information can be used to provide precision therapeutic options to patients. In addition, the shorter time interval needed to detect these changes offers a financial advantage to clinical trials.

Limitations and future directions

This work is limited by the lack of histological data. Despite demonstrating clinical validation, the biological underpinnings of texture features remain poorly understood. Neuropathological associations are required to identify texture features' sensitivity to specific degenerative processes in ALS. As stated above, it is possible that different texture features have variable correlations towards different pathological processes in which case using a combination of texture features would prove to be the better approach in detecting and monitoring the disease. It should be pointed out, however, that post-mortem studies were being conducted for this purpose during the time of this work; however, these were not included in this dissertation due to time constraints. Another limitation is the lack of cerebral associations with neuropsychometric

data. Texture abnormalities detected in the frontotemporal regions in ALS in cross-sectional and longitudinal analyses should be assessed for associations with cognitive and behavioural function. This is important given the multisystem nature of the disease and to further clinically validate the extra-motor findings of texture analysis. This work is also limited by the lack an incidence-based patient cohort. MRI studies of clinic-based populations, on average, represent patients that are less functionally impaired; there is a selection bias towards patients that are able to tolerate MRI assessments and cooperative with an extensive battery of clinical and cognitive tests. As such, to obtain a wider and a more representative spectrum of the disease, an incidence-based cohort of ALS patients should be sought.

Future work should aim to study texture features at an individual level. This dissertation provided support for texture analysis as a source of biomarkers at the group level; however, validation studies at the individual level are needed before texture features can be implemented in clinical practice and clinical trials. Additionally, work should be done to understand the pathological cascade of ALS and its temporal characteristics, including MRI studies of pre-symptomatic, or early-diagnosis patients. Doing so will optimize the use of biomarkers for patients in specific stages of the disease and reveal windows of therapeutic opportunity.

References

1. Goetz CG. Amyotrophic lateral sclerosis: early contributions of Jean-Martin Charcot. Muscle Nerve 2000;23:336-343.
2. Phukan J, Elamin M, Bede P, et al. The syndrome of cognitive impairment in amyotrophic lateral sclerosis: a population-based study. J Neurol Neurosurg Psychiatry 2012;83:102-108.
3. Ravits J. Focality, stochasticity and neuroanatomic propagation in ALS pathogenesis. Exp Neurol 2014;262 Pt B:121-126.
4. Arai T, Hasegawa M, Akiyama H, et al. TDP-43 is a component of ubiquitin-positive tau-negative inclusions in frontotemporal lobar degeneration and amyotrophic lateral sclerosis. Biochem Biophys Res Commun 2006;351:602-611.
5. Neumann M, Sampathu DM, Kwong LK, et al. Ubiquitinated TDP-43 in frontotemporal lobar degeneration and amyotrophic lateral sclerosis. Science 2006;314:130-133.
6. Renton AE, Chio A, Traynor BJ. State of play in amyotrophic lateral sclerosis genetics. Nat Neurosci 2014;17:17-23.
7. Chio A, Calvo A, Moglia C, Mazzini L, Mora G, group Ps. Phenotypic heterogeneity of amyotrophic lateral sclerosis: a population based study. J Neurol Neurosurg Psychiatry 2011;82:740-746.
8. Logroscino G, Traynor BJ, Hardiman O, et al. Incidence of amyotrophic lateral sclerosis in Europe. J Neurol Neurosurg Psychiatry 2010;81:385-390.
9. Wolfson C, Kilborn S, Oskoui M, Genge A. Incidence and prevalence of amyotrophic lateral sclerosis in Canada: a systematic review of the literature. Neuroepidemiology 2009;33:79-88.

10. Chio A, Logroscino G, Traynor BJ, et al. Global epidemiology of amyotrophic lateral sclerosis: a systematic review of the published literature. Neuroepidemiology 2013;41:118-130.
11. Joensen P. Incidence of amyotrophic lateral sclerosis in the Faroe Islands. Acta Neurol Scand 2012;126:62-66.
12. Chen L, Zhang B, Chen R, et al. Natural history and clinical features of sporadic amyotrophic lateral sclerosis in China. J Neurol Neurosurg Psychiatry 2015;86:1075-1081.
13. de Lau LM, Breteler MM. Epidemiology of Parkinson's disease. Lancet Neurol 2006;5:525-535.
14. Renton AE, Majounie E, Waite A, et al. A hexanucleotide repeat expansion in C9ORF72 is the cause of chromosome 9p21-linked ALS-FTD. Neuron 2011;72:257-268.
15. Laaksovirta H, Peuralinna T, Schymick JC, et al. Chromosome 9p21 in amyotrophic lateral sclerosis in Finland: a genome-wide association study. Lancet Neurol 2010;9:978-985.
16. Chio A, Borghero G, Pugliatti M, et al. Large proportion of amyotrophic lateral sclerosis cases in Sardinia due to a single founder mutation of the TARDBP gene. Arch Neurol 2011;68:594-598.
17. Zaldivar T, Gutierrez J, Lara G, Carbonara M, Logroscino G, Hardiman O. Reduced frequency of ALS in an ethnically mixed population: a population-based mortality study. Neurology 2009;72:1640-1645.
18. Roberts AL, Johnson NJ, Chen JT, Cudkowicz ME, Weisskopf MG. Race/ethnicity, socioeconomic status, and ALS mortality in the United States. Neurology 2016;87:2300-2308.

19. Rosen DR, Siddique T, Patterson D, et al. Mutations in Cu/Zn superoxide dismutase gene are associated with familial amyotrophic lateral sclerosis. Nature 1993;362:59-62.

20. Zou ZY, Zhou ZR, Che CH, Liu CY, He RL, Huang HP. Genetic epidemiology of amyotrophic lateral sclerosis: a systematic review and meta-analysis. J Neurol Neurosurg Psychiatry 2017;88:540-549.

21. van Blitterswijk M, van Es MA, Hennekam EA, et al. Evidence for an oligogenic basis of amyotrophic lateral sclerosis. Hum Mol Genet 2012;21:3776-3784.

22. van Rheenen W, Shatunov A, Dekker AM, et al. Genome-wide association analyses identify new risk variants and the genetic architecture of amyotrophic lateral sclerosis. Nat Genet 2016;48:1043-1048.

23. Sreedharan J, Blair IP, Tripathi VB, et al. TDP-43 mutations in familial and sporadic amyotrophic lateral sclerosis. Science 2008;319:1668-1672.

24. Kwiatkowski TJ, Jr., Bosco DA, Leclerc AL, et al. Mutations in the FUS/TLS gene on chromosome 16 cause familial amyotrophic lateral sclerosis. Science 2009;323:1205-1208.

25. Vance C, Rogelj B, Hortobagyi T, et al. Mutations in FUS, an RNA processing protein, cause familial amyotrophic lateral sclerosis type 6. Science 2009;323:1208-1211.

26. DeJesus-Hernandez M, Mackenzie IR, Boeve BF, et al. Expanded GGGGCC hexanucleotide repeat in noncoding region of C9ORF72 causes chromosome 9p-linked FTD and ALS. Neuron 2011;72:245-256.

27. Andersen PM, Forsgren L, Binzer M, et al. Autosomal recessive adult-onset amyotrophic lateral sclerosis associated with homozygosity for Asp90Ala CuZn-superoxide dismutase mutation. A clinical and genealogical study of 36 patients. Brain 1996;119 (Pt 4):1153-1172.

28. Cudkowicz ME, McKenna-Yasek D, Chen C, Hedley-Whyte ET, Brown RH, Jr. Limited corticospinal tract involvement in amyotrophic lateral sclerosis subjects with the A4V mutation in the copper/zinc superoxide dismutase gene. Ann Neurol 1998;43:703-710.

29. Millecamps S, Salachas F, Cazeneuve C, et al. SOD1, ANG, VAPB, TARDBP, and FUS mutations in familial amyotrophic lateral sclerosis: genotype-phenotype correlations. J Med Genet 2010;47:554-560.

30. Lagier-Tourenne C, Cleveland DW. Rethinking ALS: the FUS about TDP-43. Cell 2009;136:1001-1004.

31. Rademakers R, Stewart H, Dejesus-Hernandez M, et al. Fus gene mutations in familial and sporadic amyotrophic lateral sclerosis. Muscle Nerve 2010;42:170-176.

32. Morita M, Al-Chalabi A, Andersen PM, et al. A locus on chromosome 9p confers susceptibility to ALS and frontotemporal dementia. Neurology 2006;66:839-844.

33. Vance C, Al-Chalabi A, Ruddy D, et al. Familial amyotrophic lateral sclerosis with frontotemporal dementia is linked to a locus on chromosome 9p13.2-21.3. Brain 2006;129:868-876.

34. Shatunov A, Mok K, Newhouse S, et al. Chromosome 9p21 in sporadic amyotrophic lateral sclerosis in the UK and seven other countries: a genome-wide association study. Lancet Neurol 2010;9:986-994.

35. Cooper-Knock J, Hewitt C, Highley JR, et al. Clinico-pathological features in amyotrophic lateral sclerosis with expansions in C9ORF72. Brain 2012;135:751-764.

36. van der Zee J, Gijselinck I, Dillen L, et al. A pan-European study of the C9orf72 repeat associated with FTLD: geographic prevalence, genomic instability, and intermediate repeats. Hum Mutat 2013;34:363-373.

37. Taylor JP, Brown RH, Jr., Cleveland DW. Decoding ALS: from genes to mechanism. Nature 2016;539:197-206.

38. Byrne S, Elamin M, Bede P, et al. Cognitive and clinical characteristics of patients with amyotrophic lateral sclerosis carrying a C9orf72 repeat expansion: a population-based cohort study. Lancet Neurol 2012;11:232-240.

39. Byrne S, Walsh C, Lynch C, et al. Rate of familial amyotrophic lateral sclerosis: a systematic review and meta-analysis. J Neurol Neurosurg Psychiatry 2011;82:623-627.

40. Andersen PM, Al-Chalabi A. Clinical genetics of amyotrophic lateral sclerosis: what do we really know? Nat Rev Neurol 2011;7:603-615.

41. Scarmeas N, Shih T, Stern Y, Ottman R, Rowland LP. Premorbid weight, body mass, and varsity athletics in ALS. Neurology 2002;59:773-775.

42. Turner MR, Wotton C, Talbot K, Goldacre MJ. Cardiovascular fitness as a risk factor for amyotrophic lateral sclerosis: indirect evidence from record linkage study. J Neurol Neurosurg Psychiatry 2012;83:395-398.

43. Gallo V, Wark PA, Jenab M, et al. Prediagnostic body fat and risk of death from amyotrophic lateral sclerosis: the EPIC cohort. Neurology 2013;80:829-838.

44. Huisman MH, Seelen M, de Jong SW, et al. Lifetime physical activity and the risk of amyotrophic lateral sclerosis. J Neurol Neurosurg Psychiatry 2013;84:976-981.

45. Pupillo E, Messina P, Logroscino G, Beghi E, Group S. Long-term survival in amyotrophic lateral sclerosis: a population-based study. Ann Neurol 2014;75:287-297.

46. Armon C. Smoking may be considered an established risk factor for sporadic ALS. Neurology 2009;73:1693-1698.

47. Gallo V, Bueno-De-Mesquita HB, Vermeulen R, et al. Smoking and risk for amyotrophic lateral sclerosis: analysis of the EPIC cohort. Ann Neurol 2009;65:378-385.

48. Alonso A, Logroscino G, Hernan MA. Smoking and the risk of amyotrophic lateral sclerosis: a systematic review and meta-analysis. J Neurol Neurosurg Psychiatry 2010;81:1249-1252.

49. Belbasis L, Bellou V, Evangelou E. Environmental Risk Factors and Amyotrophic Lateral Sclerosis: An Umbrella Review and Critical Assessment of Current Evidence from Systematic Reviews and Meta-Analyses of Observational Studies. Neuroepidemiology 2016;46:96-105.

50. Sutedja NA, Veldink JH, Fischer K, et al. Exposure to chemicals and metals and risk of amyotrophic lateral sclerosis: a systematic review. Amyotroph Lateral Scler 2009;10:302-309.

51. Bradley WG, Mash DC. Beyond Guam: the cyanobacteria/BMAA hypothesis of the cause of ALS and other neurodegenerative diseases. Amyotroph Lateral Scler 2009;10 Suppl 2:7-20.

52. Masseret E, Banack S, Boumediene F, et al. Dietary BMAA exposure in an amyotrophic lateral sclerosis cluster from southern France. PLoS One 2013;8:e83406.

53. Koerner DR. Amyotrophic lateral sclerosis on Guam. Ann Intern Med 1952;37:1204-1220.

54. Al-Chalabi A, Hardiman O. The epidemiology of ALS: a conspiracy of genes, environment and time. Nat Rev Neurol 2013;9:617-628.

55. Robberecht W, Philips T. The changing scene of amyotrophic lateral sclerosis. Nat Rev Neurosci 2013;14:248-264.

56. Henstridge CM, Sideris DI, Carroll E, et al. Synapse loss in the prefrontal cortex is associated with cognitive decline in amyotrophic lateral sclerosis. Acta Neuropathol 2018;135:213-226.

57. Nijssen J, Comley LH, Hedlund E. Motor neuron vulnerability and resistance in amyotrophic lateral sclerosis. Acta Neuropathol 2017;133:863-885.

58. Braak H, Brettschneider J, Ludolph AC, Lee VM, Trojanowski JQ, Del Tredici K. Amyotrophic lateral sclerosis--a model of corticofugal axonal spread. Nat Rev Neurol 2013;9:708-714.

59. Eisen A, Braak H, Del Tredici K, Lemon R, Ludolph AC, Kiernan MC. Cortical influences drive amyotrophic lateral sclerosis. J Neurol Neurosurg Psychiatry 2017;88:917-924.

60. Hynd MR, Scott HL, Dodd PR. Glutamate-mediated excitotoxicity and neurodegeneration in Alzheimer's disease. Neurochem Int 2004;45:583-595.

61. Cleveland DW, Rothstein JD. From Charcot to Lou Gehrig: deciphering selective motor neuron death in ALS. Nat Rev Neurosci 2001;2:806-819.

62. Rothstein JD, Tsai G, Kuncl RW, et al. Abnormal excitatory amino acid metabolism in amyotrophic lateral sclerosis. Ann Neurol 1990;28:18-25.

63. Spreux-Varoquaux O, Bensimon G, Lacomblez L, et al. Glutamate levels in cerebrospinal fluid in amyotrophic lateral sclerosis: a reappraisal using a new HPLC method with coulometric detection in a large cohort of patients. J Neurol Sci 2002;193:73-78.

64. Foerster BR, Pomper MG, Callaghan BC, et al. An imbalance between excitatory and inhibitory neurotransmitters in amyotrophic lateral sclerosis revealed by use of 3-T proton magnetic resonance spectroscopy. JAMA Neurol 2013;70:1009-1016.

65. Pioro EP, Majors AW, Mitsumoto H, Nelson DR, Ng TC. 1H-MRS evidence of neurodegeneration and excess glutamate + glutamine in ALS medulla. Neurology 1999;53:71-79.

66. Rothstein JD, Van Kammen M, Levey AI, Martin LJ, Kuncl RW. Selective loss of glial glutamate transporter GLT-1 in amyotrophic lateral sclerosis. Ann Neurol 1995;38:73-84.

67. Rothstein JD, Dykes-Hoberg M, Pardo CA, et al. Knockout of glutamate transporters reveals a major role for astroglial transport in excitotoxicity and clearance of glutamate. Neuron 1996;16:675-686.

68. Howland DS, Liu J, She Y, et al. Focal loss of the glutamate transporter EAAT2 in a transgenic rat model of SOD1 mutant-mediated amyotrophic lateral sclerosis (ALS). Proc Natl Acad Sci U S A 2002;99:1604-1609.

69. Guo H, Lai L, Butchbach ME, et al. Increased expression of the glial glutamate transporter EAAT2 modulates excitotoxicity and delays the onset but not the outcome of ALS in mice. Hum Mol Genet 2003;12:2519-2532.

70. Boillee S, Yamanaka K, Lobsiger CS, et al. Onset and progression in inherited ALS determined by motor neurons and microglia. Science 2006;312:1389-1392.

71. Beers DR, Henkel JS, Xiao Q, et al. Wild-type microglia extend survival in PU.1 knockout mice with familial amyotrophic lateral sclerosis. Proc Natl Acad Sci U S A 2006;103:16021-16026.

72. Brettschneider J, Toledo JB, Van Deerlin VM, et al. Microglial activation correlates with disease progression and upper motor neuron clinical symptoms in amyotrophic lateral sclerosis. PLoS One 2012;7:e39216.

73. Brettschneider J, Libon DJ, Toledo JB, et al. Microglial activation and TDP-43 pathology correlate with executive dysfunction in amyotrophic lateral sclerosis. Acta Neuropathol 2012;123:395-407.

74. Turner MR, Cagnin A, Turkheimer FE, et al. Evidence of widespread cerebral microglial activation in amyotrophic lateral sclerosis: an [11C](R)-PK11195 positron emission tomography study. Neurobiol Dis 2004;15:601-609.

75. Clement AM, Nguyen MD, Roberts EA, et al. Wild-type nonneuronal cells extend survival of SOD1 mutant motor neurons in ALS mice. Science 2003;302:113-117.

76. Lee Y, Morrison BM, Li Y, et al. Oligodendroglia metabolically support axons and contribute to neurodegeneration. Nature 2012;487:443-448.

77. Kang SH, Li Y, Fukaya M, et al. Degeneration and impaired regeneration of gray matter oligodendrocytes in amyotrophic lateral sclerosis. Nat Neurosci 2013;16:571-579.

78. Philips T, Bento-Abreu A, Nonneman A, et al. Oligodendrocyte dysfunction in the pathogenesis of amyotrophic lateral sclerosis. Brain 2013;136:471-482.

79. Ferraiuolo L, Meyer K, Sherwood TW, et al. Oligodendrocytes contribute to motor neuron death in ALS via SOD1-dependent mechanism. Proc Natl Acad Sci U S A 2016;113:E6496-E6505.

80. Saberi S, Stauffer JE, Schulte DJ, Ravits J. Neuropathology of Amyotrophic Lateral Sclerosis and Its Variants. Neurol Clin 2015;33:855-876.

81. Leigh PN, Whitwell H, Garofalo O, et al. Ubiquitin-immunoreactive intraneuronal inclusions in amyotrophic lateral sclerosis. Morphology, distribution, and specificity. Brain 1991;114 (Pt 2):775-788.

82. Mizuno Y, Amari M, Takatama M, Aizawa H, Mihara B, Okamoto K. Immunoreactivities of p62, an ubiqutin-binding protein, in the spinal anterior horn cells of patients with amyotrophic lateral sclerosis. J Neurol Sci 2006;249:13-18.

83. Pankiv S, Clausen TH, Lamark T, et al. p62/SQSTM1 binds directly to Atg8/LC3 to facilitate degradation of ubiquitinated protein aggregates by autophagy. J Biol Chem 2007;282:24131-24145.

84. Lehman NL. The ubiquitin proteasome system in neuropathology. Acta Neuropathol 2009;118:329-347.

85. Giordana MT, Piccinini M, Grifoni S, et al. TDP-43 redistribution is an early event in sporadic amyotrophic lateral sclerosis. Brain Pathol 2010;20:351-360.

86. Fecto F, Yan J, Vemula SP, et al. SQSTM1 mutations in familial and sporadic amyotrophic lateral sclerosis. Arch Neurol 2011;68:1440-1446.

87. Deng HX, Chen W, Hong ST, et al. Mutations in UBQLN2 cause dominant X-linked juvenile and adult-onset ALS and ALS/dementia. Nature 2011;477:211-215.

88. Sellier C, Campanari ML, Julie Corbier C, et al. Loss of C9ORF72 impairs autophagy and synergizes with polyQ Ataxin-2 to induce motor neuron dysfunction and cell death. EMBO J 2016;35:1276-1297.

89. Webster CP, Smith EF, Bauer CS, et al. The C9orf72 protein interacts with Rab1a and the ULK1 complex to regulate initiation of autophagy. EMBO J 2016;35:1656-1676.

90. Buratti E, Baralle FE. Multiple roles of TDP-43 in gene expression, splicing regulation, and human disease. Front Biosci 2008;13:867-878.

91. Strong MJ, Volkening K, Hammond R, et al. TDP43 is a human low molecular weight neurofilament (hNFL) mRNA-binding protein. Mol Cell Neurosci 2007;35:320-327.

92. Strong MJ, Kesavapany S, Pant HC. The pathobiology of amyotrophic lateral sclerosis: a proteinopathy? J Neuropathol Exp Neurol 2005;64:649-664.

93. Menzies FM, Grierson AJ, Cookson MR, et al. Selective loss of neurofilament expression in Cu/Zn superoxide dismutase (SOD1) linked amyotrophic lateral sclerosis. J Neurochem 2002;82:1118-1128.

94. Wong NK, He BP, Strong MJ. Characterization of neuronal intermediate filament protein expression in cervical spinal motor neurons in sporadic amyotrophic lateral sclerosis (ALS). J Neuropathol Exp Neurol 2000;59:972-982.

95. Lagier-Tourenne C, Polymenidou M, Hutt KR, et al. Divergent roles of ALS-linked proteins FUS/TLS and TDP-43 intersect in processing long pre-mRNAs. Nat Neurosci 2012;15:1488-1497.

96. Polymenidou M, Lagier-Tourenne C, Hutt KR, et al. Long pre-mRNA depletion and RNA missplicing contribute to neuronal vulnerability from loss of TDP-43. Nat Neurosci 2011;14:459-468.

97. Tollervey JR, Curk T, Rogelj B, et al. Characterizing the RNA targets and position-dependent splicing regulation by TDP-43. Nat Neurosci 2011;14:452-458.

98. Arnold ES, Ling SC, Huelga SC, et al. ALS-linked TDP-43 mutations produce aberrant RNA splicing and adult-onset motor neuron disease without aggregation or loss of nuclear TDP-43. Proc Natl Acad Sci U S A 2013;110:E736-745.

99. Yang C, Wang H, Qiao T, et al. Partial loss of TDP-43 function causes phenotypes of amyotrophic lateral sclerosis. Proc Natl Acad Sci U S A 2014;111:E1121-1129.

100. Shiihashi G, Ito D, Yagi T, Nihei Y, Ebine T, Suzuki N. Mislocated FUS is sufficient for gain-of-toxic-function amyotrophic lateral sclerosis phenotypes in mice. Brain 2016;139:2380-2394.

101. Elden AC, Kim HJ, Hart MP, et al. Ataxin-2 intermediate-length polyglutamine expansions are associated with increased risk for ALS. Nature 2010;466:1069-1075.

102. Becker LA, Huang B, Bieri G, et al. Therapeutic reduction of ataxin-2 extends lifespan and reduces pathology in TDP-43 mice. Nature 2017;544:367-371.

103. Gijselinck I, Van Langenhove T, van der Zee J, et al. A C9orf72 promoter repeat expansion in a Flanders-Belgian cohort with disorders of the frontotemporal lobar degeneration-amyotrophic lateral sclerosis spectrum: a gene identification study. Lancet Neurol 2012;11:54-65.

104. Koppers M, Blokhuis AM, Westeneng HJ, et al. C9orf72 ablation in mice does not cause motor neuron degeneration or motor deficits. Ann Neurol 2015;78:426-438.

105. Lagier-Tourenne C, Baughn M, Rigo F, et al. Targeted degradation of sense and antisense C9orf72 RNA foci as therapy for ALS and frontotemporal degeneration. Proc Natl Acad Sci U S A 2013;110:E4530-4539.

106. Todd PK, Paulson HL. RNA-mediated neurodegeneration in repeat expansion disorders. Ann Neurol 2010;67:291-300.

107. Mori K, Lammich S, Mackenzie IR, et al. hnRNP A3 binds to GGGGCC repeats and is a constituent of p62-positive/TDP43-negative inclusions in the hippocampus of patients with C9orf72 mutations. Acta Neuropathol 2013;125:413-423.

108. Freibaum BD, Lu Y, Lopez-Gonzalez R, et al. GGGGCC repeat expansion in C9orf72 compromises nucleocytoplasmic transport. Nature 2015;525:129-133.

109. Zhang K, Donnelly CJ, Haeusler AR, et al. The C9orf72 repeat expansion disrupts nucleocytoplasmic transport. Nature 2015;525:56-61.

110. Zhang YJ, Gendron TF, Grima JC, et al. C9ORF72 poly(GA) aggregates sequester and impair HR23 and nucleocytoplasmic transport proteins. Nat Neurosci 2016;19:668-677.

111. Jovicic A, Mertens J, Boeynaems S, et al. Modifiers of C9orf72 dipeptide repeat toxicity connect nucleocytoplasmic transport defects to FTD/ALS. Nat Neurosci 2015;18:1226-1229.

112. Jucker M, Walker LC. Self-propagation of pathogenic protein aggregates in neurodegenerative diseases. Nature 2013;501:45-51.

113. Zoccolella S, Beghi E, Palagano G, et al. Signs and symptoms at diagnosis of amyotrophic lateral sclerosis: a population-based study in southern Italy. Eur J Neurol 2006;13:789-792.

114. Turner MR, Wicks P, Brownstein CA, et al. Concordance between site of onset and limb dominance in amyotrophic lateral sclerosis. J Neurol Neurosurg Psychiatry 2011;82:853-854.

115. Battistini S, Giannini F, Greco G, et al. SOD1 mutations in amyotrophic lateral sclerosis. Results from a multicenter Italian study. J Neurol 2005;252:782-788.

116. Orrell RW, Habgood JJ, Malaspina A, et al. Clinical characteristics of SOD1 gene mutations in UK families with ALS. J Neurol Sci 1999;169:56-60.

117. Millecamps S, Boillee S, Le Ber I, et al. Phenotype difference between ALS patients with expanded repeats in C9ORF72 and patients with mutations in other ALS-related genes. J Med Genet 2012;49:258-263.

118. Corcia P, Valdmanis P, Millecamps S, et al. Phenotype and genotype analysis in amyotrophic lateral sclerosis with TARDBP gene mutations. Neurology 2012;78:1519-1526.

119. Brooks BR, Miller RG, Swash M, Munsat TL, World Federation of Neurology Research Group on Motor Neuron D. El Escorial revisited: revised criteria for the diagnosis of amyotrophic lateral sclerosis. Amyotroph Lateral Scler Other Motor Neuron Disord 2000;1:293-299.

120. Sabatelli M, Zollino M, Luigetti M, et al. Uncovering amyotrophic lateral sclerosis phenotypes: clinical features and long-term follow-up of upper motor neuron-dominant ALS. Amyotroph Lateral Scler 2011;12:278-282.

121. Soraru G, Ermani M, Logroscino G, et al. Natural history of upper motor neuron-dominant ALS. Amyotroph Lateral Scler 2010;11:424-429.

122. Wijesekera LC, Mathers S, Talman P, et al. Natural history and clinical features of the flail arm and flail leg ALS variants. Neurology 2009;72:1087-1094.

123. Al-Chalabi A, Hardiman O, Kiernan MC, Chio A, Rix-Brooks B, van den Berg LH. Amyotrophic lateral sclerosis: moving towards a new classification system. Lancet Neurol 2016;15:1182-1194.

124. Brooks BR. El Escorial World Federation of Neurology criteria for the diagnosis of amyotrophic lateral sclerosis. Subcommittee on Motor Neuron Diseases/Amyotrophic Lateral Sclerosis of the World Federation of Neurology Research Group on Neuromuscular Diseases and the El Escorial "Clinical limits of amyotrophic lateral sclerosis" workshop contributors. J Neurol Sci 1994;124 Suppl:96-107.

125. Meininger V, Genge A, van den Berg LH, et al. Safety and efficacy of ozanezumab in patients with amyotrophic lateral sclerosis: a randomised, double-blind, placebo-controlled, phase 2 trial. Lancet Neurol 2017;16:208-216.
126. Writing G, Edaravone ALSSG. Safety and efficacy of edaravone in well defined patients with amyotrophic lateral sclerosis: a randomised, double-blind, placebo-controlled trial. Lancet Neurol 2017;16:505-512.
127. Chio A, Logroscino G, Hardiman O, et al. Prognostic factors in ALS: A critical review. Amyotroph Lateral Scler 2009;10:310-323.
128. Ringholz GM, Appel SH, Bradshaw M, Cooke NA, Mosnik DM, Schulz PE. Prevalence and patterns of cognitive impairment in sporadic ALS. Neurology 2005;65:586-590.
129. Cellura E, Spataro R, Taiello AC, La Bella V. Factors affecting the diagnostic delay in amyotrophic lateral sclerosis. Clin Neurol Neurosurg 2012;114:550-554.
130. de Carvalho M, Dengler R, Eisen A, et al. Electrodiagnostic criteria for diagnosis of ALS. Clin Neurophysiol 2008;119:497-503.
131. Geevasinga N, Menon P, Scherman DB, et al. Diagnostic criteria in amyotrophic lateral sclerosis: A multicenter prospective study. Neurology 2016;87:684-690.
132. Schrooten M, Smetcoren C, Robberecht W, Van Damme P. Benefit of the Awaji diagnostic algorithm for amyotrophic lateral sclerosis: a prospective study. Ann Neurol 2011;70:79-83.
133. Roche JC, Rojas-Garcia R, Scott KM, et al. A proposed staging system for amyotrophic lateral sclerosis. Brain 2012;135:847-852.
134. Balendra R, Jones A, Jivraj N, et al. Use of clinical staging in amyotrophic lateral sclerosis for phase 3 clinical trials. J Neurol Neurosurg Psychiatry 2015;86:45-49.

135. Crockford C, Newton J, Lonergan K, et al. ALS-specific cognitive and behavior changes associated with advancing disease stage in ALS. Neurology 2018;91:e1370-e1380.
136. Swinnen B, Robberecht W. The phenotypic variability of amyotrophic lateral sclerosis. Nat Rev Neurol 2014;10:661-670.
137. Singer MA, Statland JM, Wolfe GI, Barohn RJ. Primary lateral sclerosis. Muscle Nerve 2007;35:291-302.
138. Tartaglia MC, Rowe A, Findlater K, Orange JB, Grace G, Strong MJ. Differentiation between primary lateral sclerosis and amyotrophic lateral sclerosis: examination of symptoms and signs at disease onset and during follow-up. Arch Neurol 2007;64:232-236.
139. Gordon PH, Cheng B, Katz IB, et al. The natural history of primary lateral sclerosis. Neurology 2006;66:647-653.
140. D'Amico E, Pasmantier M, Lee YW, Weimer L, Mitsumoto H. Clinical evolution of pure upper motor neuron disease/dysfunction (PUMMD). Muscle Nerve 2013;47:28-32.
141. Kim WK, Liu X, Sandner J, et al. Study of 962 patients indicates progressive muscular atrophy is a form of ALS. Neurology 2009;73:1686-1692.
142. van der Graaff MM, Sage CA, Caan MW, et al. Upper and extra-motoneuron involvement in early motoneuron disease: a diffusion tensor imaging study. Brain 2011;134:1211-1228.
143. Ince PG, Evans J, Knopp M, et al. Corticospinal tract degeneration in the progressive muscular atrophy variant of ALS. Neurology 2003;60:1252-1258.
144. Riku Y, Atsuta N, Yoshida M, et al. Differential motor neuron involvement in progressive muscular atrophy: a comparative study with amyotrophic lateral sclerosis. BMJ Open 2014;4:e005213.

145. Montuschi A, Iazzolino B, Calvo A, et al. Cognitive correlates in amyotrophic lateral sclerosis: a population-based study in Italy. J Neurol Neurosurg Psychiatry 2015;86:168-173.
146. Bang J, Spina S, Miller BL. Frontotemporal dementia. Lancet 2015;386:1672-1682.
147. Rascovsky K, Hodges JR, Knopman D, et al. Sensitivity of revised diagnostic criteria for the behavioural variant of frontotemporal dementia. Brain 2011;134:2456-2477.
148. Saxon JA, Harris JM, Thompson JC, et al. Semantic dementia, progressive non-fluent aphasia and their association with amyotrophic lateral sclerosis. J Neurol Neurosurg Psychiatry 2017;88:711-712.
149. Witgert M, Salamone AR, Strutt AM, et al. Frontal-lobe mediated behavioral dysfunction in amyotrophic lateral sclerosis. Eur J Neurol 2010;17:103-110.
150. Lillo P, Mioshi E, Zoing MC, Kiernan MC, Hodges JR. How common are behavioural changes in amyotrophic lateral sclerosis? Amyotroph Lateral Scler 2011;12:45-51.
151. Elamin M, Bede P, Byrne S, et al. Cognitive changes predict functional decline in ALS: a population-based longitudinal study. Neurology 2013;80:1590-1597.
152. Elamin M, Phukan J, Bede P, et al. Executive dysfunction is a negative prognostic indicator in patients with ALS without dementia. Neurology 2011;76:1263-1269.
153. Strong MJ, Abrahams S, Goldstein LH, et al. Amyotrophic lateral sclerosis - frontotemporal spectrum disorder (ALS-FTSD): Revised diagnostic criteria. Amyotroph Lateral Scler Frontotemporal Degener 2017;18:153-174.
154. Diamond A. Executive functions. Annu Rev Psychol 2013;64:135-168.

155. Beeldman E, Raaphorst J, Klein Twennaar M, de Visser M, Schmand BA, de Haan RJ. The cognitive profile of ALS: a systematic review and meta-analysis update. J Neurol Neurosurg Psychiatry 2016;87:611-619.
156. Tsermentseli S, Leigh PN, Goldstein LH. The anatomy of cognitive impairment in amyotrophic lateral sclerosis: more than frontal lobe dysfunction. Cortex 2012;48:166-182.
157. Abrahams S, Goldstein LH, Kew JJ, et al. Frontal lobe dysfunction in amyotrophic lateral sclerosis. A PET study. Brain 1996;119 (Pt 6):2105-2120.
158. Wicks P, Turner MR, Abrahams S, et al. Neuronal loss associated with cognitive performance in amyotrophic lateral sclerosis: an (11C)-flumazenil PET study. Amyotroph Lateral Scler 2008;9:43-49.
159. Abrahams S, Goldstein LH, Simmons A, et al. Word retrieval in amyotrophic lateral sclerosis: a functional magnetic resonance imaging study. Brain 2004;127:1507-1517.
160. Taylor LJ, Brown RG, Tsermentseli S, et al. Is language impairment more common than executive dysfunction in amyotrophic lateral sclerosis? J Neurol Neurosurg Psychiatry 2013;84:494-498.
161. Bora E. Meta-analysis of social cognition in amyotrophic lateral sclerosis. Cortex 2017;88:1-7.
162. Carluer L, Mondou A, Buhour MS, et al. Neural substrate of cognitive theory of mind impairment in amyotrophic lateral sclerosis. Cortex 2015;65:19-30.
163. Cerami C, Dodich A, Canessa N, et al. Emotional empathy in amyotrophic lateral sclerosis: a behavioural and voxel-based morphometry study. Amyotroph Lateral Scler Frontotemporal Degener 2014;15:21-29.

164. Crespi C, Cerami C, Dodich A, et al. Microstructural white matter correlates of emotion recognition impairment in Amyotrophic Lateral Sclerosis. Cortex 2014;53:1-8.

165. Meier SL, Charleston AJ, Tippett LJ. Cognitive and behavioural deficits associated with the orbitomedial prefrontal cortex in amyotrophic lateral sclerosis. Brain 2010;133:3444-3457.

166. Watermeyer TJ, Brown RG, Sidle KC, et al. Executive dysfunction predicts social cognition impairment in amyotrophic lateral sclerosis. J Neurol 2015;262:1681-1690.

167. Abrahams S, Newton J, Niven E, Foley J, Bak TH. Screening for cognition and behaviour changes in ALS. Amyotroph Lateral Scler Frontotemporal Degener 2014;15:9-14.

168. Niven E, Newton J, Foley J, et al. Validation of the Edinburgh Cognitive and Behavioural Amyotrophic Lateral Sclerosis Screen (ECAS): A cognitive tool for motor disorders. Amyotroph Lateral Scler Frontotemporal Degener 2015;16:172-179.

169. Fujimura-Kiyono C, Kimura F, Ishida S, et al. Onset and spreading patterns of lower motor neuron involvements predict survival in sporadic amyotrophic lateral sclerosis. J Neurol Neurosurg Psychiatry 2011;82:1244-1249.

170. Korner S, Kollewe K, Fahlbusch M, et al. Onset and spreading patterns of upper and lower motor neuron symptoms in amyotrophic lateral sclerosis. Muscle Nerve 2011;43:636-642.

171. Ravits J, Laurie P, Fan Y, Moore DH. Implications of ALS focality: rostral-caudal distribution of lower motor neuron loss postmortem. Neurology 2007;68:1576-1582.

172. Ravits J, Paul P, Jorg C. Focality of upper and lower motor neuron degeneration at the clinical onset of ALS. Neurology 2007;68:1571-1575.

173. Turner MR, Brockington A, Scaber J, et al. Pattern of spread and prognosis in lower limb-onset ALS. Amyotroph Lateral Scler 2010;11:369-373.

174. Cedarbaum JM, Stambler N, Malta E, et al. The ALSFRS-R: a revised ALS functional rating scale that incorporates assessments of respiratory function. BDNF ALS Study Group (Phase III). J Neurol Sci 1999;169:13-21.

175. Gordon PH, Cheng B, Salachas F, et al. Progression in ALS is not linear but is curvilinear. J Neurol 2010;257:1713-1717.

176. Bali T, Self W, Liu J, et al. Defining SOD1 ALS natural history to guide therapeutic clinical trial design. J Neurol Neurosurg Psychiatry 2017;88:99-105.

177. Rooney J, Burke T, Vajda A, Heverin M, Hardiman O. What does the ALSFRS-R really measure? A longitudinal and survival analysis of functional dimension subscores in amyotrophic lateral sclerosis. J Neurol Neurosurg Psychiatry 2017;88:381-385.

178. Thivard L, Pradat PF, Lehericy S, et al. Diffusion tensor imaging and voxel based morphometry study in amyotrophic lateral sclerosis: relationships with motor disability. J Neurol Neurosurg Psychiatry 2007;78:889-892.

179. Canu E, Agosta F, Riva N, et al. The topography of brain microstructural damage in amyotrophic lateral sclerosis assessed using diffusion tensor MR imaging. AJNR Am J Neuroradiol 2011;32:1307-1314.

180. Neudert C, Oliver D, Wasner M, Borasio GD. The course of the terminal phase in patients with amyotrophic lateral sclerosis. J Neurol 2001;248:612-616.

181. Gil J, Funalot B, Verschueren A, et al. Causes of death amongst French patients with amyotrophic lateral sclerosis: a prospective study. Eur J Neurol 2008;15:1245-1251.

182. Czaplinski A, Yen AA, Appel SH. Forced vital capacity (FVC) as an indicator of survival and disease progression in an ALS clinic population. J Neurol Neurosurg Psychiatry 2006;77:390-392.

183. Pinto S, de Carvalho M. Comparison of slow and forced vital capacities on ability to predict survival in ALS. Amyotroph Lateral Scler Frontotemporal Degener 2017;18:528-533.

184. Kimura F, Fujimura C, Ishida S, et al. Progression rate of ALSFRS-R at time of diagnosis predicts survival time in ALS. Neurology 2006;66:265-267.

185. Proudfoot M, Jones A, Talbot K, Al-Chalabi A, Turner MR. The ALSFRS as an outcome measure in therapeutic trials and its relationship to symptom onset. Amyotroph Lateral Scler Frontotemporal Degener 2016;17:414-425.

186. Qureshi M, Schoenfeld DA, Paliwal Y, Shui A, Cudkowicz ME. The natural history of ALS is changing: improved survival. Amyotroph Lateral Scler 2009;10:324-331.

187. Chio A, Ilardi A, Cammarosano S, Moglia C, Montuschi A, Calvo A. Neurobehavioral dysfunction in ALS has a negative effect on outcome and use of PEG and NIV. Neurology 2012;78:1085-1089.

188. Govaarts R, Beeldman E, Kampelmacher MJ, et al. The frontotemporal syndrome of ALS is associated with poor survival. J Neurol 2016;263:2476-2483.

189. Cudkowicz ME, McKenna-Yasek D, Sapp PE, et al. Epidemiology of mutations in superoxide dismutase in amyotrophic lateral sclerosis. Ann Neurol 1997;41:210-221.

190. Hardiman O, van den Berg LH, Kiernan MC. Clinical diagnosis and management of amyotrophic lateral sclerosis. Nat Rev Neurol 2011;7:639-649.

191. Miller RG, Mitchell JD, Moore DH. Riluzole for amyotrophic lateral sclerosis (ALS)/motor neuron disease (MND). Cochrane Database Syst Rev 2012:CD001447.

192. Wang SJ, Wang KY, Wang WC. Mechanisms underlying the riluzole inhibition of glutamate release from rat cerebral cortex nerve terminals (synaptosomes). Neuroscience 2004;125:191-201.

193. Azbill RD, Mu X, Springer JE. Riluzole increases high-affinity glutamate uptake in rat spinal cord synaptosomes. Brain Res 2000;871:175-180.

194. Kalra S, Cashman NR, Genge A, Arnold DL. Recovery of N-acetylaspartate in corticomotor neurons of patients with ALS after riluzole therapy. Neuroreport 1998;9:1757-1761.

195. Rothstein JD. Edaravone: A new drug approved for ALS. Cell 2017;171:725.

196. Edaravone Acute Infarction Study G. Effect of a novel free radical scavenger, edaravone (MCI-186), on acute brain infarction. Randomized, placebo-controlled, double-blind study at multicenters. Cerebrovasc Dis 2003;15:222-229.

197. Hardiman O, van den Berg LH. Edaravone: a new treatment for ALS on the horizon? Lancet Neurol 2017;16:490-491.

198. Diagnosis ETFo, Management of Amyotrophic Lateral S, Andersen PM, et al. EFNS guidelines on the clinical management of amyotrophic lateral sclerosis (MALS)--revised report of an EFNS task force. Eur J Neurol 2012;19:360-375.

199. Miller RG, Jackson CE, Kasarskis EJ, et al. Practice parameter update: the care of the patient with amyotrophic lateral sclerosis: multidisciplinary care, symptom management, and cognitive/behavioral impairment (an evidence-based review): report of the Quality Standards Subcommittee of the American Academy of Neurology. Neurology 2009;73:1227-1233.

200. Chio A, Bottacchi E, Buffa C, Mutani R, Mora G, Parals. Positive effects of tertiary centres for amyotrophic lateral sclerosis on outcome and use of hospital facilities. J Neurol Neurosurg Psychiatry 2006;77:948-950.

201. Traynor BJ, Alexander M, Corr B, Frost E, Hardiman O. Effect of a multidisciplinary amyotrophic lateral sclerosis (ALS) clinic on ALS survival: a population based study, 1996-2000. J Neurol Neurosurg Psychiatry 2003;74:1258-1261.

202. Van den Berg JP, Kalmijn S, Lindeman E, et al. Multidisciplinary ALS care improves quality of life in patients with ALS. Neurology 2005;65:1264-1267.

203. Marin B, Desport JC, Kajeu P, et al. Alteration of nutritional status at diagnosis is a prognostic factor for survival of amyotrophic lateral sclerosis patients. J Neurol Neurosurg Psychiatry 2011;82:628-634.

204. Dupuis L, Pradat PF, Ludolph AC, Loeffler JP. Energy metabolism in amyotrophic lateral sclerosis. Lancet Neurol 2011;10:75-82.

205. Miller RG, Jackson CE, Kasarskis EJ, et al. Practice parameter update: the care of the patient with amyotrophic lateral sclerosis: drug, nutritional, and respiratory therapies (an evidence-based review): report of the Quality Standards Subcommittee of the American Academy of Neurology. Neurology 2009;73:1218-1226.

206. Mazzini L, Corra T, Zaccala M, Mora G, Del Piano M, Galante M. Percutaneous endoscopic gastrostomy and enteral nutrition in amyotrophic lateral sclerosis. J Neurol 1995;242:695-698.

207. Bourke SC, Tomlinson M, Williams TL, Bullock RE, Shaw PJ, Gibson GJ. Effects of non-invasive ventilation on survival and quality of life in patients with amyotrophic lateral sclerosis: a randomised controlled trial. Lancet Neurol 2006;5:140-147.

208. Yoshida M. Amyotrophic lateral sclerosis with dementia: the clinicopathological spectrum. Neuropathology 2004;24:87-102.

209. Hudson AJ, Kiernan JA, Munoz DG, Pringle CE, Brown WF, Ebers GC. Clinicopathological features of primary lateral sclerosis are different from amyotrophic lateral sclerosis. Brain Res Bull 1993;30:359-364.

210. Pringle CE, Hudson AJ, Munoz DG, Kiernan JA, Brown WF, Ebers GC. Primary lateral sclerosis. Clinical features, neuropathology and diagnostic criteria. Brain 1992;115 (Pt 2):495-520.

211. Lawyer T, Jr., Netsky MG. Amyotrophic lateral sclerosis. AMA Arch Neurol Psychiatry 1953;69:171-192.

212. Maekawa S, Al-Sarraj S, Kibble M, et al. Cortical selective vulnerability in motor neuron disease: a morphometric study. Brain 2004;127:1237-1251.

213. Nihei K, McKee AC, Kowall NW. Patterns of neuronal degeneration in the motor cortex of amyotrophic lateral sclerosis patients. Acta Neuropathol 1993;86:55-64.

214. Hammer RP, Jr., Tomiyasu U, Scheibel AB. Degeneration of the human Betz cell due to amyotrophic lateral sclerosis. Exp Neurol 1979;63:336-346.

215. Udaka F, Kameyama M, Tomonaga M. Degeneration of Betz cells in motor neuron disease. A Golgi study. Acta Neuropathol 1986;70:289-295.

216. Rivara CB, Sherwood CC, Bouras C, Hof PR. Stereologic characterization and spatial distribution patterns of Betz cells in the human primary motor cortex. Anat Rec A Discov Mol Cell Evol Biol 2003;270:137-151.

217. Gredal O, Pakkenberg H, Karlsborg M, Pakkenberg B. Unchanged total number of neurons in motor cortex and neocortex in amyotrophic lateral sclerosis: a stereological study. J Neurosci Methods 2000;95:171-176.

218. Sofroniew MV. Molecular dissection of reactive astrogliosis and glial scar formation. Trends Neurosci 2009;32:638-647.

219. Kamo H, Haebara H, Akiguchi I, Kameyama M, Kimura H, McGeer PL. A distinctive distribution of reactive astroglia in the precentral cortex in amyotrophic lateral sclerosis. Acta Neuropathol 1987;74:33-38.

220. Kushner PD, Stephenson DT, Wright S. Reactive astrogliosis is widespread in the subcortical white matter of amyotrophic lateral sclerosis brain. J Neuropathol Exp Neurol 1991;50:263-277.

221. Murayama S, Inoue K, Kawakami H, Bouldin TW, Suzuki K. A unique pattern of astrocytosis in the primary motor area in amyotrophic lateral sclerosis. Acta Neuropathol 1991;82:456-461.

222. Piao YS, Wakabayashi K, Kakita A, et al. Neuropathology with clinical correlations of sporadic amyotrophic lateral sclerosis: 102 autopsy cases examined between 1962 and 2000. Brain Pathol 2003;13:10-22.

223. Graves MC, Fiala M, Dinglasan LA, et al. Inflammation in amyotrophic lateral sclerosis spinal cord and brain is mediated by activated macrophages, mast cells and T cells. Amyotroph Lateral Scler Other Motor Neuron Disord 2004;5:213-219.

224. Neumann H, Kotter MR, Franklin RJ. Debris clearance by microglia: an essential link between degeneration and regeneration. Brain 2009;132:288-295.

225. Finsterer J, Erdorf M, Mamoli B, Fuglsang-Frederiksen A. Needle electromyography of bulbar muscles in patients with amyotrophic lateral sclerosis: evidence of subclinical involvement. Neurology 1998;51:1417-1422.

226. Higo R, Tayama N, Nito T. Longitudinal analysis of progression of dysphagia in amyotrophic lateral sclerosis. Auris Nasus Larynx 2004;31:247-254.

227. Swash M, Leader M, Brown A, Swettenham KW. Focal loss of anterior horn cells in the cervical cord in motor neuron disease. Brain 1986;109 (Pt 5):939-952.

228. Terao S, Sobue G, Hashizume Y, Mitsuma T, Takahashi A. Disease-specific patterns of neuronal loss in the spinal ventral horn in amyotrophic lateral sclerosis, multiple system atrophy and X-linked recessive bulbospinal neuronopathy, with special reference to the loss of small neurons in the intermediate zone. J Neurol 1994;241:196-203.

229. Tsukagoshi H, Yanagisawa N, Oguchi K, Nagashima K, Murakami T. Morphometric quantification of the cervical limb motor cells in controls and in amyotrophic lateral sclerosis. J Neurol Sci 1979;41:287-297.

230. Schiffer D, Autilio-Gambetti L, Chio A, et al. Ubiquitin in motor neuron disease: study at the light and electron microscope. J Neuropathol Exp Neurol 1991;50:463-473.

231. Henkel JS, Engelhardt JI, Siklos L, et al. Presence of dendritic cells, MCP-1, and activated microglia/macrophages in amyotrophic lateral sclerosis spinal cord tissue. Ann Neurol 2004;55:221-235.

232. Kawamata T, Akiyama H, Yamada T, McGeer PL. Immunologic reactions in amyotrophic lateral sclerosis brain and spinal cord tissue. Am J Pathol 1992;140:691-707.

233. Okamoto K, Mizuno Y, Fujita Y. Bunina bodies in amyotrophic lateral sclerosis. Neuropathology 2008;28:109-115.

234. Kuroda S, Ishizu H, Kawai K, Otsuki S. Bunina bodies in dendrites of patients with amyotrophic lateral sclerosis. Acta Med Okayama 1990;44:41-45.

235. Mochizuki A, Komatsuzaki Y, Iwamoto H, Shoji S. Frontotemporal dementia with ubiquitinated neuronal inclusions presenting with primary lateral sclerosis and parkinsonism: clinicopathological report of an autopsy case. Acta Neuropathol 2004;107:377-380.

236. Kimura T, Jiang H, Konno T, et al. Bunina bodies in motor and non-motor neurons revisited: a pathological study of an ALS patient after long-term survival on a respirator. Neuropathology 2014;34:392-397.

237. Ross CA, Poirier MA. Protein aggregation and neurodegenerative disease. Nat Med 2004;10 Suppl:S10-17.

238. Leigh PN, Anderton BH, Dodson A, Gallo JM, Swash M, Power DM. Ubiquitin deposits in anterior horn cells in motor neurone disease. Neurosci Lett 1988;93:197-203.

239. Lowe J, Aldridge F, Lennox G, et al. Inclusion bodies in motor cortex and brainstem of patients with motor neurone disease are detected by immunocytochemical localisation of ubiquitin. Neurosci Lett 1989;105:7-13.

240. Murayama S, Bouldin TW, Suzuki K. Immunocytochemical and ultrastructural studies of upper motor neurons in amyotrophic lateral sclerosis. Acta Neuropathol 1992;83:518-524.

241. Hasegawa M, Arai T, Nonaka T, et al. Phosphorylated TDP-43 in frontotemporal lobar degeneration and amyotrophic lateral sclerosis. Ann Neurol 2008;64:60-70.

242. Sumi H, Kato S, Mochimaru Y, Fujimura H, Etoh M, Sakoda S. Nuclear TAR DNA binding protein 43 expression in spinal cord neurons correlates with the clinical course in amyotrophic lateral sclerosis. J Neuropathol Exp Neurol 2009;68:37-47.

243. Nishihira Y, Tan CF, Onodera O, et al. Sporadic amyotrophic lateral sclerosis: two pathological patterns shown by analysis of distribution of TDP-43-immunoreactive neuronal and glial cytoplasmic inclusions. Acta Neuropathol 2008;116:169-182.

244. Tan RH, Kril JJ, Fatima M, et al. TDP-43 proteinopathies: pathological identification of brain regions differentiating clinical phenotypes. Brain 2015;138:3110-3122.

245. Halliday GM, Kiernan MC, Kril JJ, et al. TDP-43 in the hypoglossal nucleus identifies amyotrophic lateral sclerosis in behavioral variant frontotemporal dementia. J Neurol Sci 2016;366:197-201.

246. Brettschneider J, Arai K, Del Tredici K, et al. TDP-43 pathology and neuronal loss in amyotrophic lateral sclerosis spinal cord. Acta Neuropathol 2014;128:423-437.

247. Geser F, Martinez-Lage M, Robinson J, et al. Clinical and pathological continuum of multisystem TDP-43 proteinopathies. Arch Neurol 2009;66:180-189.

248. Al-Chalabi A, Jones A, Troakes C, King A, Al-Sarraj S, van den Berg LH. The genetics and neuropathology of amyotrophic lateral sclerosis. Acta Neuropathol 2012;124:339-352.

249. Mackenzie IR, Bigio EH, Ince PG, et al. Pathological TDP-43 distinguishes sporadic amyotrophic lateral sclerosis from amyotrophic lateral sclerosis with SOD1 mutations. Ann Neurol 2007;61:427-434.

250. Tan CF, Eguchi H, Tagawa A, et al. TDP-43 immunoreactivity in neuronal inclusions in familial amyotrophic lateral sclerosis with or without SOD1 gene mutation. Acta Neuropathol 2007;113:535-542.

251. Okamoto Y, Shirakashi Y, Ihara M, et al. Colocalization of 14-3-3 proteins with SOD1 in Lewy body-like hyaline inclusions in familial amyotrophic lateral sclerosis cases and the animal model. PLoS One 2011;6:e20427.

252. Shibata N, Hirano A, Kobayashi M, et al. Intense superoxide dismutase-1 immunoreactivity in intracytoplasmic hyaline inclusions of familial amyotrophic lateral sclerosis with posterior column involvement. J Neuropathol Exp Neurol 1996;55:481-490.

253. Ince PG, Tomkins J, Slade JY, Thatcher NM, Shaw PJ. Amyotrophic lateral sclerosis associated with genetic abnormalities in the gene encoding Cu/Zn superoxide dismutase: molecular pathology of five new cases, and comparison with previous reports and 73 sporadic cases of ALS. J Neuropathol Exp Neurol 1998;57:895-904.

254. Kerman A, Liu HN, Croul S, et al. Amyotrophic lateral sclerosis is a non-amyloid disease in which extensive misfolding of SOD1 is unique to the familial form. Acta Neuropathol 2010;119:335-344.

255. Liu HN, Sanelli T, Horne P, et al. Lack of evidence of monomer/misfolded superoxide dismutase-1 in sporadic amyotrophic lateral sclerosis. Ann Neurol 2009;66:75-80.

256. Forsberg K, Andersen PM, Marklund SL, Brannstrom T. Glial nuclear aggregates of superoxide dismutase-1 are regularly present in patients with amyotrophic lateral sclerosis. Acta Neuropathol 2011;121:623-634.

257. Da Cruz S, Bui A, Saberi S, et al. Misfolded SOD1 is not a primary component of sporadic ALS. Acta Neuropathol 2017;134:97-111.

258. Blair IP, Williams KL, Warraich ST, et al. FUS mutations in amyotrophic lateral sclerosis: clinical, pathological, neurophysiological and genetic analysis. J Neurol Neurosurg Psychiatry 2010;81:639-645.

259. Hewitt C, Kirby J, Highley JR, et al. Novel FUS/TLS mutations and pathology in familial and sporadic amyotrophic lateral sclerosis. Arch Neurol 2010;67:455-461.

260. Mackenzie IR, Ansorge O, Strong M, et al. Pathological heterogeneity in amyotrophic lateral sclerosis with FUS mutations: two distinct patterns correlating with disease severity and mutation. Acta Neuropathol 2011;122:87-98.

261. Deng HX, Zhai H, Bigio EH, et al. FUS-immunoreactive inclusions are a common feature in sporadic and non-SOD1 familial amyotrophic lateral sclerosis. Ann Neurol 2010;67:739-748.

262. Keller BA, Volkening K, Droppelmann CA, Ang LC, Rademakers R, Strong MJ. Co-aggregation of RNA binding proteins in ALS spinal motor neurons: evidence of a common pathogenic mechanism. Acta Neuropathol 2012;124:733-747.

263. Mackenzie IR, Frick P, Neumann M. The neuropathology associated with repeat expansions in the C9ORF72 gene. Acta Neuropathol 2014;127:347-357.

264. Stewart H, Rutherford NJ, Briemberg H, et al. Clinical and pathological features of amyotrophic lateral sclerosis caused by mutation in the C9ORF72 gene on chromosome 9p. Acta Neuropathol 2012;123:409-417.

265. Murray ME, DeJesus-Hernandez M, Rutherford NJ, et al. Clinical and neuropathologic heterogeneity of c9FTD/ALS associated with hexanucleotide repeat expansion in C9ORF72. Acta Neuropathol 2011;122:673-690.

266. Al-Sarraj S, King A, Troakes C, et al. p62 positive, TDP-43 negative, neuronal cytoplasmic and intranuclear inclusions in the cerebellum and hippocampus define the pathology of C9orf72-linked FTLD and MND/ALS. Acta Neuropathol 2011;122:691-702.

267. Mori K, Weng SM, Arzberger T, et al. The C9orf72 GGGGCC repeat is translated into aggregating dipeptide-repeat proteins in FTLD/ALS. Science 2013;339:1335-1338.

268. Mackenzie IR, Frick P, Grasser FA, et al. Quantitative analysis and clinico-pathological correlations of different dipeptide repeat protein pathologies in C9ORF72 mutation carriers. Acta Neuropathol 2015;130:845-861.

269. Mackenzie IR, Feldman HH. Ubiquitin immunohistochemistry suggests classic motor neuron disease, motor neuron disease with dementia, and frontotemporal dementia of the motor neuron disease type represent a clinicopathologic spectrum. J Neuropathol Exp Neurol 2005;64:730-739.

270. Geser F, Brandmeir NJ, Kwong LK, et al. Evidence of multisystem disorder in whole-brain map of pathological TDP-43 in amyotrophic lateral sclerosis. Arch Neurol 2008;65:636-641.

271. Prudlo J, Konig J, Schuster C, et al. TDP-43 pathology and cognition in ALS: A prospective clinicopathologic correlation study. Neurology 2016;87:1019-1023.

272. Cykowski MD, Powell SZ, Peterson LE, et al. Clinical Significance of TDP-43 Neuropathology in Amyotrophic Lateral Sclerosis. J Neuropathol Exp Neurol 2017;76:402-413.

273. Hsiung GY, DeJesus-Hernandez M, Feldman HH, et al. Clinical and pathological features of familial frontotemporal dementia caused by C9ORF72 mutation on chromosome 9p. Brain 2012;135:709-722.

274. Brettschneider J, Del Tredici K, Toledo JB, et al. Stages of pTDP-43 pathology in amyotrophic lateral sclerosis. Ann Neurol 2013;74:20-38.

275. Catani M, Dell'acqua F, Vergani F, et al. Short frontal lobe connections of the human brain. Cortex 2012;48:273-291.

276. Nambu A. A new dynamic model of the cortico-basal ganglia loop. Prog Brain Res 2004;143:461-466.

277. Kassubek J, Muller HP, Del Tredici K, et al. Diffusion tensor imaging analysis of sequential spreading of disease in amyotrophic lateral sclerosis confirms patterns of TDP-43 pathology. Brain 2014;137:1733-1740.

278. Kassubek J, Muller HP, Del Tredici K, et al. Imaging the pathoanatomy of amyotrophic lateral sclerosis in vivo: targeting a propagation-based biological marker. J Neurol Neurosurg Psychiatry 2018;89:374-381.

279. Benatar M, Boylan K, Jeromin A, et al. ALS biomarkers for therapy development: State of the field and future directions. Muscle Nerve 2016;53:169-182.

280. Kalra S. Magnetic Resonance Spectroscopy in ALS. Front Neurol 2019;10:482.

281. Lule D, Ludolph AC, Kassubek J. MRI-based functional neuroimaging in ALS: an update. Amyotroph Lateral Scler 2009;10:258-268.

282. Jack CR, Jr., Knopman DS, Jagust WJ, et al. Tracking pathophysiological processes in Alzheimer's disease: an updated hypothetical model of dynamic biomarkers. Lancet Neurol 2013;12:207-216.

283. Turner MR, Grosskreutz J, Kassubek J, et al. Towards a neuroimaging biomarker for amyotrophic lateral sclerosis. Lancet Neurol 2011;10:400-403.

284. Currie S, Hoggard N, Craven IJ, Hadjivassiliou M, Wilkinson ID. Understanding MRI: basic MR physics for physicians. Postgrad Med J 2013;89:209-223.

285. Fischl B. FreeSurfer. Neuroimage 2012;62:774-781.

286. Jenkinson M, Beckmann CF, Behrens TE, Woolrich MW, Smith SM. Fsl. Neuroimage 2012;62:782-790.

287. Wright IC, McGuire PK, Poline JB, et al. A voxel-based method for the statistical analysis of gray and white matter density applied to schizophrenia. Neuroimage 1995;2:244-252.

288. Mori S, Barker PB. Diffusion magnetic resonance imaging: its principle and applications. Anat Rec 1999;257:102-109.

289. Beaulieu C. The basis of anisotropic water diffusion in the nervous system - a technical review. NMR Biomed 2002;15:435-455.

290. Pierpaoli C, Barnett A, Pajevic S, et al. Water diffusion changes in Wallerian degeneration and their dependence on white matter architecture. Neuroimage 2001;13:1174-1185.

291. Douaud G, Jbabdi S, Behrens TE, et al. DTI measures in crossing-fibre areas: increased diffusion anisotropy reveals early white matter alteration in MCI and mild Alzheimer's disease. Neuroimage 2011;55:880-890.

292. Jeurissen B, Leemans A, Tournier JD, Jones DK, Sijbers J. Investigating the prevalence of complex fiber configurations in white matter tissue with diffusion magnetic resonance imaging. Hum Brain Mapp 2013;34:2747-2766.

293. Toosy AT, Werring DJ, Orrell RW, et al. Diffusion tensor imaging detects corticospinal tract involvement at multiple levels in amyotrophic lateral sclerosis. J Neurol Neurosurg Psychiatry 2003;74:1250-1257.

294. Smith SM, Jenkinson M, Johansen-Berg H, et al. Tract-based spatial statistics: voxelwise analysis of multi-subject diffusion data. Neuroimage 2006;31:1487-1505.

295. Shen D, Cui L, Fang J, Cui B, Li D, Tai H. Voxel-Wise Meta-Analysis of Gray Matter Changes in Amyotrophic Lateral Sclerosis. Front Aging Neurosci 2016;8:64.

296. Acosta-Cabronero J, Machts J, Schreiber S, et al. Quantitative Susceptibility MRI to Detect Brain Iron in Amyotrophic Lateral Sclerosis. Radiology 2018;289:195-203.

297. Raaphorst J, van Tol MJ, de Visser M, et al. Prose memory impairment in amyotrophic lateral sclerosis patients is related to hippocampus volume. Eur J Neurol 2015;22:547-554.
298. Rajagopalan V, Yue GH, Pioro EP. Do preprocessing algorithms and statistical models influence voxel-based morphometry (VBM) results in amyotrophic lateral sclerosis patients? A systematic comparison of popular VBM analytical methods. J Magn Reson Imaging 2014;40:662-667.
299. Roccatagliata L, Bonzano L, Mancardi G, Canepa C, Caponnetto C. Detection of motor cortex thinning and corticospinal tract involvement by quantitative MRI in amyotrophic lateral sclerosis. Amyotroph Lateral Scler 2009;10:47-52.
300. Verstraete E, Veldink JH, Hendrikse J, Schelhaas HJ, van den Heuvel MP, van den Berg LH. Structural MRI reveals cortical thinning in amyotrophic lateral sclerosis. J Neurol Neurosurg Psychiatry 2012;83:383-388.
301. Walhout R, Westeneng HJ, Verstraete E, et al. Cortical thickness in ALS: towards a marker for upper motor neuron involvement. J Neurol Neurosurg Psychiatry 2015;86:288-294.
302. Zhang J, Yin X, Zhao L, et al. Regional alterations in cortical thickness and white matter integrity in amyotrophic lateral sclerosis. J Neurol 2014;261:412-421.
303. Bede P, Bokde A, Elamin M, et al. Grey matter correlates of clinical variables in amyotrophic lateral sclerosis (ALS): a neuroimaging study of ALS motor phenotype heterogeneity and cortical focality. J Neurol Neurosurg Psychiatry 2013;84:766-773.
304. Schuster C, Kasper E, Machts J, et al. Focal thinning of the motor cortex mirrors clinical features of amyotrophic lateral sclerosis and their phenotypes: a neuroimaging study. J Neurol 2013;260:2856-2864.

305. Kwan JY, Meoded A, Danielian LE, Wu T, Floeter MK. Structural imaging differences and longitudinal changes in primary lateral sclerosis and amyotrophic lateral sclerosis. Neuroimage Clin 2012;2:151-160.

306. Agosta F, Spinelli EG, Riva N, et al. Survival prediction models in motor neuron disease. Eur J Neurol 2019.

307. Agosta F, Pagani E, Petrolini M, et al. Assessment of white matter tract damage in patients with amyotrophic lateral sclerosis: a diffusion tensor MR imaging tractography study. AJNR Am J Neuroradiol 2010;31:1457-1461.

308. Ellis CM, Simmons A, Jones DK, et al. Diffusion tensor MRI assesses corticospinal tract damage in ALS. Neurology 1999;53:1051-1058.

309. Sarica A, Cerasa A, Valentino P, et al. The corticospinal tract profile in amyotrophic lateral sclerosis. Hum Brain Mapp 2017;38:727-739.

310. Turner MR, Verstraete E. What does imaging reveal about the pathology of amyotrophic lateral sclerosis? Curr Neurol Neurosci Rep 2015;15:45.

311. Alruwaili AR, Pannek K, Coulthard A, Henderson R, Kurniawan ND, McCombe P. A combined tract-based spatial statistics and voxel-based morphometry study of the first MRI scan after diagnosis of amyotrophic lateral sclerosis with subgroup analysis. J Neuroradiol 2018;45:41-48.

312. Ciccarelli O, Behrens TE, Johansen-Berg H, et al. Investigation of white matter pathology in ALS and PLS using tract-based spatial statistics. Hum Brain Mapp 2009;30:615-624.

313. Sage CA, Van Hecke W, Peeters R, et al. Quantitative diffusion tensor imaging in amyotrophic lateral sclerosis: revisited. Hum Brain Mapp 2009;30:3657-3675.

314. Menke RA, Abraham I, Thiel CS, et al. Fractional anisotropy in the posterior limb of the internal capsule and prognosis in amyotrophic lateral sclerosis. Arch Neurol 2012;69:1493-1499.
315. Blain CR, Williams VC, Johnston C, et al. A longitudinal study of diffusion tensor MRI in ALS. Amyotroph Lateral Scler 2007;8:348-355.
316. Menke RA, Korner S, Filippini N, et al. Widespread grey matter pathology dominates the longitudinal cerebral MRI and clinical landscape of amyotrophic lateral sclerosis. Brain 2014;137:2546-2555.
317. Wang S, Poptani H, Bilello M, et al. Diffusion tensor imaging in amyotrophic lateral sclerosis: volumetric analysis of the corticospinal tract. AJNR Am J Neuroradiol 2006;27:1234-1238.
318. Agosta F, Pagani E, Petrolini M, et al. MRI predictors of long-term evolution in amyotrophic lateral sclerosis. Eur J Neurosci 2010;32:1490-1496.
319. Muller HP, Agosta F, Riva N, et al. Fast progressive lower motor neuron disease is an ALS variant: A two-centre tract of interest-based MRI data analysis. Neuroimage Clin 2018;17:145-152.
320. Prudlo J, Bissbort C, Glass A, et al. White matter pathology in ALS and lower motor neuron ALS variants: a diffusion tensor imaging study using tract-based spatial statistics. J Neurol 2012;259:1848-1859.
321. Rosenbohm A, Muller HP, Hubers A, Ludolph AC, Kassubek J. Corticoefferent pathways in pure lower motor neuron disease: a diffusion tensor imaging study. J Neurol 2016;263:2430-2437.

322. Agosta F, Galantucci S, Riva N, et al. Intrahemispheric and interhemispheric structural network abnormalities in PLS and ALS. Hum Brain Mapp 2014;35:1710-1722.
323. Iwata NK, Kwan JY, Danielian LE, et al. White matter alterations differ in primary lateral sclerosis and amyotrophic lateral sclerosis. Brain 2011;134:2642-2655.
324. Foerster BR, Dwamena BA, Petrou M, Carlos RC, Callaghan BC, Pomper MG. Diagnostic accuracy using diffusion tensor imaging in the diagnosis of ALS: a meta-analysis. Acad Radiol 2012;19:1075-1086.
325. Foerster BR, Dwamena BA, Petrou M, et al. Diagnostic accuracy of diffusion tensor imaging in amyotrophic lateral sclerosis: a systematic review and individual patient data meta-analysis. Acad Radiol 2013;20:1099-1106.
326. Chapman MC, Jelsone-Swain L, Johnson TD, Gruis KL, Welsh RC. Diffusion tensor MRI of the corpus callosum in amyotrophic lateral sclerosis. J Magn Reson Imaging 2014;39:641-647.
327. Filippini N, Douaud G, Mackay CE, Knight S, Talbot K, Turner MR. Corpus callosum involvement is a consistent feature of amyotrophic lateral sclerosis. Neurology 2010;75:1645-1652.
328. Karandreas N, Papadopoulou M, Kokotis P, Papapostolou A, Tsivgoulis G, Zambelis T. Impaired interhemispheric inhibition in amyotrophic lateral sclerosis. Amyotroph Lateral Scler 2007;8:112-118.
329. Wittstock M, Wolters A, Benecke R. Transcallosal inhibition in amyotrophic lateral sclerosis. Clin Neurophysiol 2007;118:301-307.

330. Muller HP, Unrath A, Huppertz HJ, Ludolph AC, Kassubek J. Neuroanatomical patterns of cerebral white matter involvement in different motor neuron diseases as studied by diffusion tensor imaging analysis. Amyotroph Lateral Scler 2012;13:254-264.
331. Smith MC. Nerve Fibre Degeneration in the Brain in Amyotrophic Lateral Sclerosis. J Neurol Neurosurg Psychiatry 1960;23:269-282.
332. Sugiyama M, Takao M, Hatsuta H, et al. Increased number of astrocytes and macrophages/microglial cells in the corpus callosum in amyotrophic lateral sclerosis. Neuropathology 2013;33:591-599.
333. Agosta F, Pagani E, Rocca MA, et al. Voxel-based morphometry study of brain volumetry and diffusivity in amyotrophic lateral sclerosis patients with mild disability. Hum Brain Mapp 2007;28:1430-1438.
334. Christidi F, Karavasilis E, Riederer F, et al. Gray matter and white matter changes in non-demented amyotrophic lateral sclerosis patients with or without cognitive impairment: A combined voxel-based morphometry and tract-based spatial statistics whole-brain analysis. Brain Imaging Behav 2018;12:547-563.
335. Lillo P, Mioshi E, Burrell JR, Kiernan MC, Hodges JR, Hornberger M. Grey and white matter changes across the amyotrophic lateral sclerosis-frontotemporal dementia continuum. PLoS One 2012;7:e43993.
336. Mezzapesa DM, Ceccarelli A, Dicuonzo F, et al. Whole-brain and regional brain atrophy in amyotrophic lateral sclerosis. AJNR Am J Neuroradiol 2007;28:255-259.
337. Chang JL, Lomen-Hoerth C, Murphy J, et al. A voxel-based morphometry study of patterns of brain atrophy in ALS and ALS/FTLD. Neurology 2005;65:75-80.

338. Rajagopalan V, Pioro EP. Distinct patterns of cortical atrophy in ALS patients with or without dementia: an MRI VBM study. Amyotroph Lateral Scler Frontotemporal Degener 2014;15:216-225.

339. Schuster C, Kasper E, Dyrba M, et al. Cortical thinning and its relation to cognition in amyotrophic lateral sclerosis. Neurobiol Aging 2014;35:240-246.

340. Cirillo M, Esposito F, Tedeschi G, et al. Widespread microstructural white matter involvement in amyotrophic lateral sclerosis: a whole-brain DTI study. AJNR Am J Neuroradiol 2012;33:1102-1108.

341. Senda J, Atsuta N, Watanabe H, et al. Structural MRI correlates of amyotrophic lateral sclerosis progression. J Neurol Neurosurg Psychiatry 2017;88:901-907.

342. Kamminga J, Leslie FVC, Hsieh S, et al. Syntactic comprehension deficits across the FTD-ALS continuum. Neurobiol Aging 2016;41:11-18.

343. Leslie FV, Hsieh S, Caga J, et al. Semantic deficits in amyotrophic lateral sclerosis. Amyotroph Lateral Scler Frontotemporal Degener 2015;16:46-53.

344. Long Z, Irish M, Piguet O, Kiernan MC, Hodges JR, Burrell JR. Clinical and neuroimaging investigations of language disturbance in frontotemporal dementia-motor neuron disease patients. J Neurol 2019;266:921-933.

345. Ash S, Olm C, McMillan CT, et al. Deficits in sentence expression in amyotrophic lateral sclerosis. Amyotroph Lateral Scler Frontotemporal Degener 2015;16:31-39.

346. Karageorgiou E, Miller BL. Frontotemporal lobar degeneration: a clinical approach. Semin Neurol 2014;34:189-201.

347. Omer T, Finegan E, Hutchinson S, et al. Neuroimaging patterns along the ALS-FTD spectrum: a multiparametric imaging study. Amyotroph Lateral Scler Frontotemporal Degener 2017;18:611-623.

348. Kaan E, Swaab TY. The brain circuitry of syntactic comprehension. Trends Cogn Sci 2002;6:350-356.

349. Terada T, Miyata J, Obi T, et al. Frontal assessment battery and frontal atrophy in amyotrophic lateral sclerosis. Brain Behav 2017;7:e00707.

350. Agosta F, Ferraro PM, Riva N, et al. Structural brain correlates of cognitive and behavioral impairment in MND. Hum Brain Mapp 2016;37:1614-1626.

351. Sarro L, Agosta F, Canu E, et al. Cognitive functions and white matter tract damage in amyotrophic lateral sclerosis: a diffusion tensor tractography study. AJNR Am J Neuroradiol 2011;32:1866-1872.

352. Trojsi F, Caiazzo G, Siciliano M, et al. Microstructural correlates of Edinburgh Cognitive and Behavioural ALS Screen (ECAS) changes in amyotrophic lateral sclerosis. Psychiatry Res Neuroimaging 2019;288:67-75.

353. Woolley SC, Zhang Y, Schuff N, Weiner MW, Katz JS. Neuroanatomical correlates of apathy in ALS using 4 Tesla diffusion tensor MRI. Amyotroph Lateral Scler 2011;12:52-58.

354. Consonni M, Cappa SF, Dalla Bella E, Contarino VE, Lauria G. Cortical correlates of behavioural change in amyotrophic lateral sclerosis. J Neurol Neurosurg Psychiatry 2019;90:380-386.

355. Rolls ET. Limbic systems for emotion and for memory, but no single limbic system. Cortex 2015;62:119-157.

356. Abdulla S, Machts J, Kaufmann J, et al. Hippocampal degeneration in patients with amyotrophic lateral sclerosis. Neurobiol Aging 2014;35:2639-2645.

357. Machts J, Vielhaber S, Kollewe K, Petri S, Kaufmann J, Schoenfeld MA. Global Hippocampal Volume Reductions and Local CA1 Shape Deformations in Amyotrophic Lateral Sclerosis. Front Neurol 2018;9:565.

358. Raz N, Lindenberger U, Rodrigue KM, et al. Regional brain changes in aging healthy adults: general trends, individual differences and modifiers. Cereb Cortex 2005;15:1676-1689.

359. Bede P, Hardiman O. Longitudinal structural changes in ALS: a three time-point imaging study of white and gray matter degeneration. Amyotroph Lateral Scler Frontotemporal Degener 2018;19:232-241.

360. Cardenas-Blanco A, Machts J, Acosta-Cabronero J, et al. Structural and diffusion imaging versus clinical assessment to monitor amyotrophic lateral sclerosis. Neuroimage Clin 2016;11:408-414.

361. de Albuquerque M, Branco LM, Rezende TJ, de Andrade HM, Nucci A, Franca MC, Jr. Longitudinal evaluation of cerebral and spinal cord damage in Amyotrophic Lateral Sclerosis. Neuroimage Clin 2017;14:269-276.

362. Menke RAL, Proudfoot M, Talbot K, Turner MR. The two-year progression of structural and functional cerebral MRI in amyotrophic lateral sclerosis. Neuroimage Clin 2018;17:953-961.

363. Senda J, Kato S, Kaga T, et al. Progressive and widespread brain damage in ALS: MRI voxel-based morphometry and diffusion tensor imaging study. Amyotroph Lateral Scler 2011;12:59-69.

364. Shen DC, Xu YY, Hou B, et al. Monitoring Value of Multimodal Magnetic Resonance Imaging in Disease Progression of Amyotrophic Lateral Sclerosis: A Prospective Observational Study. Chin Med J (Engl) 2018;131:2904-2909.

365. Jacob S, Finsterbusch J, Weishaupt JH, Khorram-Sefat D, Frahm J, Ehrenreich H. Diffusion tensor imaging for long-term follow-up of corticospinal tract degeneration in amyotrophic lateral sclerosis. Neuroradiology 2003;45:598-600.

366. Sage CA, Peeters RR, Gorner A, Robberecht W, Sunaert S. Quantitative diffusion tensor imaging in amyotrophic lateral sclerosis. Neuroimage 2007;34:486-499.

367. Mitsumoto H, Ulug AM, Pullman SL, et al. Quantitative objective markers for upper and lower motor neuron dysfunction in ALS. Neurology 2007;68:1402-1410.

368. Nickerson JP, Koski CJ, Boyer AC, Burbank HN, Tandan R, Filippi CG. Linear longitudinal decline in fractional anisotropy in patients with amyotrophic lateral sclerosis: preliminary results. Klin Neuroradiol 2009;19:129-134.

369. Avants B, Khan A, McCluskey L, Elman L, Grossman M. Longitudinal cortical atrophy in amyotrophic lateral sclerosis with frontotemporal dementia. Arch Neurol 2009;66:138-139.

370. Agosta F, Rocca MA, Valsasina P, et al. A longitudinal diffusion tensor MRI study of the cervical cord and brain in amyotrophic lateral sclerosis patients. J Neurol Neurosurg Psychiatry 2009;80:53-55.

371. Agosta F, Gorno-Tempini ML, Pagani E, et al. Longitudinal assessment of grey matter contraction in amyotrophic lateral sclerosis: A tensor based morphometry study. Amyotroph Lateral Scler 2009;10:168-174.

372. Zhang Y, Schuff N, Woolley SC, et al. Progression of white matter degeneration in amyotrophic lateral sclerosis: A diffusion tensor imaging study. Amyotroph Lateral Scler 2011;12:421-429.

373. Keil C, Prell T, Peschel T, Hartung V, Dengler R, Grosskreutz J. Longitudinal diffusion tensor imaging in amyotrophic lateral sclerosis. BMC Neurosci 2012;13:141.

374. Schuster C, Kasper E, Machts J, et al. Longitudinal course of cortical thickness decline in amyotrophic lateral sclerosis. J Neurol 2014;261:1871-1880.

375. Verstraete E, Veldink JH, van den Berg LH, van den Heuvel MP. Structural brain network imaging shows expanding disconnection of the motor system in amyotrophic lateral sclerosis. Hum Brain Mapp 2014;35:1351-1361.

376. Westeneng HJ, Verstraete E, Walhout R, et al. Subcortical structures in amyotrophic lateral sclerosis. Neurobiol Aging 2015;36:1075-1082.

377. Steinbach R, Loewe K, Kaufmann J, et al. Structural hallmarks of amyotrophic lateral sclerosis progression revealed by probabilistic fiber tractography. J Neurol 2015;262:2257-2270.

378. Floeter MK, Bageac D, Danielian LE, Braun LE, Traynor BJ, Kwan JY. Longitudinal imaging in C9orf72 mutation carriers: Relationship to phenotype. Neuroimage Clin 2016;12:1035-1043.

379. Wirth AM, Khomenko A, Baldaranov D, et al. Combinatory Biomarker Use of Cortical Thickness, MUNIX, and ALSFRS-R at Baseline and in Longitudinal Courses of Individual Patients With Amyotrophic Lateral Sclerosis. Front Neurol 2018;9:614.

380. Stampfli P, Sommer S, Czell D, et al. Investigation of Neurodegenerative Processes in Amyotrophic Lateral Sclerosis Using White Matter Fiber Density. Clin Neuroradiol 2018.

381. Floeter MK, Danielian LE, Braun LE, Wu T. Longitudinal diffusion imaging across the C9orf72 clinical spectrum. J Neurol Neurosurg Psychiatry 2018;89:53-60.

382. Alruwaili AR, Pannek K, Henderson RD, Gray M, Kurniawan ND, McCombe PA. Tract integrity in amyotrophic lateral sclerosis: 6-month evaluation using MR diffusion tensor imaging. BMC Med Imaging 2019;19:19.

383. Moffett JR, Ross B, Arun P, Madhavarao CN, Namboodiri AM. N-Acetylaspartate in the CNS: from neurodiagnostics to neurobiology. Prog Neurobiol 2007;81:89-131.

384. Pohl C, Block W, Karitzky J, et al. Proton magnetic resonance spectroscopy of the motor cortex in 70 patients with amyotrophic lateral sclerosis. Arch Neurol 2001;58:729-735.

385. Suhy J, Miller RG, Rule R, et al. Early detection and longitudinal changes in amyotrophic lateral sclerosis by (1)H MRSI. Neurology 2002;58:773-779.

386. van der Graaff MM, Lavini C, Akkerman EM, et al. MR spectroscopy findings in early stages of motor neuron disease. AJNR Am J Neuroradiol 2010;31:1799-1806.

387. Gredal O, Rosenbaum S, Topp S, Karlsborg M, Strange P, Werdelin L. Quantification of brain metabolites in amyotrophic lateral sclerosis by localized proton magnetic resonance spectroscopy. Neurology 1997;48:878-881.

388. Kaufmann P, Pullman SL, Shungu DC, et al. Objective tests for upper motor neuron involvement in amyotrophic lateral sclerosis (ALS). Neurology 2004;62:1753-1757.

389. Pioro EP, Antel JP, Cashman NR, Arnold DL. Detection of cortical neuron loss in motor neuron disease by proton magnetic resonance spectroscopic imaging in vivo. Neurology 1994;44:1933-1938.

390. Kalra S, Vitale A, Cashman NR, Genge A, Arnold DL. Cerebral degeneration predicts survival in amyotrophic lateral sclerosis. J Neurol Neurosurg Psychiatry 2006;77:1253-1255.

391. Govind V, Sharma KR, Maudsley AA, Arheart KL, Saigal G, Sheriff S. Comprehensive evaluation of corticospinal tract metabolites in amyotrophic lateral sclerosis using whole-brain 1H MR spectroscopy. PLoS One 2012;7:e35607.

392. Stagg CJ, Knight S, Talbot K, Jenkinson M, Maudsley AA, Turner MR. Whole-brain magnetic resonance spectroscopic imaging measures are related to disability in ALS. Neurology 2013;80:610-615.

393. Strong MJ, Grace GM, Orange JB, Leeper HA, Menon RS, Aere C. A prospective study of cognitive impairment in ALS. Neurology 1999;53:1665-1670.

394. Kalra S, Tai P, Genge A, Arnold DL. Rapid improvement in cortical neuronal integrity in amyotrophic lateral sclerosis detected by proton magnetic resonance spectroscopic imaging. J Neurol 2006;253:1060-1063.

395. Abe K, Takanashi M, Watanabe Y, et al. Decrease in N-acetylaspartate/creatine ratio in the motor area and the frontal lobe in amyotrophic lateral sclerosis. Neuroradiology 2001;43:537-541.

396. Quinn C, Elman L, McCluskey L, et al. Frontal lobe abnormalities on MRS correlate with poor letter fluency in ALS. Neurology 2012;79:583-588.

397. Sharma KR, Saigal G, Maudsley AA, Govind V. 1H MRS of basal ganglia and thalamus in amyotrophic lateral sclerosis. NMR Biomed 2011;24:1270-1276.

398. Usman U, Choi C, Camicioli R, et al. Mesial prefrontal cortex degeneration in amyotrophic lateral sclerosis: a high-field proton MR spectroscopy study. AJNR Am J Neuroradiol 2011;32:1677-1680.

399. Bowen BC, Pattany PM, Bradley WG, et al. MR imaging and localized proton spectroscopy of the precentral gyrus in amyotrophic lateral sclerosis. AJNR Am J Neuroradiol 2000;21:647-658.

400. Bitsch A, Bruhn H, Vougioukas V, et al. Inflammatory CNS demyelination: histopathologic correlation with in vivo quantitative proton MR spectroscopy. AJNR Am J Neuroradiol 1999;20:1619-1627.

401. Rothermundt M, Ohrmann P, Abel S, et al. Glial cell activation in a subgroup of patients with schizophrenia indicated by increased S100B serum concentrations and elevated myo-inositol. Prog Neuropsychopharmacol Biol Psychiatry 2007;31:361-364.

402. Hattingen E, Raab P, Franz K, Zanella FE, Lanfermann H, Pilatus U. Myo-inositol: a marker of reactive astrogliosis in glial tumors? NMR Biomed 2008;21:233-241.

403. Ratai EM, Alshikho MJ, Zurcher NR, et al. Integrated imaging of [(11)C]-PBR28 PET, MR diffusion and magnetic resonance spectroscopy (1)H-MRS in amyotrophic lateral sclerosis. Neuroimage Clin 2018;20:357-364.

404. Kalra S, Hanstock CC, Martin WR, Allen PS, Johnston WS. Detection of cerebral degeneration in amyotrophic lateral sclerosis using high-field magnetic resonance spectroscopy. Arch Neurol 2006;63:1144-1148.

405. Han J, Ma L. Study of the features of proton MR spectroscopy ((1)H-MRS) on amyotrophic lateral sclerosis. J Magn Reson Imaging 2010;31:305-308.

406. Ziemann U, Winter M, Reimers CD, Reimers K, Tergau F, Paulus W. Impaired motor cortex inhibition in patients with amyotrophic lateral sclerosis. Evidence from paired transcranial magnetic stimulation. Neurology 1997;49:1292-1298.

407. Foerster BR, Callaghan BC, Petrou M, Edden RA, Chenevert TL, Feldman EL. Decreased motor cortex gamma-aminobutyric acid in amyotrophic lateral sclerosis. Neurology 2012;78:1596-1600.

408. Atassi N, Xu M, Triantafyllou C, et al. Ultra high-field (7tesla) magnetic resonance spectroscopy in Amyotrophic Lateral Sclerosis. PLoS One 2017;12:e0177680.

409. Lloyd CM, Richardson MP, Brooks DJ, Al-Chalabi A, Leigh PN. Extramotor involvement in ALS: PET studies with the GABA(A) ligand [(11)C]flumazenil. Brain 2000;123 (Pt 11):2289-2296.

410. Foerster BR, Carlos RC, Dwamena BA, et al. Multimodal MRI as a diagnostic biomarker for amyotrophic lateral sclerosis. Ann Clin Transl Neurol 2014;1:107-114.

411. Cervo A, Cocozza S, Sacca F, et al. The combined use of conventional MRI and MR spectroscopic imaging increases the diagnostic accuracy in amyotrophic lateral sclerosis. Eur J Radiol 2015;84:151-157.

412. Charil A, Corbo M, Filippi M, et al. Structural and metabolic changes in the brain of patients with upper motor neuron disorders: a multiparametric MRI study. Amyotroph Lateral Scler 2009;10:269-279.

413. Gore JC. Principles and practice of functional MRI of the human brain. J Clin Invest 2003;112:4-9.

414. Kew JJ, Goldstein LH, Leigh PN, et al. The relationship between abnormalities of cognitive function and cerebral activation in amyotrophic lateral sclerosis. A

neuropsychological and positron emission tomography study. Brain 1993;116 (Pt 6):1399-1423.

415. Mohammadi B, Kollewe K, Samii A, Dengler R, Munte TF. Functional neuroimaging at different disease stages reveals distinct phases of neuroplastic changes in amyotrophic lateral sclerosis. Hum Brain Mapp 2011;32:750-758.

416. Schoenfeld MA, Tempelmann C, Gaul C, et al. Functional motor compensation in amyotrophic lateral sclerosis. J Neurol 2005;252:944-952.

417. Kollewe K, Munte TF, Samii A, Dengler R, Petri S, Mohammadi B. Patterns of cortical activity differ in ALS patients with limb and/or bulbar involvement depending on motor tasks. J Neurol 2011;258:804-810.

418. Poujois A, Schneider FC, Faillenot I, et al. Brain plasticity in the motor network is correlated with disease progression in amyotrophic lateral sclerosis. Hum Brain Mapp 2013;34:2391-2401.

419. Jelsone-Swain L, Persad C, Burkard D, Welsh RC. Action processing and mirror neuron function in patients with amyotrophic lateral sclerosis: an fMRI study. PLoS One 2015;10:e0119862.

420. Li H, Chen Y, Li Y, et al. Altered cortical activation during action observation in amyotrophic lateral sclerosis patients: a parametric functional MRI study. Eur Radiol 2015;25:2584-2592.

421. Proudfoot M, Bede P, Turner MR. Imaging Cerebral Activity in Amyotrophic Lateral Sclerosis. Front Neurol 2018;9:1148.

422. Douaud G, Filippini N, Knight S, Talbot K, Turner MR. Integration of structural and functional magnetic resonance imaging in amyotrophic lateral sclerosis. Brain 2011;134:3470-3479.

423. Goldstein LH, Newsom-Davis IC, Bryant V, Brammer M, Leigh PN, Simmons A. Altered patterns of cortical activation in ALS patients during attention and cognitive response inhibition tasks. J Neurol 2011;258:2186-2198.

424. Keller J, Bohm S, Aho-Ozhan HEA, et al. Functional reorganization during cognitive function tasks in patients with amyotrophic lateral sclerosis. Brain Imaging Behav 2018;12:771-784.

425. Passamonti L, Fera F, Tessitore A, et al. Dysfunctions within limbic-motor networks in amyotrophic lateral sclerosis. Neurobiol Aging 2013;34:2499-2509.

426. Aho-Ozhan HE, Keller J, Heimrath J, et al. Perception of Emotional Facial Expressions in Amyotrophic Lateral Sclerosis (ALS) at Behavioural and Brain Metabolic Level. PLoS One 2016;11:e0164655.

427. Raichle ME, MacLeod AM, Snyder AZ, Powers WJ, Gusnard DA, Shulman GL. A default mode of brain function. Proc Natl Acad Sci U S A 2001;98:676-682.

428. Raichle ME. The brain's default mode network. Annu Rev Neurosci 2015;38:433-447.

429. Mohammadi B, Kollewe K, Samii A, Krampfl K, Dengler R, Munte TF. Changes of resting state brain networks in amyotrophic lateral sclerosis. Exp Neurol 2009;217:147-153.

430. Tedeschi G, Trojsi F, Tessitore A, et al. Interaction between aging and neurodegeneration in amyotrophic lateral sclerosis. Neurobiol Aging 2012;33:886-898.

431. Jelsone-Swain LM, Fling BW, Seidler RD, Hovatter R, Gruis K, Welsh RC. Reduced Interhemispheric Functional Connectivity in the Motor Cortex during Rest in Limb-Onset Amyotrophic Lateral Sclerosis. Front Syst Neurosci 2010;4:158.

432. Agosta F, Valsasina P, Absinta M, et al. Sensorimotor functional connectivity changes in amyotrophic lateral sclerosis. Cereb Cortex 2011;21:2291-2298.

433. Heimrath J, Gorges M, Kassubek J, et al. Additional resources and the default mode network: Evidence of increased connectivity and decreased white matter integrity in amyotrophic lateral sclerosis. Amyotroph Lateral Scler Frontotemporal Degener 2014;15:537-545.

434. Chenji S, Jha S, Lee D, et al. Investigating Default Mode and Sensorimotor Network Connectivity in Amyotrophic Lateral Sclerosis. PLoS One 2016;11:e0157443.

435. Haralick RM, Shanmugam K, Dinstein IH. Textural features for image classification. IEEE Trans Syst Man Cybern 1973;SMC-3:610-621.

436. Castellano G, Bonilha L, Li LM, Cendes F. Texture analysis of medical images. Clin Radiol 2004;59:1061-1069.

437. Mahmoud-Ghoneim D, Alkaabi MK, de Certaines JD, Goettsche FM. The impact of image dynamic range on texture classification of brain white matter. BMC Med Imaging 2008;8:18.

438. Kassner A, Thornhill RE. Texture analysis: a review of neurologic MR imaging applications. AJNR Am J Neuroradiol 2010;31:809-816.

439. Maani R, Yang YH, Emery D, Kalra S. Cerebral Degeneration in Amyotrophic Lateral Sclerosis Revealed by 3-Dimensional Texture Analysis. Front Neurosci 2016;10:120.

440. Maani R, Yang YH, Kalra S. Voxel-based texture analysis of the brain. PLoS One 2015;10:e0117759.

441. Kassner A, Liu F, Thornhill RE, Tomlinson G, Mikulis DJ. Prediction of hemorrhagic transformation in acute ischemic stroke using texture analysis of postcontrast T1-weighted MR images. J Magn Reson Imaging 2009;30:933-941.

442. Mayerhoefer ME, Breitenseher MJ, Kramer J, Aigner N, Hofmann S, Materka A. Texture analysis for tissue discrimination on T1-weighted MR images of the knee joint in a multicenter study: Transferability of texture features and comparison of feature selection methods and classifiers. J Magn Reson Imaging 2005;22:674-680.

443. Freeborough PA, Fox NC. MR image texture analysis applied to the diagnosis and tracking of Alzheimer's disease. IEEE Trans Med Imaging 1998;17:475-479.

444. Zhang J, Yu C, Jiang G, Liu W, Tong L. 3D texture analysis on MRI images of Alzheimer's disease. Brain Imaging Behav 2012;6:61-69.

445. Braak H, Braak E. Staging of Alzheimer's disease-related neurofibrillary changes. Neurobiol Aging 1995;16:271-278; discussion 278-284.

446. Feng F, Wang P, Zhao K, et al. Radiomic Features of Hippocampal Subregions in Alzheimer's Disease and Amnestic Mild Cognitive Impairment. Front Aging Neurosci 2018;10:290.

447. de Oliveira MS, Balthazar ML, D'Abreu A, et al. MR imaging texture analysis of the corpus callosum and thalamus in amnestic mild cognitive impairment and mild Alzheimer disease. AJNR Am J Neuroradiol 2011;32:60-66.

448. Luk CC, Ishaque A, Khan M, et al. Alzheimer's disease: 3-Dimensional MRI texture for prediction of conversion from mild cognitive impairment. Alzheimers Dement (Amst) 2018;10:755-763.

449. Sorensen L, Igel C, Liv Hansen N, et al. Early detection of Alzheimer's disease using MRI hippocampal texture. Hum Brain Mapp 2016;37:1148-1161.

450. Zhang Y. MRI texture analysis in multiple sclerosis. Int J Biomed Imaging 2012;2012:762804.

451. Mathias JM, Tofts PS, Losseff NA. Texture analysis of spinal cord pathology in multiple sclerosis. Magn Reson Med 1999;42:929-935.

452. Zhang Y, Zhu H, Mitchell JR, Costello F, Metz LM. T2 MRI texture analysis is a sensitive measure of tissue injury and recovery resulting from acute inflammatory lesions in multiple sclerosis. Neuroimage 2009;47:107-111.

453. Yu O, Steibel J, Mauss Y, et al. Remyelination assessment by MRI texture analysis in a cuprizone mouse model. Magn Reson Imaging 2004;22:1139-1144.

454. Zhang Y, Wells J, Buist R, Peeling J, Yong VW, Mitchell JR. A novel MRI texture analysis of demyelination and inflammation in relapsing-remitting experimental allergic encephalomyelitis. Med Image Comput Comput Assist Interv 2006;9:760-767.

455. Zhang Y, Moore GR, Laule C, et al. Pathological correlates of magnetic resonance imaging texture heterogeneity in multiple sclerosis. Ann Neurol 2013;74:91-99.

456. de Albuquerque M, Anjos LG, Maia Tavares de Andrade H, et al. MRI Texture Analysis Reveals Deep Gray Nuclei Damage in Amyotrophic Lateral Sclerosis. J Neuroimaging 2016;26:201-206.

457. Ishaque A, Maani R, Satkunam J, et al. Texture Analysis to Detect Cerebral Degeneration in Amyotrophic Lateral Sclerosis. Can J Neurol Sci 2018;45:533-539.

458. Statland JM, Moore D, Wang Y, et al. Rasagiline for amyotrophic lateral sclerosis: A randomized, controlled trial. Muscle Nerve 2019;59:201-207.

459. Filippi M, Agosta F, Grosskreutz J, et al. Progress towards a neuroimaging biomarker for amyotrophic lateral sclerosis. Lancet Neurol 2015;14:786-788.

460. Lassek AM. The human pyramidal tract. IV. A study of the mature, myelinated fibers of the pyramid. Journal of Comparative Neurology 1942;76:217-225.

461. Russell-Schulz B, Laule C, Li DK, MacKay AL. What causes the hyperintense T2-weighting and increased short T2 signal in the corticospinal tract? Magn Reson Imaging 2013;31:329-335.

462. Aboitiz F, Scheibel AB, Fisher RS, Zaidel E. Fiber composition of the human corpus callosum. Brain Res 1992;598:143-153.

463. Hanstock C, Sun K, Choi C, et al. Spectroscopic markers of neurodegeneration in the mesial prefrontal cortex predict survival in ALS. Amyotroph Lateral Scler Frontotemporal Degener 2020:1-6.